INFORMATION TO USERS

This manuscript has been reproduced from the microfilm master. UMI films the text directly from the original or copy submitted. Thus, some thesis and dissertation copies are in typewriter face, while others may be from any type of computer printer.

The quality of this reproduction is dependent upon the quality of the copy submitted. Broken or indistinct print, colored or poor quality illustrations and photographs, print bleedthrough, substandard margins, and improper alignment can adversely affect reproduction.

In the unlikely event that the author did not send UMI a complete manuscript and there are missing pages, these will be noted. Also, if unauthorized copyright material had to be removed, a note will indicate the deletion.

Oversize materials (e.g., maps, drawings, charts) are reproduced by sectioning the original, beginning at the upper left-hand corner and continuing from left to right in equal sections with small overlaps.

Photographs included in the original manuscript have been reproduced xerographically in this copy. Higher quality 6" x 9" black and white photographic prints are available for any photographs or illustrations appearing in this copy for an additional charge. Contact UMI directly to order.

Bell & Howell Information and Learning
300 North Zeeb Road, Ann Arbor, MI 48106-1346 USA
800-521-0600

The Effect of Long Chain Branching on the Rheological Behavior of Polyethylenes Synthesized Using Constrained Geometry and Metallocene Catalysts

by

Paula Marie Wood-Adams

Department of Chemical Engineering
McGill University, Montreal
October 1998

A thesis submitted to the Faculty of Graduate Studies in partial fulfillment of the requirements of the degree of Doctor of Philosophy

Abstract

Constrained Geometry catalysts make it possible to control independently molecular weight (MW), molecular weight distribution (MWD), homogeneity of short chain branching (SCB), and degree of long chain branching (LCB). This catalyst technology provides us with a unique opportunity to study the effects of molecular structure on the rheological behavior of polyethylene. In particular the effects of low levels of long chain branching (LCB) have never been studied in commercial polyethylenes, because it was impossible to vary the degree of branching while maintaining the backbone molecular weight and molecular weight distribution using traditional polymerization techniques.

Nine constrained geometry catalyzed and metallocene polyethylenes (together referred to as mPE) with approximately the same MWDs but varying degrees of LCB were subjected to an intensive study including linear viscoelastic behavior and nonlinear shear and extensional flow behavior. Using these results, it was found that low levels of LCB manifest themselves mostly in the linear regime and not in nonlinear extensional flow behavior as was previously thought. LCB extended the relaxation spectrum to longer relaxation times, increased the zero shear viscosity and the shear sensitivity, and resulted in a complex viscosity curve that was slightly sigmoidal in shape. It was also found that these branched materials followed the Cox-Merz rule and the Gleissle mirror relations. Separable stress relaxation behavior was exhibited in step strain experiments with increasing degree of LCB resulting in increasing damping. LCB increased the nonlinearity in the fluids' response to large amplitude oscillatory shear (LAOS). The damping functions determined from step strain experiments were consistent with experimental data for steady simple shear and LAOS.

A study of the effect of molecular weight and short chain branching on the linear viscoelastic behavior was also performed. A set of three additional linear mPEs with the same polydispersities but varying average molecular weights was studied. The usual exponential dependence of the zero shear viscosity on the molecular weight was found with coefficient and exponent values consistent with previously reported results for

polyethylene. To determine the effect of short chain branching a set of three butene copolymers with the same polydispersity but varying degrees of SCB was included. It was found that any effect of SCB on the LVE behavior was smaller than the variation in the experimental data.

A procedure was developed for inferring the degree of LCB using linear viscoelastic data and backbone MWD information. Such a procedure is particularly important in the case of ethylene-octene copolymers for which it is difficult to measure the degree of long chain branching using nuclear magnetic resonance techniques. This technique was shown to be robust and not likely to give false predictions of LCB in the case of linear materials. A method for evaluating the reliability of the predicted degree of LCB that involves only complex viscosity data was also presented.

Resumé

Aujourd'hui, les catalyseurs contraintes géométriques nous laissent controller indépendamment le poids moléculaire (MW), la distribution du poids moléculaire (MWD), l'homogéneité des ramifications courtes (SCB), et le degré des ramifications longues (LCB). Cette technologie nous donne une occasion unique pour étudier les effets moléculaires sur les propriétés rhéologiques du polyéthylène. C'est surtout le cas pour l'effet du niveau de ramifications longues sur la rhéologie: avec les techniques de polymérization traditionnelles, il était impossible de changer le degré de ramifications sans altérer le poids moléculaire du tronc et la distribution du poids moléculaire.

Neuf polyéthylènes contraintes géométriques catalysés et metallocènes ont été étudiés en cisaillement linéaire, cisaillement non-linéaire, et en extension. Ces polymères avaient tous la même distribution de poids moléculaires, mais avec des degrés différents de ramifications longues. Dans cette étude, nous avons découvert que les bas niveaux de ramifications courtes se manifestent dans le régime linéaire et non dans le régime d'extension non-linéaire. On a découvert que les ramifications courtes elargissent le spectre linéaire à des temps plus élevés, augmentent la viscosité á cisaillement nul, augmentent la sensibilité au cisaillement et donnent une forme sigmoidale à la courbe de viscosité. On a aussi demontré que ces matériaux suivent la règle de Cox-Merz et les relations mirroirs Gleisse. La relaxation des contraintes après des deformations étagé est séparable et on a observé qu'une augmentation du degré de ramifications longues augmente l'amortissement. Le degré de ramifications longues a aussi augmenté la non-linéarité de la réponse du fluide au cisaillement oscillatoire à grande amplitude. L'ammortissement calculé à partir des deformations étagé était en accord avec les résultats obtenus en cisaillement simple et en cisaillement oscillatoire à grande amplitude.

On a aussi étudié l'effet du poids moléculaire et du degré de ramifications courtes sur le régime viscoélastique linéaire. Trois polyéthylènes à base de catalyseurs metallocènes ont été utilisés. Ces polymères ont tous la même polydispersité mais varient en poids moleculaire. On a mesuré une dépendance exponentielle de la viscosité á cisaillement nul sur le poids moléculaire. Les valeurs obtenues pour le coefficient et

l'éxposant sont en accord avec celles publiées dans la littérature pour le polyéthylène. Pour déterminer l'effet des ramifications courtes, trois copolymères de butène avec la même polydispersité mais avec différents degrés de ramifications courtes ont été inclus dans l'étude. On a trouvé que l'effet des branchements courts sur la viscoélasticité linéaire étaient inférieur à la variation normale des résultats expérimentaux.

Une procédure a été conçue pour déterminer le degré de ramifications longues à partir des résultats viscoélastiques linéaires et des propriétés de la distribution moléculaire du tronc. Cette procédure est particulièrement importante pour les copolymères éthylene-octène, où il est difficile de mesurer le degré de ramifications longues en utilisant les techniques de résonance magnétique nucléaire. On a démontré que notre technique est robuste et ne donne pas de prédictions fausses pour les matériaux linéaires. Une méthode pour évaluer la fiabilité de la prédiction du degré de ramifications longues est aussi présentée. Cette technique utilise seulement la viscosité complexe.

Acknowledgements

My first acknowledgement must go to my advisor and mentor John Dealy who unfailingly teaches, inspires and pushes towards success all who have the good fortune to be his students. He is an expert, and I have learned a great deal from him. I am grateful for his patience, his belief in me, and for all of the opportunities that he has afforded me.

I would also like to thank my husband, Myles, whose constant support and encouragement gave me the strength to get through many difficulties. My daughter, Emily, is without doubt the one who sacrificed the most for this thesis and I will be ever grateful for her loving nature and her happy acceptance of my hectic schedule.

This work would not have been possible without The Dow Chemical Company, who supplied financial support and made their research resources available to my many requests. Many individuals at Dow Chemical went out of their way to help me, including Rudy Koopmans, Marc Mangnus, Steve Chum, Ravi Ramanathan, Willem Degroot, and Teresa Karjala. I appreciate very much their personal interest in my work.

One of the experiences that I value the most is having had the opportunity to work as a part of such a great research team. The cooperative atmosphere and the easy sharing of results and ideas resulted in far better science than would otherwise have been possible. I am especially grateful to my fellow students, François Koran and Marie-Claude Heuzey who for five years have been a source of motivation and inspiration. I would also like to thank the other graduate students who added so much to my experience at McGill; Valerie Gilbert, Yalda Farhoudi, Mazen Samara, Seungh-oh Kim, Martin Sentmanat, Michael Reimers, Ranjit Jeyaleelan, and Mélanie Boudreault. A sincere thank you also to Akram Sabaie and Ka Wing Ng who each sacrificed a summer to collect experimental results for me.

I am also indebted to Joachim Meissner and Thomas Schweizer who graciously received me at their lab at the Institue für Polymere, ETH Zürich and provided training and valuable advice on the use of an extensional rheometer. I appreciate very much the excellent experimental work done by Thomas Schweizer and his company, Plastech Engineering AG.

I would like to thank Helmut Münstedt of the University of Erlangen-Nürnberg, for putting me in touch with his graduate student Jens Hepperle, with whom I had several useful communications.

Finally, I would like to thank the many people outside of McGill who listened with unfailing interest to many grumblings and were there also to celebrate the successes: my parents and assorted siblings, my family-in-law, my friends; Krista Gilliland, Charlotte Orrell-Hoskins, Paula McGarrigle, Denise Kokaram, Wendy Yiu, and Annie Simard. I am also grateful to my Aunt Christine who encouraged to me to become a teacher.

Table of Contents

List of Figures

List of Tables

Chapter 1

Introduction to Metallocene Polyethylenes

In the past decade a new commercial class has been added to the traditional line-up of polyethylenes that includes low density polyethylene (LDPE), linear low density polyethylene (LLDPE), and high density polyethylene (HDPE). This new class, referred to as mPE, contains materials that differ from traditional resins in terms of molecular structure, melt rheological behavior and solid state physical properties. The general class of mPE consists of constrained geometry catalyzed and metallocene polyethylenes.

mPEs are interesting from a commercial point of view because of their good physical properties and the better control of molecular structure. Generally, mPEs exhibit higher toughness, better optical properties, better heat-sealing characteristics and higher crosslink efficiency[1] than traditional polyethylenes. For most mPEs, improved physical properties come at the price of reduced processability, however, which is an important factor when determining the utility of a polymer for a particular product.

Metallocene polyethylenes are interesting to rheologists because of their unique and precisely controlled molecular structures (described in Section 1.2). Using these materials it is possible to study independently the effects of various molecular characteristics on rheological behavior. This type of study was impossible with traditional polyethylenes.

In the present work, the relationship between molecular structure and melt rheology of mPE is studied. The dependence of various rheological parameters on molecular weight, short chain branching and long chain branching is described. Also, a technique for inferring degree of LCB from rheological data is presented.

1.1 Single Site Metallocene Catalysts for the Production of Polyolefins

Catalysts are said to be "single-site" when reactions can occur only at one place on the catalyst molecule. Typically, single site metallocene catalysts are referred to as "metallocene catalysts" without mention of the number of active sites. Since it is possible to have metallocene catalysts with multiple active sites this designation can be misleading. However, as it is the accepted terminology in the literature and it is less cumbersome we will use the term metallocene catalyst to mean single site metallocene catalyst. Conventional Zieger-Natta catalysts used for the production of the polyethylene have multiple active sites with different reactivity ratios for different olefins. The multiple active sites result in a polymeric system that is a mixture of many kinds of molecules. The single site catalysts offer much more control over the molecular structure of the polymer.

Figure 1.1 shows the general chemical structure of the catalyst used by Dow Chemical to produce its AFFINITY* resins[2]. This catalyst is a constrained geometry catalyst. However, for convenience purpose the industry also calls this catalyst a "metallocene" catalyst and the polymer made from this catalyst system, mPE. In this figure the R' groups contain up to 10 carbon atoms. The metal ion is the active site and is surrounded by the rest of the catalyst complex in a constrained geometry. This feature allows for precise and independent control of the molecular weight, homogeneity of short chain branching and degree of long chain branching.

The polyethylenes produced with metallocene catalysts are called 'metallocene polyethylenes' (mPEs). As with the catalyst, this is perhaps not the most accurate name but is the accepted terminology in the literature. In this work, we use metallocene polyethylene and mPE to refer to polyethylenes produced with single site catalysts.

---

* Trademark of the Dow Chemical Company

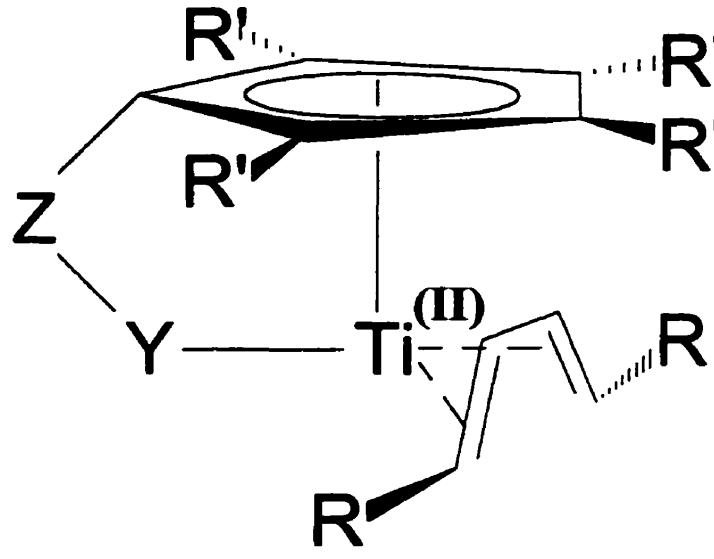

Figure 1.1 Chemical Structure of INSITE* Metallocene Catalyst

1.2 Unique Molecular Characteristic of Metallocene Polyethylenes

In Figure 1.2 the molecular structures of traditional and metallocene polyethylenes are shown schematically. Traditional linear polyethylenes, such as HDPE and LLDPE, have broad molecular weight distributions (MWD), and in the case of LLDPE, broad short chain branching distributions. The short chain branches (SCB) are distributed non-uniformly along the backbones and heterogeneously among the molecules[3]. These materials are said to be "linear" because they have no long chain branches (LCB). They can be contrasted to LDPE, which has branches of many different lengths distributed non-uniformly throughout the system.

In comparison, mPEs have narrow MWDs with polydispersity indexes of approximately 2. In the case of ethylene α-olefin copolymers produced with metallocene catalysts, the SCB are distributed randomly and uniformly along the backbone and homogeneously among the molecules. Within the general class of metallocene polyethylenes there are two subclasses: linear and branched mPEs. In this context "branched" refers to the presence of long chain branches. The linear mPEs, have either

no branches or only short chain branches but no LCB. The branched mPEs (AFFINITY Resins) are made using the constrained geometry catalysts and have precisely controlled low levels of LCB. These materials are referred to as substantially linear, to distinguish them from highly branched LDPE.

The narrow MWD is the source of both the benefits and the disadvantages of mPE. The narrow MWD allows the good physical properties characteristic of mPE[4]. However, a narrow MWD also causes decreased shear thinning resulting in higher energy requirements for processing. The low levels of LCB in the AFFINITY™ polymers increase the amount of shear thinning and therefore improve their processability. The LCB also increases melt strength and reduces susceptibility to melt fracture and draw resonance[5].

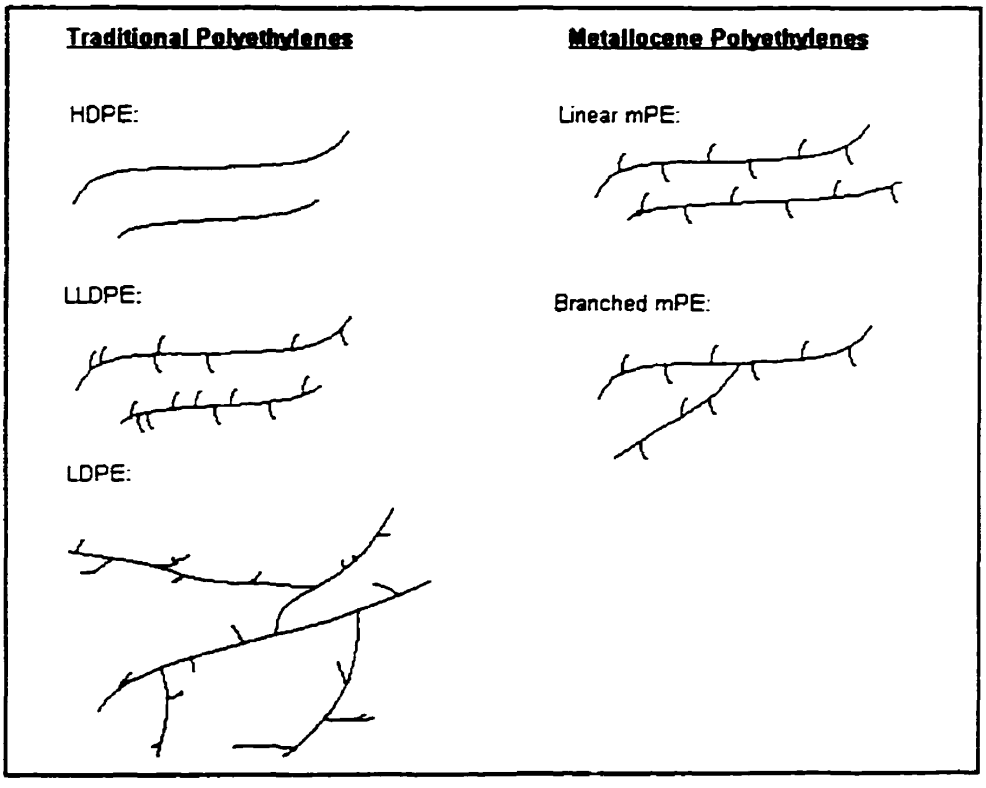

Figure 1.2 Schematic of Molecular Structures of Different Polyethylenes

1.3 Rheological Behavior of mPEs – A Review of the Current Literature

There has been considerable interest in mPE because of its superior physical properties, but, as mentioned in the previous section, many linear mPEs are difficult to process. Figure 1.3 compares qualitatively the processability of various types of polyethylene[6]. In an effort to understand the processing behavior of mPE a number of rheological studies have been performed with these materials. These studies are summarized in this section.

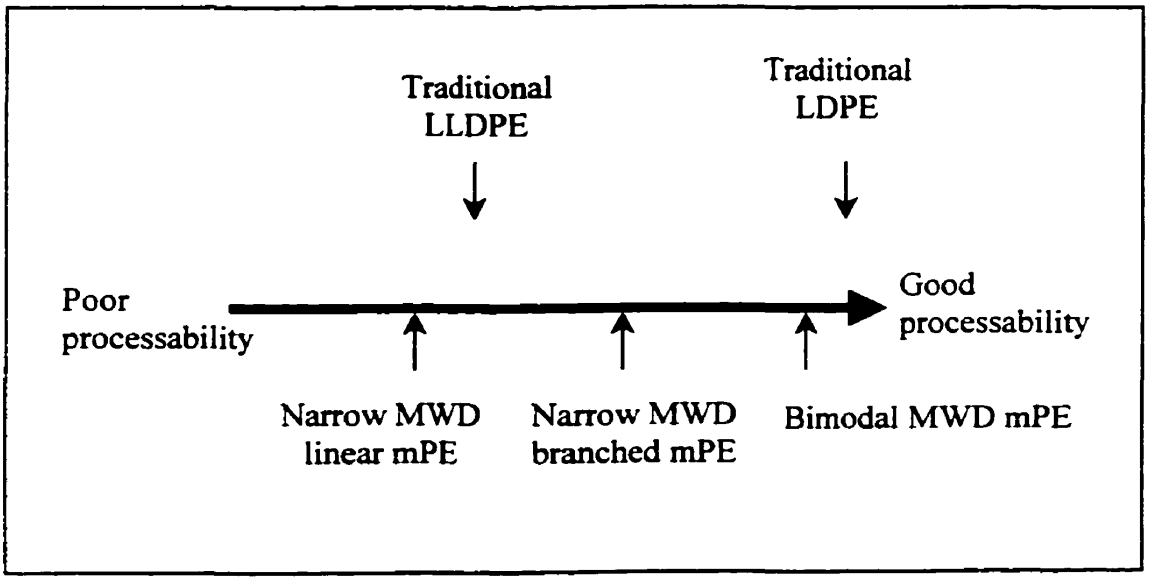

Figure 1.3 Comparing the Processability of Traditional and Metallocene Polyethylenes (Reference 6)

Lai and coworkers[5] compared the shear rheology of linear and branched mPEs. They found that the viscosity curves of all linear mPEs (with $M_W/M_N \approx 2$) could be described by a master curve using the Cross Equation (Equation 1.1).

$$\frac{\eta}{\eta_o} = \frac{1}{1+(\dot{\gamma}\tau_o)^m} \qquad [1.1]$$

$$\eta_o = 3.65 \times 10^6 \tau_o \qquad [1.2]$$

where η_o (Poise) and τ_o (s) result from nonlinear regression fits of the Cross Equation to experimental viscosity data. They also found that branched mPEs do not follow the master curve and that branched mPEs exhibit more shear thinning. The authors used the master curve for the linear mPEs as the basis of a method to quantify the effect of LCB on viscosity. They defined a parameter parameter, the Dow Rheology Index (DRI), that is zero for linear mPEs and increases as the degree of LCB increases. The determination of the DRI is described in Section 9.1.

Kim and coworkers[3] studied a number of traditional and metallocene polyethylenes and compared their shear and temperature sensitivities. They observed increased shear thinning behavior with level of LCB. They also found that mPEs are thermo-rheologically simple over the temperature range 170°C to 250°C, in that the Arrhenius Equation (shown below) can describe the effect of temperature on the viscosity.

$$\frac{\eta(T)}{\eta(T_o)} = \exp\left[\frac{E_a}{R}\left(\frac{1}{T} - \frac{1}{T_o}\right)\right] \qquad [1.3]$$

In Equation 1.3, E_a is the flow activation energy, which is independent of temperature. The authors found that branched mPEs have much higher activation energies than linear mPEs. This means that branched mPEs are much more sensitive to temperature than linear mPEs. They also found that for the materials they studied the activation energy of linear mPEs is not affected by short chain branch length (i.e. type of comonomer).

Recently Vega and coworkers have compared rheological properties of some traditional and metallocene polyethylenes[7,8]. They studied various commercial HDPE and LLDPE grades and some specially prepared mPEs. In their first publication they

present some anomalous results[7]. They found that the zero shear viscosity of the mPEs did not follow the same dependence on M_w as the traditional polyethylenes. The traditional PEs followed Equation 1.4 using the coefficients determined earlier by Raju and coworkers[9]. In this equation η_o has units of Pa.s.

$$\eta_o(190°C) = 3.4 \times 10^{-15} (M_w)^{3.6} \qquad [1.4]$$

However, they reported that the mPEs had higher zero shear viscosities than those calculated using Equation 1.4. According to their results for the mPEs, the exponent in Equation 1.4 was 4.2. They also found that in the temperature range of 140 to 210°C the effect of temperature on the dynamic LVE data could be described by the Arrhenius Equation (Equation 1.3) for both the traditional PEs and the mPEs. However, they found that the mPEs had significantly higher activation energies than the traditional PEs. Furthermore, they found that the relaxation spectra for the mPEs were significantly higher at longer relaxation times than the spectra for the traditional polyethylenes. Unable to explain these unusual results, the authors hypothesized that they were due to the absence of short chain branches in the mPEs.

Shortly after the first publication of Vega and coworkers[7], Carella[10] suggested that the unusual observations for the mPEs were due to the presence of low levels of LCB. In particular, increased zero shear viscosity, larger exponent for dependence on M_W (weight average molecular weight), higher values of the relaxation spectrum at long times, and higher activation energy for flow were cited as characteristic of LCB.

Vega and coworkers then published additional data following the same trend as in their 1996 results, which they now attribute to low levels of LCB[8]. They also defined a LCB index that can be calculated from flow activation energy. It is important to note that the presence of LCB in their original samples was not supported by their carbon-13 NMR measurements (an analytical technique for detecting branching described in Section 2.2). It is unlikely that LCB were formed during the polymerization process that the authors

the presence of LCB in their original samples was not supported by their carbon-13 NMR measurements (an analytical technique for detecting branching described in Section 2.2). It is unlikely that LCB were formed during the polymerization process that the authors described and two other explanations for the rheological behavior observed by Vega and coworkers are: incomplete removal of co-catalyst residues, and/or cross-linking during sample molding or LVE measurement. Further work must be done to resolve this issue.

In 1997 Wasserman presented a technique for evaluating the processabilty of mPEs using dynamic LVE data[11]. The author defines the RSI (relaxation spectrum index) that is a measure of the breadth of the relaxation spectrum (Equation 1.5).

$$RSI = \frac{\lambda_{II}}{\lambda_{I}}$$

$$\text{where:} \qquad [1.5]$$

$$\lambda_{I} = \frac{\sum g_i}{\sum g_i/\lambda_i} \qquad \lambda_{II} = \frac{\sum g_i \lambda_i}{\sum g_i}$$

Higher values of the RSI correspond to better processing behavior. The author presents results for two sets of mPEs. The first set, known as "High Performance mLLDPE", has RSI values ranging from 1.5 to 7. The second set, "Easy Processing mLLDPE", has RSI values in the range of 2 to 65. The author attributes the higher RSIs in the second set to differences in molecular structure but does not describe these differences.

Koopmans[12] compared the linear viscoelastic behavior of four polyethylenes, including an LDPE, an LLDPE and two branched mPEs. All four resins had approximately the same melt index (MI) and density. The author found that the complex viscosity of the LLDPE was significantly different from those of the other three resins (which were all very similar). In particular, he found that the branched materials had higher zero shear viscosities and exhibited more shear thinning than the linear material. The author also noted that there is a significant difference between the loss angles of the

branched materials and those of the linear materials. Thus the branched mPEs exhibited linear viscoelastic behavior that was closer to that of an LDPE than an LLDPE.

Very few extensional flow data have been published for mPEs[12,13]. Ramanathan and coworkers[13] used flow visualization experiments to compare the behavior of an LLDPE, a linear mPE and five branched mPEs in a 4:1 abrupt contraction. They found that for extension rates between 1 and 10 s^{-1}, extension thinning increases as the degree of LCB increases. The linear materials did not exhibit extension thinning in the range of rates studied. Koopmans performed uniaxial extension experiments at extension rates below 1 s^{-1} using the extensional rheometer described in Chapter 7 for the resins discussed in the preceding paragraph. He found that the LLDPE exhibited essentially no strain hardening behavior, which is defined as an increase in the tensile stress growth coefficient over the linear viscoelastic response, whereas the branched materials (LDPE and two mPEs) exhibited strain hardening at all the extension rates studied. The strain hardening behavior of all three branched materials was qualitatively and quantitatively similar, leading to the conclusion that at low extension rates, the branched mPEs act more like LDPEs than LLDPEs.

List of References

[1] Schwank, Don, *Single-site metallocene catalysts yield tailor-made polyolefin resins*, Modern Plastics, August (1993), p. 49-50

[2] Lai, S.Y. *et al*, United States Patent, 5 272 236, 1993

[3] Kim, Y.S., *et al*, J. Appl. Polym. Sci., Vol. 59, 125-137 (1996)

[4] Lai, S. and G.W. Knight, SPE-ANTEC, 1188-1192 (1993)

[5] Lai, S. *et al*, SPE-ANTEC, 1814-1815 (1994)

[6] Colvin, R., *Modern Plastics*, 62-67, May (1997)

[7] Vega, J.F., *et al, Macromolecules*, Vol. 29, No. 3, 960-965 (1996)

[8] Vega, J.F., *et al, Macromolecules*, Vol. 31, No. 11, 3639-3647 (1998)

[9] Raju, V.R., *et al, J. Polym. Sci., Polym. Phys. Ed., 17, 1183-1195 (1979)*

[10] Carella, J.M., *Macromolecules*, 29, No. 25, 8280-8281 (1996)

[11] Wasserman, S.H., SPE-ANTEC, 43, 1129-1133 (1997)

[12] Koopmans, R.J., SPE ANTEC, 43, 1006-1006 (1997)

[13] Ramanathan, R. *et al*, SPE ANTEC, 41, 1073-1077 (1995)

Chapter 2

Background Information on Long Chain Branching

Long chain branching (LCB) is an important aspect of the molecular structure of mPEs. Its presence improves processability without adversely affecting the good physical properties of the final product. In the present work the rheological behavior of several mPEs, including both linear and branched materials, was studied. A summary of the current literature discussing the effect of LCB on rheology is presented in Section 2.1. The various rheological properties are defined in later chapters (e.g. linear viscoelastic properties are defined in *Chapter 5. Linear Viscoelasticity*). In Section 2.2 analytical techniques for quantifying LCB are described.

2.1 The Effect of LCB on Rheological Behavior

The presence of long chain branches can result in complex rheological behavior that cannot be explained simply by the additional molecular weight due to the branches. Furthermore, the degree, length, and structure of the branching all affect the rheological behavior in various ways. Studies of the effect of LCB on rheological behavior are further complicated by a variation in molecular weight distribution, since it is often impossible to control independently these two characteristics. Because of these complications and the fact that much work in this area has been based on comparing resins that are different in more than one aspect of molecular structure, we do not have a clear understanding of the effect of LCB on rheological behavior of commercial polyolefins. However, there has been a significant amount of work done with model polymers such as stars or combs (Figure 2.1), which have very narrow molecular weight distributions and uniform structures. Comprehensive summaries of these studies have been presented by Bersted[1] and by Gell and coworkers[2].

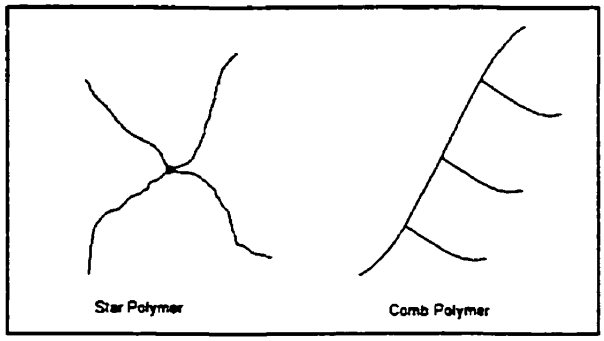

Figure 2.1 Schematic Diagram of Model Branched Polymers

Commercial, branched polymers are typically randomly branched, which means that the idea of a molecule consisting of a backbone with branches distributed along it is not useful, and it is very difficult to make meaningful comparisons among randomly branched materials. Studies of such materials involve either introducing controlled degrees of random LCB to make "model" polymers or the use of analytical methods to characterize the molecular structure of whole polymer systems, which are then compared. Both of these approaches are less than ideal and care must be taken when interpreting the results.

2.1.1 Zero Shear Viscosity

The dependence of the zero shear viscosity on degree of branching is not straightforward. For star polymers the zero shear viscosity of a branched material is generally lower than the zero shear viscosity of a linear material of the same molecular weight. However at molecular weights around 10^6 the zero shear viscosity of the star approaches and may even exceed that of a linear material of the same molecular weight[1]. The effect of LCB in star polymers below a certain critical molecular weight can be explained by the adjustment for molecular size using the g parameter, as shown below. Above this critical molecular weight, the zero shear viscosity of the star is higher than the zero shear viscosity of a linear material with the same molecular size (gM_W).

$$\eta_o = k(gM_w)^{\alpha} \qquad [2.1]$$

In this equation **g** is the ratio of the mean squared radius of gyration of the branched molecule to that of a linear molecule with the same molecular weight and **k** and α are constants. For linear materials **g** is, by definition 1 and it is less than 1 for branched materials. For regular stars **g** is given by Equation 2.2

$$g = \frac{3f - 2}{f^2} \qquad [2.2]$$

where f is the number of arms. Above the critical molecular weight, when Equation 2.1 fails, the zero shear viscosity is described by Equation 2.3, where Γ is the viscosity enhancement factor which can be estimated with Equation 2.4.

$$\eta_o = k(gM_w)^{\alpha}\Gamma \qquad [2.3]$$

$$\Gamma \equiv K_b \exp\left(\frac{M_{arm}}{M_e}\right) \qquad [2.4]$$

In Equation 2.4, M_e is the molecular weight between entanglements. Depending on the values of **g** and Γ the zero shear viscosity of a branched material can be either higher or lower than the zero shear viscosity of a linear material at the same molecular weight. Therefore, when studying the effect of LCB on the rheological behavior, it is necessary to compare materials of similar molecular size (gM_w) rather than similar molecular weight.

Graessley and coworkers[3] studied a series of solutions of star branched polyisoprenes with various molecular weights. Their results for 4 arm stars are shown in Figure 2.2. Viscosity enhancement clearly occurs for the branched materials at the higher molecular sizes, whereas at the lower molecular sizes the data for the linear and branched materials superpose.

Raju and coworkers demonstrated the effect of branch or arm molecular weight, M_a, on the viscosity enhancement of symmetric stars[4] of hydrogenated polybutadiene. The exponential relationship of Equation 2.4 was found to describe accurately the dependence of viscosity enhancement on branch molecular weight (Figure 2.3).

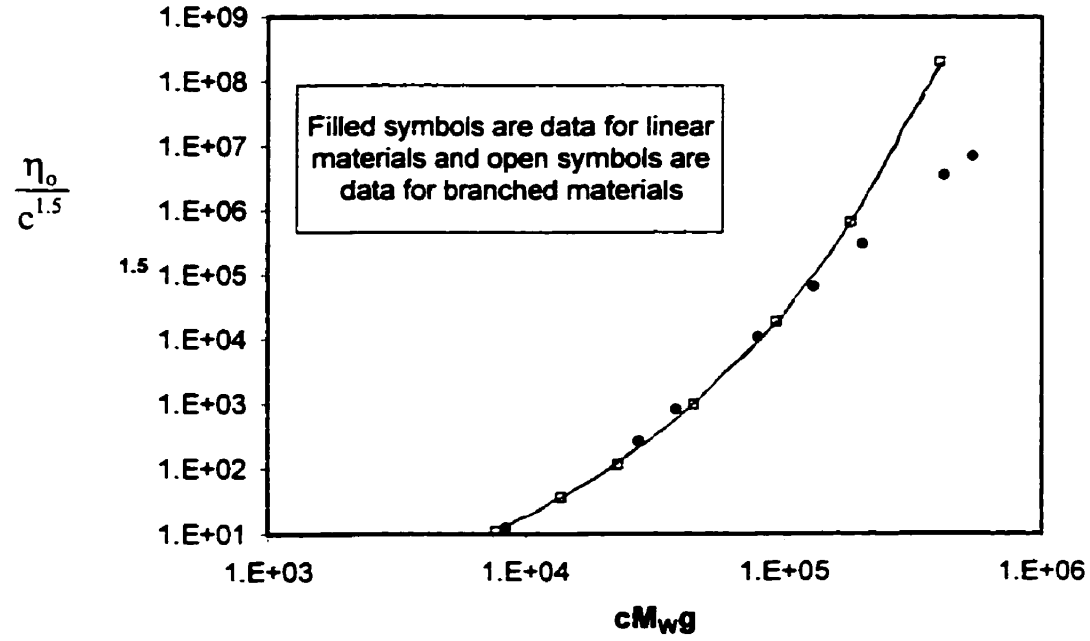

Figure 2.2 The Relationship between Zero Shear Viscosity and Molecular Size for Solutions of 4 Arm Polyisoprene Stars
(Data taken from Ref. 3, units of viscosity are Poise, units of concentration are g/cm^3)

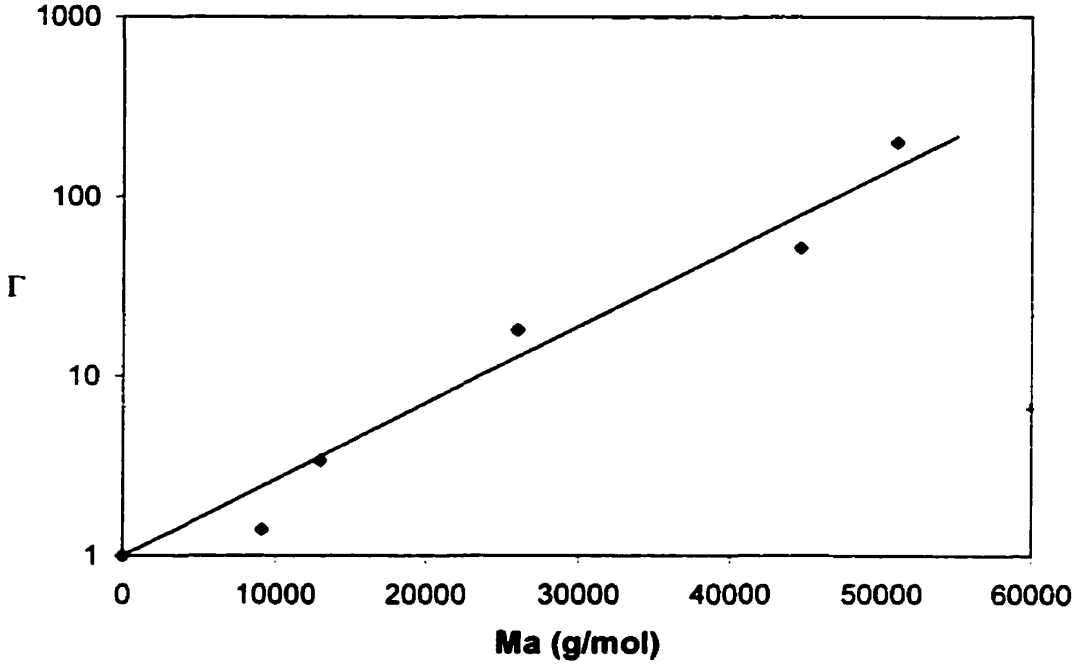

Figure 2.3. The Effect of Arm Molecular Weight on the Viscosity Enhancement of Symmetric Star Polymers
(Data taken from Reference 4)

More recently, Gell and coworkers[2] studied a series of asymmetric 3 arm star polymers to evaluate the effect of branch length on the rheological behavior. The molecular characteristics of these Poly(ethylene-*alt*-propylene)s or PEPs are given in Table 2.1. The dependence of the zero shear viscosity on molecular size is shown in Figure 2.4. For the asymmetric stars, **g** was calculated as for symmetric stars, *i.e.* for all stars **g** was assigned a value of 0.78. The relationship between η_o (at 100°C, Poise) and M_w for linear PEPs is given by Equation 2.5. Using the data for S42, the symmetric star, the parameter K_b in Equation 2.4 was calculated. Using the experimental value for K_b and Equations 2.3 through 2.5, we arrive at Equation 2.6, which describes the relationship between η_o (at 100°C, Poise) and molecular weight for 3 arm symmetric PEP stars.

$$\eta_o = 6 \times 10^{-13} M_w^{3.46} \qquad [2.5]$$

$$\eta_o = 3.2\times10^{-19} M_w^{3.46}\left[\exp\left(\frac{M_w}{6900}\right)\right] \qquad [2.6]$$

From Figure 2.4 we see that an asymmetric star polymer exhibits a higher η_o than a linear material of the same molecular size. Also, an asymmetric star polymer has a higher η_o than a symmetric star of the same molecular size. If we define the viscosity enhancement of an asymmetric star with respect to a symmetric star of the same molecular size as in Equation 2.7 (η_o in Poise), we can evaluate the effect of branch length on zero shear viscosity, as in Figure 2.5. In Figure 2.5 M_b is the molecular weight of the branch and M_{bb} is molecular weight of the backbone. At the shorter branch lengths we see an increase in Γ_{asym} as branch length increases. As the branch length approaches ½ M_{bb}, Γ_{asym} must become 1, indicating that there is a maximum in the Γ_{asym} vs. branch length function.

$$\Gamma_{asym} \equiv \frac{\eta_o}{3.2\times10^{-19} M_w^{3.46}\left[\exp\left(\frac{M_w}{6900}\right)\right]} \qquad [2.7]$$

Table 2.1 Poly(ethylene-*alt*-propylene) Star Polymers from Reference 2

Sample	$M_{backbone}$	M_{branch}
S00	88 000	0
S01	90 000	1 100
S06	96 000	5 500
S17	80 000	17 000
S42	84 000	42 000

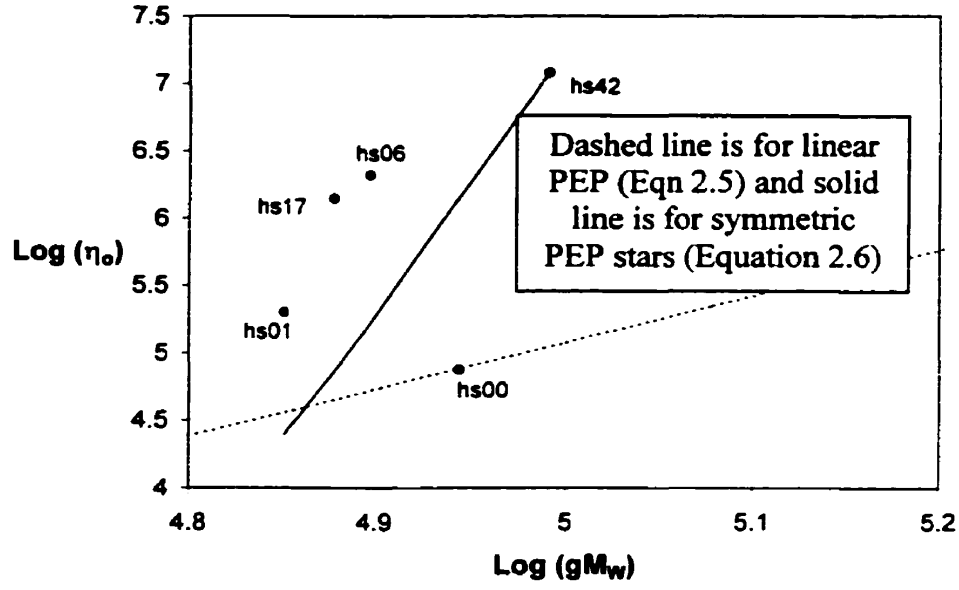

Figure 2.4 The Relationship between Zero Shear Viscosity (Poise) and Molecular Size for Asymmetric Star Polymers (100°C)
(Data taken from Reference 2)

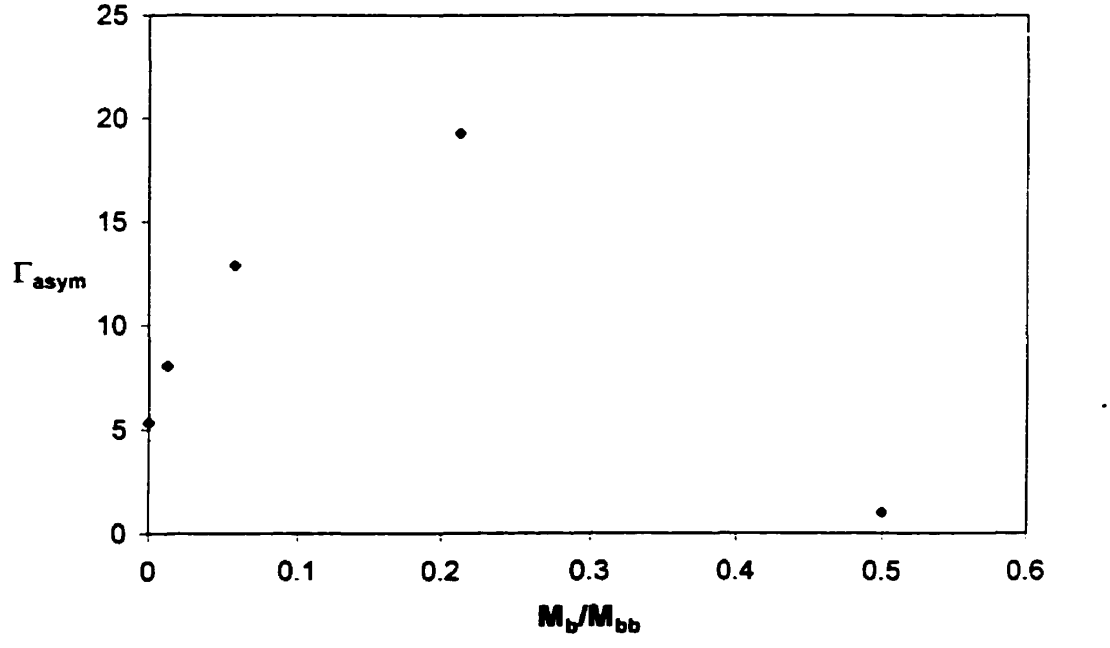

Figure 2.5 The Effect of Branch Length on the Viscosity Enhancement of Asymmetric Star Polymers with respect to Symmetric Stars of the same gM_W
(Data taken from Reference 2)

Comb and H-branched polymers also exhibit viscosity enhancement when compared to linear materials of equivalent molecular size. For these materials the degree of enhancement is typically much higher than with star polymers of the same molecular size[1].

Randomly branched polymers present a much more complicated situation, and for such polymers with very low levels of LCB not all of the molecules are branched. Such systems have been modeled as mixtures of linear and branched materials. Bersted and coworkers[5] have shown that the zero shear viscosities of such materials can be described by Equation 2.8. Therefore, as shown by Equation 2.8, for low levels of LCB the zero shear viscosity increases as LCB increases.

$$\eta_{o,\,mixture} = \left(\eta_{o,\,linear}\right)^{w_L}\left(\eta_{o,\,branched}\right)^{w_B} \qquad [2.8]$$
$$\text{where } w_B = 1 - w_L$$

At higher levels of LCB the dependence of the zero shear viscosity on molecular size can be described by Equation 2.1 but with a much higher value of α than is found for linear materials. The values for the parameters in Equation 2.1 found for linear polyethylenes[6] and for highly branched polyethylenes (LDPE)[7] at 190°C are given in Table 2.2. The relationships between zero shear viscosity and molecular size for linear and branched polyethylenes are compared in Figure 2.6.

Table 2.2 Parameters for Equation 2.1 for Linear and Branched PE at 190°C (η_o in Pa.s)

Structure	Log k	α
Linear	-14.47	3.6
Branched	-49.79	11.4

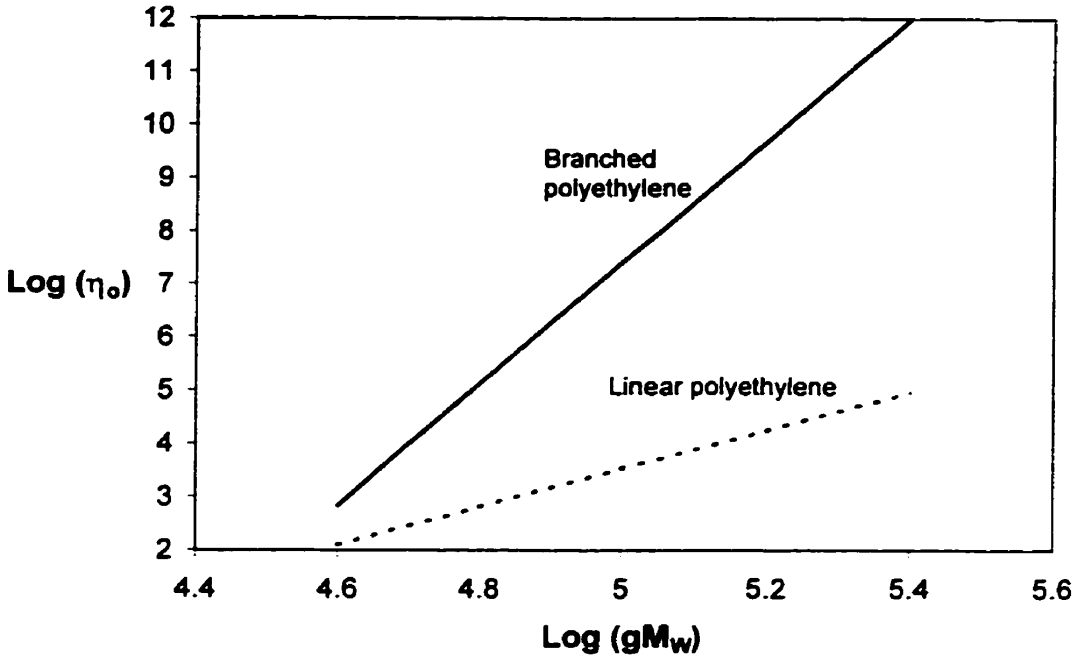

Figure 2.6 Relationship between Zero Shear Viscosity (Pa.s) and Molecular Size for Linear and Branched Polyethylenes

For high levels of LCB, an increase in LCB at constant M_w typically causes a decrease in the zero shear viscosity. Since, as was discussed earlier, at very low levels of LCB the zero shear viscosity increases with LCB, there is a maximum in the η_o vs. LCB function. According to the results of Constantin[8] and Bersted[7], this maximum should occur at approximately 2.4 LCB/10^4 C at a molecular weight of 120 000.

2.1.2 Thermorheological Behavior

For linear polymers, the temperature dependence of rheological behavior can be described by a single shift factor a_T.

$$\eta_0(T) = a_T \eta_o(T_o) \qquad [2.9]$$

In Equation 2.9, T_o is the reference temperature. Materials that exhibit this behavior are said to be thermorheologically simple, because simple shifts along the frequency axis will

result in superposition of dynamic moduli data for various temperatures. For some branched polymers however the effect of temperature cannot be explained by a simple shift along the frequency axis[1]. In these cases a different shift factor is needed at each frequency. Raju and coworkers[4] found that for star-branched hydrogenated polybutadiene the shift factor varied as a function of frequency. At high frequencies, the shift factor required for superposition is approximately equal to the shift fact for linear polybutadiene, while at low frequencies it is higher. This can be explained by the greater temperature sensitivity of the long relaxation times due to the LCB. The authors demonstrated that the maximum apparent activation energy (which occurs at low frequency) increased linearly with branch length (Figure 2.7). Thermorheological complexity was also demonstrated for stars of poly(ethylene-*alt*-propylene) and of high vinyl polybutadiene[9]. Previous research has shown that stars of polystyrene[10] and polybutadiene[11] can be thermorheologically simple. In contrast with the results of Carella and cowrokers[9], Gell and coworkers[2] found that 3 arm poly(ethylene-*alt*-propylene) stars were thermorheologically simple. Gell and coworkers also found that temperature sensitivity increased with degree of LCB. Kasehagen[30] measured rheological properties of long chain randomly branched polybutadiene and found no correlation between branching content and activation energy.

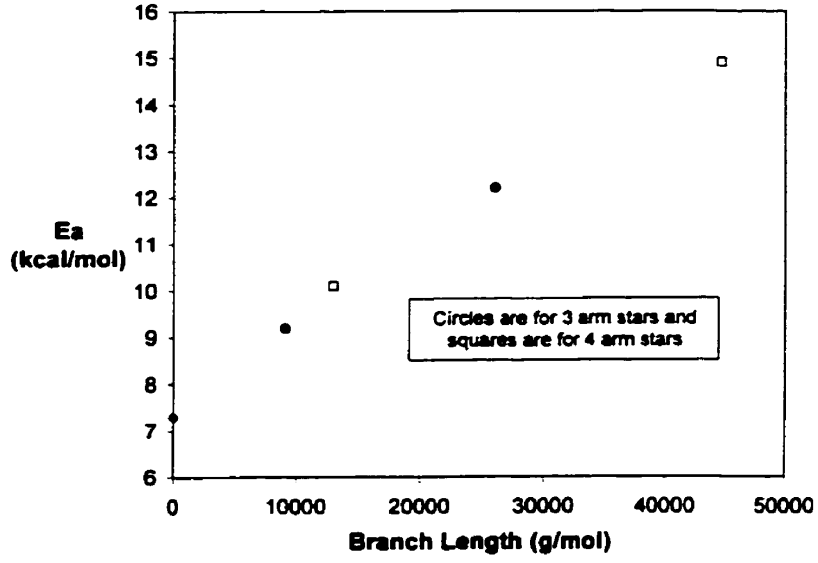

Figure 2.7 Relationship between Branch Length and Maximum Apparent Activation Energy for Stars of Hydrogenated Polybutadiene (Ref. 4)

Bersted examined the effect of low levels of LCB on the temperature sensitivity of polyethylene[7] by measuring the effective activation energy corresponding to a frequency range of 1 to 10 rad/s over a temperature range of 150°C to 190°C. He did not address the issue of thermorheological complexity. He studied 3 sets of branched PEs. The first set consisted of an HDPE resin that had been exposed to increasing amounts of peroxide, resulting in tetra-functional branches. The second set consisted of several HDPEs that were subjected to various thermal and mechanical histories to induce LCB. The final set consisted of 4 commercial, low-density polyethylenes. The results of this study are shown in Figure 2.8. The author concluded that the samples with the peroxide induced branches exhibited a stronger dependence of E_a on the degree of LCB. It seems likely, however, that the difference between the peroxide samples and the thermal degradation samples is not significant. At low levels of LCB, E_a follows a linear relationship with degree of LCB, and at very high levels of LCB it becomes independent of degree of LCB.

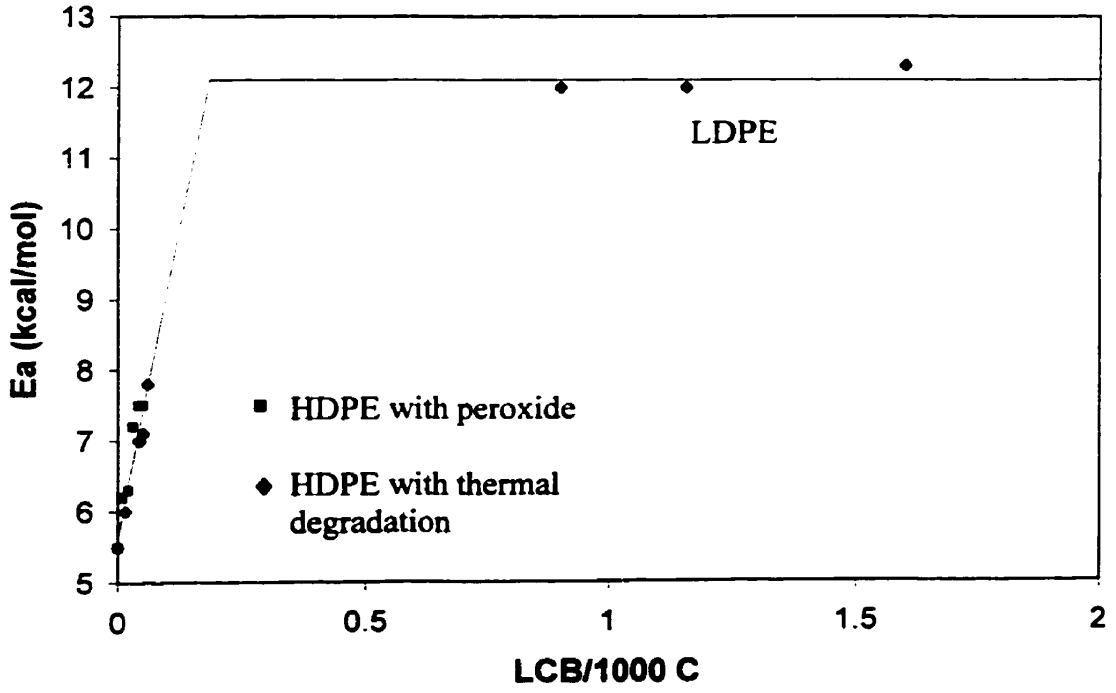

Figure 2.8 The Effect of Degree of Long Chain Branching on the Apparent Activation Energy of Polyethylene (1 to 10 rad/s, 150 to 190°C)
(Data taken from Reference 7)

2.1.3 Linear Viscoelasticity

Long chain branching also significantly affects linear viscoelastic behavior. In particular, LCB increases elasticity in the linear regime, *i.e.* it extends the relaxation spectrum to much longer relaxation times. In the case of star polymers the terminal to plateau transition is broadened with respect to the behavior of a linear material. Gell and coworkers[2] found that the broadening of this transition zone increased as branch length increased for asymmetric stars (described in Table 2.1). Some linear viscoelastic data for these materials are presented in Figures 2.9 through 2.12. For the material with the shortest branch (S01), the authors found that the shape of the modulus curve differed little from that of the linear material. The next material in the sequence, S06, exhibited two maxima in the loss modulus curve. The first occurred at a low frequency and was due to the relaxation of the large-scale conformation, and the high frequency maximum was attributed to the relaxation of the branch. As the branch length increased from this point, the loss modulus response became a single very broad peak, which is characteristic of symmetric stars. In Figures 2.9 and 2.10 the loss and storage moduli of the linear material and two of the branched materials (S06 and S42) are compared. The effect of branch length on the loss angle is shown in Figure 2.11. The shape of the loss angle curve of the material with the shortest branch is very similar to that of the linear material. However, there is a significant difference at longer branch lengths. For resins S06 and S42, we see a plateau in the loss angle that is not present in the data for S01 and S00. A plateau in the loss angles indicates that the loss and storage moduli curves are parallel. Hingmann and Marczinke[12] noted the same effect of LCB on the dynamic moduli of polypropylene.

The complex viscosity curves of the star polymers are compared in Figure 2.11. Since the effect of molecular size on the complex viscosity is confounded with the effect of branch length (see Section 2.1.1) the differences between the curves in Figure 2.12 cannot be attributed solely to branch length. The effect of branch length on recoverable compliance is shown in Figure 2.13. This parameter is independent of molecular weight,

and the differences between the recoverable compliances of the series of stars of PEP can therefore be attributed to branch length. The recoverable compliance, which is a measure of elasticity in the linear regime, increases with branch length and approaches a maximum as the molecule becomes symmetric.

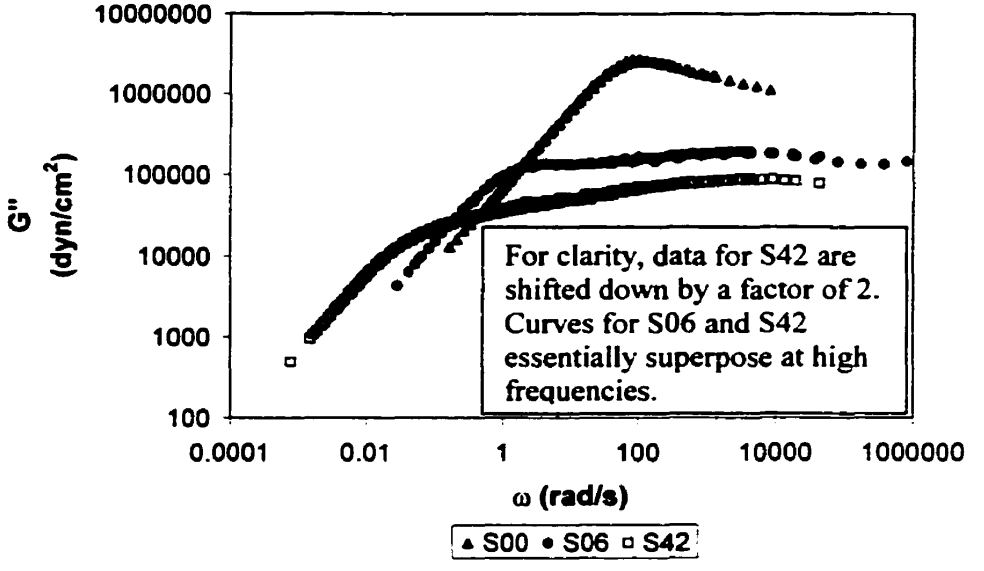

Figure 2.9 Effect of Branch Length on Loss Modulus of Stars of PEP
(Data from Reference 2, Samples are described in Table 2.1)

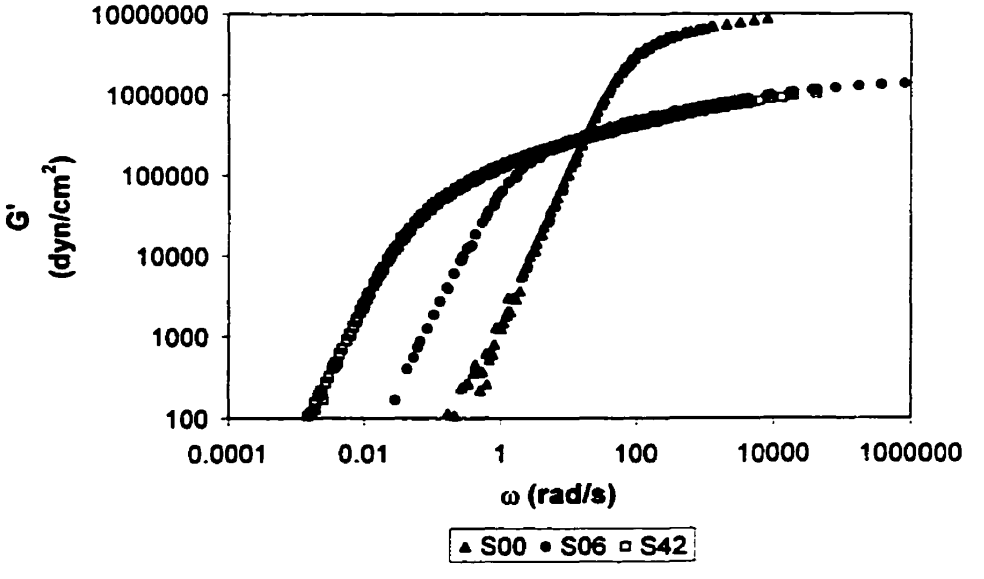

Figure 2.10 Effect of Branch Length on Storage Modulus of Stars of PEP
(Data from Reference 2, Samples are described in Table 2.1)

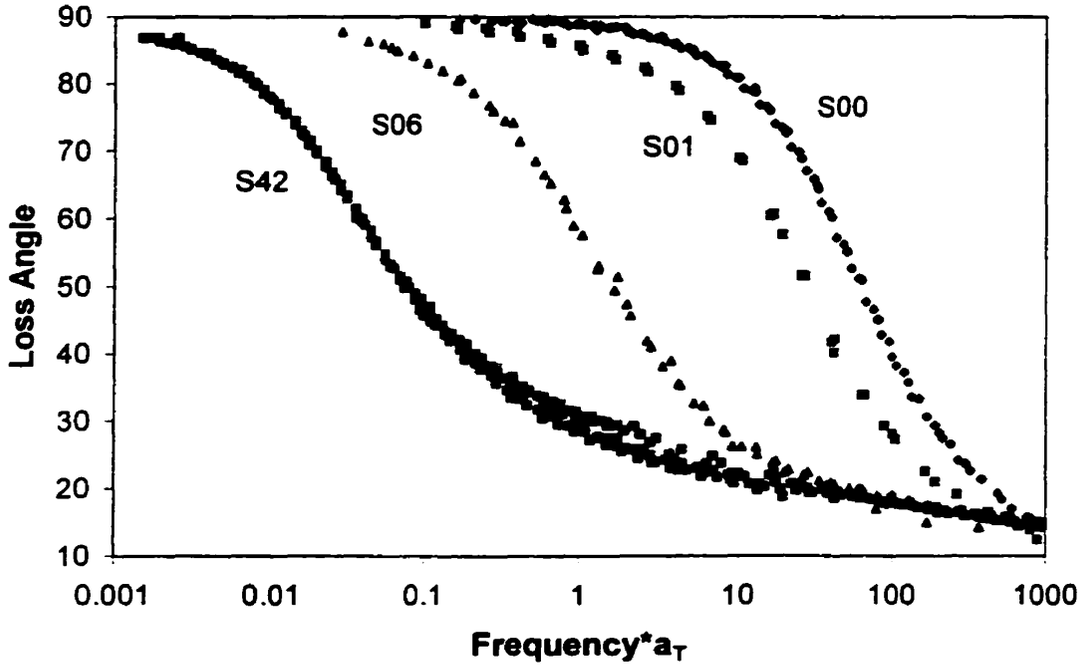

Figure 2.11 Effect of Branch Length on Loss Angle of Stars of PEP
(Data from Reference 2, Samples are described in Table 2.1)

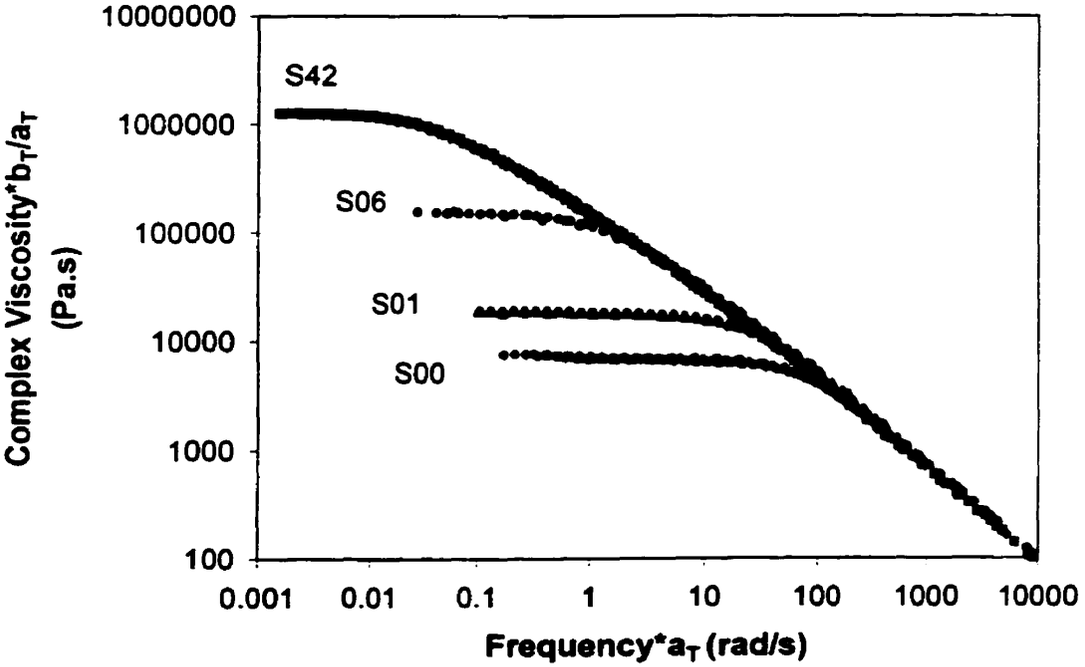

Figure 2.12 Complex Viscosity Curves of a Series of Asymmetric Stars of PEP
(Data from Reference 2, Samples are described in Table 2.1)

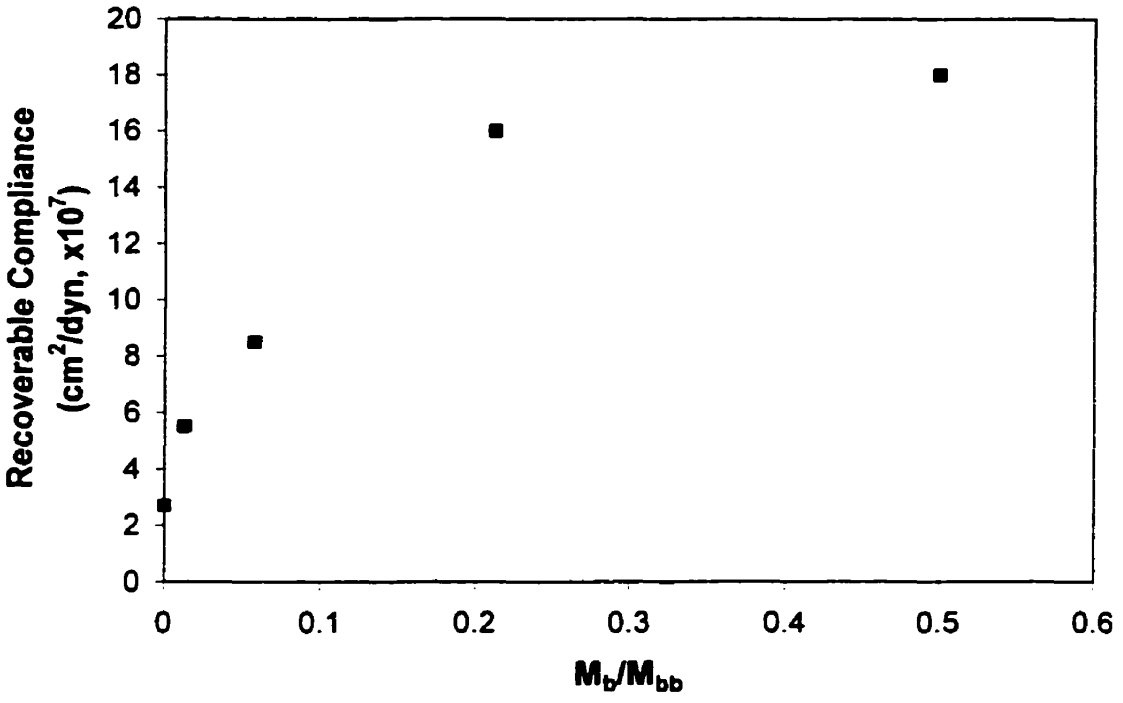

Figure 2.13 Effect of Branch Length on Recoverable Compliance of Stars of PEP
(Data from Reference 2)

Linear viscoelastic behavior is strongly affected by both MWD and LCB. Therefore, looking at the effect of LCB on the LVE behavior of randomly branched materials is difficult, since polydispersity cannot usually be controlled independently from LCB for these materials. The effect of MWD on the recoverable compliance of linear polymers can be approximated by Equation 2.10.

$$J_s^0 = \left(J_s^0\right)_{monodisperse} \frac{\overline{M}_{Z+1}\overline{M}_Z}{\left(\overline{M}_w\right)^2} \qquad [2.10]$$

Pederson and Ram[13] found that the recoverable compliance of highly branched polyethylenes could be described by a relation analogous to Equation 2.10 with **M** replaced by **gM** (Figure 2.14).

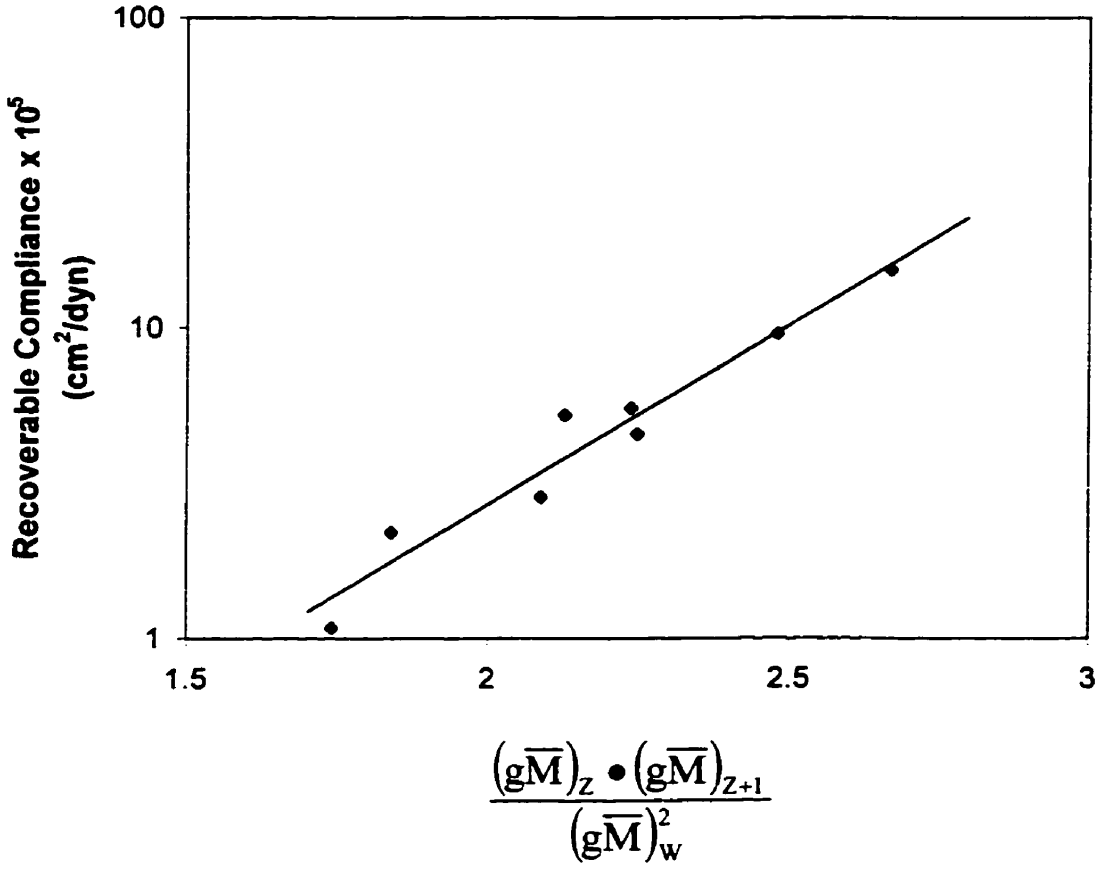

Figure 2.14 Relationship between MWD and Recoverable Compliance for Highly Branched Polyethylenes with Varying Degrees of LCB (190°C)
(Data taken from Reference 13)

2.1.4 Nonlinear Viscoelasticity in Shear

Because of experimental difficulties in making nonlinear viscoelastic measurements and in producing large amounts of model polymers, little work has been done in the area of the relationship between LCB and nonlinear viscoelasticity. Generally, the easiest nonlinear behavior to study is the shear rate dependence of viscosity, and several studies of this type will be discussed later in this section. Several techniques have been employed to determine the effect of LCB on the damping function, often with conflicting results.

2.1.4.1 Shear Rate Dependence of Viscosity

For randomly branched materials at low levels of LCB, LCB increases shear sensitivity. Bersted and coworkers[5] showed that for blends of linear HDPE and highly branched LDPE the viscosity could be described by the logarithmic blending rule (Equation 2.8) at all rates. Later Bersted and coworkers[7] demonstrated that low levels of LCB introduced in HDPE by thermal or mechanical degradation resulted in more shear thinning behavior. Therefore, even though a branched material has a higher zero shear viscosity than a linear material of the same molecular weight, at high rates the viscosity can be lower.

For highly branched LDPE, shear thinning behavior does not necessarily correlate with degree of LCB. Laun and Schuch[14] presented data for two LDPE melts that had similar zero shear viscosities but slightly different degrees of LCB. They found that the material with the higher degree of LCB exhibited less shear thinning than did the material with less LCB. Also, when comparing two LDPE resins having very different degrees of LCB, they found that the more highly branched resin displayed less shear sensitivity, even though its MWD was much broader.

2.1.4.2 Nonlinear Relaxation Modulus

Osaki and coworkers[15] studied the rheological behavior of solutions of 4-arm star branched and linear polystyrenes. They performed step strain experiments in a cone and plate rheometer to determine the nonlinear relaxation modulus. They found that the characteristic time, which is the time at which the relaxation moduli at various strains can be superposed by a vertical shift, increased with branch length for stars of polystyrene. They also found that the damping function, $h(\gamma)$, was independent of branch length for the stars. However, they did find that the damping function for the stars was different that for the linear polystyrenes. In particular, $h(\gamma)$ fell below 1 at smaller strains for the branched materials than for the linear materials. Also, the branched materials exhibited more damping at all strains than did the linear materials. The damping function for the

branched materials was in agreement with the prediction of the Doi-Edwards theory with the independent alignment assumption, which is approximated by Equation 2.11. The data for the linear polystyrenes could be described by a damping function of the same form as Equation 2.11 but with a coefficient on the order of 0.14 in place of 0.2.

$$h(\gamma) = \frac{1}{1 + 0.2\gamma^2} \qquad [2.11]$$

The results of Osaki and coworkers, described above, are in contradiction with results seen by Archer and Varshney[16] and Macosko and Kasehagen[17]. Archer and Varshney studied the relaxation behavior of multi-arm polybutadiene melts (of the general form A_3AA_3) in step strain experiments. The authors found that linear polybutadiene had a damping function that was more strain dependent than that of the branched materials. In fact, the damping function of the linear material was in quite good agreement with the Doi-Edwards theory with the independent alignment assumption. Macosko and Kasehagen[17] also studied branched polybutadienes. They determined the linear relaxation modulus and the damping function by fitting Wagner's constitutive equation to the results of start-up of steady simple shear experiments. The Wagner constitutive equation in shear, together with the damping function used by Macosko and Kasehagen, is given below.

$$\sigma = \int_{-\infty}^{t} m(t - t')\left(\frac{1}{1 + a\gamma^2}\right)\gamma dt' \qquad [2.12]$$

Macosko and Kasehagen found that for the linear material the fitted value **a** was 0.26 and the values for the branched materials decreased with degree of LCB down to 0.07 for the most highly branched material. Weaker damping for branched materials has also been observed when comparing LDPE with HDPE and LLDPE[18,19].

Yoshikawa and coworkers[20] compared the behavior of three HDPEs and their fractions. One of the HDPE resins had 1 LCB/10^4 C. Based on step strain experiments, they concluded that this level of LCB had no effect on the damping function.

2.1.5 Non-linear Viscoelasticity in Extension

Studying extensional flow behavior is even more difficult than studying nonlinear shear flow behavior and very few reliable data exist. Although various techniques for inferring extensional flow properties from non-homogeneous flows have been proposed, in this section only studies employing uniaxial extension will be discussed.

Over 30 years ago, Laun and Münstedt[21,22,23] demonstrated that shear flow properties are insufficient to describe behavior in extensional flows. For example, Laun and Münstedt[21,22,23] found that LDPE exhibited a maximum in the extensional viscosity curve, behavior often referred to as "strain hardening", which had no counterpart in shear. In a further study of the relationship between molecular structure and extensional flow behavior,[24] they studied several LDPE and HDPE melts with various polydispersities and degrees of LCB. In general, the authors found that both LCB and MWD affected extensional flow behavior, and they were unable to distinguish between these effects. They demonstrated that the height of the maximum in the extensional viscosity curve divided by $3\eta_0$ was related to degree of LCB for highly branched materials as shown in Figure 2.15. Increased degrees of LCB resulted in higher maxima in the extensional viscosity curve.

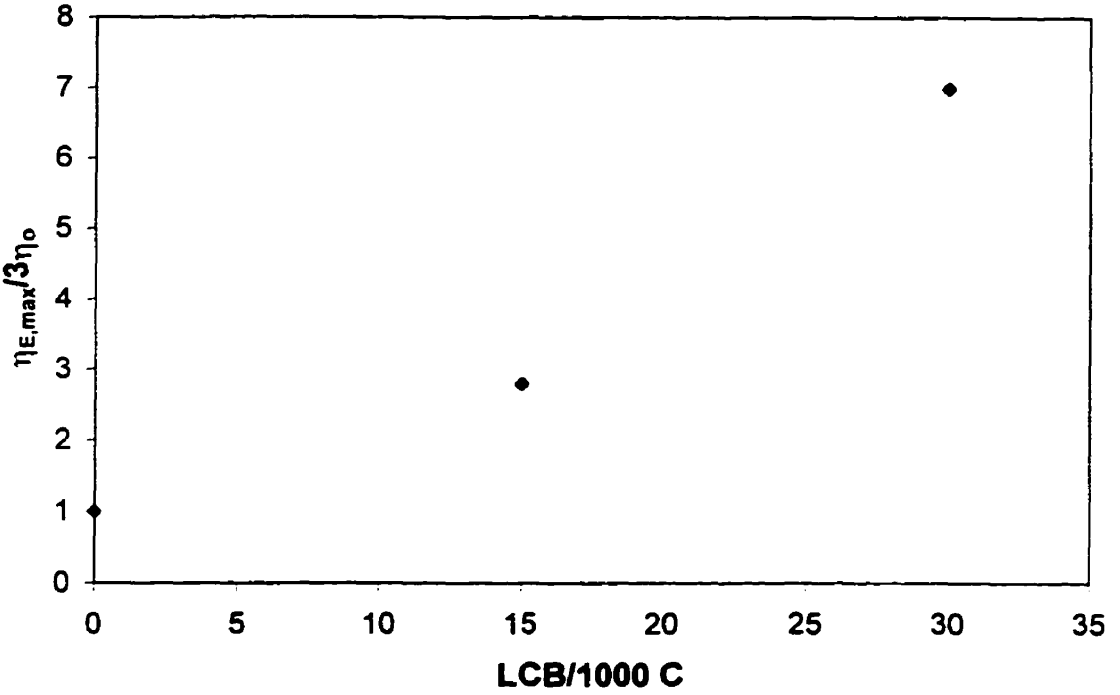

Figure 2.15. The Effect of LCB on the Maximum in the Extensional Viscosity of Polyethylene
(Data taken from Reference 24)

More recently, Laun and Schuch[14] found that MWD has very little effect on the maximum in the extensional viscosity curve. They concluded that some of the results for "HDPE" presented earlier, which had indicated that a maximum in the extensional viscosity curve could be caused by a very broad MWD, were in fact due to low levels of LCB introduced by thermal degradation.

Hingmann and Marczinke[12] studied three polypropylene melts with various degrees of LCB introduced by means of cross-linking agents. The degree of LCB was estimated from the concentration of cross-linking agent. They found that the branched materials exhibited a maximum in their extensional viscosity curves, while the linear material did not. The dependence of the height of this maximum on degree of LCB is shown in Figure 2.16. These results are in good qualitative agreement with those of Münstedt and Laun[24].

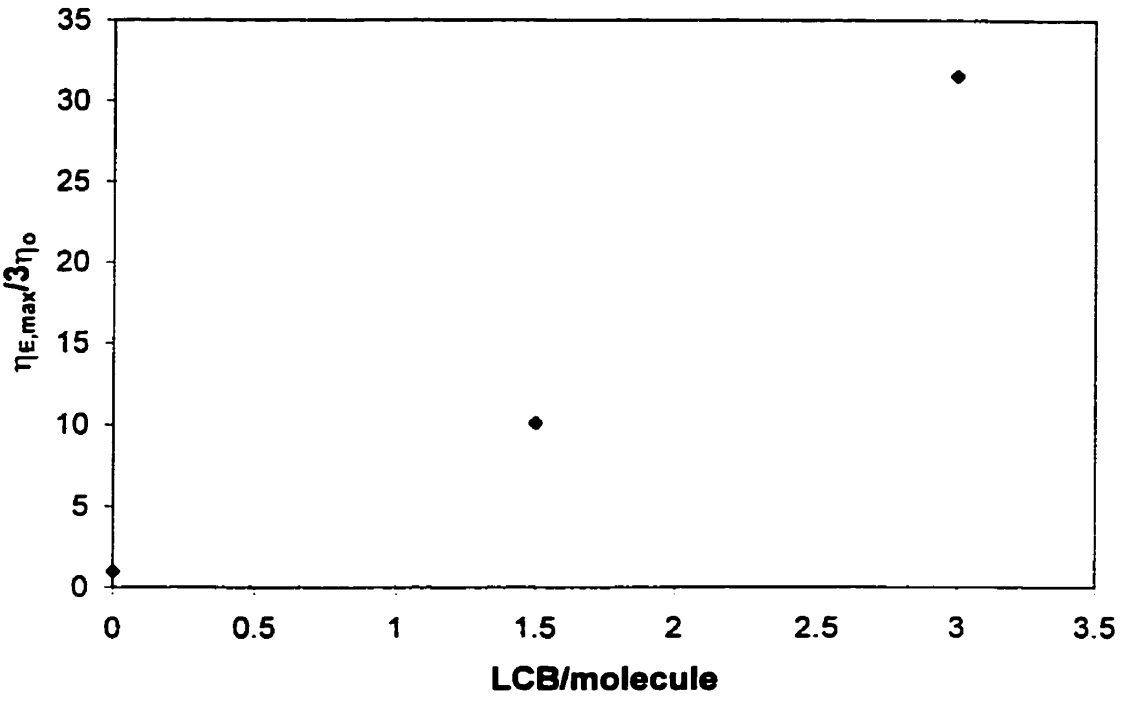

Figure 2.16 The Effect of LCB on the Maximum in Extensional Viscosity of Polypropylene
(Data taken from Reference 12)

Macosko and Kasehagen[17] studied the extensional flow behavior of linear and branched polybutadiene. As steady state was not achieved in their extensional experiments, they reported transient stress responses. To compare the strain hardening behavior of the various materials they used the ratio of $\eta_E^+(t)$ to $\eta^+(t)$ at a Hencky strain of 2. For a linear response this ratio is equal to 3, for strain hardening it is greater than 3, and for strain softening it is less than 3. The effect of degree of LCB on strain hardening is shown in Figure 2.17. Again we see that increased LCB results in increased strain hardening.

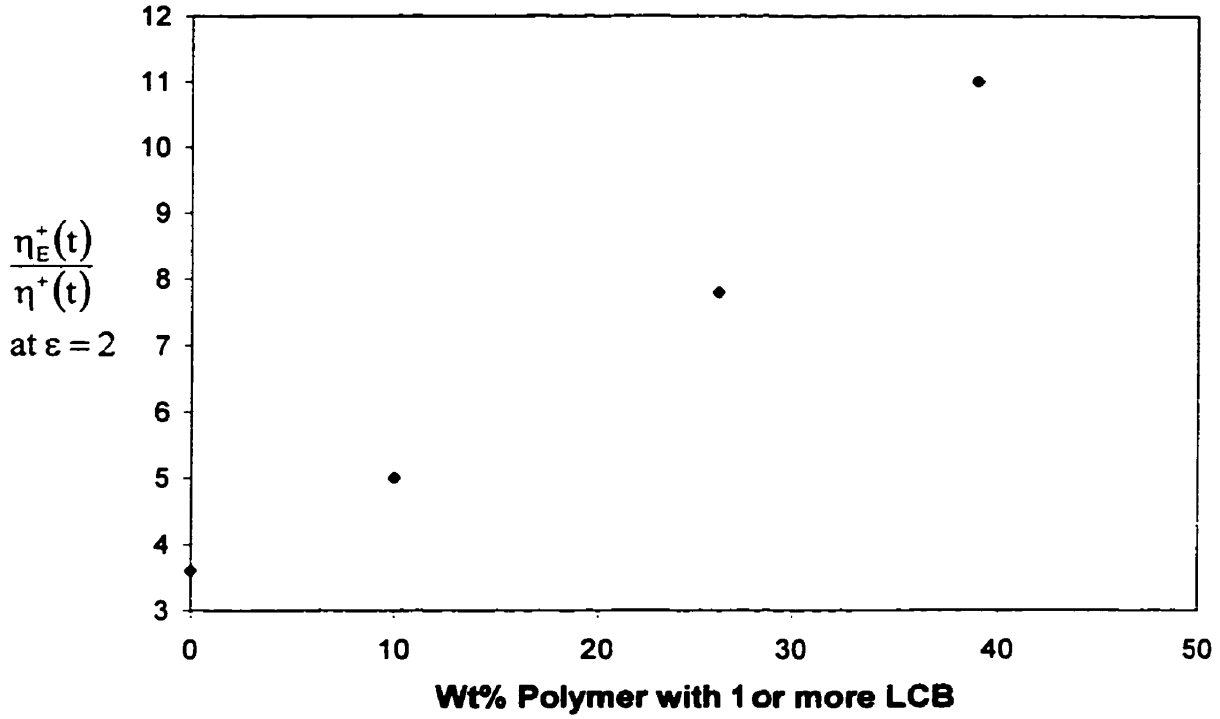

Figure 2.17 Effect of LCB on Strain Hardening Behavior of Polybutadiene
(Data taken from Reference 17)

2.2 Quantifying Long Chain Branching Using Analytical Techniques

The long-chain branches present in materials produced according to the teachings of Lai and coworkers[25] allow these materials to be processed with much greater ease than the strictly linear materials while retaining the good solid state properties associated with their narrow molecular weight distributions. Because of this, the presence and detection of LCB in constrained geometry catalyzed polymers is of interest.

Two analytical techniques have been used for quantifying LCB in LDPEs: high field carbon-13 nuclear magnetic resonance (NMR) and size exclusion chromatography. The Carbon-13 NMR spectra for branches that are 6 or more carbons in length are very similar. Since AFFINITY resins are octene copolymers and therefore contain short

chain branches that are 6 carbons in length, it is difficult to quantify LCB in these resins using this technique[26]. Size exclusion chromatography is very useful for quantifying high levels of LCB[27,28,29]. Solution techniques have also been used to quantify LCB in constrained geometry catalyzed polymers[31,32,33]. Since we know that the rheological behavior of polymers is significantly affected by long chain branching, using rheological measurements to infer LCB characteristics of these materials is a viable alternative.

List of References

[1] Bersted, B.H., *Encyclopedia of Fluid Mechanics*, Vol. 7, Chapter 22, Gulf Publishing Company (1988)

[2] Gell, C.B. *et al*, *J. Polym. Sci. B: Polym. Phys.*, Vol. 35, 1943-1954 (1997)

[3] Graessley, W.W. *et al*, *Macromolecules*, Vol. 9, 127-141 (1976)

[4] Raju, V.R., *et al*, *J. Polym. Sci., Poly. Phys. Ed.*, Vol.17, 1223 (1979)

[5] Bersted, B.H. *et al*, *J. Appl. Polym. Sci.*, Vol. 26, 1001 (1981)

[6] Raju, V.R., G.G. Smith, G. Marin, J.R. Knox, W.W. Graessley, J. Polym. Sci.: Phys. Ed., 17, 1183-1195 (1979).

[7] Bersted, B.H., *J. Appl. Poly. Sci.*, Vol. 30, 3751-3765 (1985)

[8] Constantin, D., *Polym. Eng. Sci.*, 24, 268 (1984)

[9] Carella, J.M. *et al*, *Macromolecules*, Vol. 19, 659, (1986)

[10] Graessley, W.W. and J. Roovers, *Macromolecules*, Vol. 12, 959 (1979)

[11] Rochefort, W.E., *et al*, *J. Polym. Sci: Polym. Phys. Ed.*, Vol. 17, 1197 (1979)

[12] Hingmann, R. and B.L. Marczinke, *J. Rheol.*, Vol. 38, No. 3, 573 (1994)

[13] Pederson, S. and A. Ram, *Polym. Eng. Sci.*, Vol. 18, 990 (1978)

[14] Laun, H.M. and H. Schuch, *J. Rheol.*, 33(1), 119-175 (1989)

[15] Osaki, K. *et al*, *Macromolecules*, Vol. 23, No. 20, 4392 (1990)

[16] Archer, A.R. and S.K. Varshey, work submitted for publication (1998)

[17] Macosko, C.W. and Kasehagen, work submitted to *J. Rheol.* for publication (1998)

[18] Laun, H.M., *Rheol. Acta.*,Vol. 17, 1-15 (1978)

[19] Osaki, K, *Rheol. Acta.*, Vol. 32, 429-437 (1993)

[20] Yoshikawa, K. *et al*, *Polymer Rheology and Processing*, Edited by A.A. Collyer and L.A. Utracki, Chapter 2,Elsevior Science Publishers Ltd. (1990)

[21] Laun, H.M. and H. Münstedt, *Rheol. Acta*, Vol. 15, 517 (1976)

[22] Laun, H.M. and H. Münstedt, *Rheol. Acta*, Vol. 17, 415 (1978)

[23] Münstedt, H. and H.M. Laun, *Rheol. Acta*, Vol. 18, 492 (1979)

[24] Münstedt, H. and H.M. Laun, *Rheol. Acta*, Vol. 20, 679 (1981)

[25] Lai, S.Y. *et al*, United States Patent, 5 272 236, 1993

[26] Randall, J.C., *American Chemical Society Symposium Series 142*, 93-118 (1980)

[27] Mirabella, F.M. and L. Wild, *American Chemical Society Advances in Chemistry Series 227*, 23-44 (1990)

[28] Pang, S. and A. Rudin, *American Chemical Society Symposium Series 521*, 254-269 (1993)

[29] Rudin, A. *et al*, *J. Liquid Chrom.*, Vol. 7 (9), 1809-1821 (1984)

[30] Kasehagen, L.J. *et al*, *J. Rheol.* 40(4), 689-709 (1996)

[31] Chum, P.S. and A.W. deGroot, FA CSS XXI (1994)

[32] de Groot, A.W. *et al*, ISPAC-II (1998)

[33] deGroot, A.W., *et al*, *Waters International GPC Conference* (1998)

Chapter 3

Objectives of Research

Constrained geometry catalyst technology provides us with a unique opportunity to study independently the effects of various molecular characteristics on the rheological behavior of polyethylene. In particular, the effects of low levels of long chain branching (LCB) have never been studied in commercial polyethylenes, because it was impossible to vary the degree of branching while maintaining the backbone molecular weight and molecular weight distribution using traditional polymerization techniques. Because of the unique capabilities of constrained geometry catalysts it was possible to set the following objectives.

(1) To carry out a thorough study of the rheological behavior of mPEs.
(2) To determine the effects of LCB level on rheological behavior.
(3) To develop a procedure for inferring the level of LCB using rheological data.
(4) To determine the likelihood that variations in other molecular characteristics (molecular weight, molecular weight distribution, and short chain branching) would result in falsely predicting LCB.

Chapter 4

Polymers Included in Study

To meet the objectives of the project it was necessary to make a judicious choice of the materials to be included. For our experimental study we chose sets of 4 low density and 5 high density mPEs that have approximately the same MWDs but different degrees of LCB. Also included in our discussion and data analysis is a set of linear mPEs and a set of linear traditional polyethylenes.

Three sets of mPEs were studied. The first set consisted of low density copolymers that were representative of commercial mPEs (Table 4.1).

Table 4.1 Characteristics of Low Density mPEs

Resin	Comonomer	Density	Mw	Mw/Mn
LDL1	Butene	0.911	118 400	2.30
LDB1	Octene	0.908	109 300	2.21
LDB2	Octene	0.908	90 300	2.21
LDB3	Octene	0.908	89 400	2.32

To infer the degree of LCB in octene copolymers using analytical techniques, a series of comparative homopolymers with increasing degrees of LCB was chosen to meet objectives 2 and 3. The characteristics of these resins are given in Table 4.2.

Table 4.2 Characteristics of High Density Polyethylenes				
Resin	**Density**	**Mw**	**Mw/Mn**	**LCB/ 10^4 C**
HDL1*	0.9351	100 900	2.08	0
HDB1	0.9592	88 400	1.98	0.12
HDB2	0.9583	96 500	1.93	0.37
HDB3	0.9575	101 500	1.99	0.42
HDB4	0.9565	90 200	2.14	1.21

To partially meet the requirements for the fourth objective a set of linear mPE homopolymers with varying molecular weights was selected. These materials (Table 4.3) comprised a set that allowed the examination of a molecular weight range of 41 900 to 359 000.

Table 4.3 Characteristics of Linear Homopolymers		
Resin	**Mw**	**Mw/Mn**
HDL2	41 900	1.90
HDL3	122 200	2.02
HDL4	359 000	2.08

To examine the effects of short chain branching two linear butene-ethylene copolymers were also included. These materials along with LDL1 and HDL1 covered a comonomer content range of 1.44 to 21.2 weight % (Table 4.4).

* HDL1 is a butene copolymer with a very low comonomer content

Table 4.4 Characteristic of Linear Butene Copolymers			
Resin	**Mw**	**Mw/Mn**	**wt% Butene**
HDL1	100 900	2.08	1.44
LDL1	118 400	2.30	11.4
LDL2	105 600	2.08	14.83
LDL3	130 400	2.12	21.2

To complete the requirements for the fourth objective 2 linear low density polyethylenes were included.

Table 4.5 Characteristics of Traditional Linear Polyethylenes				
Resin	**Comonomer**	**Density**	**Mw**	**Mw/Mn**
LLDPE1	octene	0.91	158 000	4.54
LLDPE2	octene	0.91	145 500	3.50

The data in Tables 4.1 to 4.5 were supplied by The Dow Chemical Company. Molecular weight distributions were determined by gel permeation chromatography, LCB by C^{13}-NMR, and density by ASTMD-792.

Chapter 5.

Linear Viscoelasticity

Linear viscoelastic (LVE) behavior occurs at low deformation rates, small strains, or short times and follows the Boltzmann superposition principle, which states that stresses due to successive strains are additive[1]. LVE data are important, because they provide an essential element of models for nonlinear flows and because they are highly dependent upon molecular structure.

The linear relaxation modulus, defined by Equation 5.1, is a way of describing a material's response to a step strain deformation, and can be used to determine its response to any other linear deformation.

$$G(t) = \sigma(t)/\gamma \qquad [5.1]$$

Often it is not possible to determine the relaxation modulus experimentally, because of the difficulties associated with generating nearly instantaneous strains and accurately measuring small stresses. Therefore, rheologists generally use small amplitude oscillatory shear to study the LVE behavior of polymers. In this experiment the sample is subjected to the sinusoidal strain given by Equation 5.2.

$$\gamma(t) = \gamma_o \sin(\omega t) \qquad [5.2]$$

The measured stress is also sinusoidal and has the same frequency as the strain but is shifted in time as shown in Equation 5.3

$$\sigma(t) = \gamma_o G_d \sin(\omega t + \delta) = \gamma_o [G'(\omega)\sin(\omega t) + G''(\omega)\cos(\omega t)] \qquad [5.3]$$

where G' and G'' are the storage and loss moduli. The stress can also be written as shown in Equation 5.4

$$\sigma(t) = \dot{\gamma}_o[\eta'(\omega)\sin(\omega t) + \eta''(\omega)\cos(\omega t)] \qquad [5.4]$$

where η' and η'' have units of viscosity. The complex viscosity is given by Equation 5.5, and its absolute value is given by Equation 5.6.

$$\eta^*(\omega) \equiv \eta'(\omega) - i\eta''(\omega) \qquad [5.5]$$

$$|\eta^*| = \sigma_o/\dot{\gamma}_o = \sqrt{(\eta')^2 + (\eta'')^2} \qquad [5.6]$$

The absolute value of the complex viscosity is referred to in this work as the complex viscosity.

Dynamic LVE data can be used to determine the discrete relaxation spectrum [G_i λ_i] which models the relaxation modulus:

$$G(t) = \sum G_i \exp(-t/\lambda_i) \qquad [5.7]$$

5.1 Experimental Procedures

The dynamic LVE data were collected for LDL1, LDB1-3, HDB1-4 and HDL1 by use of a Rheometrics Dynamic Analyzer II (RDA II) in parallel plate (25 mm diameter) configuration with a gap of 1 mm. All experiments were performed under a nitrogen atmosphere, and resin stability under testing conditions was verified. This instrument has a spring torque transducer with a range of 2-2000 gmf cm, and torques

above 5 gmf cm were assumed to be reliable. Prior to performing frequency sweeps, strain sweeps were performed to establish the linear region at each frequency. For the frequency sweeps the variable strain technique was used, which entails using the maximum strain still within the linear region for each frequency. Figure 5.1 shows an example of a strain sweep that was used to determine the appropriate strain for HDB4 at a frequency of 0.5 rad/s.

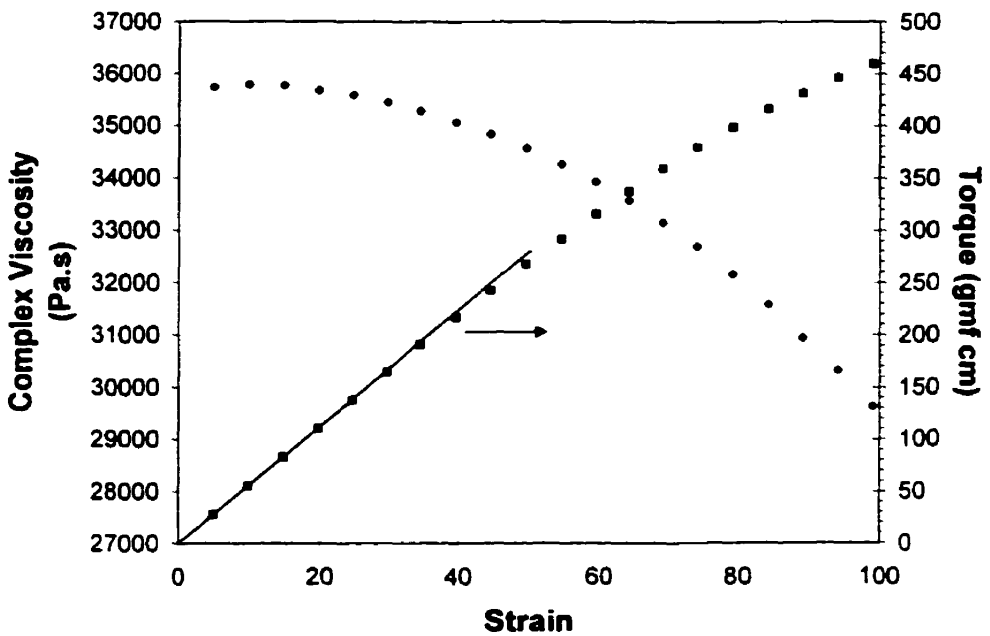

Figure 5.1 Strain Sweep Results for HDB4 at 0.5 rad/s

For the case shown in Figure 5.1 the linear region ends at a strain level of approximately 20%. To ensure that measurements would be well within the linear region, a strain of 10% was chosen for HDB4 at 0.5 rad/s.

Table 5.1 gives the strains used at each frequency for all the resins. The measurements for HDB1-4 and HDL1 were taken at 150°C. A time temperature superposition study was conducted on LDB1-3 and LDL1, which included measurements at 130°C, 150°C and 170°C[2]. Differential scanning calorimetry data showing the melting ranges of these materials are presented in Appendix E. For each material (and

temperature) at least five frequency sweeps were performed using five different samples. All LVE data sets discussed are therefore averages of multiple runs. LVE data are tabulated in Appendix A.

Table 5.1 % Strain Used During Dynamic LVE Data Collection

Frequency Range rad/s	0.005-0.05	0.05-0.5	0.5-5	5-500
LDL1	100	30	10	5
LDB1	50	15	10	5
LDB2	40	25	15	5
LDB3	35	10	10	5
HDL1	250	200	80	10
HDB1	60	25	5	5
HDB2	30 to 0.0186 rad/s and 20 to 0.05 rad/s	15	5	5
HDB3	25 to .0259 rad/s and 20 to 0.05 rad/s	10	5	5
HDB4	30	20	10	5

Samples for the RDA II were molded using a Carver Laboratory Press at a temperature between 185 and 190°C. The compression molding conditions are given in Table 5.2.

Table 5.2 Compression Molding Procedure

Force (metric tonnes)	Holding Time (min)
0	5 [14[A]]
5	5 [12]
10	5 [12]
15	5 [12]

[A] Holding times for LDL1 are higher than for other resins

5.2 Temperature Dependence of LVE Behavior

The effect of temperature on the complex viscosity of LDL1 and LDB3 is shown in Figure 5.2. The master curves in Figure 5.3 were generated by applying time-temperature superposition to the LVE data at 130, 150 and 170°C with a reference temperature of 150°C. The shift factor, a_T, can be determined using Equation 5.8 or by plotting $G'(\omega)$ and $G''(\omega)$ versus ωa_T for various temperatures and varying a_T until the curves superpose at a reference temperature. For some materials, especially long chain branched materials, it is necessary to include a correction for the temperature dependence of density in the form of b_T, which is a vertical shift in the moduli (Equation 5.9). In this work the values for b_T were found empirically rather than by using Equation 5.9. The shift factor values for LDL1-3 and LDL1 are given in Table 5.3 and plotted in Figure 5.4. From this table and graph we can see that temperature sensitivity of rheological behavior is increased with degree of LCB.

$$a_T = \frac{\eta_0(T)}{\eta_0(T_o)} \qquad [5.8]$$

$$b_T = \frac{T_o \rho_o}{T \rho} \qquad [5.9]$$

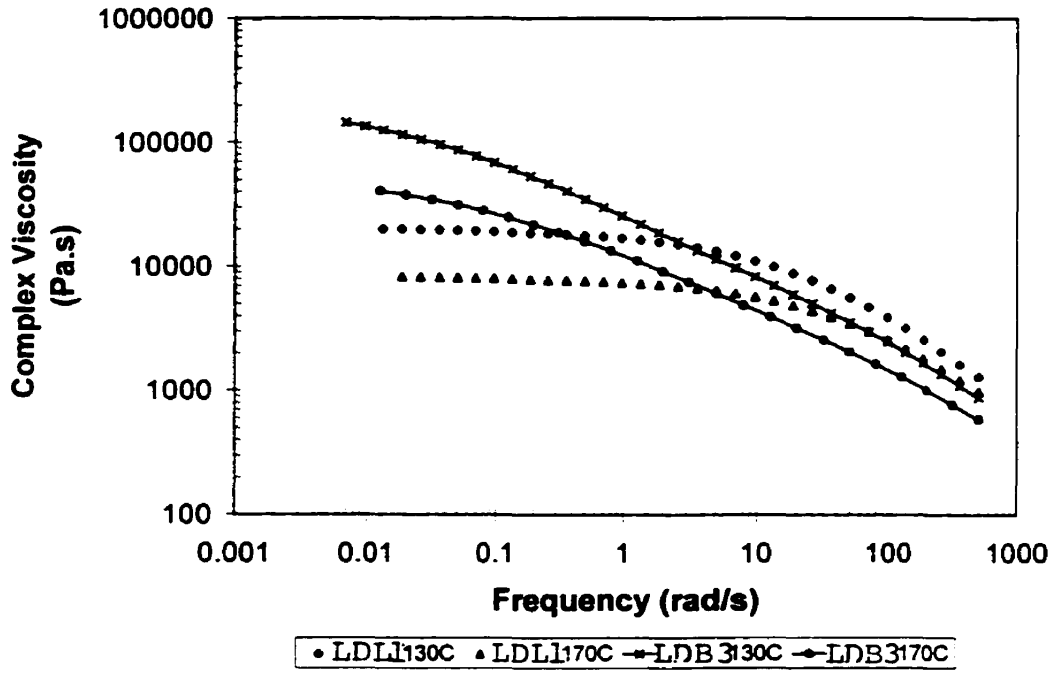

Figure 5.2. The Effect of Temperature on Complex Viscosity for LDL1 and LDB3

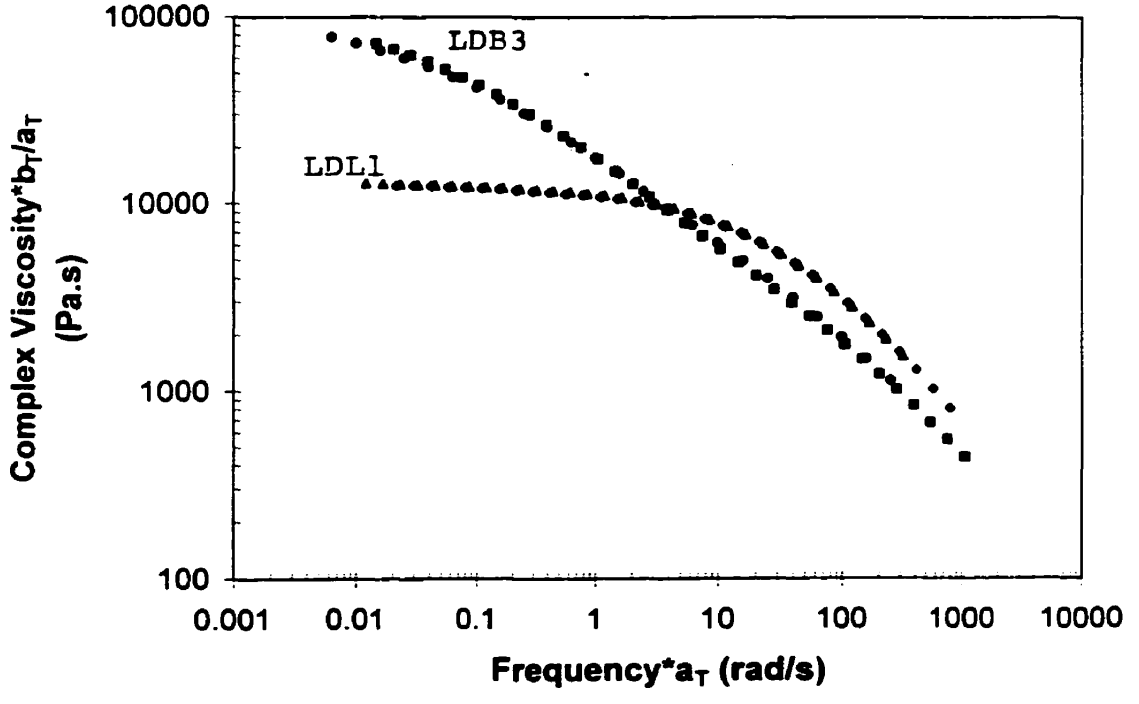

Figure 5.3 Complex Viscosity Master Curves for LDL1 and LDB3 for a Reference Temperature of 150°C

Table 5.3 Temperature Shift Factors for the Low Density mPEs with a Reference Temperature of 150°C				
Material	130°C		170°C	
	a_T	b_T	a_T	b_T
LDL1	1.59	1	0.64	1
LDB1	1.75	1	0.61	1
LDB2	1.85	0.95	0.57	1
LDB3	2.10	1.05	0.50	0.97

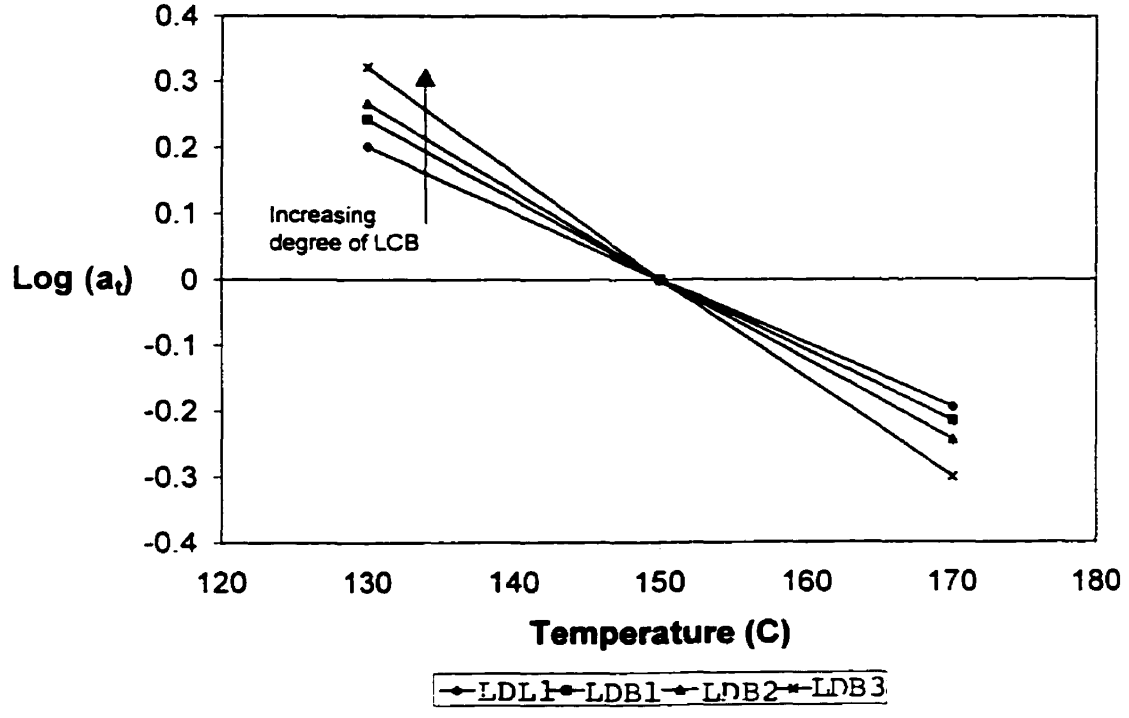

Figure 5.4 The Effect of Temperature on Temperature Shift Factor for LDL1 and LDB1-3

The effect of temperature on the shift factor, a_T, can be described by the Arrhenius Equation over the fairly small temperature ranges studied.

$$a_T = \exp\left[\frac{E_a}{R}\left(\frac{1}{T} - \frac{1}{T_o}\right)\right] \qquad [5.10]$$

In Equation 5.10, E_a is an activation energy. The linear relationship between $\log(a_T)$ and temperature that we see in Figure 5.4 indicates that the Arrhenius Equation is valid for these materials over this temperature range, *i.e.* that E_a is independent of temperature. Materials that have frequency independent shift factors are said to be "thermorheologically simple". LDPE, which has a high degree of LCB, is not thermorheologically simple. The activation energies determined by fitting Equation 5.10 to the experimental data are plotted in Figure 5.5. Since these four materials have very similar molecular weights and polydispersities, and are free of extraneous effects such as impurities and high comonomer contents, the trend that we see in the activation energies is assumed to be due to LCB.

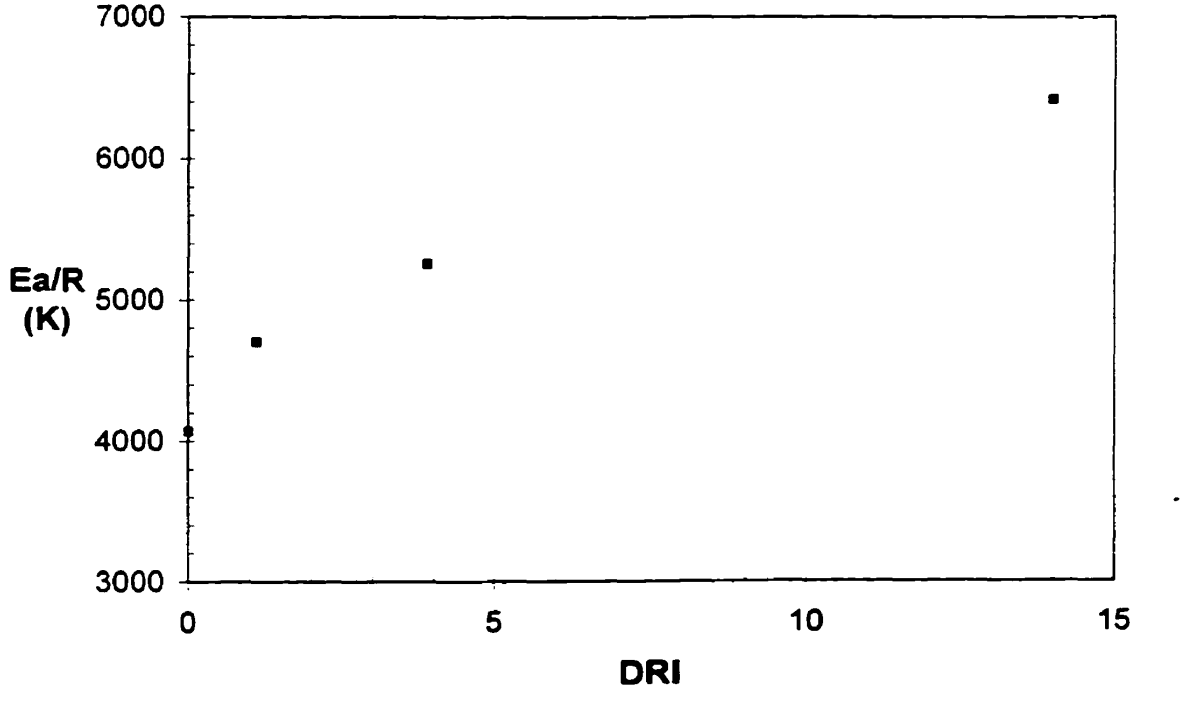

Figure 5.5 The Effect of LCB on the Arrhenius Activation Energy
DRI is an empirical measure of LCB in mPEs

5.3 Effect of Long Chain Branching on LVE Behavior

The LVE data presented and discussed in this section have not been time-temperature super-posed. Each data set is the result of measurements at a single temperature.

5.3.1 High Density mPEs

The complex viscosity curves for the high-density mPEs, HDB1-4 and HDL1, are compared in Figure 5.6. The presence of LCB has 4 main effects on the complex viscosity: (1) the zero shear viscosity is increased for the same backbone molecular weight, (2) the amount of shear thinning is increased, (3) the transition zone between the zero shear viscosity and the power law zone is broadened, and (4) two points of inflection are added within the transition zone.

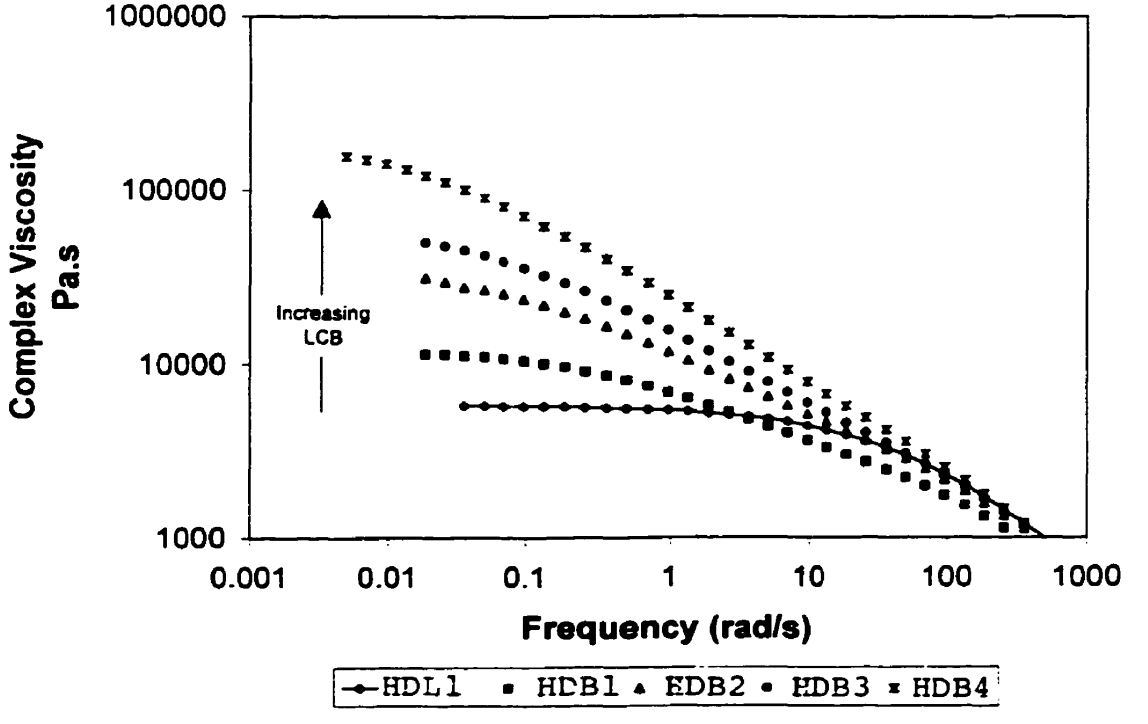

Figure 5.6 Complex Viscosity Data for High Density mPEs

These points of inflection can be seen more clearly in Figure 5.7, which shows the complex viscosity curves for HDL1 (linear material) and HDB4 (1.21 LCB/10 000C). The circles on the HDB4 curve indicate the locations of the inflection points. In comparison, the curve for HDL1 is concave downward over the entire frequency range. As will be explained in Chapter 9, inflection points in complex viscosity curves are often indicators of the presence of LCB in mPEs.

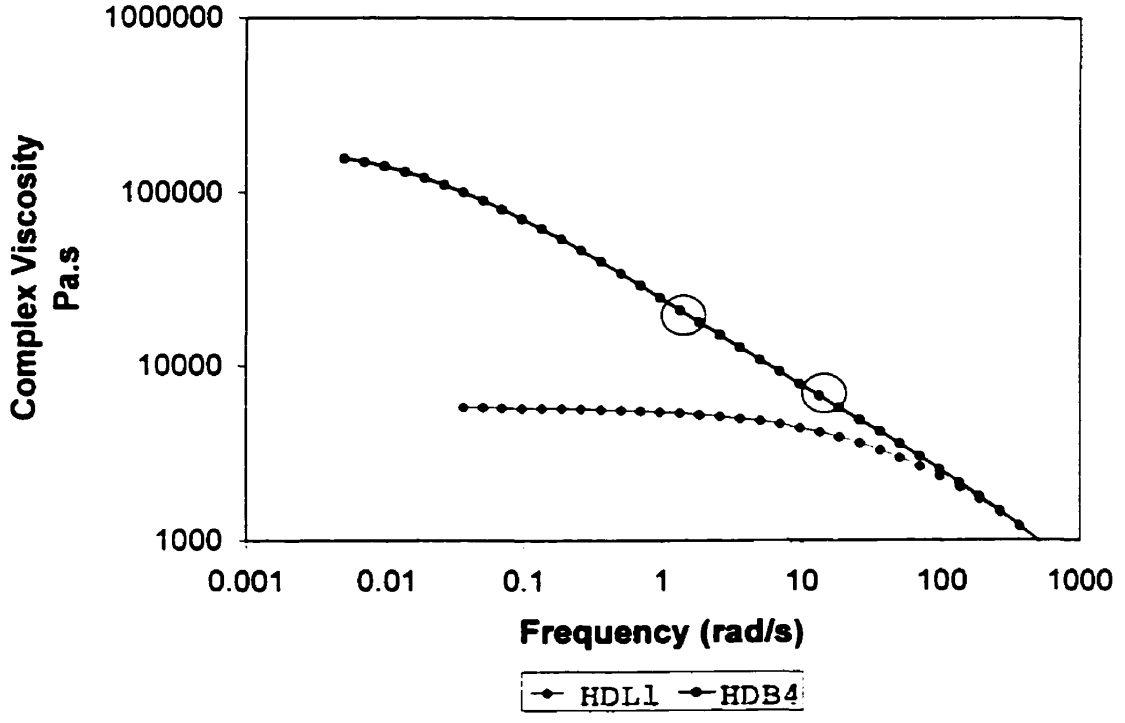

Figure 5.7 Comparison of Complex Viscosity Curves for HDB4 and HDL1

The effects of LCB can also be seen in other LVE properties such as the dynamic moduli, shown in Figure 5.8 and the loss angle, shown in Figure 5.9. In Figure 5.8 the dynamic moduli for HDB4 (branched) and HDL1 (linear) are plotted. LCB changes entirely the shapes of the moduli curves. This point can be seen more clearly by looking

at the loss angle (Figure 5.9) which is the inverse tangent of the ratio of the loss modulus to the storage modulus. We recall that all polymers in this set have similar molecular weights and polydispersities so the differences observed in Figure 5.9 are presumed due to LCB. The loss angle curve for the linear material is what we would expect for a narrow MWD linear polymer. However, the curves for the branched materials are completely different. We see a plateau in the loss angle the magnitude and breadth of which depend upon degree of LCB. This observation is in accordance with results published by Koopmans[3] who noted the same effect of LCB on loss angle when comparing an LDPE, an LLDPE and two branched mPEs.

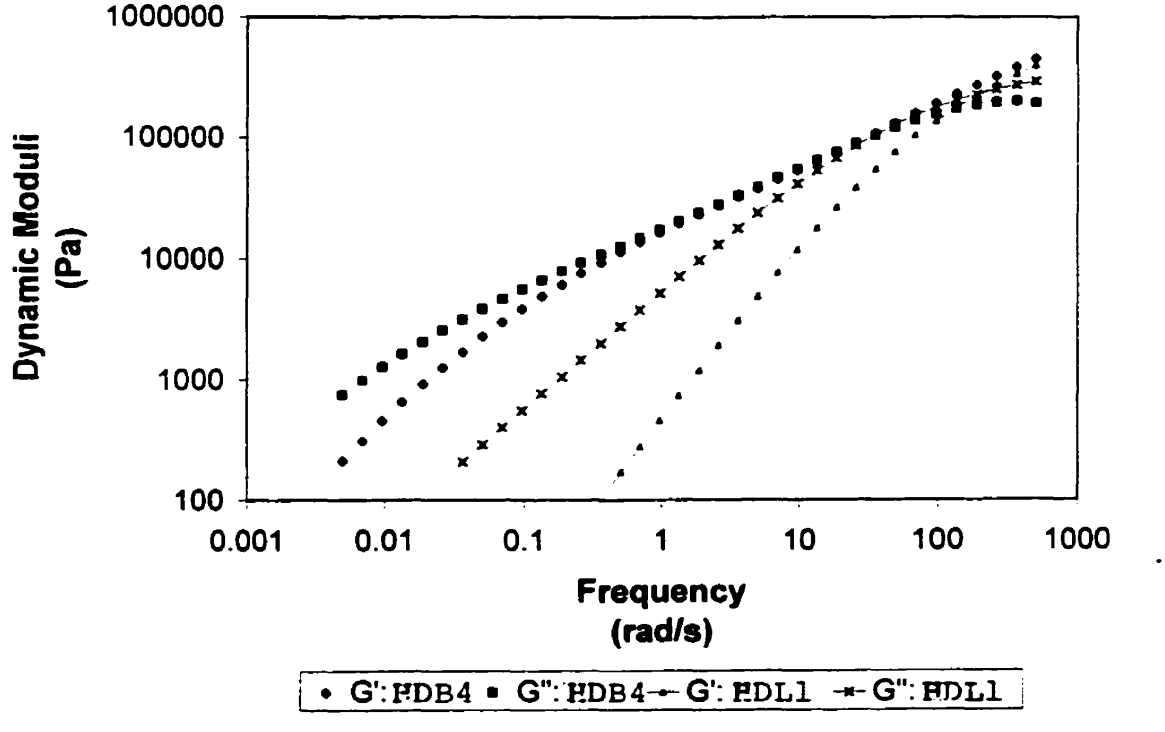

Figure 5.8 Comparison of Dynamic Moduli for HDB4 and HDL1

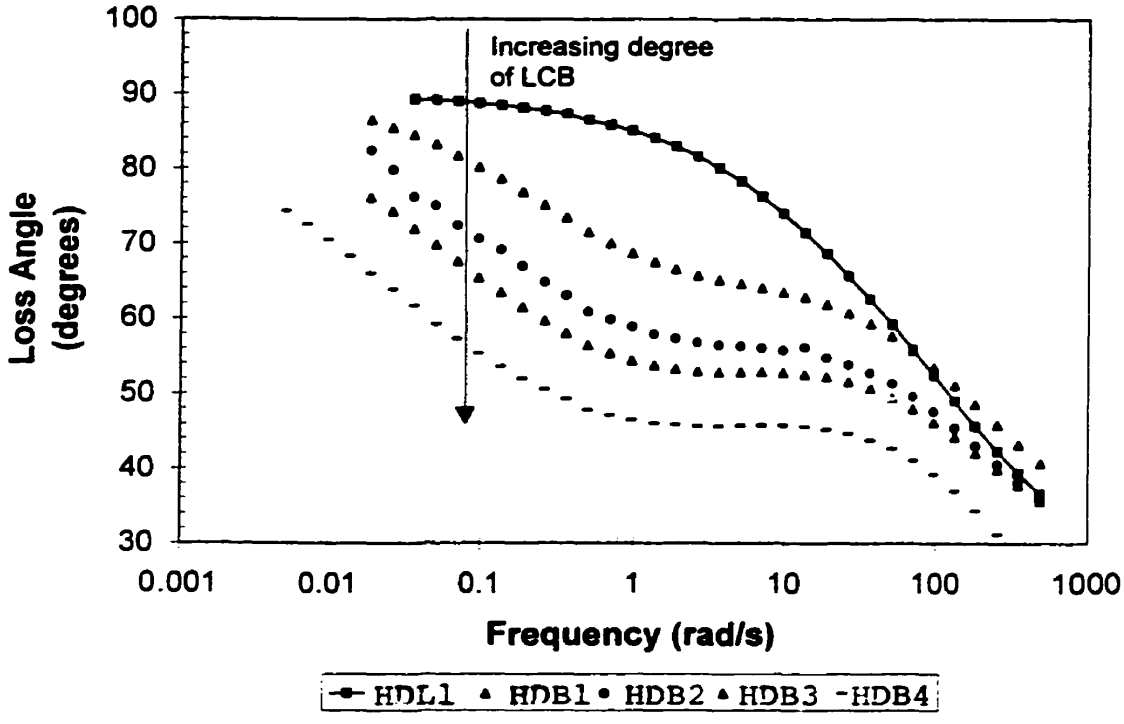

Figure 5.9 The Effect of LCB on Loss Angle High Density mPEs at 150°C

In Table 5.4 the estimated zero shear viscosities (calculated using discrete spectra) and the cross over moduli and frequencies are given for the high density materials at 150°C. The relationship between zero shear viscosity and degree of LCB is shown in Figure 5.10. Once again, all of the polymers in this set have similar molecular weights and polydispersities.

Table 5.4 Dynamical Parameters for High Density mPEs

Resin	η_o^* Pa.s	Cross-over Modulus kPa	Cross-over Frequency rad/s
HDL1	5 800	221	188
HDB1	11 700	223	293
HDB2	31 600	188	153
HDB3	56 600	174	117
HDB4	241 140	84	22

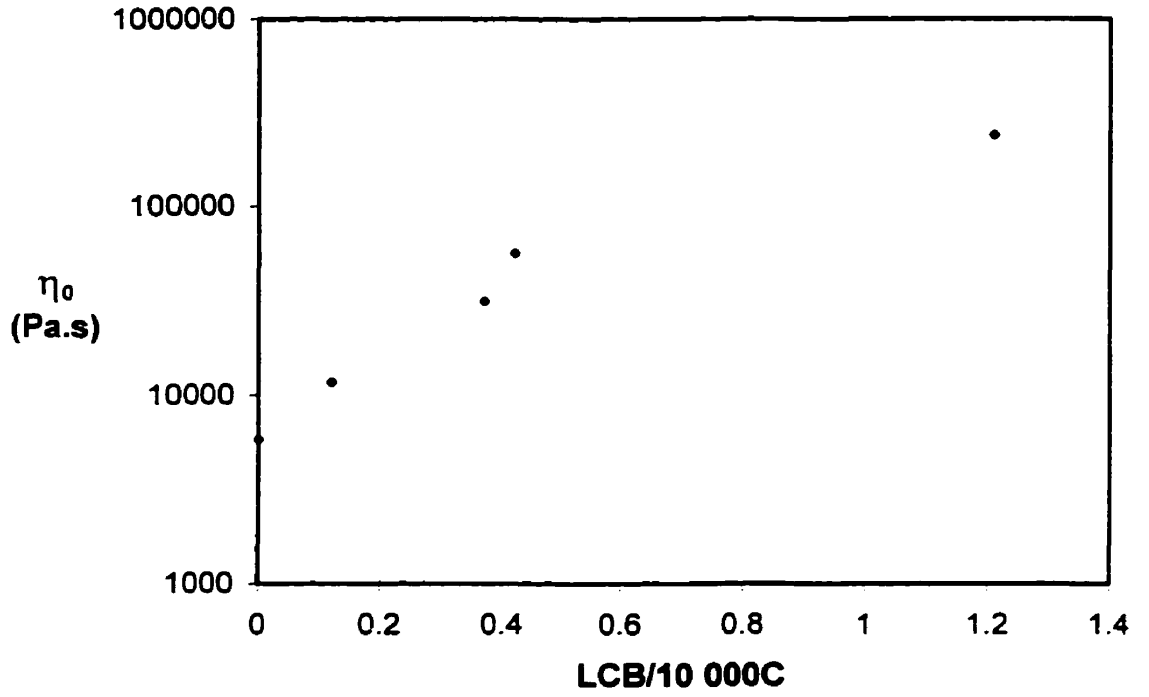

Figure 5.10 The Relationship between η_0 (150°C) and LCB (High Density mPEs having similar Mw and Mw/Mn)

The discrete spectra (tabulated in Appendix A) were determined using IRIS[4] software; this software fits the dynamic moduli to a series of Maxwell relaxation modes (Equations 5.11 and 5.12). The discrete spectrum can be used to calculate a material's response to any deformation within the linear viscoelastic regime, and, as will be discussed in Chapter 8, it is also an essential element of the simulation of nonlinear flow using a constitutive equation. The relaxation spectra of the high density mPEs are compared in Figure 5.11. As expected, the curves come together at short times, and the differences between the materials are evident only at long times.

$$G'(\omega) = \sum_{i=1}^{N} G_i \frac{(\omega\lambda_i)^2}{1+(\omega\lambda_i)^2} \qquad [5.11]$$

$$G''(\omega) = \sum_{i=1}^{N} G_i \frac{\omega\lambda_i}{1+(\omega\lambda_i)^2} \qquad [5.12]$$

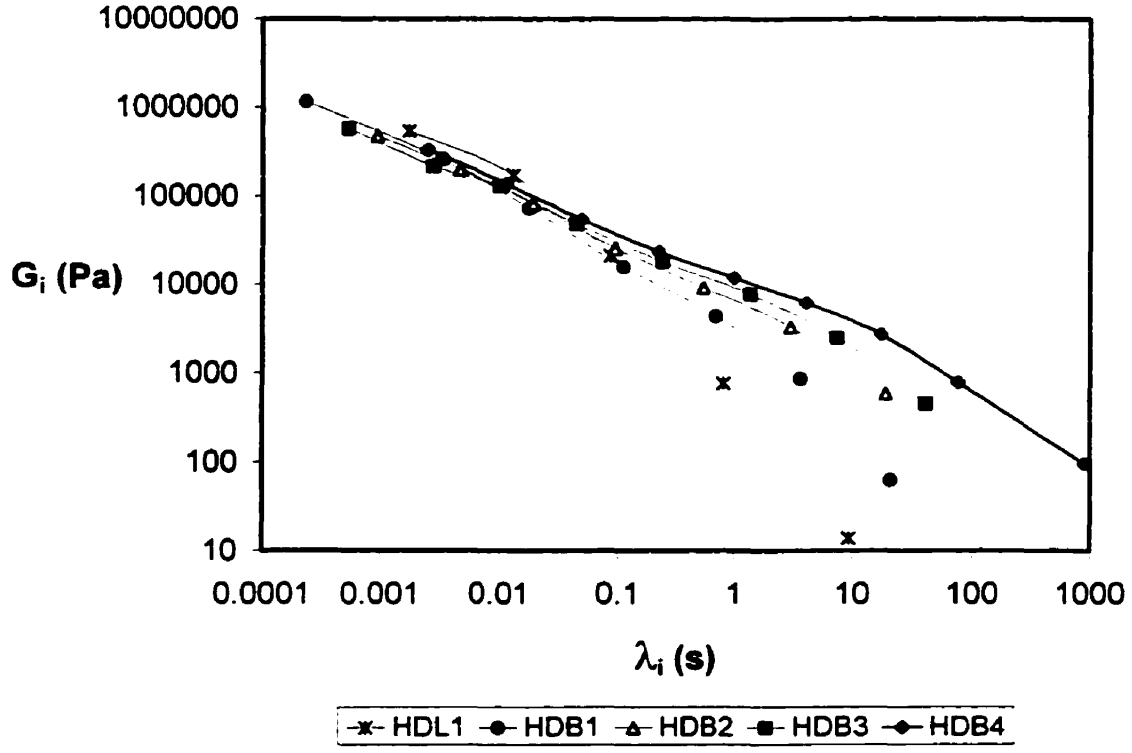

Figure 5.11 The Effect of LCB on the Discrete Relaxation Spectrum
(lines are only to aid the eye)

Wassermen[5] has developed a method of comparing the LVE behavior of different resins based on the breadth of the relaxation spectra as described by the Relaxation Spectrum Index (RSI). The RSI is a ratio of two moments of the relaxation spectrum (Equations 5.13 and 5.14) and is analogous to the polydispersity index, which is used to describe the breadth of the MWD.

$$\lambda_I = \frac{\sum G_i}{\sum G_i / \lambda_i} \qquad [5.13]$$

$$\lambda_{II} = \frac{\sum G_i \lambda_i}{\sum G_i} \qquad [5.14]$$

$$RSI = \lambda_{II} / \lambda_I \qquad [5.15]$$

The RSI values for the high density mPEs are given in Table 5.5. The RSI is dependent on weight average molecular weight (M_w), MWD, LCB and temperature. To look at the effect of LCB only, a reduced RSI (rRSI) can be calculated for these materials, which is simply the ratio of the RSI to the RSI of a linear material of the same M_w and MWD, at the same temperature. As expected, we see that increasing LCB level results in a broader relaxation spectrum.

Table 5.5 RSI Values for High Density mPEs

Resin	RSI	rRSI
HDL1	3.5	1
HDB1	25.9	7.44
HDB2	27.8	7.98
HDB3	66.5	19.07
HDB4	108.9	31.24

5.3.2 Low Density mPEs

LCB has much the same effect on the LVE behavior of the low density mPEs as we saw with the high density materials in the last section. The complex viscosity curves for these materials are plotted in Figure 5.12. Once again with increasing LCB there is an increase in the zero shear viscosity and the amount of shear thinning, the transition zone is broadened, and points of inflection are added within the transition zone. In Figure 5.13 the loss angle curves for the low density mPEs are plotted. As with the high density mPEs, the loss angle curve for the linear material (in this case, LDL1) has an entirely different shape than those of the branched LDB1-3.

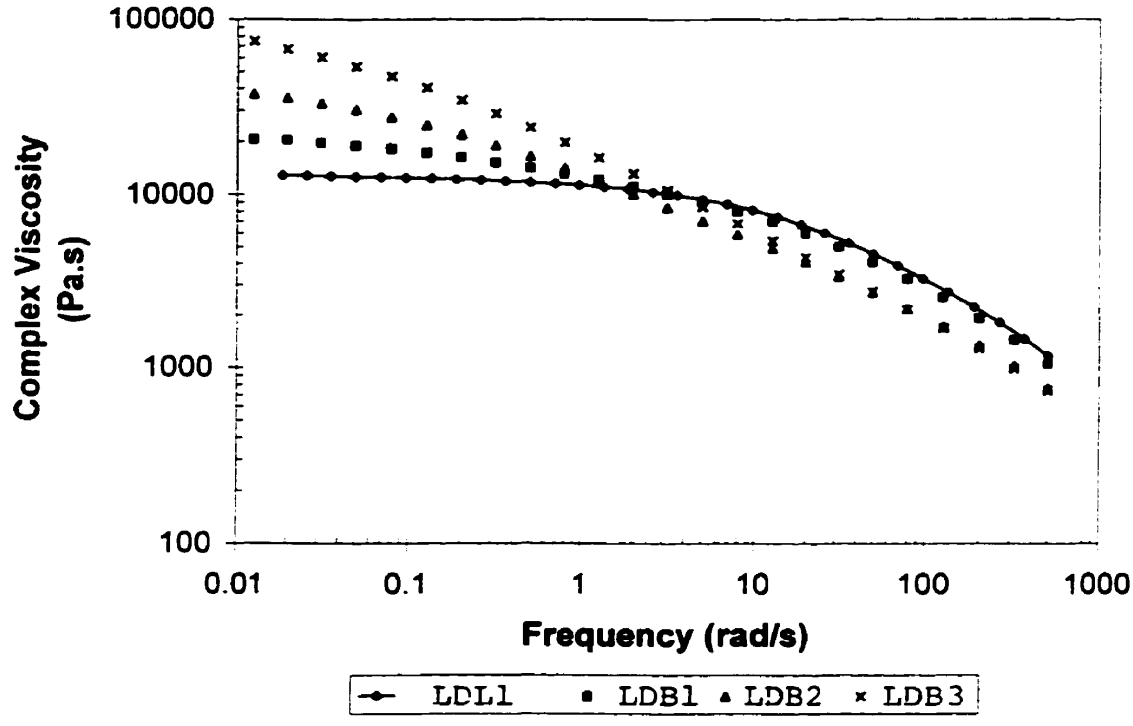

Figure 5.12 Complex Viscosity Curves for Low Density MPEs (150°C)

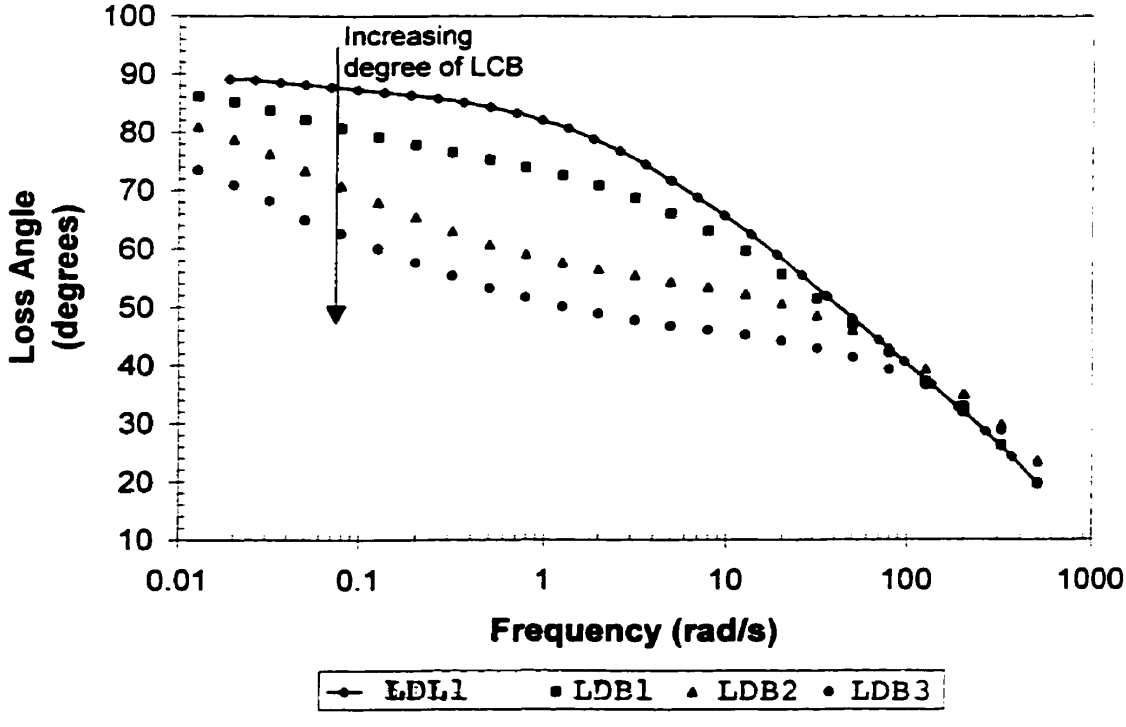

Figure 5.13 The Effect of LCB on Loss Angle Low Density mPEs at 150°C

Table 5.6 lists the dynamical parameters at 130°C for LDB1-3 and LDL1. Figure 5.14 shows the relationship between zero shear viscosity and the DRI (an indicator of degree of LCB). For a complete definition of the DRI see section 9.1.

Table 5.6 Dynamical Parameters for Low Density mPEs (130°C)

Resin	η_o Pa.s	Cross-over Modulus KPa	Cross-over Frequency rad/s
LDL1	19 850	162	33
LDB1	37 290	170	40
LDB2	80 600	113	36
LDB3	175 270	51	8

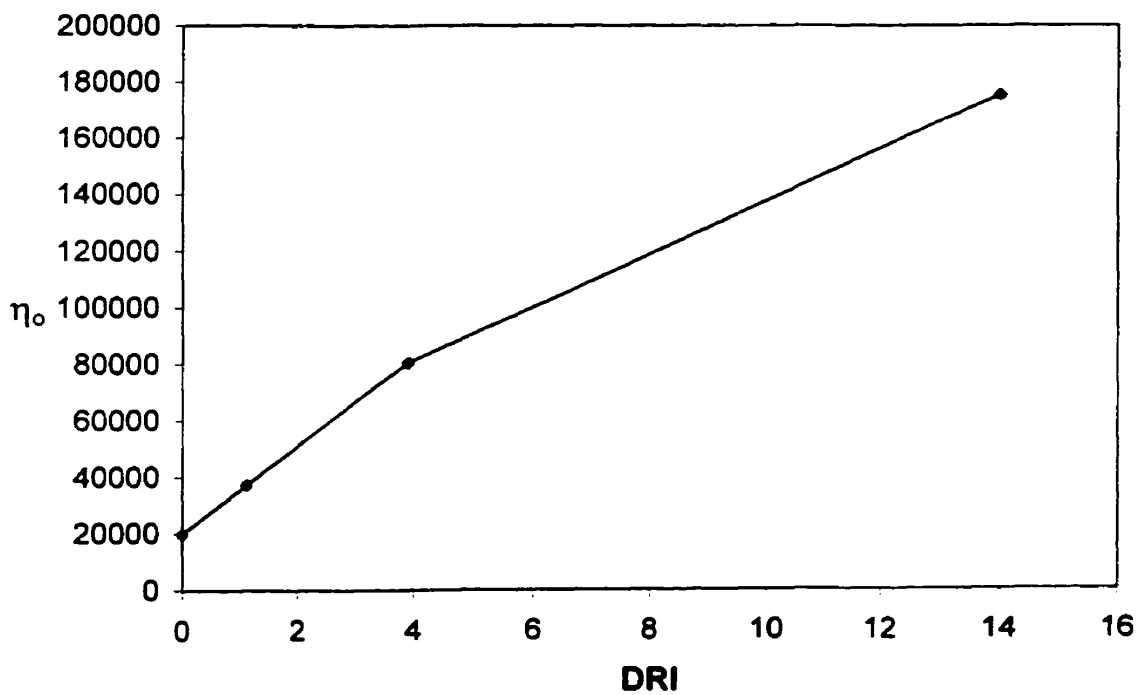

Figure 5.14 Relationship between η_o (130°C, Pa.s) and DRI for Low Density mPEs

It is interesting to note that the effect of increasing degree of LCB on the LVE behavior of mPEs is qualitatively similar to the effect of increasing branch length of asymmetric stars that was seen by Gell and coworkers[6]. The data from this reference are discussed in detail in section 2.1.3.

5.4 Effect of Molecular Weight on LVE Behavior of mPEs

Six linear mPEs were used to study the effect of molecular weight on the LVE behavior. The molecular weights ranged from 41 900 (HDL2) to 359 000 (HDL4). All of the materials included in this study have polydispersities of approximately 2. Therefore the differences in the complex viscosity curves (Figure 5.15) are primarily due to molecular weight variation. An increase in molecular weight causes an increase in the zero shear viscosity and a decrease in the frequency at which shear thinning begins.

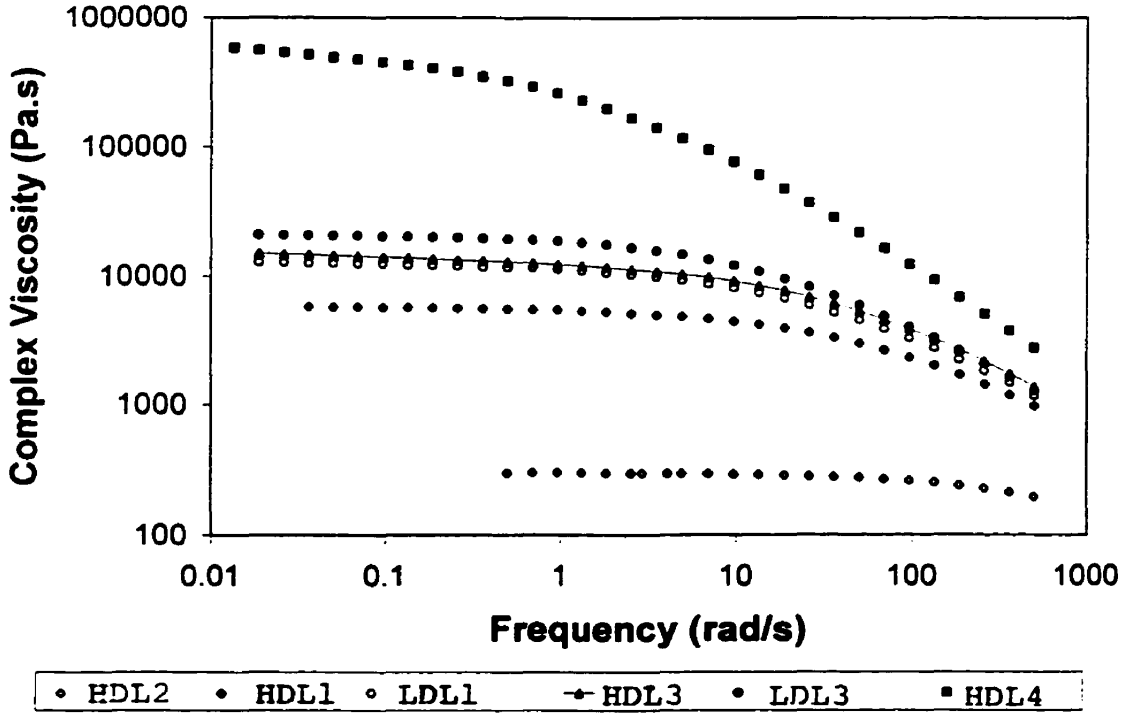

Figure 5.15 Effect of M_W on Complex Viscosity of Linear mPEs (150°C)

The relationship between molecular weight and zero shear viscosity is well documented. For linear polymers above a critical molecular weight the relation shown below is followed.

$$\eta_o = K(M_w)^{\alpha} \qquad [5.16]$$

In Equation 5.16, α is usually found to be approximately 3.4, although it is not unusual to see slightly higher values. The zero shear viscosities are plotted against weight average molecular weight in Figure 5.16 on a double logarithmic plot. In accord with Equation 5.16, the data fall on a straight line. The parameters that result from fitting these data to Equation 5.16 are given in Table 5.7. These values are in good agreement with those reported by Raju and coworkers[7] for polyethylene at 190°C ($K=3.4\times10^{-15}$, $\alpha=3.6$).

Table 5.7 Paramters for Relating η_o to M_W (Equation 5.16)

K	α
3.9×10^{-15}	3.65

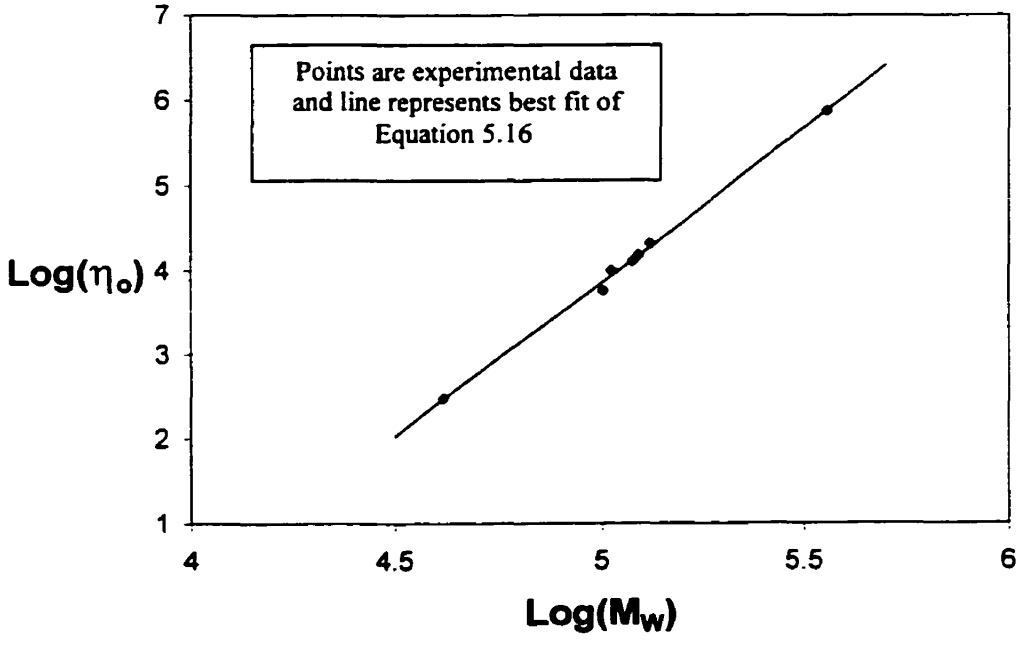

Figure 5.16 Relationship between Zero Shear Viscosity (Pa.s) and M_W for Linear mPEs (150°C)

5.5 Effect of Short Chain Branching on LVE Behavior of mPEs

Traditionally it is assumed that short chain branching (SCB) has little or no effect on the rheological behavior of polyethylenes. The linear mPEs included in this work provide an opportunity to test this theory, since they have the same polydispersities but varying levels of SCB. In Table 5.8 the molecular characteristics of three linear mPEs are given.

Table 5.8 Linear mPEs Included in SCB Study

Resin	M_w	$PI = \frac{M_w}{M_n}$	wt% butene
HDL1	100 900	2.1	1.44
LDL2	105 600	2.1	14.83
LDL3	130 400	2.1	21.1

To remove the effects of MW on the complex viscosity the data are plotted as in Figure 5.17. This type of plot allows one to look at the effect of SCB only. It appears that there is a difference between the three curves, with those for the two materials with the higher levels of SCB are slightly above that for HDL1 at low frequencies. At higher frequencies the curve for HDL1 (lowest level of SCB) is the highest, followed by that for LDL2 and then that for LDL3. However, when the error bars on the complex viscosity representing the 95% confidence limits on the mean are added (Figure 5.18), we see that there is no meaningful difference between the three curves. Based on this observation, we conclude that the differences in complex viscosity are less than the experimental error and that there is no significant effect of SCB on the viscosity function.

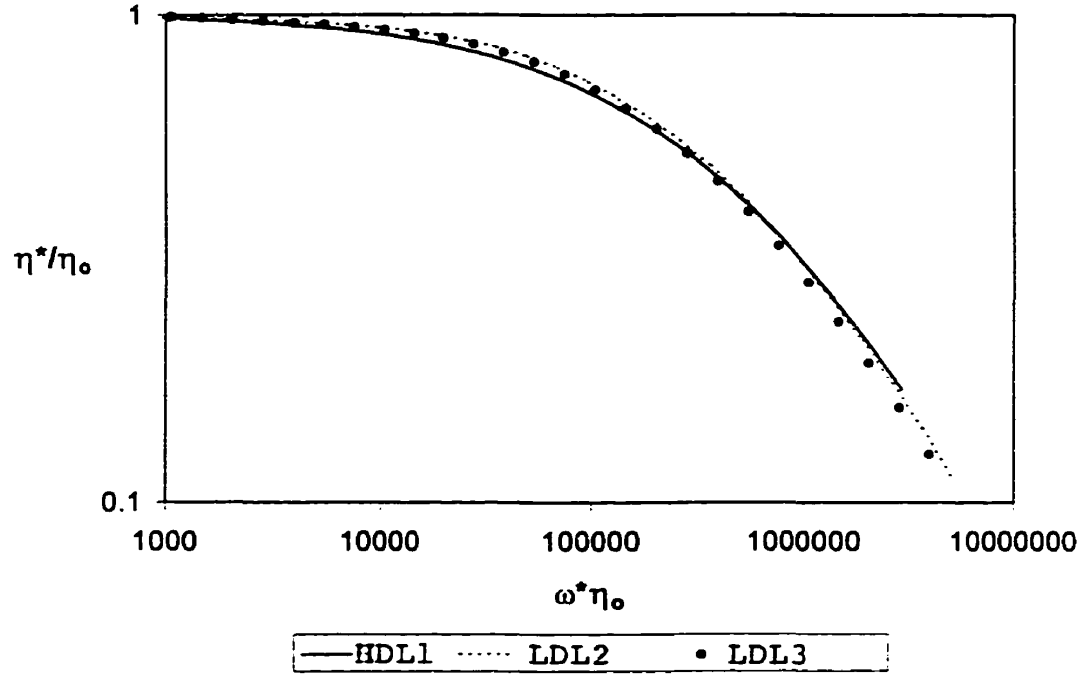

Figure 5.17 The Effect of SCB on Complex Viscosity
(The units of η_o and ω are Pa.s and rad/s)

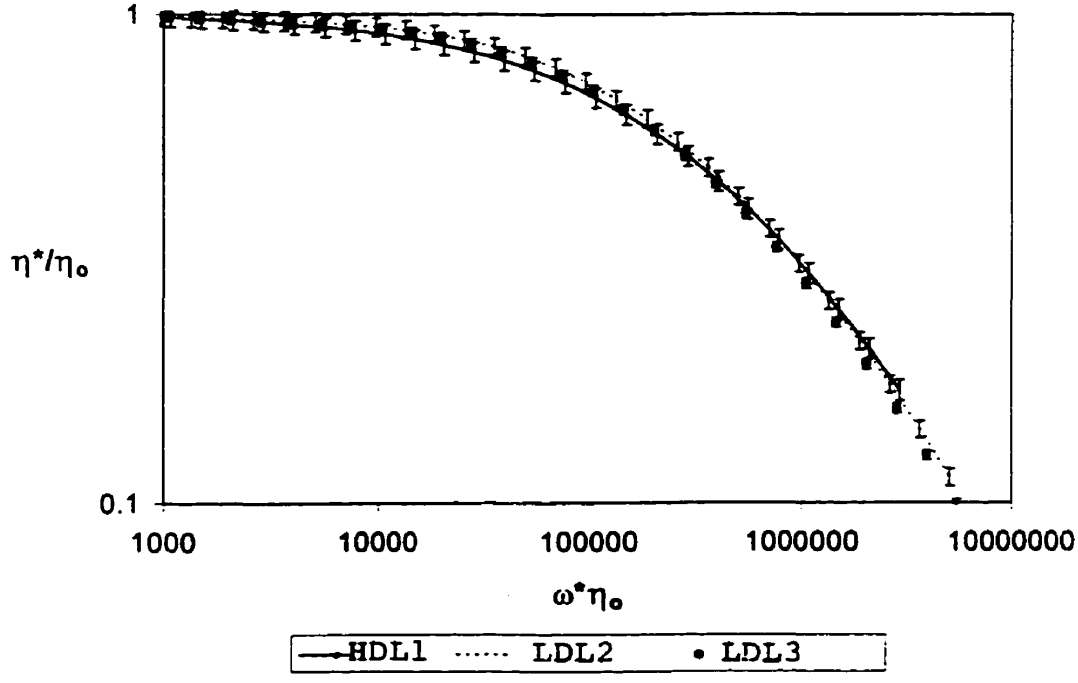

Figure 5.18 The Effect of SCB on Complex Viscosity – Error Bars Represent 95% Confidence Limits of the Complex Viscosity at each Frequency
(Same units as Figure 5.17)

List of References

[1] John M. Dealy and Kurt F. Wissbrun, *Melt Rheology and its Role in Plastics Processing: Theory and Applications*, Van Nostrand Reinhold New York (1990)

[2] Seungoh Kim, unpublished work, McGill University (1998)

[3] Koopmans, R.J. SPE ANTEC 43, 1006-1009, (1997)

[4] Baumgaertel, M. and H.H. Winter, *Rheol. Acta*, 22, 425 (1983)

[5] Wasserman, S.H., SPE ANTEC 43, 1129-1133 (1997)

[6] Gell, C.B. *et al*, *J. Polym. Sci. B; Polym. Phys.*, Vol 35, 1943-1954 (1997)

[7] Raju, V.R., G.G. Smith, G. Marin, J.R. Knox, W.W. Graessley, J. Polym. Sci.: Phys. Ed., 17, 1183-1195 (1979)

Chapter 6

Nonlinear Viscoelasticity in Shear

Polymer melts display nonlinear viscoelasticity under fast, large deformations. This means that the material's response depends on the size, rate and kinematics of the deformation, and it is not possible to use information about its behavior in one deformation to predict its behavior in a different deformation[1]. Nonlinear viscoelastic behavior is important, because plastics forming processes involve high rates and large deformations. To understand how a material will behave in a processing situation, it is necessary to have information about its nonlinear viscoelastic behavior. Since nonlinear phenomena are dependent on kinematics, we must study the material's response to many types of deformation. One can, in principle, use the resulting data to fit the parameters of a constitutive equation, which can then be used in the simulation of complex flows. In the present study both the linear and nonlinear viscoelastic behavior were studied to determine the effect of long chain branching (LCB) and to identify the rheological behavior most affected by the presence of LCB.

For the present study three shearing tests were used: (1) step strain, (2) steady simple shear, and (3) large amplitude oscillatory shear (LAOS). A step strain experiment involves subjecting the material to a sudden strain, γ_o, and monitoring the stress as it decays over time. This type of experiment allows one to determine the nonlinear relaxation modulus, defined as follows.

$$G(t,\gamma) = \sigma(t,\gamma)/\gamma \qquad [6.1]$$

Steady simple shear experiments can be used to determine the viscosity and the first normal stress coefficient (Equations 6.2 and 6.3) by subjecting the material to a constant shear rate and measuring the shear stress and first normal stress difference.

$$\eta(\dot{\gamma}) = \frac{\sigma_{12}(\dot{\gamma})}{\dot{\gamma}} \qquad [6.2]$$

$$\psi_1(\dot{\gamma}) = \frac{\sigma_{11}(\dot{\gamma}) - \sigma_{22}(\dot{\gamma})}{\dot{\gamma}} \qquad [6.3]$$

In LAOS the material is subjected to a sinusoidal shear strain (Equation 5.2), and the periodic stress is measured. If the strain amplitude is large enough that the behavior is nonlinear, the stress signal is not sinusoidal. LAOS is a useful test because it allows the independent variation of the amplitudes of strain and strain rate, but the analysis of the data is more complicated than for other shear flows. The Fourier series, shown by Equation 6.4 can describe the stress.

$$\sigma(t) = \gamma_o \sum_{\substack{n=1 \\ n\ odd}} \left[G_n'(\omega, \gamma_o) \sin(n\omega t) + G_n''(\omega, \gamma_o) \cos(n\omega t) \right] \qquad [6.4]$$

The material response can be more easily evaluated in a qualitative manner by the use of closed loop plots of stress versus strain rate. Such loops are ellipses for LVE behavior and distorted ellipses for nonlinear viscoelastic behavior.

Two instruments were used for the nonlinear shear flow studies; a sliding plate rheometer[2] (SPR) and a rotational cone and plate rheometer (RMS800). The SPR was used for step strain, steady simple shear and LAOS experiments, and the RMS800 was used to measure the first normal stress under steady simple shear. The RMS800 studies were performed by Plastech Engineering AG of Zurich, Switzerland.

6.1 Steady Simple Shear Studies

6.1.1 Sliding Plate Rheometer

The viscosity was determined by subjecting the material to a constant strain rate in the sliding plate rheometer and monitoring the stress until steady state was achieved. These experiments were performed for LDB3, HDB1, HDB2, HDB3, HDB4 and HDL1 at 150°C. The range of shear rates studied was limited at the low end by very small stress values and at the high end by slip and was different for each resin. Approximately fifteen experiments at various rates were performed on each sample, and for each resin at least three samples were used. Table 6.1 shows the shear rate ranges for each resin.

Table 6.1 Steady Simple Shear Experimental Conditions

Resin	$\dot{\gamma}$ range
HDL1	0.5 – 74
HDB1	0.5 – 92
HDB2	0.2 – 28
HDB3	0.1 – 28
HDB4	0.05 – 28
LDB3	0.01 – 2.8

Samples were compression molded using the same conditions as those used to prepare the samples for dynamic linear viscoelastic testing (Section 5.1)

An example of the startup behavior observed in the sliding plate experiments is shown in Figure 6.1. We see the typical overshoot before the stress reaches its ultimate plateau value, which corresponds to the viscosity.

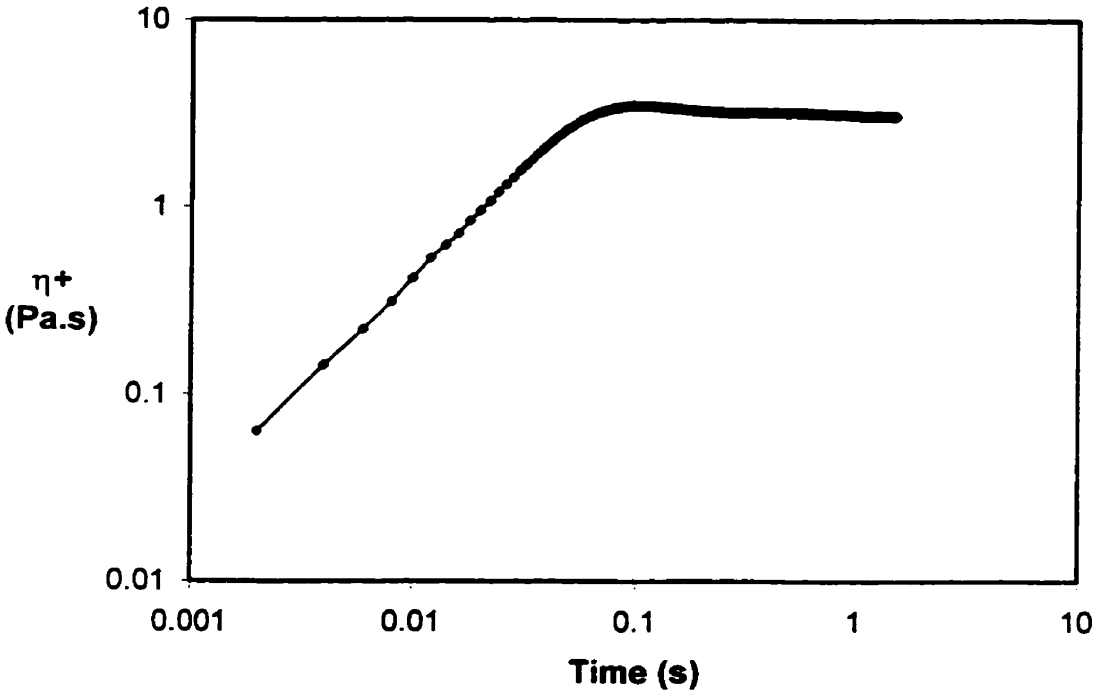

Figure 6.1 Startup Transient for HDB2 at a Shear Rate of 46.1 s^{-1}

Startup of steady simple shear can be used to gain nonlinear rheological information; but in the case of the sliding plate rheometer (SPR) the startup strain was not controlled precisely enough to allow for extraction of this information. Therefore, only the steady state behavior will be discussed. In Figure 6.2 the shear viscosity curves for HDL1, HDB1, HDB2, HDB3 and HDB4 (150°C) are compared, and the viscosity curve for LDB3 (150°C) is shown in Figure 6.3. The scatter in the low shear rate viscosity data for LDB3 is due to the extremely small stresses that occurred under those conditions. The similarity of the curves of viscosity and complex viscosity is referred to as the Cox-Merz[3] rule.

$$\eta(\dot{\gamma}) = |\eta^*(\omega)| \qquad (\omega = \dot{\gamma}) \qquad [6.5]$$

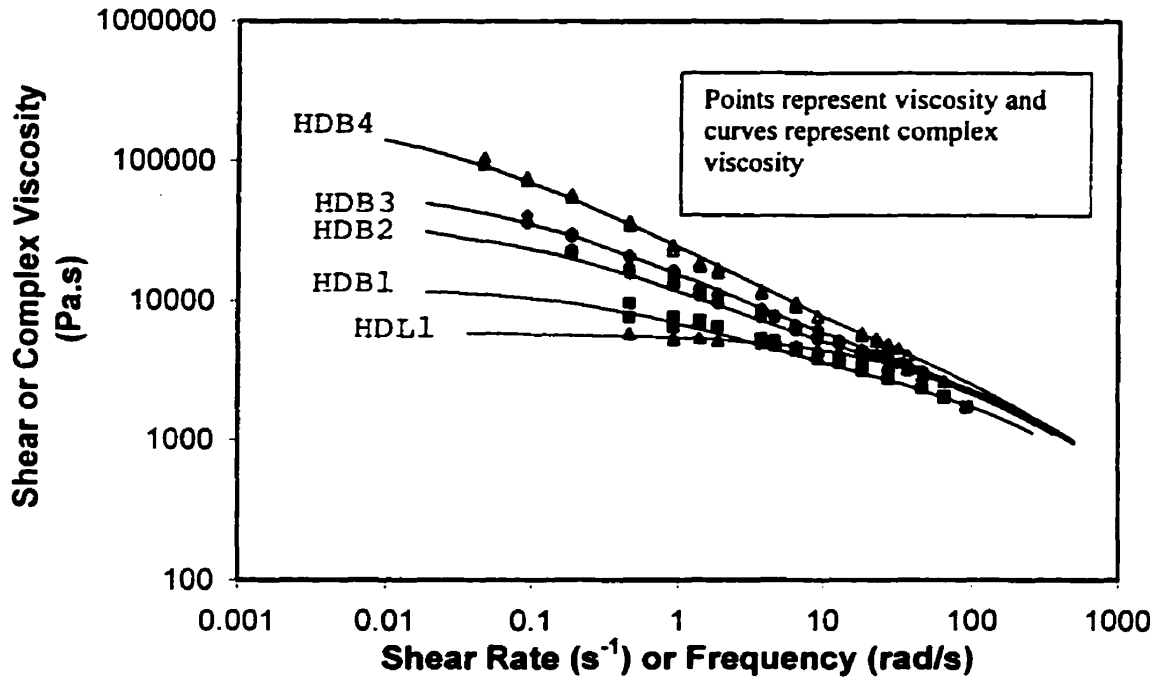

Figure 6.2 Shear and Complex Viscosity for High Density Materials

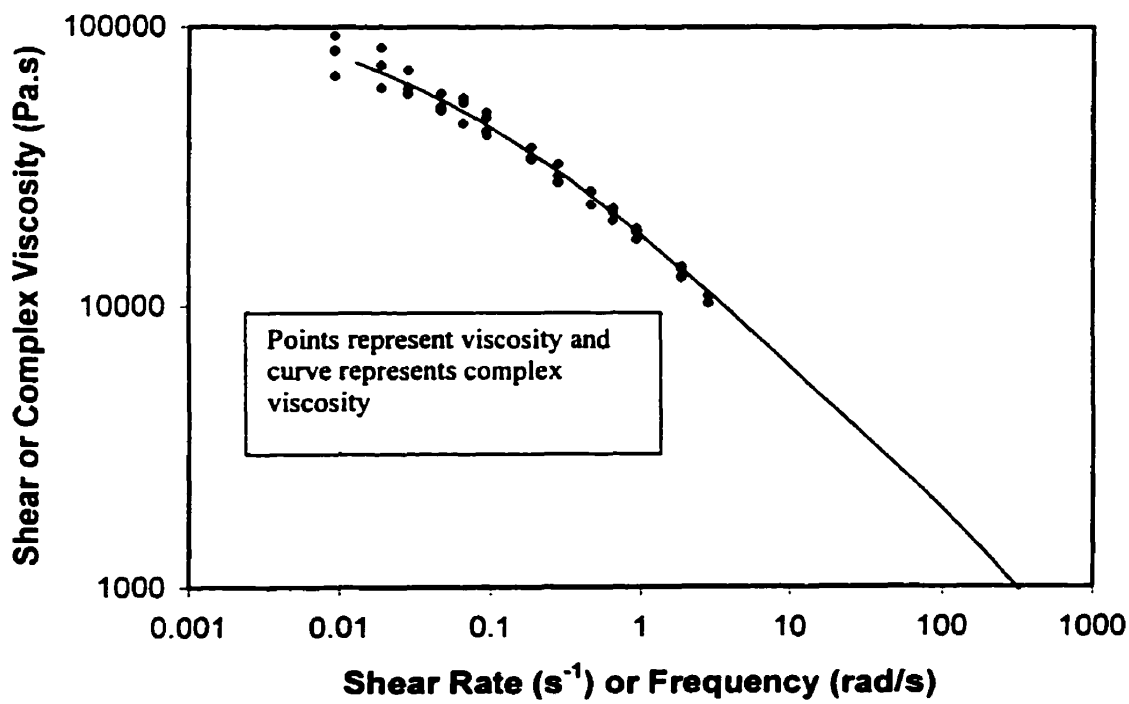

Figure 6.3 Shear and Complex Viscosity for LDB3

6.1.2 Cone and Plate Rheometer

The data presented in this section were measured by Plastech Engineering AG of Zurich, Switzerland. An RMS800 rheometer with cone and plate fixtures was used to measure the viscosity and first normal stress difference coefficient. Measurements were performed for HDB1, HDB2, HDB3, HDL1 and LDB3 at 150°C. The samples were compression molded under the conditions shown in Table 6.2. Appropriate sample diameters were used at each rate to keep the normal force within measurable limits (Table 6.3). At higher rates flow instabilities affected the measured stresses and narrowed the experimental window to shorter ranges than those shown in Table 6.3.

Table 6.2 Compression Molding Conditions for RMS800 Cone and Plate Samples

Resin	Temperature (°C)	Holding Time (min.)
HDB1	190	15
HDB2	190	15
HDB3	190	15
HDL1	180	15
LDB3	170	15

Table 6.3 Sample Diameters for RMS800 Cone and Plate Experiments

Rate (s^{-1})	0.01 (mm)	0.06	0.1	0.3	0.6	1	3	6	10	30
HDB1	18.863	18.75	15.339	15.347	15.347	15.347	12.086	10.951	9.194	8.244
HDB2	18.908	18.891	15.373	15.381	15.356	15.364	12.289	10.951	9.000	8.3618
HDB3	18.869		15.398	15.364	15.347	15.415	12.222	10.901	9.000	----
HDL1	18.925	18.869		18.908	18.908	18.891	15.381	12.204	10.312	8.303
LDB3	19.064	19.086	19.014	15.508	15.524	12.433	10.331	10.513	8.389	-----

The viscosity data measured using the RMS800 are compared with the complex viscosity and the SPR viscosity data in Figure 6.4 for four of the high density mPEs. For all four resins, the viscosity data from the SPR and the RMS800 are in excellent agreement. The RMS800 data for HDB1 appear to indicate a deviation from the Cox-Merz rule at low rates. Given the error likely to be present in the low shear rate data, we cannot be certain that this deviation is significant.

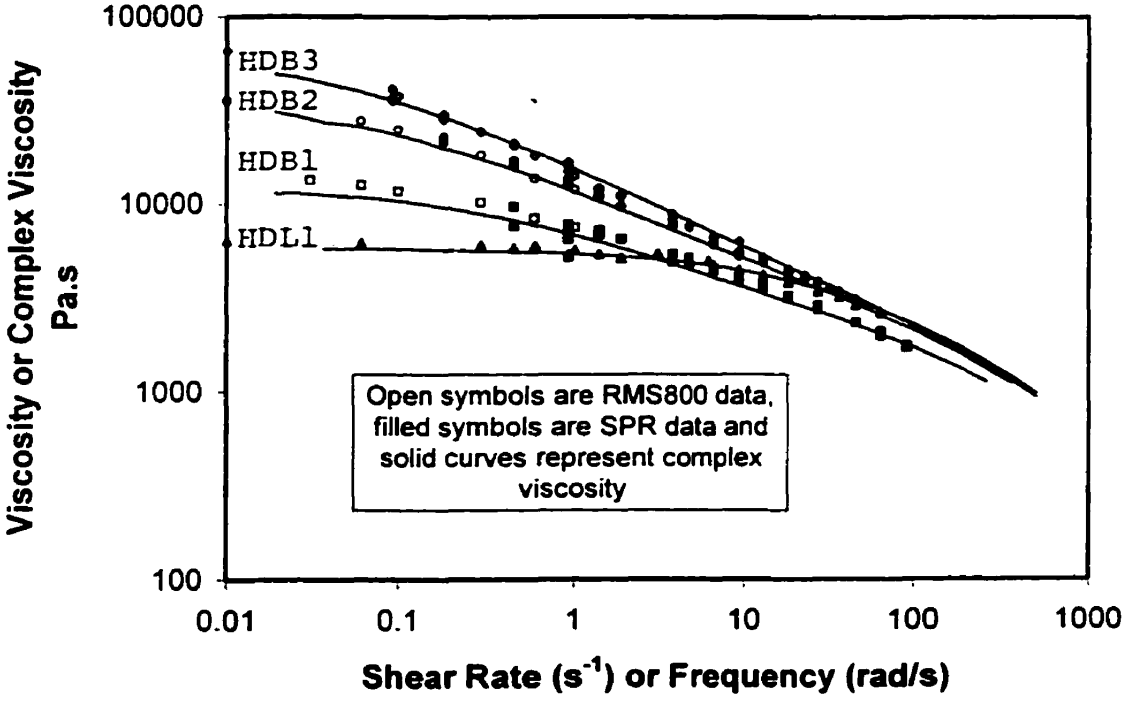

Figure 6.4 Comparison of SPR and RMS800 Data (η) with Complex Viscosity

The effect of LCB on the first normal stress coefficient is shown in Figure 6.5. In this graph we can see that the first normal stress coefficient increases with degree of LCB. There is some suggestion that the curves come together at high rates.

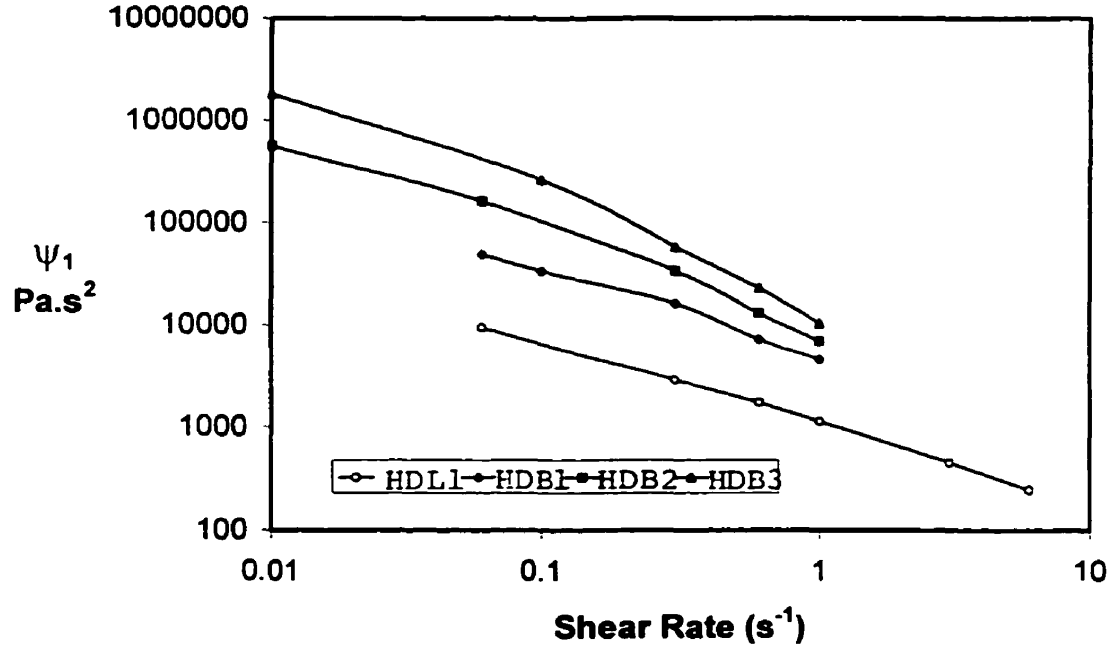

Figure 6.5 The Effect of LCB on the First Normal Stress Coefficient Function

6.1.3 Empirical Relations between Linear Properties and the Viscometric Functions

Several empirical relations have been proposed that relate the viscometric functions to linear viscoelastic properties. The Cox-Merz rule, defined in Section 6.1.2, is one such relation. A second Cox-Merz rule is given by Equation 6.6.

$$\frac{d\sigma(\dot{\gamma})}{d\dot{\gamma}} = \eta'(\omega) \quad (\omega = \dot{\gamma}) \qquad [6.6]$$

In addition, Gleissle[4] has proposed two "mirror" relations (Equations 6.7 and 6.8). These relate the linear startup of shear flow to viscometric functions.

$$\eta^+(t) = \eta(\dot{\gamma}) \quad (t = 1/\dot{\gamma}) \qquad [6.7]$$

$$\psi_1^+(t) = \psi_1(\dot{\gamma}) \quad (t = k/\dot{\gamma}) \qquad [6.8]$$

For use in Equation 6.8, $\psi_1^+(t)$ was calculated using Equation 6.9

$$\psi_1^+ = 2\int_0^t sG(s)ds = 2\sum_1^N G_i\lambda_i[\lambda_i - t\exp(-t/\lambda_i) - \lambda_i\exp(-t/\lambda_i)] \qquad [6.9]$$

Finally, Laun[5] proposed the relationship shown in Equation 6.10, which relates the first normal stress coefficient and the dynamic moduli.

$$\psi_1(\dot{\gamma}) = 2\frac{G'}{\omega^2}\left[1+\left(\frac{G'}{G''}\right)^2\right]^{0.7} \qquad [6.10]$$

We saw previously that mPEs follow the first Cox-Merz rule. However, in Figure 6.6 we can see that the second Cox-Merz rule applies only at low shear rates/frequencies for the linear material, HDL1, and not at all for the branched material, HDB3. In this figure the solid line represents $\eta'(\omega)$, and the points represent the derivative term in Equation 6.6. Neither HDB1 nor HDB2 follow the second Cox-Merz rule.

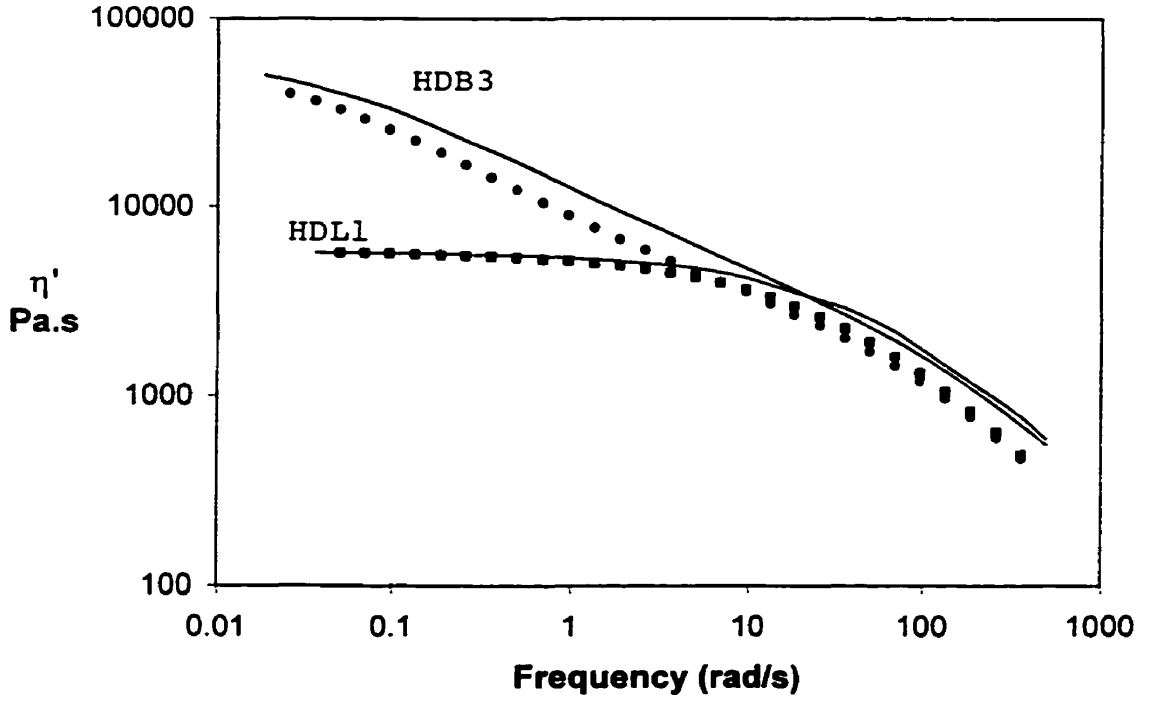

Figure 6.6 Testing of the Applicability of the Second Cox-Merz Rule (Equation 6.6)

In Figure 6.7 the first Gleissle mirror relation (Equation 6.7) is tested. The solid curves represent the shear stress growth coefficient calculated from the discrete spectra, and the points are the shear viscosity data with $t = 1/\dot{\gamma}$. The data for the linear material, HDL1, follow the rule very well. For the branched material (HDB3) the rule is followed well at long times but is less accurate at shorter times. We see much the same behavior with HDB1 and HDB2.

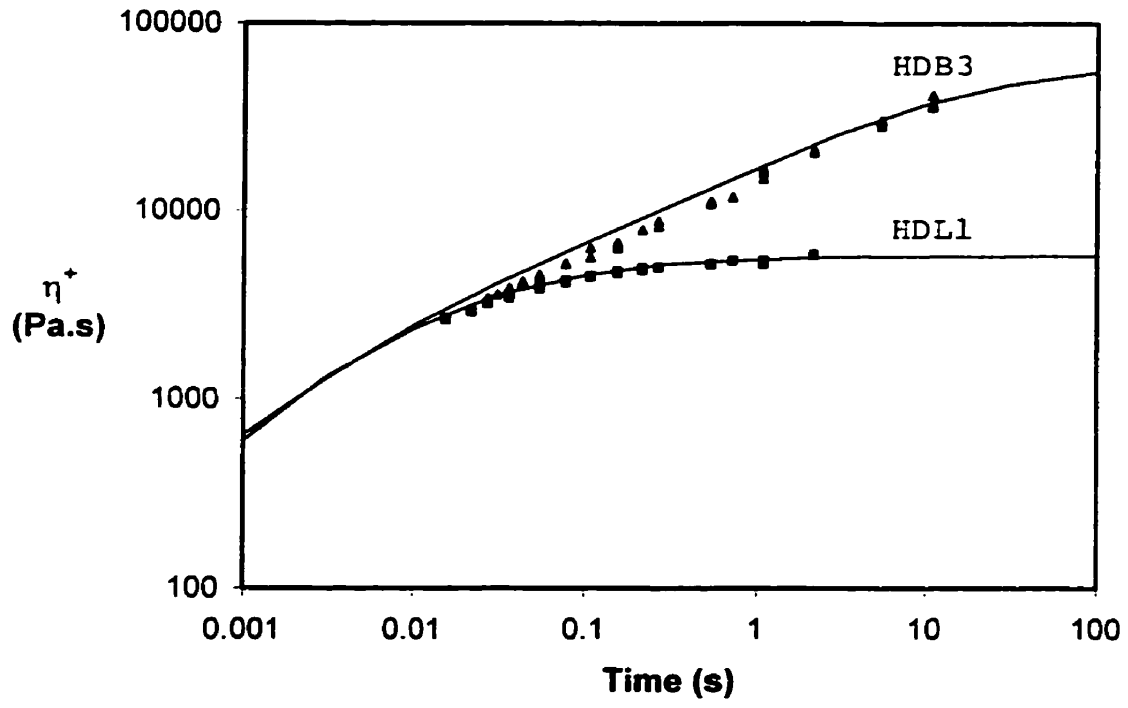

Figure 6.7 Testing the Applicability of the First Gleissle Mirror Relation (Equation 6.7)

In Figure 6.8 the applicability of the second Gleissle mirror relation is tested for four of the high density mPEs. The solid curves show $\psi_1^+(t)$ as calculated from the discrete spectrum using Equation 6.9. The points are the RMS800 data, with time calculated as shown in Equation 6.8. The **k** values in Table 6.4, were chosen to give the best agreement between ψ_1^+ and the RMS800 data. For HDL1 using a value of **k** other than 1 did not improve the agreement, since a simple shift cannot explain the difference between the two functions. From this comparison, we conclude that the second Gleissle mirror relation is valid for the branched mPEs but not for linear mPEs. This is in accordance with the findings of Larson[6] and Wissbrun[7], who show that materials with relaxation moduli that are broader functions of time display viscometric behavior that is less sensitive to the detailed form of the damping function. This means that materials with broader relaxation spectra are more likely to follow the empirical relations developed by Cox, Merz, and Gleissle.

Table 6.4 Parameter Values for Equation 6.10	
Resin	**k**
HDL1	1
HDB1	1.5
HDB2	1.2
HDB3	1.1

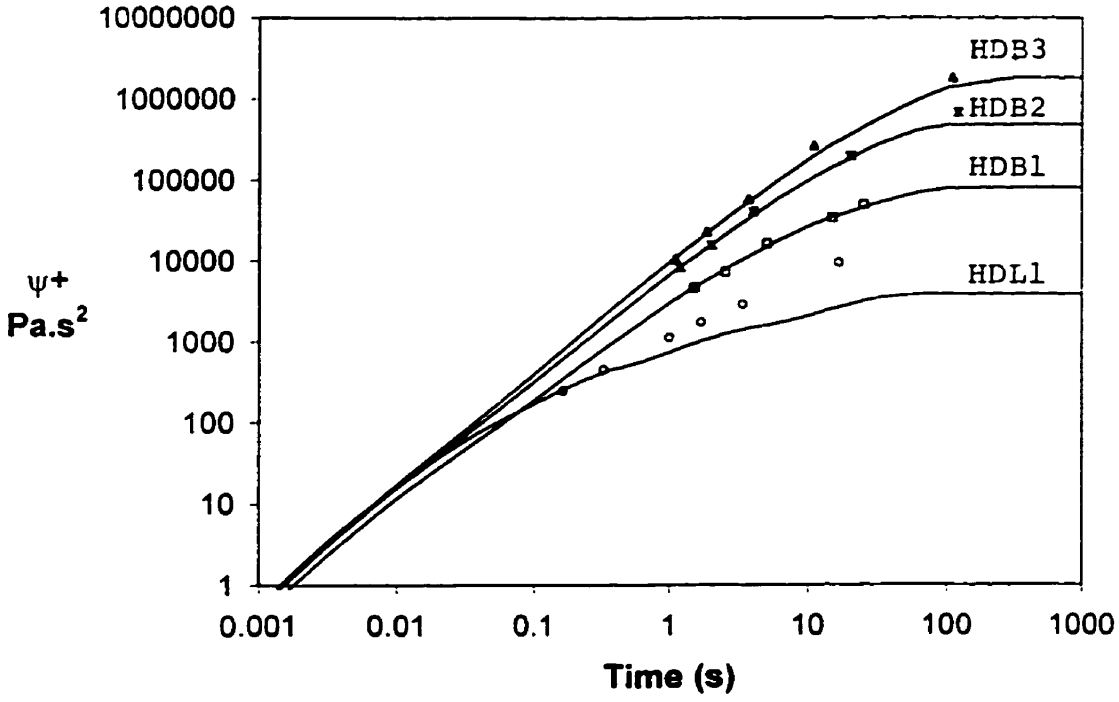

Figure 6.8 Testing the Applicability of the Second Gleissle Mirror Relation (Equation 6.8)

Using the second Gleissle relation, the first normal force coefficient curves were extended for the branched materials (Figure 6.9), indicating that these curves do, in fact, come together at high shear rates.

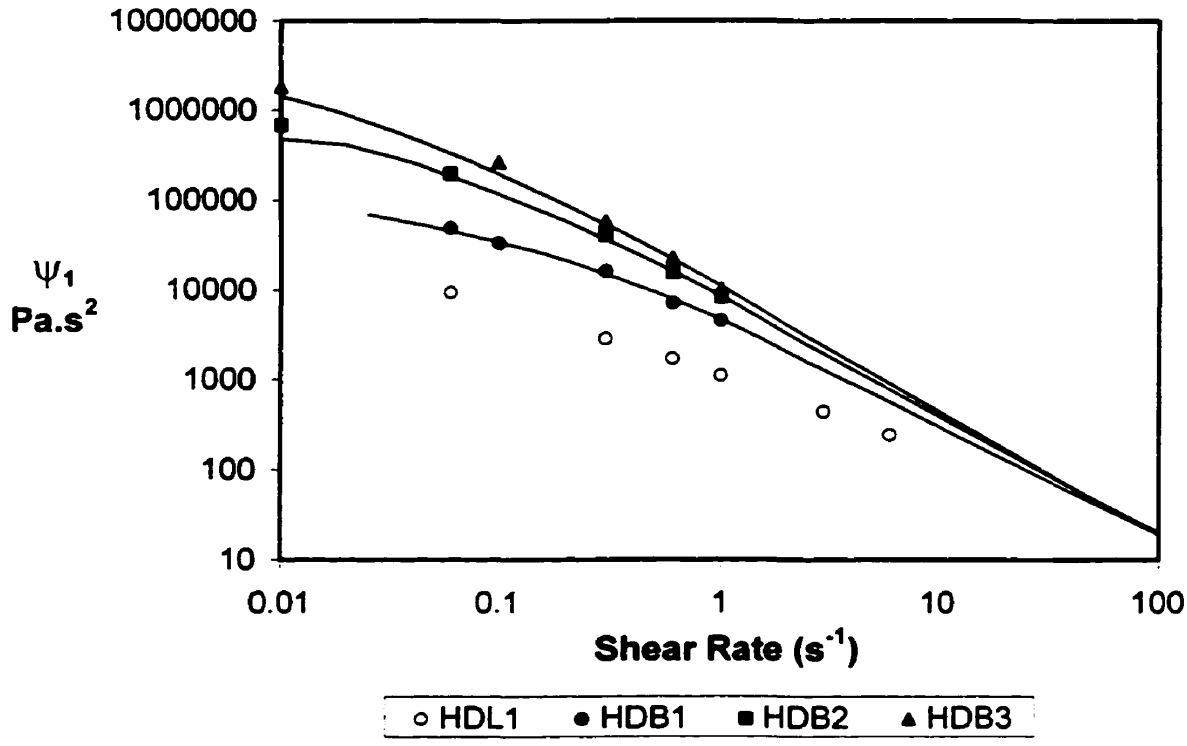

Figure 6.9 Extrapolation of First Normal Stress Coefficient Curves using the Second Gleissle Mirror Relation

In Figure 6.10 Laun's relation (Equation 6.10) is tested. The solid lines represent Laun's relation, and the points are the experimental data. This relation does not fit the experimental data as well as the second Gleissle mirror relation.

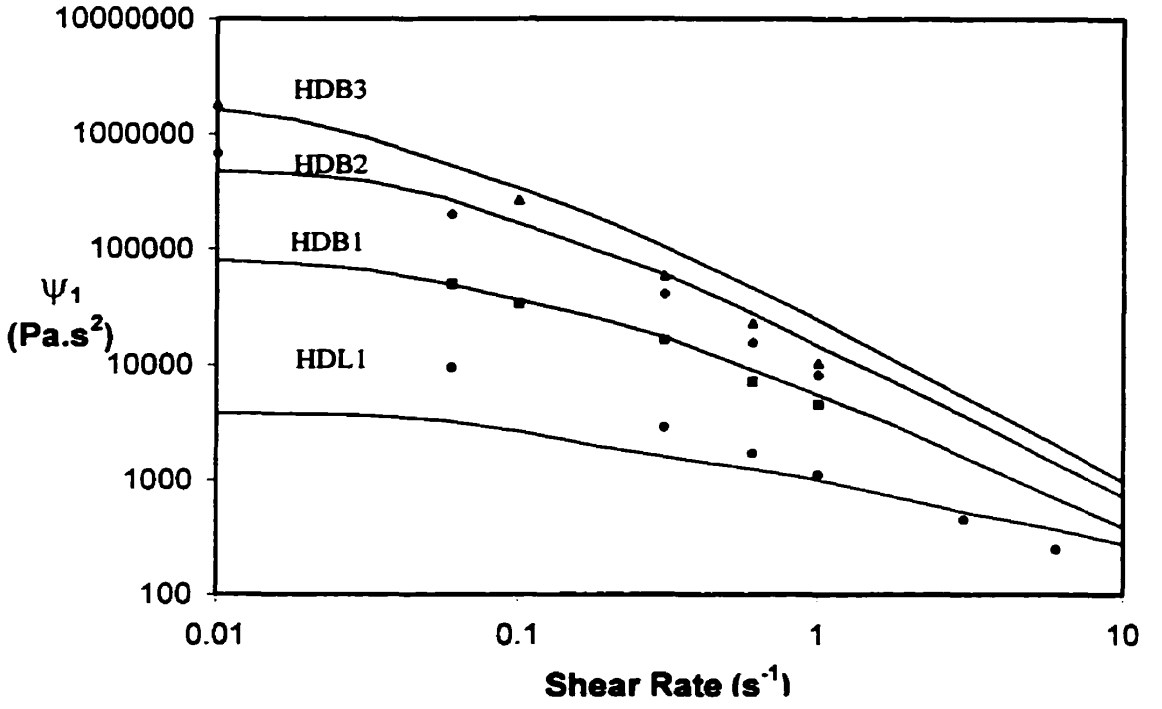

Figure 6.10. Testing the Applicability of Laun's Relation (Equation 6.10)

6.2 Step Strain

It is not possible to subject a material to a truly instantaneous step in strain, and these experiments are therefore performed by applying a strain rate, $\dot{\gamma}$, until the desired strain is reached. This is described by Equation 6.11

$$\gamma = \begin{cases} \dot{\gamma}t & 0 < t \leq \Delta t \\ \gamma_o & \Delta t < t < \infty \end{cases} \qquad [6.11]$$

where Δt is the rise time. The value of $\dot{\gamma}$ must be less than the critical rate for the onset of slip but must be as high as possible in order to minimize the rise time. Step strain experiments were conducted for materials HDL1, HDB1 and HDB3 at 150°C. The gap between the two plates was 1.085 mm and the strain was calculated from the plate displacement.

$$\gamma_o = \frac{\Delta x\,(mm)}{1.085} \qquad [6.12]$$

These experiments involved small plate displacements ranging from 0.27 to 17.36 mm, and the control system was not able to respond quickly enough to generate a constant plate speed during the ramp. This meant that the rise time could not be calculated using the strain and strain rate as in Equation 6.11. Plate position data were used to determine the actual rise time corresponding to each strain and nominal plate speed, and a straight line was fitted to the data (Equation 6.13). Other experimental conditions for this study are given in Appendix B.

$$\Delta t\,(s) = 0.9789\frac{\gamma}{\dot{\gamma}_{nominal}} + 0.0294 \qquad [6.13]$$

To account for the departure from the ideal strain history, the independent variable, 't', of the relaxation modulus is calculated as in Equation 6.14[8].

$$t = t_o - \frac{\Delta t}{2} \qquad [6.14]$$

The reliability of this method was verified for each material by using various nominal plate speeds to apply the same strain. These results are compared in Figure 6.11 and the rise times are given in Table 6.5. At times greater than 0.5 s, the three curves superpose. This indicates that Equation 6.14 is appropriate for HDB3 at a strain of 4, and that above 0.5 s the data are free of the effects of the non-ideal start-up. Therefore, in the case of HDB3, for strains up to 4, stresses measured after $1.6\Delta t$ can be used to calculate a relaxation modulus. Similar experiments were performed for each material at various strains, and the results are given in Table 6.6.

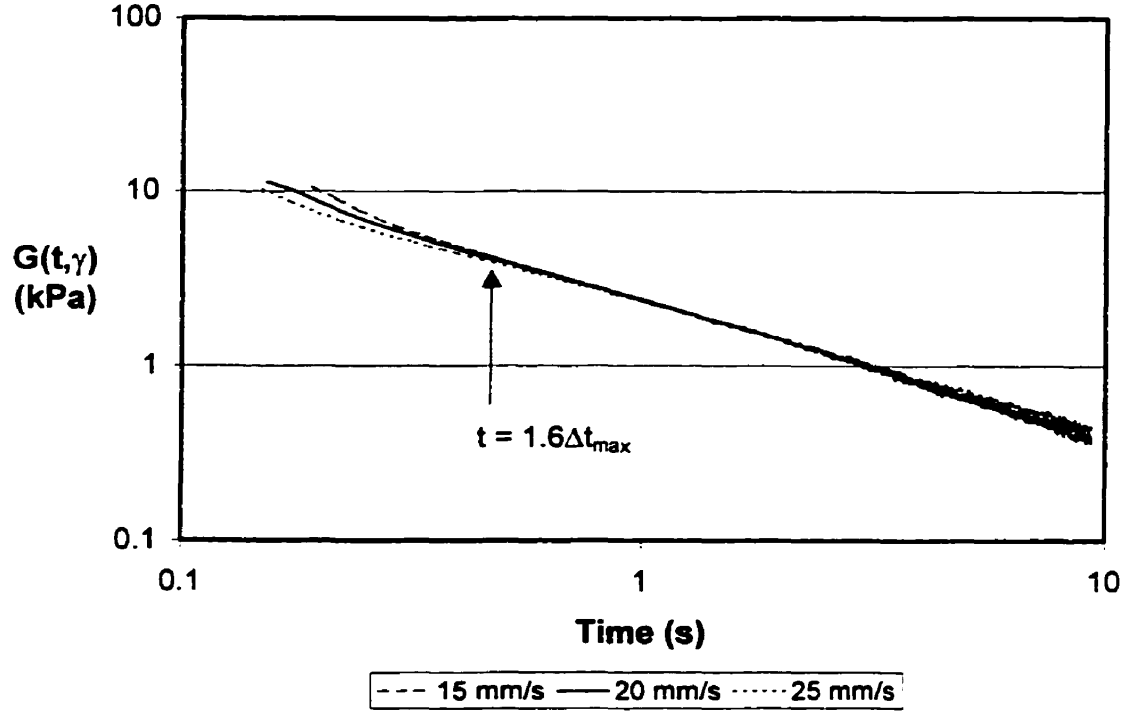

Figure 6.11 Comparison of Relaxation Moduli for HDB3 at a Strain of 4 Measured Using Four Different Nominal Plate Speeds During the Ramp
(Time calculated using Equation 6.14)

Table 6.5 Rise Times Corresponding to the Data shown in Figure 6.11	
Nominal Speed (mm/s)	**Rise Time (s)**
15	0.31
20	0.24
25	0.20

Table 6.6 Times at which Stress Data can be Used to Calculate Relaxation Modulus Values			
Resin	$\gamma_o = 1$	$\gamma_o = 4$	$\gamma_o = 16$
HDL1	Δt	$1.5\Delta t$	$1.6\Delta t$
HDB1	Δt	$1.6\Delta t$	na
HDB3	Δt	$1.6\Delta t$	$3.0\Delta t$

The non-linear relaxation moduli for HDL1, HDB1 and HDB3 are shown in Figures 6.12 through 6.14. The data presented in these three figures were collected using single samples, and replicates were performed to verify these results. For all resins, the curves at the smallest strains were independent of strain and were taken to reflect the linear relaxation moduli. At higher strains the relaxation modulus curves fall below the LVE relaxation modulus. In Figures 6.12 through 6.14, at long times there is a significant amount of noise in the data, especially for HDL1. This noise results from the very low stress levels. The non-linear relaxation moduli in Figures 6.12 to 6.14 can be superposed by vertical shifts, meaning that the time and strain dependencies can be separated as indicated by Equation 6.15.

$$G(t,\gamma) = h(\gamma)G(t) \qquad [6.15]$$

This is demonstrated by Figures 6.15 through 17, where the ratio of the nonlinear to linear relaxation modulus is plotted as a function of time for each strain. After some initial variation this ratio, $h(t,\gamma)$, becomes constant. The value of the damping function, $h(\gamma)$, can be determined at each strain from the long time value of $h(t,\gamma)$. At small strains the damping function approaches a value of 1, which corresponds to LVE behavior. The damping function falls below 1 at the onset of non-linear viscoelastic behavior and continues to decrease as the strain is increased. A lower value of **h** at a certain strain indicates a higher degree of non-linearity in the fluid's response. Damping functions were determined for HDL1, HDB1 and HDB3 and are plotted in Figure 6.18.

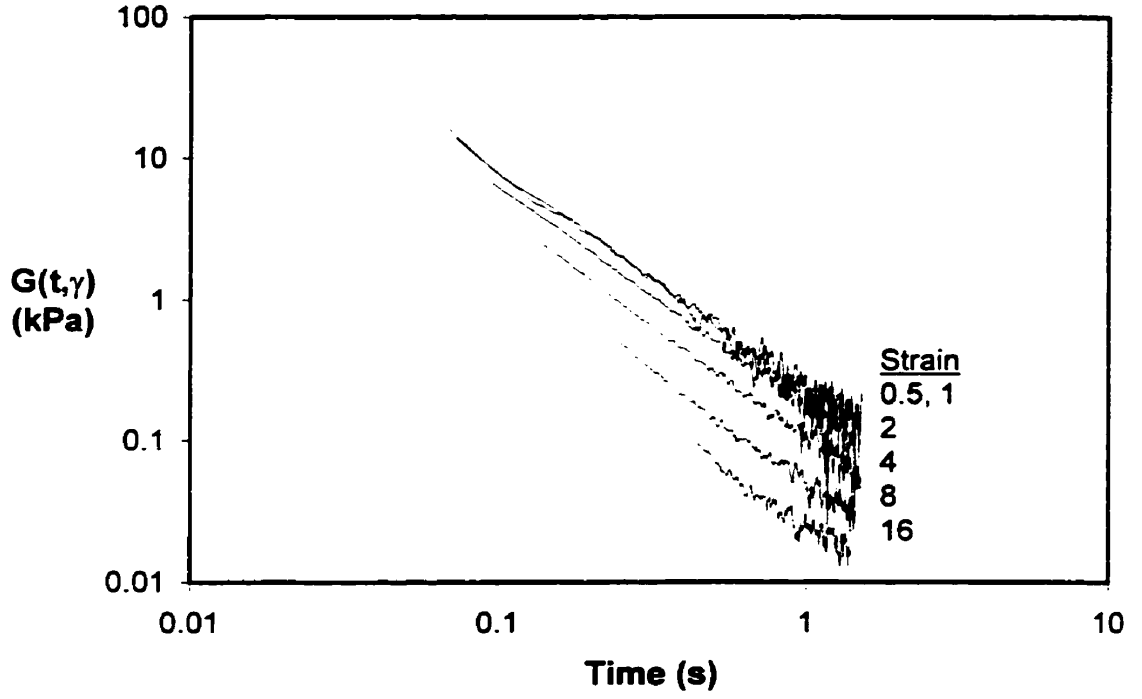

Figure 6.12 Nonlinear Relaxation Modulus Data for HDL1

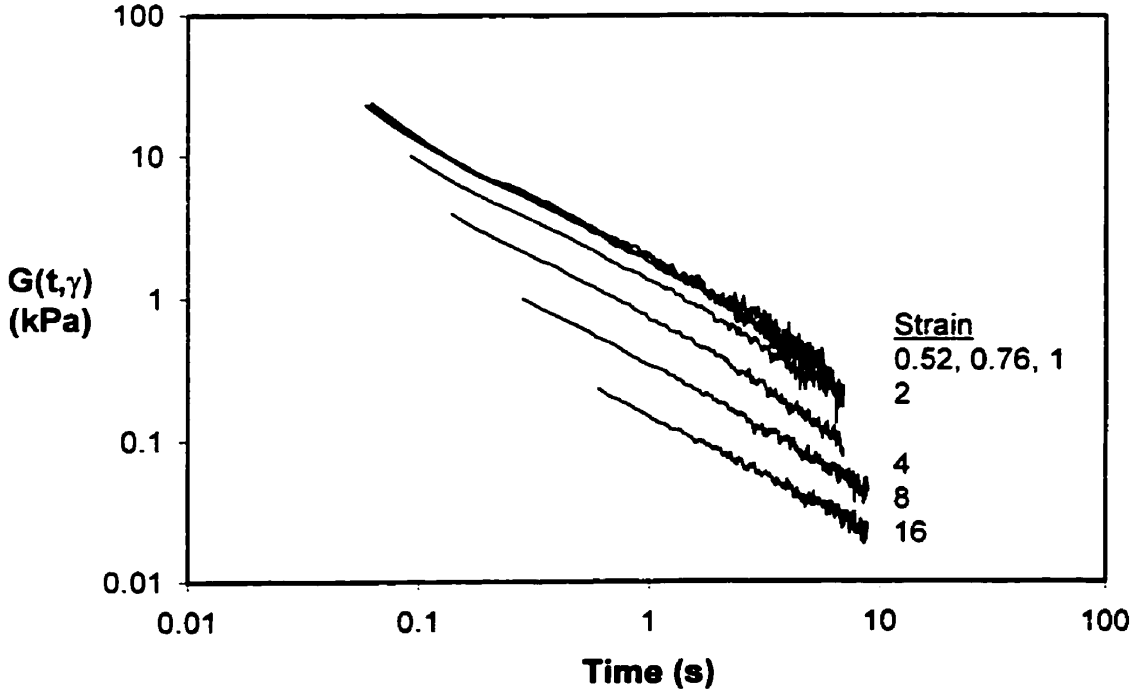

Figure 6.13 Non-linear Relaxation Modulus Data for HDB1

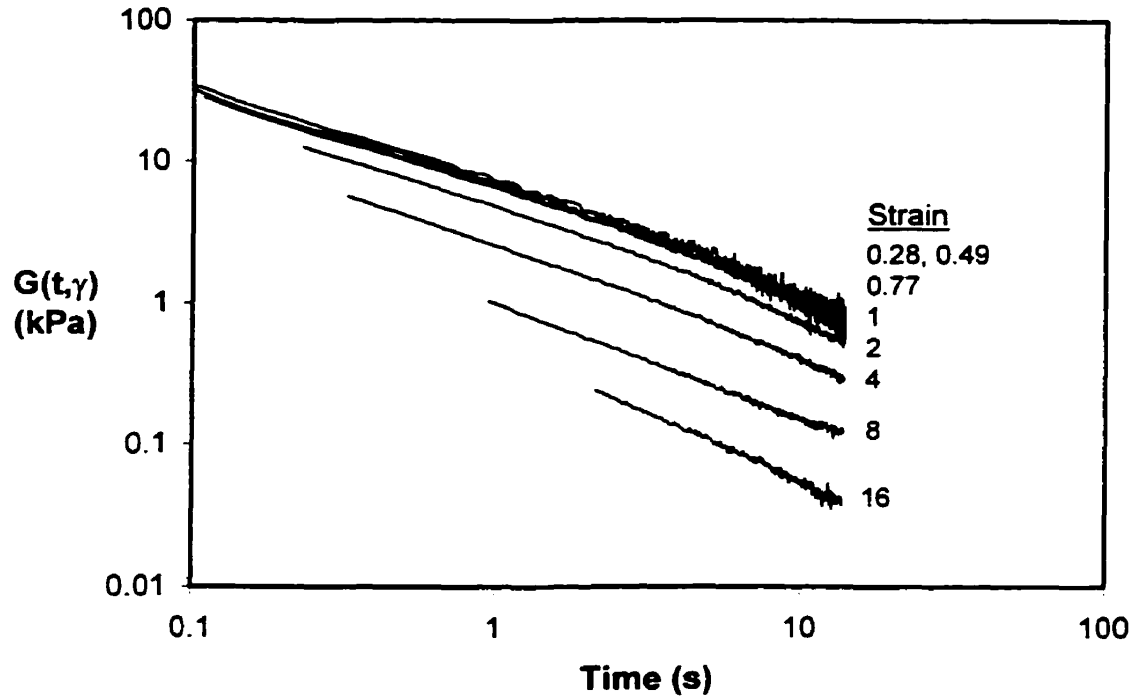

Figure 6.14 Non-linear Relaxation Modulus Data for HDB3

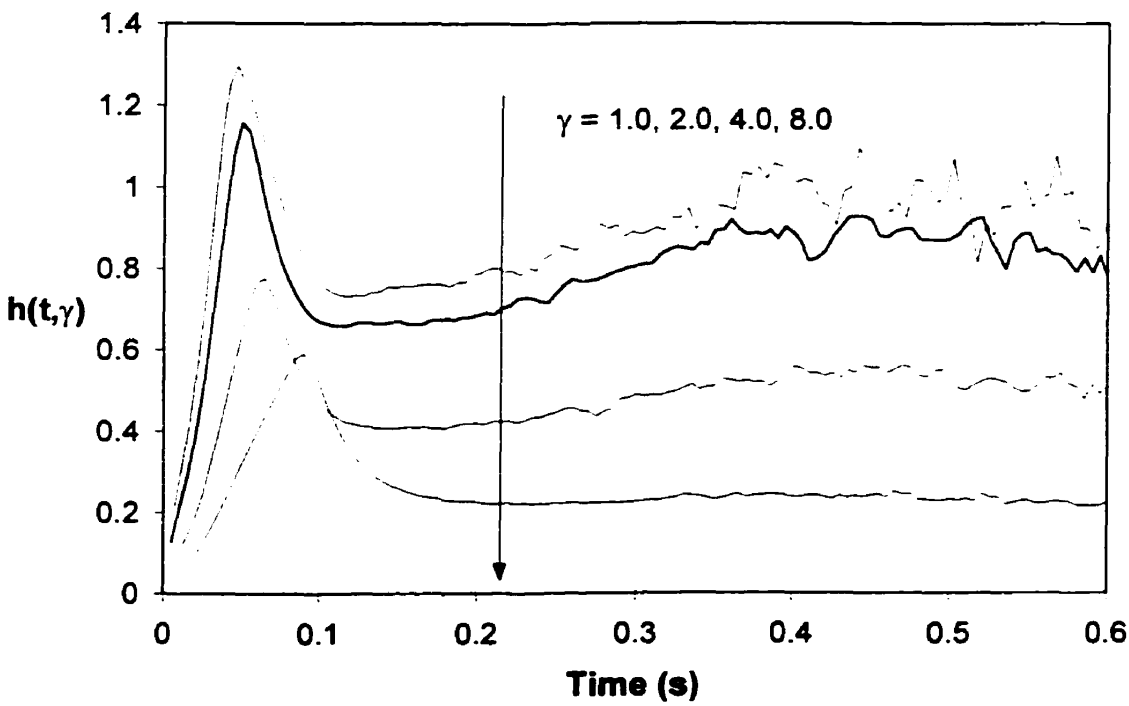

Figure 6.15 Time and Strain Dependent Damping Function for HDL1

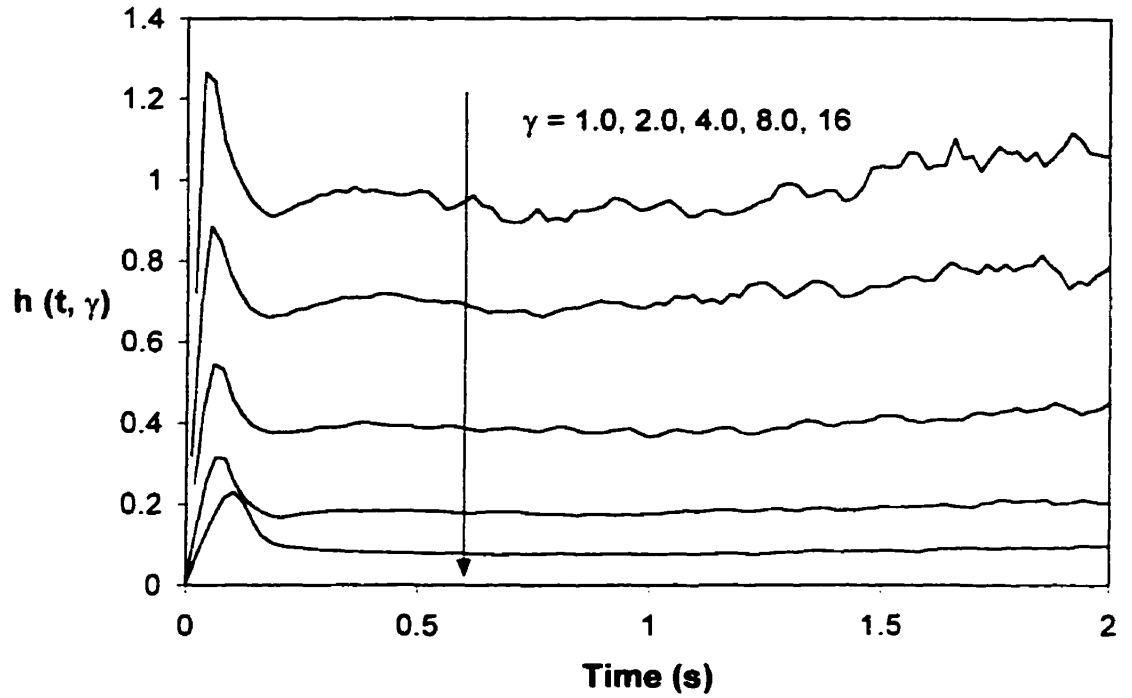

Figure 6.16 Time and Strain Dependent Damping Function for HDB1

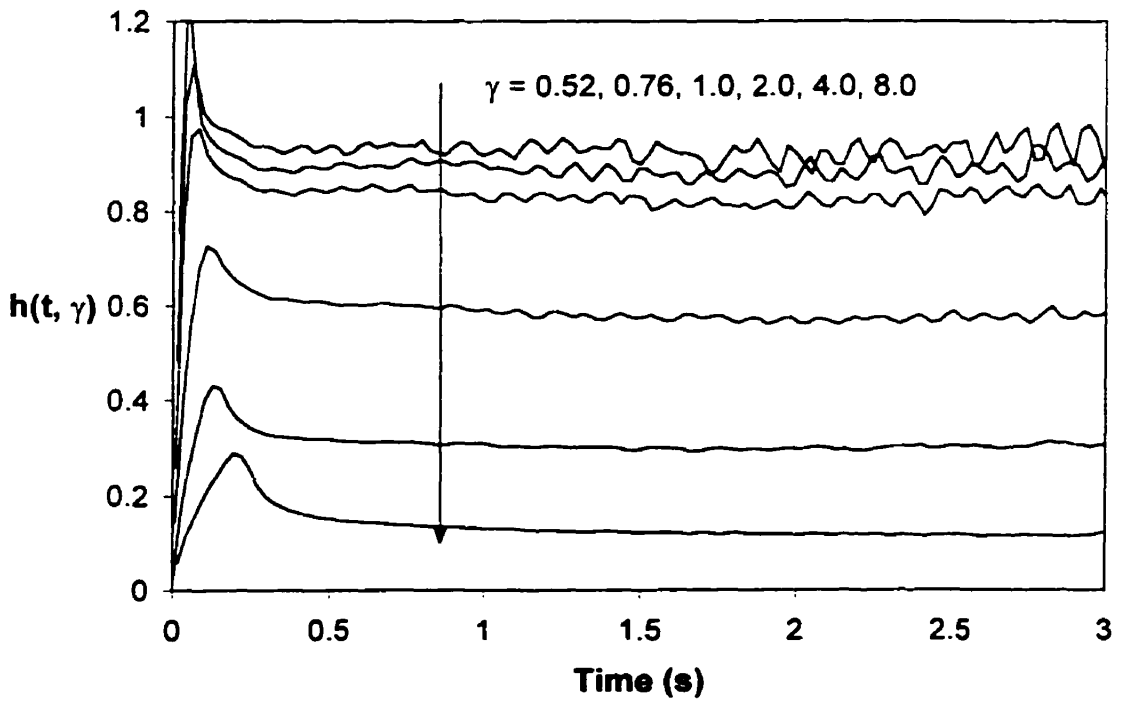

Figure 6.17 Time and Strain Dependent Damping Function for HDB3

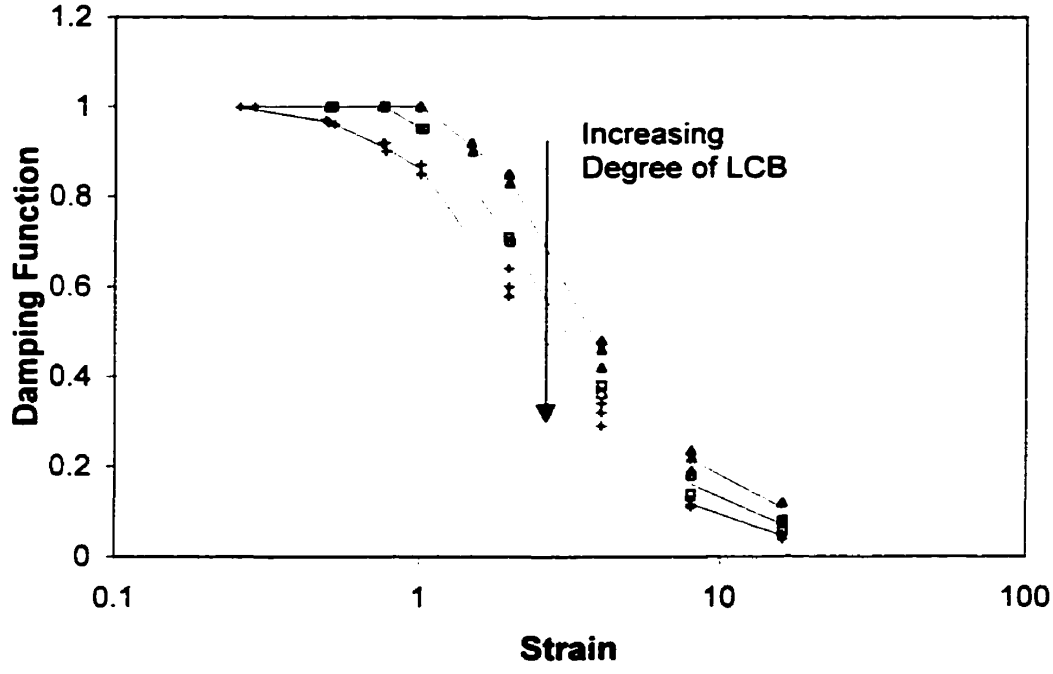

Figure 6.18 Damping Functions for HDL1, HDB1 and HDB3
Curves Represent Average Values at each Strain

In Figure 6.18, we see that LCB causes the onset of non-linear behavior to occur at lower strains and increases the degree of non-linearity at all strains up to $\gamma = 16$. LCB affects the damping function particularly in the region just beyond the LVE zone.

It is useful to fit an equation to damping function data, and several forms have been proposed. One that has been found particularly useful is Equation 6.16, which has only one parameter, **a**. The data in Figure 6.18 were fitted to Equation 16, and the results are given in Table 6.7. For these materials, '**a**' increases with degree of LCB.

$$h(\gamma) = \frac{1}{1 + a\gamma^2} \qquad [6.16]$$

The damping function curves calculated using Equation 6.16 are compared to the experimental data in Figure 6.19. Equation 6.16 fits the data for HDB3 very well at all strains. For HDL1 and HDB1, Equation 6.16 is not able to describe the small strain behavior, but it fits well at higher strains. We can compare the damping functions of the mPEs with that predicted by the Doi-Edwards theory, which is considered to represent a lower bound, and the measured damping is always less than the Doi-Edwards prediction.

Table 6.7 Results of Fitting Equation 6.16 To the Data in Figure 6.15

Resin	LCB/10 000 C	a
HDL1	0	0.05921
HDB1	0.12	0.09607
HDB3	0.42	0.1492

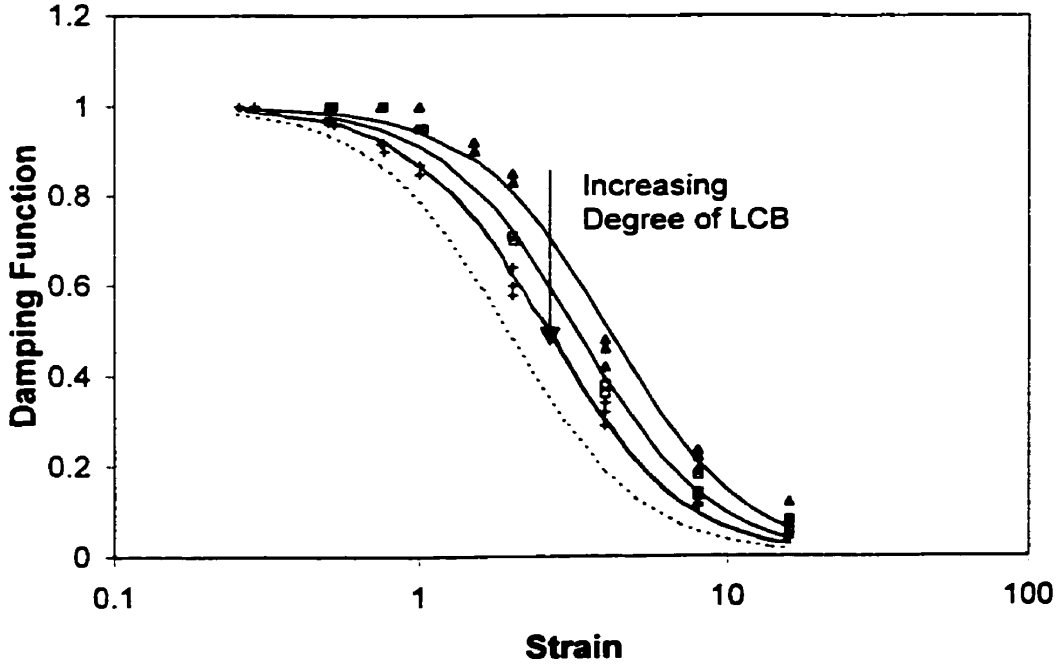

Figure 6.19 Damping Functions for HDL1, HDB1 and HDB3
(Solid curves represent best fit of Equation 6.16 and broken curve represents Doi-Edwards Model)

The results presented above do not agree with those of some published reports (see section 2.1.4.2). In general, it has been reported that LCB either has no effect on the damping function or results in less damping[9,10,11,12,13]. With the exception of the work of Yoshikawa and coworkers[13], who found that the damping function was not affected by LCB, all of these studies involved materials with much higher degrees of LCB than those present in the materials studied here. Osaki and coworkers[14], who studied solutions of star polymers with relatively low degrees of entanglement, did report that LCB resulted in enhanced damping.

In Chapter 8, we show that the damping functions determined for these materials using step strain experiments are in accord with data for steady simple shear and large amplitude oscillatory shear. This leads us to conclude that the damping functions measured here are valid and that the relationship between degree of LCB and damping that we have observed is correct.

6.3 Large Amplitude Oscillatory Shear

In these experiments the sample was subjected to the large amplitude sinusoidal strain described by Equation 6.17. In contrast to small amplitude oscillatory shear where the stress response is also sinusoidal, the stress in this case is no longer sinusoidal and can be described by Equation 6.4. The parameters in this equation are evaluated by performing discrete Fourier transforms of the data.[15]

$$\gamma = \gamma_o \sin(\omega t) \qquad [6.17]$$

Samples were compression molded using the same conditions as were used for the samples for dynamic linear viscoelastic testing (Section 5.1)

Figure 6.20 shows an example of the transient data from a large amplitude oscillatory shear (LAOS) experiment. These data can be described by fitting the parameters of Equation 6.4 using the discrete Fourier transform[15]. The effect of LCB on

LAOS behavior is shown in Figures 6.21 and 6.22, which show the first harmonic of the shear stress, σ_1, as a function of strain amplitude, at a constant frequency. Data for four of the high density mPEs are shown in these graphs. Essentially the effect of LCB is to increase σ_1, with the exception of HDB1, which has lower stresses than HDL1 at both frequencies. The increase in σ_1 is a result of the increase in zero shear viscosity due to the increased level of LCB. However, since LCB also causes greater shear thinning, at some point the shear dependent viscosity of a branched material can be lower than that of a linear material. This is why HDB1, which has a higher zero shear viscosity than HDL1, has lower σ_1 values under the conditions studied.

The degree of non-linearity in the material's response can be evaluated by looking at the magnitudes of the higher harmonics of stress. The presence of significant higher harmonics indicates that the response is nonlinear. Figure 6.23 shows the effect of strain amplitude on the third harmonic of stress for the same four resins. We see that σ_3 correlates directly with degree of LCB. In other words, increasing the degree of LCB results in an increasingly nonlinear response to LAOS.

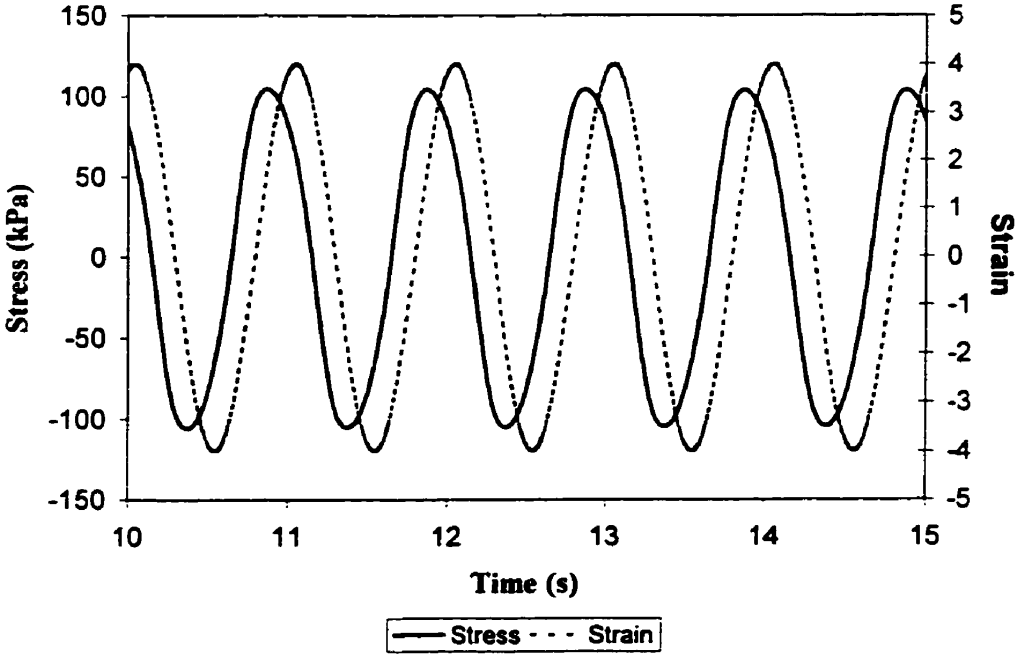

Figure 6.20 Real Time Stress and Strain Curves for HDB3 Under LAOS at $\gamma = 4$ and $\omega = 2\pi$ rad/s.

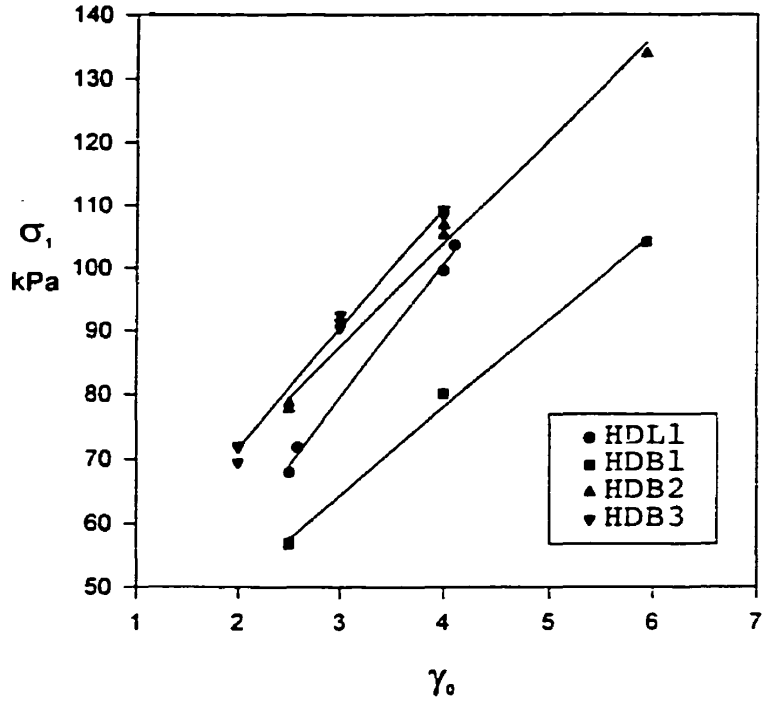

Figure 6.21 Effect of γ_o on the First Harmonic of the Shear Stress at $\omega = 2\pi$ rad/s

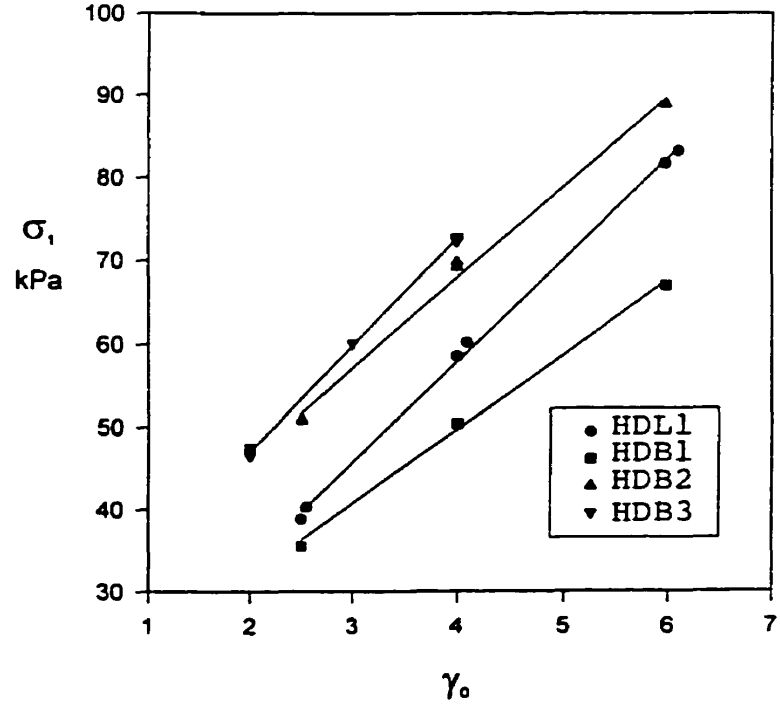

Figure 6.22 Effect of γ_o on the First Harmonic of the Shear Stress at $\omega = \pi$ rad/s

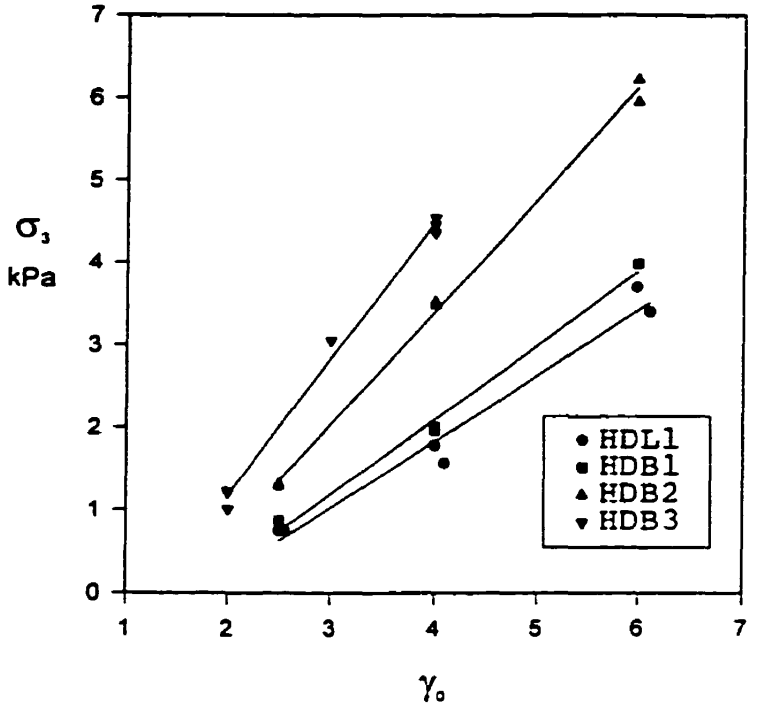

Figure 6.23 Effect of γ_o on the Third Harmonic of the Shear Stress at $\omega = \pi$ rad/s

LAOS data can also be compared qualitatively by making closed-loop stress versus strain rate plots as shown in Figures 6.24 through 6.28. Figure 6.24 shows the effect of strain amplitude on the response to LAOS for HDB3, which is a high density branched mPE. There are two effects of increasing the strain amplitude: (1) the magnitude of the stress response increases and (2) the loop departs increasingly from an ellipse. Figure 6.25 shows the effect of the strain amplitude for HDL1, the high density linear mPE. We see similar though less prominent effects of increasing strain amplitude for HDL1 in comparison with HDB3. It is the second effect, the distortion of the loop, that is the manifestation of nonlinearity in this type of plot. The higher degree of distortion in the response for HDB3 is what we expect, as we saw previously that branched materials display a higher degree of nonlineraity in their response than do linear materials. Figures 6.26 and 6.27 show the effect of increasing frequency at constant strain amplitude for HDB3 and HDL1 respectively. The distortion of the loops is even more apparent at the higher frequency.

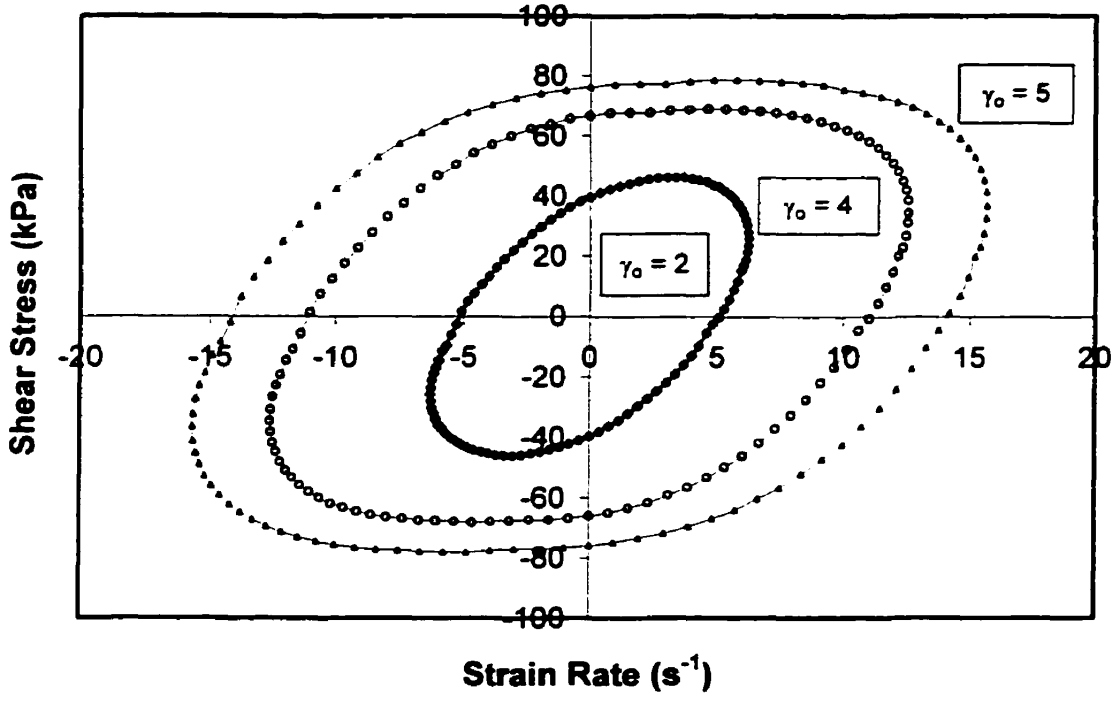

Figure 6.24 Effect of γ_o on Closed Stress vs. Strain Rate Loop HDB3, π rad/s

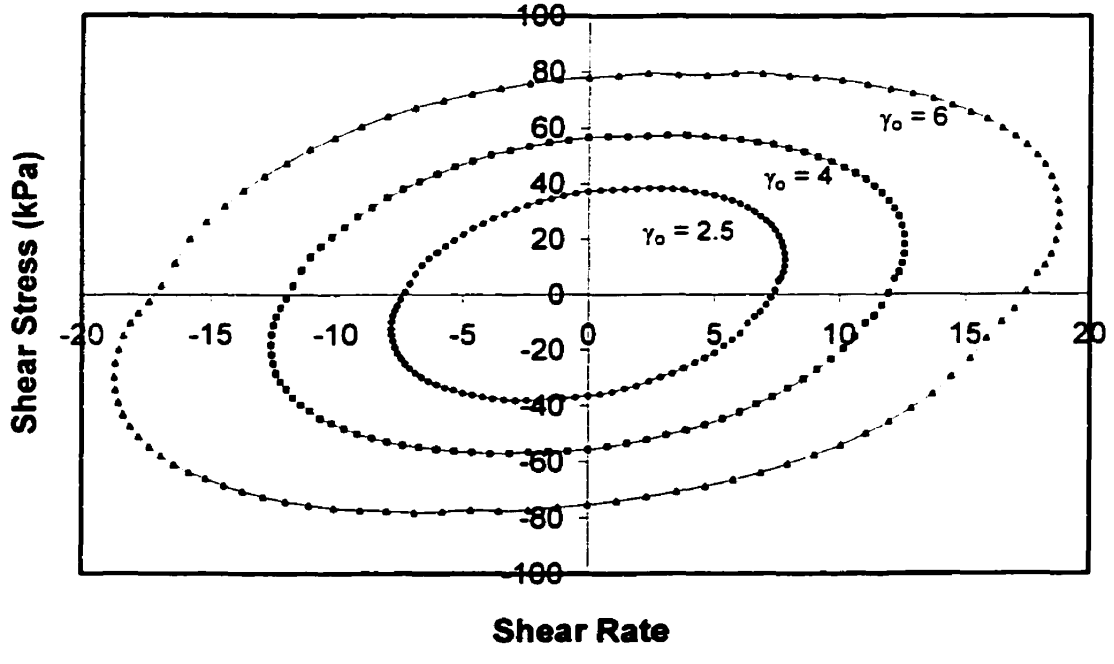

Figure 6.25 Effect of γ_o on Closed Stress vs. Strain Rate Loop HDL1, π rad/s

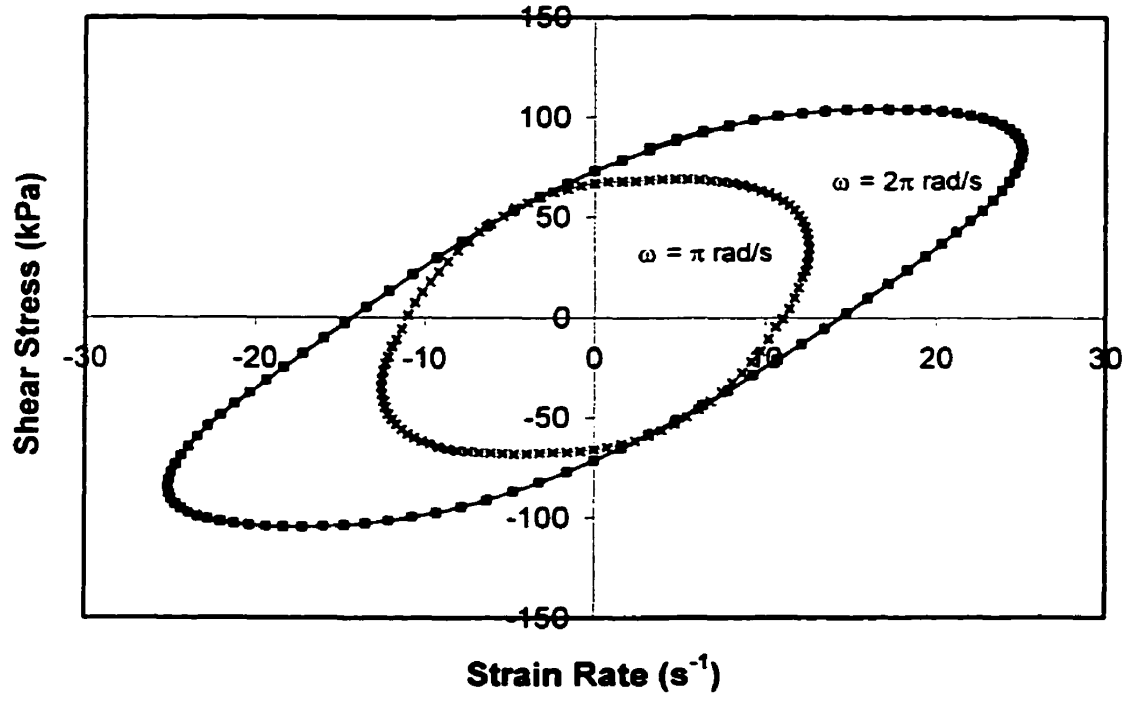

Figure 6.26 Effect of ω on Closed Stress vs. Strain Rate Loop HDB3, $\gamma_o = 4$

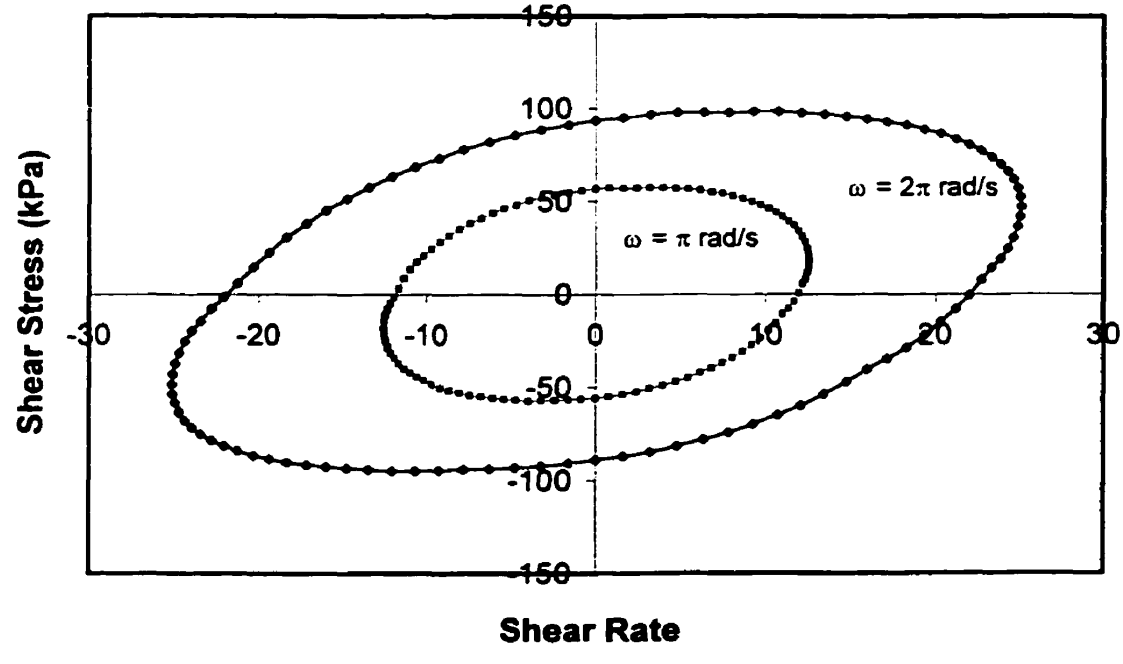

Figure 6.27 Effect of ω on Closed Stress vs. Strain Rate Loop HDL1, $\gamma_o = 4$

In Figure 6.28 the effect of LCB on the closed loop stress response is illustrated by plotting reduced shear stress against reduced shear rate for three of the high density mPEs. Once again, we see the increasing degree of distortion of the loop with increasing degree of LCB. Figures 6.29 and 6.30 show another method of comparing the behavior of different materials. In these figures, the solid curve represents the linear response at the same frequency, which was calculated using Equation 6.18

$$\frac{\sigma(t)}{\gamma_o} = G^* \sin(\omega t + \delta) \qquad [6.18]$$

where G* and δ are calculated from the discrete spectra. The points in these plots are the experimental LAOS data. The LAOS response for the branched material (HDB3) is quite different than its linear response at this frequency while the two responses for the linear material (HDL1) are very similar.

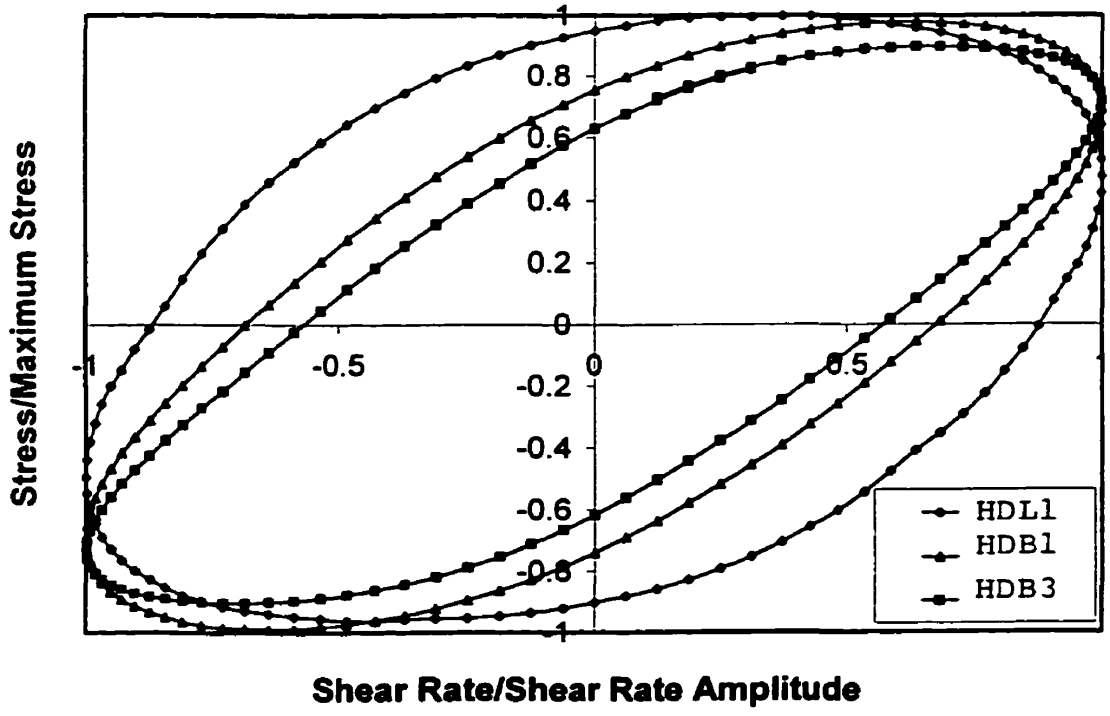

Figure 6.28 Effect of LCB on Closed Loop Stress Response to LAOS
$\omega = 2\pi$ rad/s, $\gamma_o = 4$

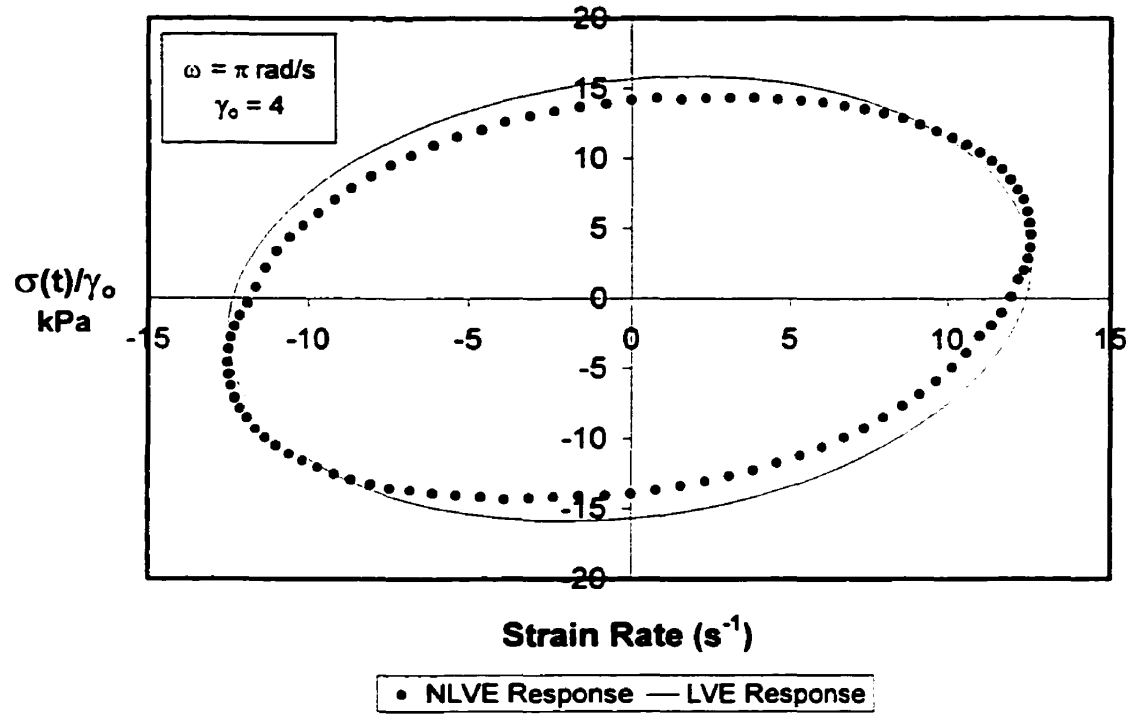

Figure 6.29 Comparison between Linear and Nonlinear Response to LAOS HDL1

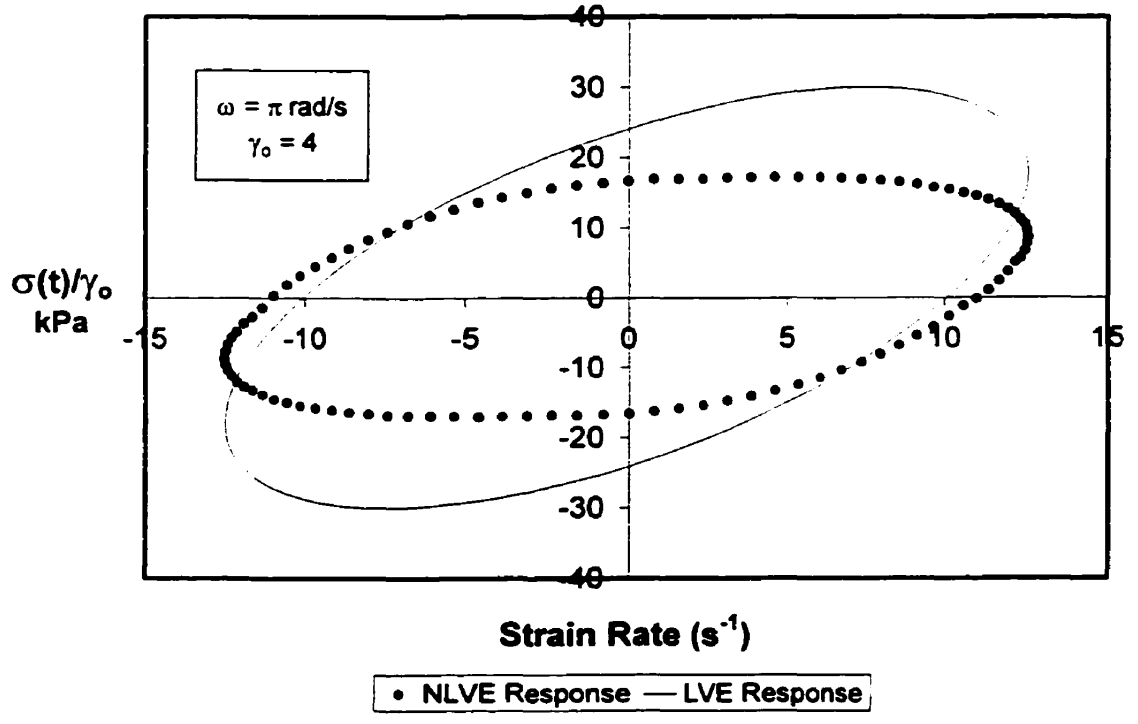

Figure 6.30 Comparison between Linear and Nonlinear Response to LAOS HDB3

List of References

[1] John M. Dealy and Kurt F. Wissbrun, *Melt Rheology and its Role in Plastics Processing: Theory and Applications*, Van Nostrand Reinhold New York, 1990

[2] François Koran, *Anomalous Wall Slip Behavior of Low Density Polyethylenes*, Master's Thesis, Department of Chemical Engineering, McGill University, July 1994.

[3] W.P. Cox and E.H. Merz, *J. Polym. Sci.*, 28:619 (1958)

[4] W. Gleissle, in *Rheology, Vol. 2*, edited by G. Astarita, G. Marrucci and L. Nicolais (Proc. 8th Intern. Congr. Rheol.) Plenum Press, New York, p. 457 (1980).

[5] H.M. Laun, *J. Rheol.*, 30:459 (1986)

[6] R.G. Larson, *Rheol. Acta.*, 24:327 (1985)

[7] K.F. Wissbrun, *J. Rheol.*, 30:1143 (1986)

[8] L.J. Zapas, J. Res. N. B. S. 75a:33 (1971)

[9] Archer, A.R. and S.K. Varshey, work submitted for publication (1998)

[10] Macosko, C.W. and Kasehagen, work submitted to *J. Rheol.* for publication (1998)

[11] Laun, H.M., *Rheol. Acta*, Vol. 17, 1-15 (1978)

[12] Osaki, K., *Rheol. Acta*, Vol.32, 429-437 (1993)

[13] Yoshikawa, K. *et al*, *Polymer Rheology and Processing*, Edited by A.A. Collyer and L.A. Utracki, Chapter 2, Elsevior Science Publishers Ltd. (1990)

[14] Osaki, K. *et al*, *Macromolecules*, Vol. 23, No. 20, 4392 (1990)

[15] A.J. Giacomin and J.M. Dealy, in *Techniques in Rheological Measurement*, edited by A.A. Collyer, Chapman and Hall, London, 1993.

Chapter 7.

Nonlinear Viscoelasticity in Extension

The response of a polymer melt to large or fast deformations is nonlinear in that it depends on the kinematics as well as the magnitude and rate of the deformation. Therefore, as was discussed in Chapter 6, in order to characterize a polymer's nonlinear viscoelastic behavior its response to many different types of deformations must be studied. In particular, one must determine the effects of both shearing and extensional deformations on the material. An extensional deformation involves stretching along the streamlines. The two uniform, shearfree, axisymmetric extensional flows are uniaxial and biaxial extension. Uniaxial extension involves stretching along the axis of symmetry and biaxial extension involves stretching in the radial direction and compression along the axis of symmetry. In the present study, uniaxial extension experiments were used.

The strain measure used for extensional deformations is the Hencky strain (Equation 7.1). The corresponding measure of deformation rate (Equation 7.2) has the useful characteristic that it does not depend upon the initial sample length.

$$\varepsilon = \ln\left(\frac{L}{L_o}\right) \qquad [7.1]$$

$$\dot{\varepsilon} = \frac{d\ln(L)}{dt} \qquad [7.2]$$

The rheologically significant stress in this flow, the extension stress, is defined in Equation 7.3.

$$\sigma_E \equiv \sigma_{11} - \sigma_{22} = \sigma_{11} - \sigma_{33} \qquad [7.3]$$

One of the tests that is most useful for studying uniaxial extensional flow behavior is the start-up of steady simple extension. In this test, the material, which is initially at rest, is subjected to a simple extension with a constant Hencky strain rate. The tensile stress growth coefficient is defined in Equation 7.4.

$$\eta_E^+(t,\dot{\varepsilon}) \equiv \frac{\sigma_E(t,\dot{\varepsilon})}{\dot{\varepsilon}} \qquad [7.4]$$

At longer times, steady state is reached and the limiting value of the extensional stress is used to calculate the extensional viscosity.

$$\eta_E = \frac{\sigma_E(\dot{\varepsilon})}{\dot{\varepsilon}} \qquad [7.5]$$

If the magnitude or the rate of the deformation is small enough the theory of linear viscoelasticity will apply and the tensile stress growth coefficient will be related to the linear relaxation modulus as shown below.

$$\eta_E^+(t) = 3\eta^+(t) = 3\int_0^t G(s)ds \qquad [7.6]$$

The measurement of extensional flow properties is more difficult than that of shear flow properties and much work has been put into developing reliable techniques. Münstedt[1] and Meissner[2] developed two of the most successful experimental techniques. In Münstedt's extensional rheometer a small sample is attached with an adhesive to a stationary bottom plate which is coupled to a load cell. The top of the sample is attached to a flexible band which is drawn upwards by a servomotor. The entire deformation takes place in a vertical oil bath. With this instrument both constant rate and constant stress

tests are possible. Meissner's extensional rheometer uses metal conveyor belt clamps to stretch the sample horizontally while supported by a cushion of nitrogen. One clamp is mounted at the bottom of two leaf springs, which are bent by the tensile force resulting from the deformation of the sample. An LVDT is used to measure the displacement of the springs, which is proportional to the force exerted by the sample. Constant rate tests are performed with this instrument.

7.1 Experimental Procedures and Data Analysis

7.1.1 Experimental Apparatus

For the present work, extensional flow experiments were performed with a Meissner type rheometer, the Rheometrics melt elongational rheometer (RME). A schematic of the clamps and sample positioning is shown in Figure 7.1. The sample, clamps, and leaf springs are housed in an oven, which is heated by electrical heater wires embedded in the walls. A cushion of nitrogen that supports the sample is formed by compressed nitrogen that flows though a frit. The nitrogen is preheated by passing it through a copper tube inserted in the electrically heated back wall of the oven. The initial sample length, L_o, is equal to the distance between the tips of the clamps (54.5 mm). The conveyor belts rotate in the directions shown in Figure 7.1 at constant rates and the sample is stretched horizontally between the two clamps. Strain rates between 0.0001 and 1 s^{-1} are possible, although useful measurements at the lowest rates are often not possible due to sample sagging and extremely small stresses.

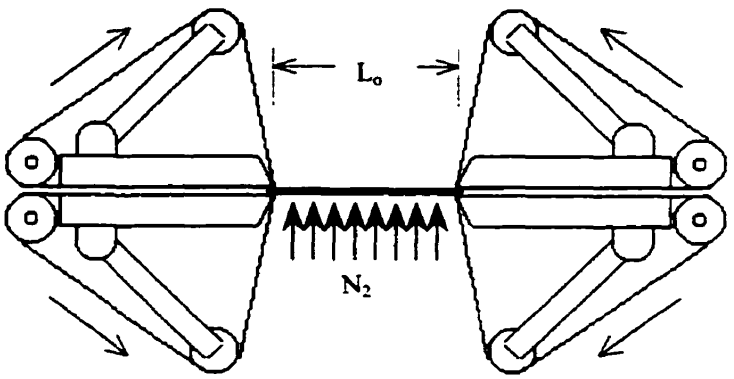

Figure 7.1 Schematic of Flow Situation in RME

The sample can be stretched up to a Hencky strain of 7 in this instrument. There are problems associated with measurements at higher strains, which will be discussed in section 7.1.3. The tensile force can be measured between 0.001 and 2 N with a resolution of 0.001 N.

Samples were prepared by compression molding. To avoid sample deformation during melting in the rheometer, care was taken to ensure that there were no significant residual stresses in the sample after molding. The samples were approximately 57 mm in length with a rectangular cross section (width 7mm, height 1.3 mm). Measurements were performed on the low density mPEs at 130°C and on the high density mPEs at 150°C. For the purpose of studying the effect of temperature on the non-linear extensional flow behavior, measurements were performed on LDB3 at both 130°C and 150°C.

7.1.2 Calculating Strain and Stress from Measured and Controlled Variables

The strain rate is related to the belt velocity as in Equation 7.7 and the strain as a function of time is given by Equation 7.8.

$$\dot{\varepsilon} = \frac{2v}{L_o} \qquad [7.7]$$

$$\varepsilon = \frac{2vt}{L_o} \qquad [7.8]$$

It is possible that the true strain rate will differ from the nominal rate applied by the belts at least at some times during the test. The true strain rate can be measured by marking the sample with small glass beads and using an image processing routine to analyze video records of the tests. When the experiments were performed for the present study the image analysis software was not available, therefore in all of the following analysis we assume that the true extension rate was defined by Equation 7.7.

As the sample is stretched at a constant extension rate its dimensions change as in Equations 7.8 and 7.9.

$$L(t) = L_o \exp(\dot{\varepsilon} t) \qquad [7.8]$$

$$A(t) = H(t)W(t) = H_o W_o \exp(-\dot{\varepsilon} t) \qquad [7.9]$$

H_o and W_o are the height and width of the sample just before the deformation begins. These dimensions are different from the dimensions of the molded sample due to thermal expansion. Thermal expansion is accounted for with Equation 7.10

$$A_o = H_{RT} W_{RT} \left(\frac{\rho_{RT}}{\rho_{TT}} \right)^{2/3} \qquad [7.10]$$

where the subscript RT and TT refer to room temperature and test temperature respectively. The melt density as a function of temperature for LDB3 is shown in Figure 7.2. These data were also used for all the high and low density mPEs since comonomer content does not affect melt density.

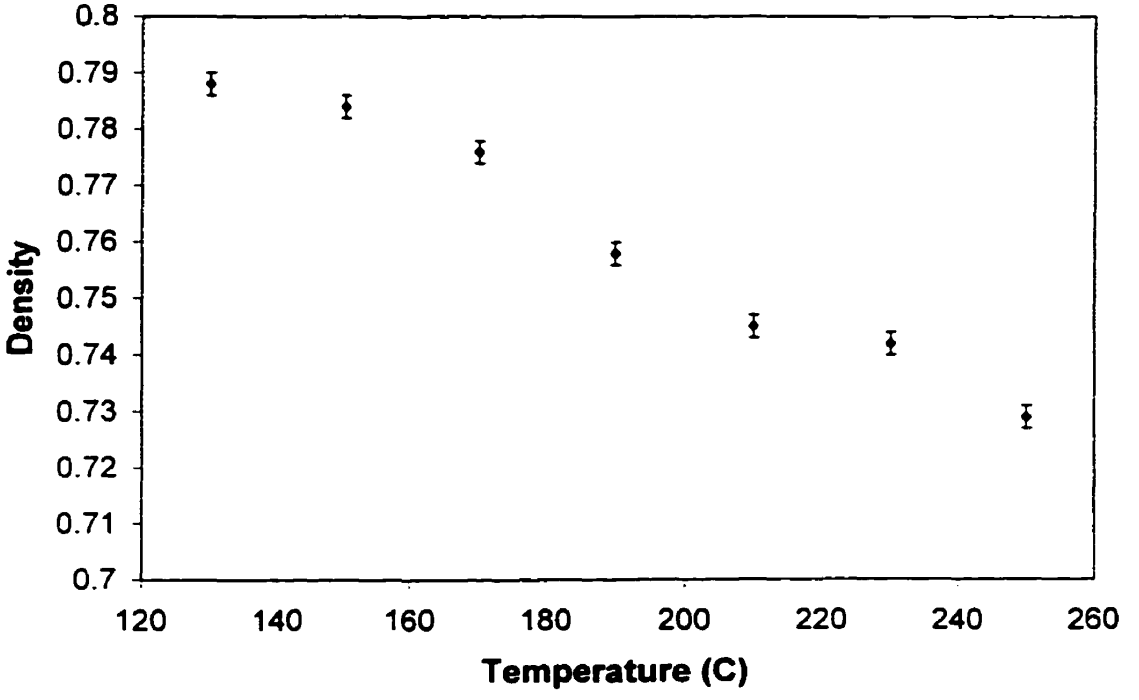

Figure 7.2 Effect of Temperature on Density (LDB3)

The extensional stress is calculated from the measured force using Equation 7.11. It is important to note that any errors in the extension rate will be magnified exponentially in the calculation of the stress.

$$\sigma_E(t) = \frac{F(t)}{A(t)} = \frac{F(t)}{A_o \exp(-\dot{\varepsilon} t)} \qquad [7.11]$$

Before the stress is calculated using Equation 7.11 the force as a function of time curve should be examined to allow the removal of erroneous data. Two types of non-ideal experimental conditions can be identified with the force curve: (1) sample sticking to or touching the nitrogen frit on top of the sample table and (2) sample breaking at high strains. In Figure 7.3, the force curve from an experiment where the sample touched the table twice is compared to the force curve that was generated at the same strain rate without touching the table. The effect of the sample touching the table is an increase in force and therefore viscosity. Once the sample has touched the table, the entire run is invalid and data should be discarded. The force curve from an experiment when the sample broke is plotted in Figure 7.4. In this case 3.42 s into the test the sample started to neck down and finally broke at 4 s. This situation results in a lower than expected force and viscosity after necking down begins and a zero force when the sample breaks. The data up until the point of necking down are valid, and thus for this run the data before 3.42 s can be used to calculate the tensile stress growth coefficient.

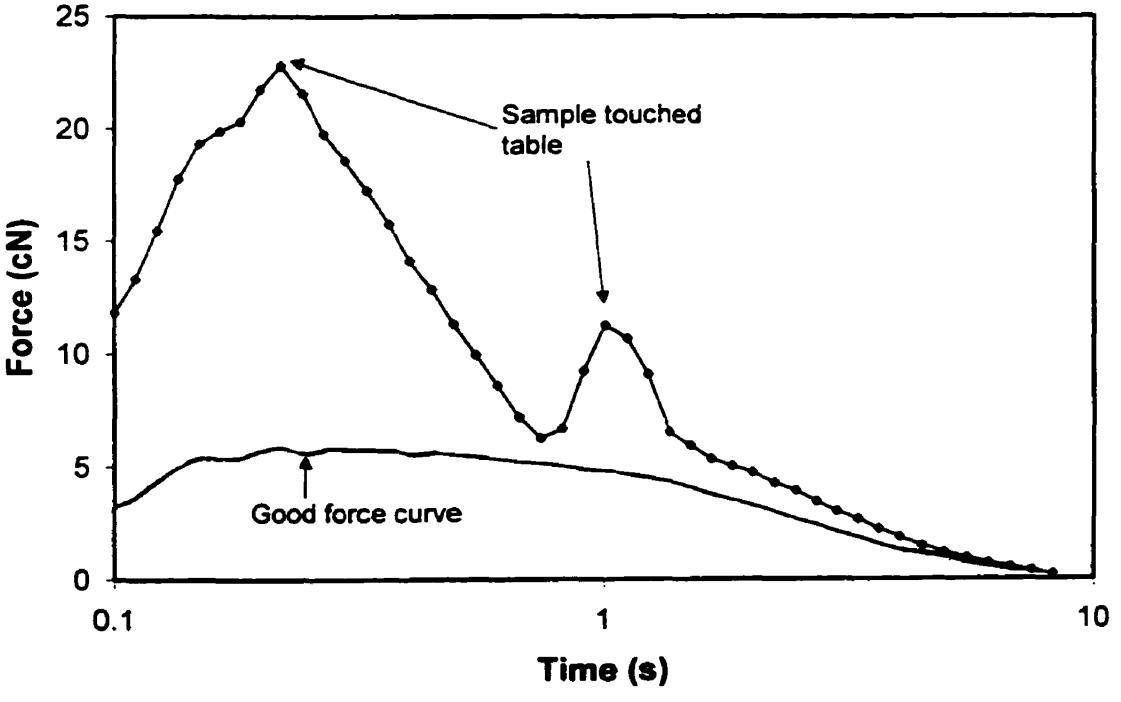

Figure 7.3 Effect of Sample Touching Table on Force Curve
HDL1, $\dot{\varepsilon} = 0.5\ s^{-1}$

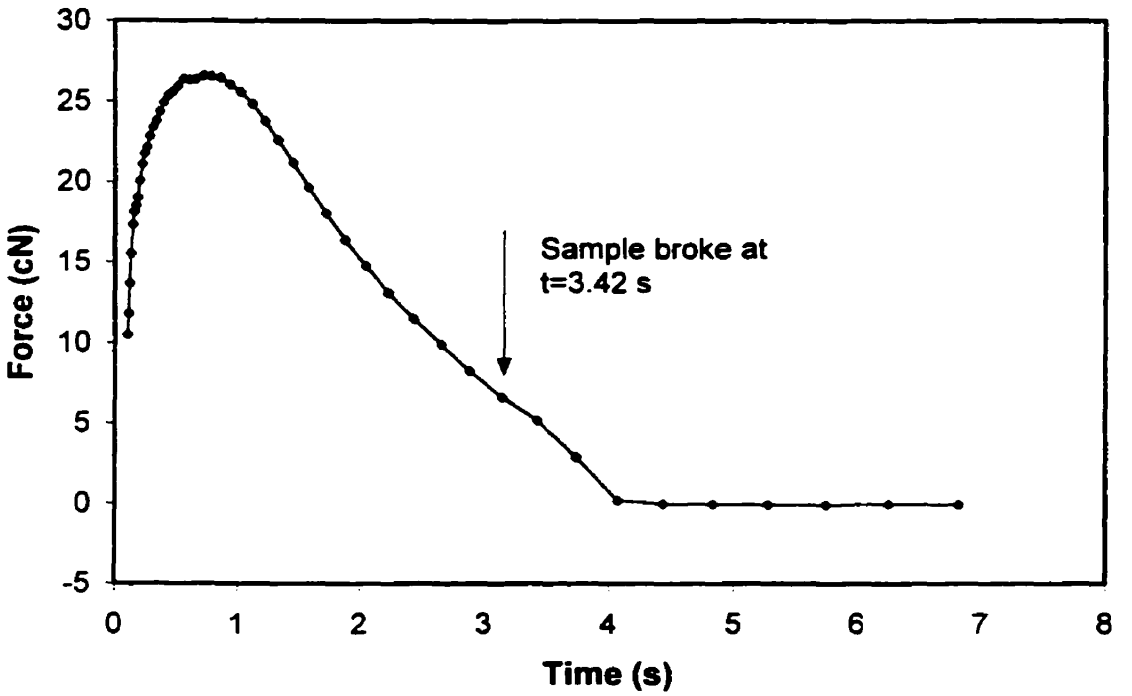

Figure 7.4 Example of a Force Curve When Sample Breaks
HDB3, $\dot{\varepsilon} = 1\,s^{-1}$

7.1.3 Sources of Error in Measurement Technique

There are several significant sources of error in the measurement technique that was used in this work. One problem is the sagging of the sample that occurs after melting and before the stretching begins. When the conveyor belts first begin to turn the slack due to the sagging of the sample is being taken up and the measured forces and therefore viscosities are lower than would be expected. Previous work has found that this problem affects the data only at the beginning of the test; at higher strains the initial sagging has little effect on the results[3]. In Figure 7.5, the tensile stress growth coefficient at $0.1s^{-1}$ is compared to the LVE response (calculated from Equation 7.6 using the discrete spectrum) for HDB3. In this case, because of the sample sag the tensile stress growth function is below the LVE response at times before about 1 s. There is good agreement between the tensile stress growth coefficient and the LVE response in the intermediate region before strain hardening begins.

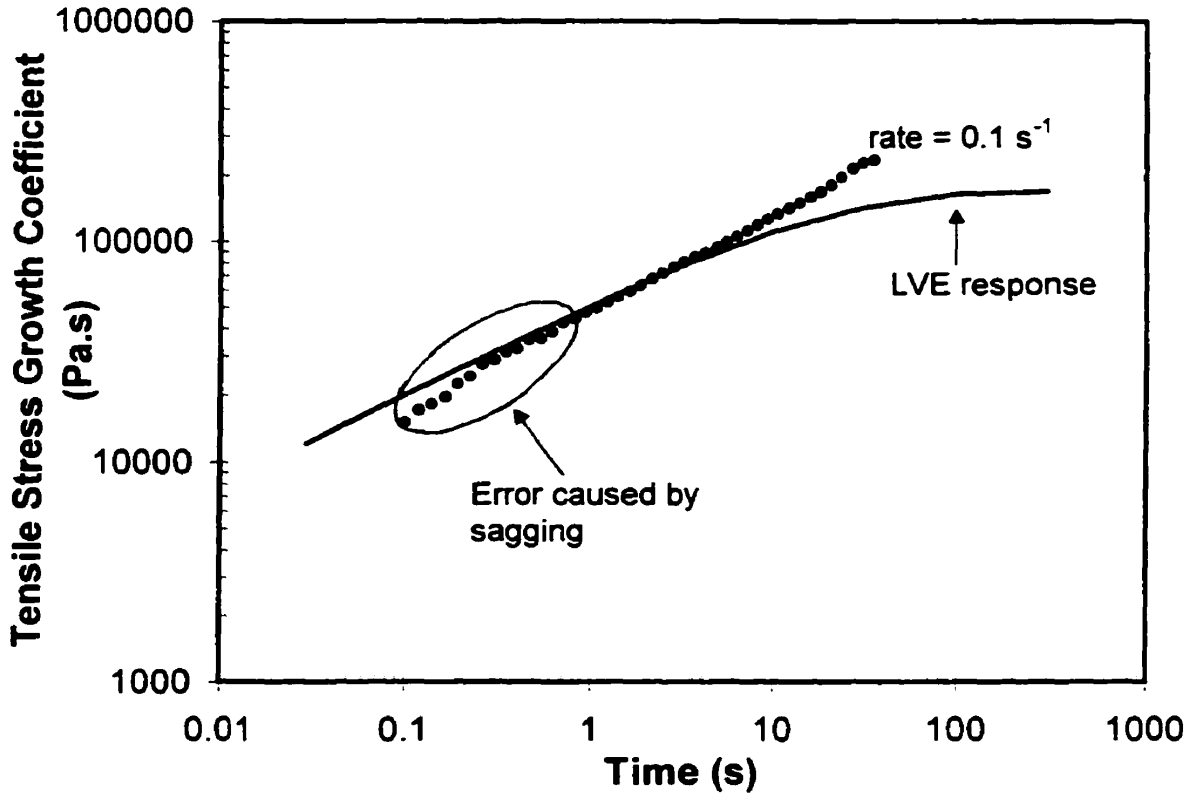

Figure 7.5 The Effect of Sample Sag on Tensile Stress Growth Coefficient

A second source of error is the uncertainty in the strain rate. Since it was not possible to measure the true strain rate, it was assumed that the strain rate was defined by Equation 7.7. Meissner and Hostettler[2] showed that this assumption results in approximately 1% error in the strain rate. The effect of this error on the stress can be determined by performing an error propagation analysis (Equation 7.12). In Equation 7.12 and all subsequent equations in this section Δ means uncertainty (i.e. Δx means uncertainty in x).

$$\Delta\sigma_E\Big|_{\dot{\varepsilon}} = \frac{\partial\sigma_E}{\partial\dot{\varepsilon}}\Delta\dot{\varepsilon} = t\left[\exp(\dot{\varepsilon}t)\right]\frac{F(t)}{A_o}\Delta\dot{\varepsilon} \qquad [7.12]$$

The relative uncertainty in the stress due to the uncertainty in the strain rate is given by Equation 7.13.

$$\left.\frac{\Delta\sigma_E}{\sigma_E}\right|_{\dot{\varepsilon}} = t\Delta\dot{\varepsilon} = \varepsilon\left(\frac{\Delta\dot{\varepsilon}}{\dot{\varepsilon}}\right) = 0.01\varepsilon \qquad [7.13]$$

Another important source of error is the uncertainty in the force measurement. The error in the stress due to the uncertainty in the force measurement is given in Equation 7.14. According to the instrument manufacturer the uncertainty in the force measurement is 0.001 N. Therefore, the relative uncertainty in the stress can be written as Equation 7.15.

$$\Delta\sigma_E\big|_F = \frac{\partial\sigma_E}{\partial F}\Delta F = \frac{\Delta F}{A(t)} = \frac{\Delta F}{A_o}\exp(\varepsilon) \qquad [7.14]$$

$$\left.\frac{\Delta\sigma_E}{\sigma_E}\right|_F = \frac{\Delta F}{F} = \frac{0.001}{F} \qquad [7.15]$$

Using Equations 7.13 and 7.15 and neglecting the uncertainty in the cross sectional area, the total relative uncertainty in the extensional stress is given by Equation 7.16.

$$\frac{\Delta\sigma_E}{\sigma_E} = \sqrt{\left(\frac{0.001}{F}\right)^2 + (0.01\varepsilon)^2} \qquad [7.16]$$

In Figures 7.6 through 7.8 the errors in the extensional stress due to the strain rate and to the force are compared to the total error. At the higher rates the uncertainty in the rate is the most significant source of error in the stress. At lower rates (and therefore lower forces) the uncertainty in the force becomes the dominant source of error. This means that the less viscous a material is the less accurate the measurements from the RME will be. In the case of the high density mPEs included in this study, HDB3 has the highest

viscosity, therefore for HDB1, HDB2 and HDL1 the extensional flow data have even more error. In Figure 7.9 the effect of extension rate on the total error in the stress is shown for HDB3. Figure 7.10 is the same type of plot for HDL1. The increased uncertainty due to the lower viscosity of HDL1 is readily apparent in this plot.

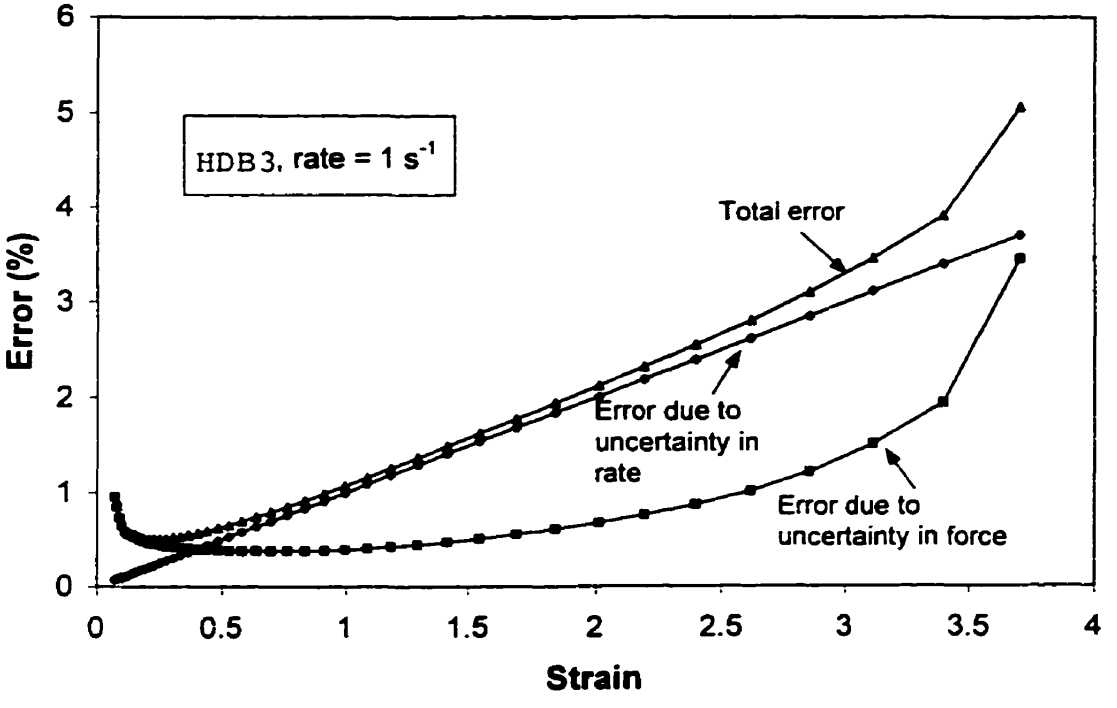

Figure 7.6 Uncertainty in Extensional Stress as a Function of Strain
HDB3, $\dot{\varepsilon} = 1\,s^{-1}$

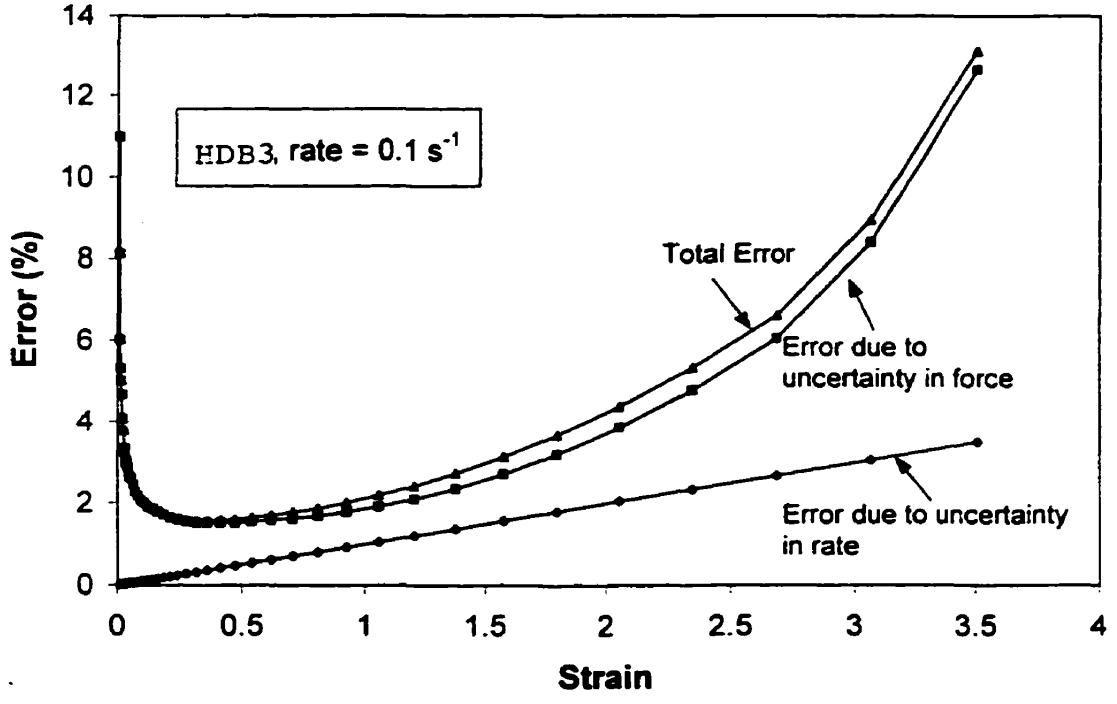

Figure 7.7 Uncertainty in Extensional Stress as a Function of Strain
HDB3, $\dot{\varepsilon} = 0.1\,s^{-1}$

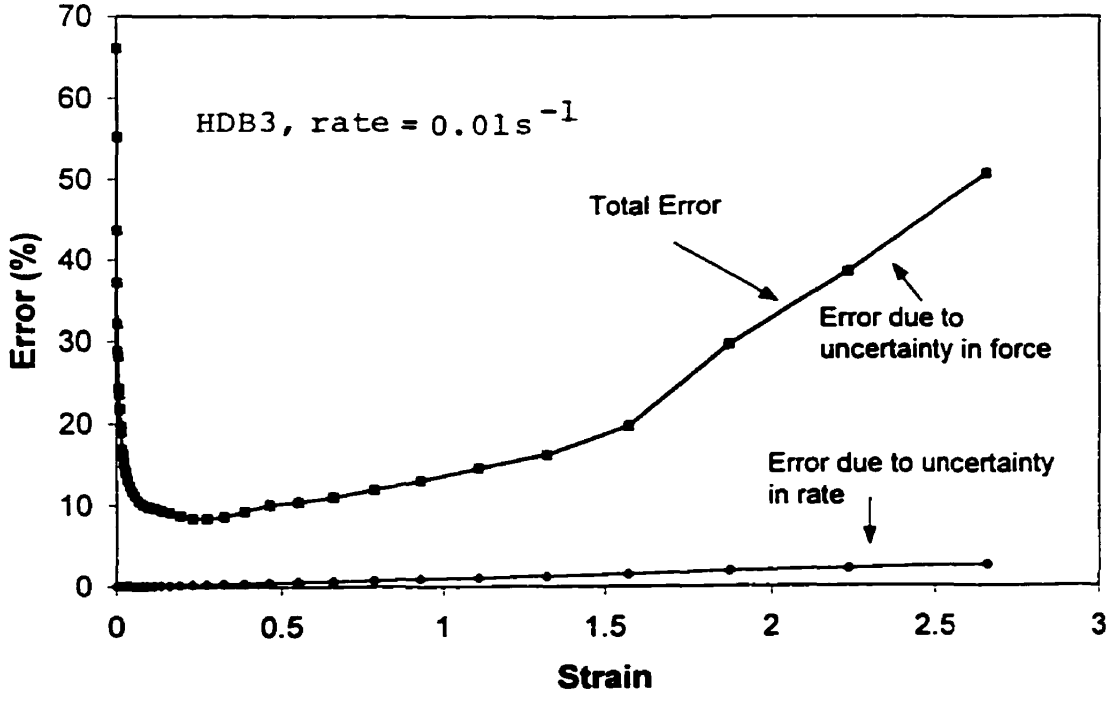

Figure 7.8 Uncertainty in Extensional Stress as a Function of Strain
HDB3, $\dot{\varepsilon} = 0.01\,s^{-1}$

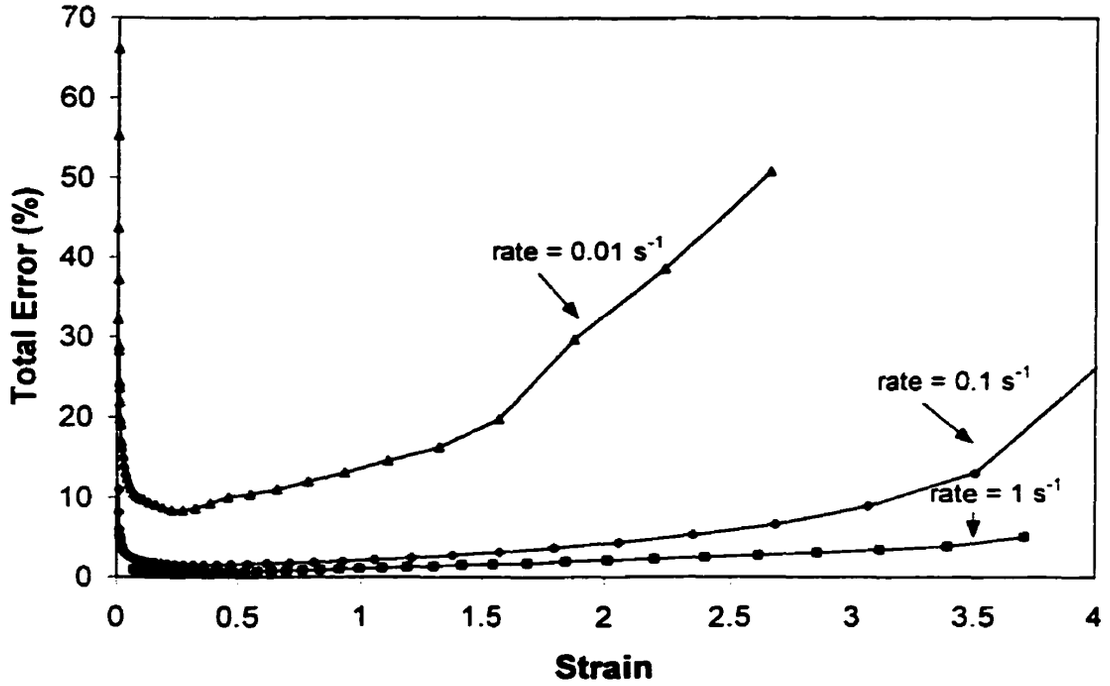

Figure 7.9 Effect of Extension Rate on Total Uncertainty in Stress for HDB3

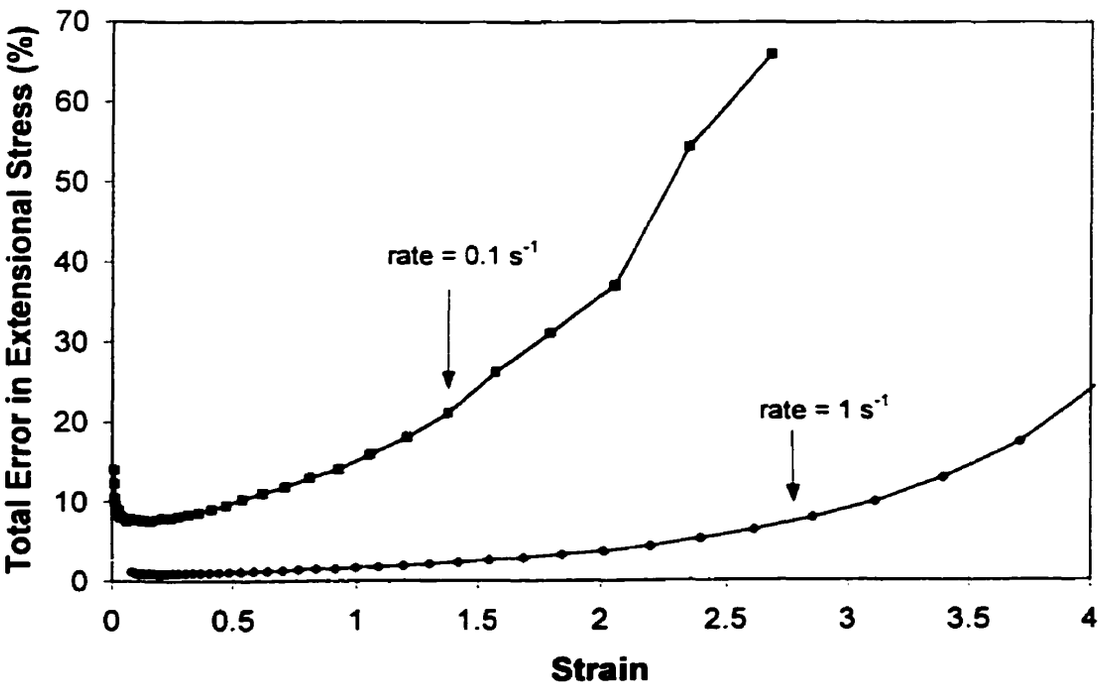

Figure 7.10 Effect of Extension Rate on Total Uncertainty in Stress for HDL1

Equation 7.17 is used to calculate the total uncertainty in the tensile stress growth coefficient due to the uncertainty in the strain rate and the force.

$$\frac{\Delta\eta_E^+}{\eta_E^+} = \sqrt{\left(\frac{\Delta\sigma_E}{\sigma_E}\right)^2 + (0.01)^2} \qquad [7.17]$$

A fourth problem that occurs in the RME data is artificial strain hardening. Hepperle and Saito[3] found that for non-strain hardening materials artificial strain hardening is often observed at high rates. They also observed artificial strain hardening with low-viscosity materials at low rates and long times. They were unable to find a cause for the artificial strain hardening at high rates, but they suggest that the artificial strain hardening at low rates could be due to calibration errors. In the case of very small forces, a small error in the force can result in a very large error in the stress. Because of the problem with artificial strain hardening care must be taken when making conclusions about strain hardening using the RME data.

7.2 Results and Discussion

7.2.1 High Density mPEs

Results from the extensional flow experiments for the high density mPEs are plotted in Figures 7.11 through 7.14. To ensure clarity in the graphs data from four or less extension rates are compared. The error bars were calculated using Equation 7.17 and represent the uncertainty in the tensile stress growth coefficient due to the uncertainty in the rate and the force. In Figure 7.11 we see that at the higher rates HDB3 exhibits significant strain hardening. At a rate of 0.01 s^{-1} the uncertainty becomes so large that the tensile data cannot be distinguished from the LVE response. The same phenomena are observed in Figures 7.12 and 7.13 for HDB2 and HDB3 although the onset of significant strain hardening occurs at a higher rate. For HDL1 (Figure 7.14), a slightly different situation is observed. At rates up to 0.5 s^{-1} no significant strain hardening occurs. At 1

s^{-1} the data appear to indicate strain hardening, but because of the possibility of artificial strain hardening at high rates we cannot conclude that strain hardening occurs for this material. The onset of strain hardening behavior is summarized for these resins in Table 7.1.

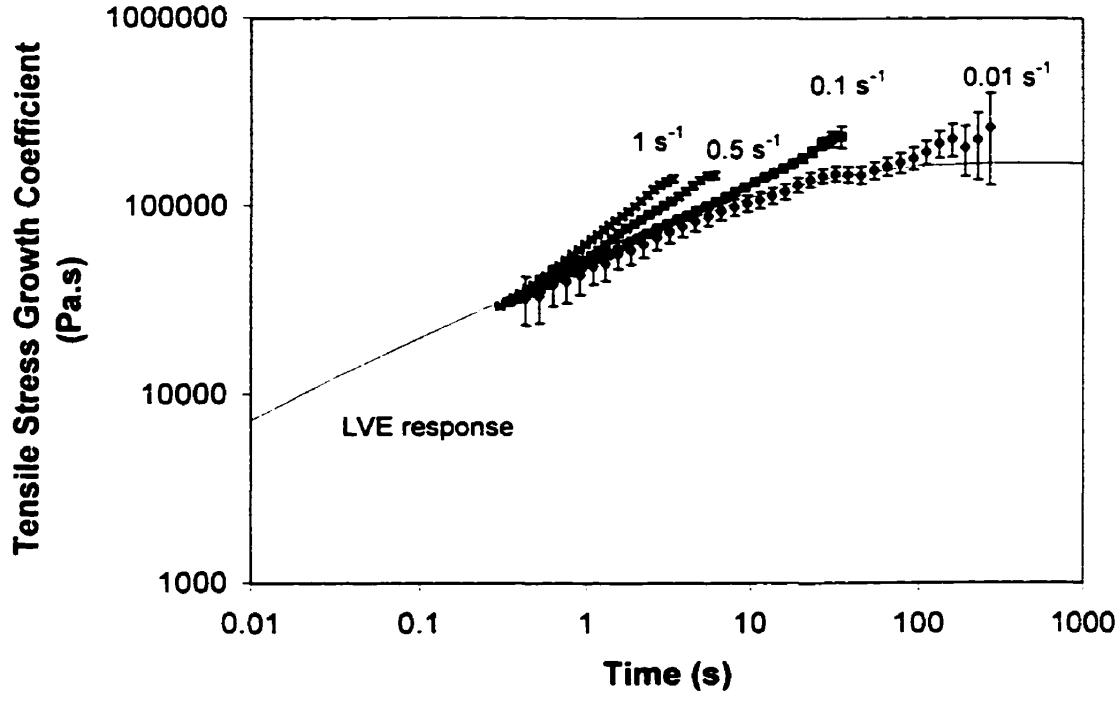

Figure 7.11 Start-up of Steady Simple Extension for HDB3

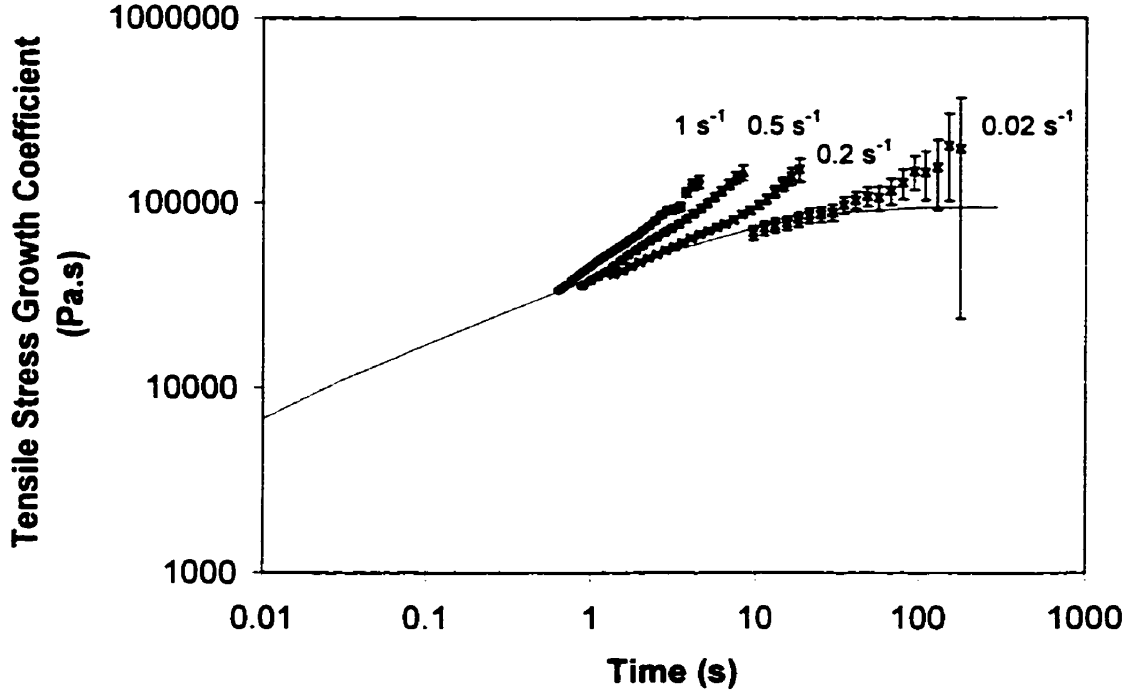

Figure 7.12 Start-up of Steady Simple Extension for HDB2

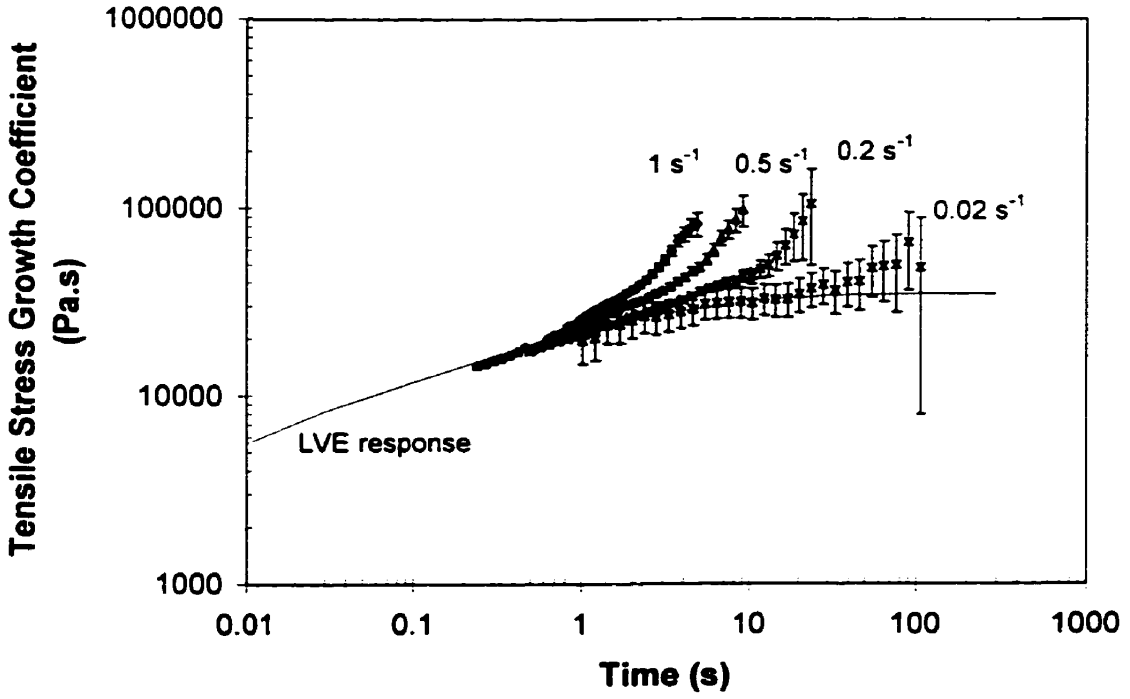

Figure 7.13 Start-up of Steady Simple Extension for HDB1

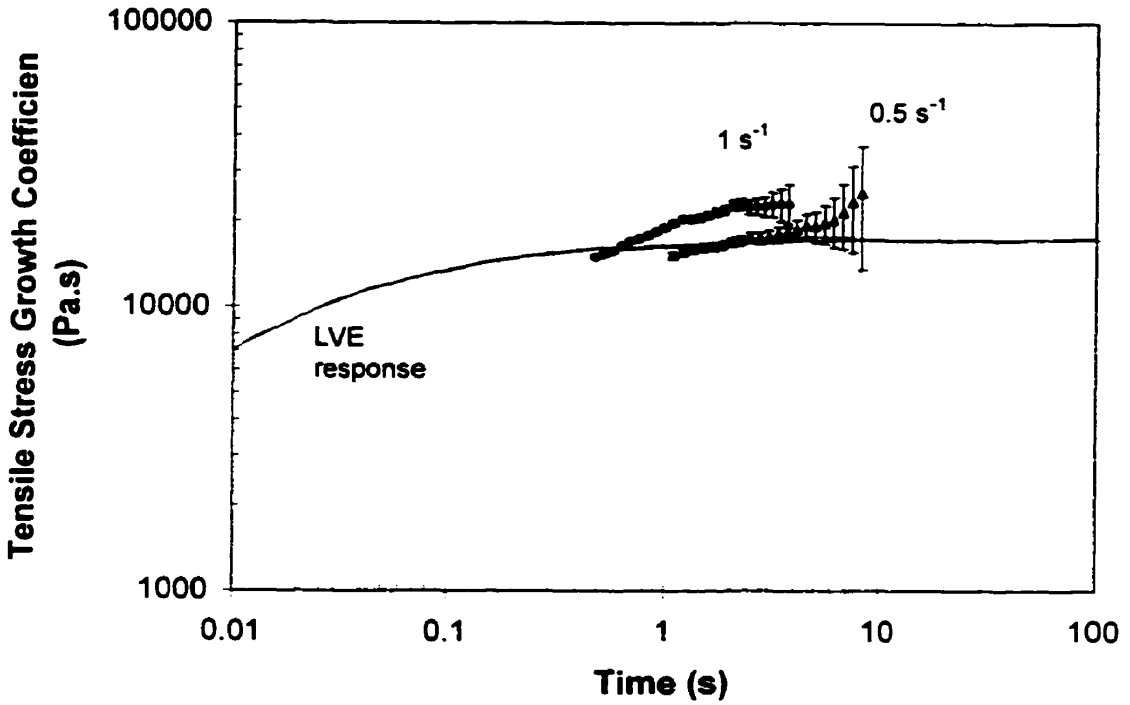

Figure 7.14 Start-up of Steady Simple Extension for HDL1

Table 7.1 Summary of Non-linear Behavior in Extensional Flow for High Density mPEs at 150°C		
Resin	$\frac{LCB}{10^4 C}$	**$\dot{\varepsilon}$ at which strain hardening is first observed (s^{-1})**
HDL1	0	No strain hardening observed
HDB1	0.12	0.05
HDB2	0.37	0.05
HDB3	0.42	0.02

It is also important to note that in the preceding figures no steady state values for the tensile stress growth coefficient were noted. In all cases the sample broke, the instrument's maximum strain of 7 was reached, or the force fell below detectable limits

before steady state was reached. This is unfortunate because it means that it was not possible to generate extensional viscosity curves for these materials.

7.2.2 Low Density mPEs

Extensional flow data for the low density mPEs are shown in Figures 7.15 through 7.18. Because these measurements were performed at a lower temperature (130°C) than the measurements for the high density mPEs (150°C) the forces were higher and therefore the data are more accurate. For LDB3 (Figure 7.15) even at a rate of 0.01 s^{-1} the error bars are very small (especially at low strains). In this set of materials the resin with the highest degree of LCB, LDB3, exhibits strain hardening at the lowest rate. As the degree of LCB decreases the rate at which strain hardening begins increases. LDL1 is a linear material and in other rheological studies it behaved as a linear material. However in the case of extensional flow behavior, the RME data for LDL1 appear to indicate strain hardening for rates above 0.1 s^{-1}. Because of the previously observed incidence of artificial strain hardening for non-strain hardening materials with this instrument we cannot conclude based on these data that LDL1 exhibits strain hardening behavior in extensional flow. Measurements for LDL1 should be performed with another type of extensional rheometer to confirm or invalidate the RME data. The onset of strain hardening behavior for the low density mPEs is summarized in Table 7.2.

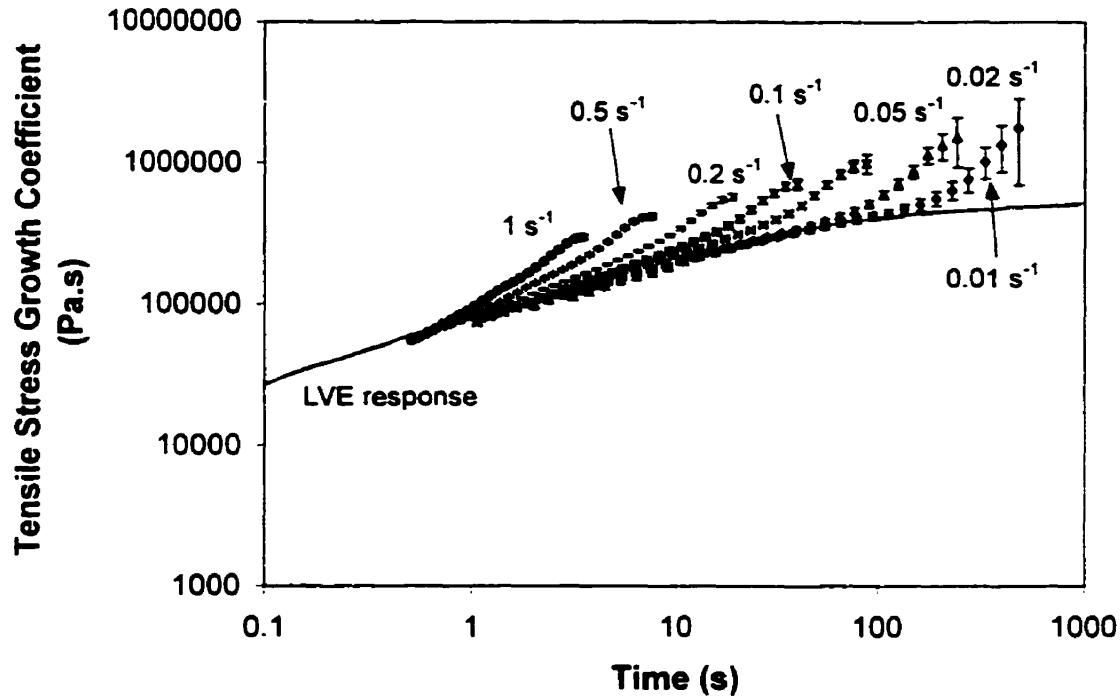

Figure 7.15 Start-up of Steady Simple Extension for LDB3

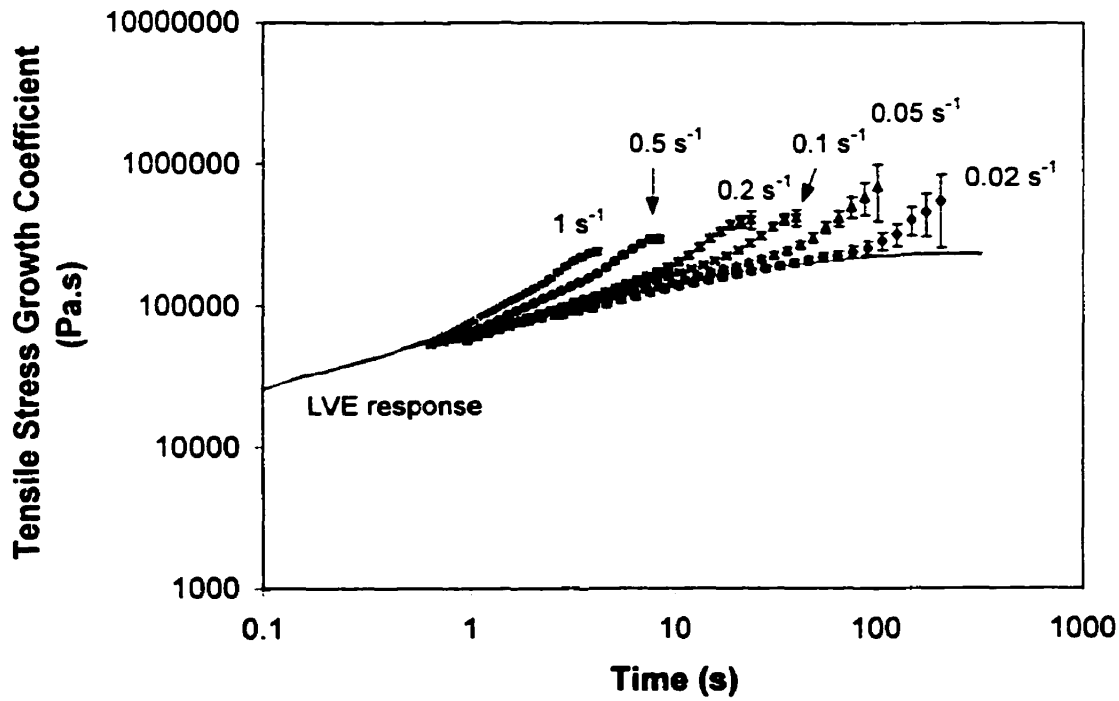

Figure 7.16 Start-up of Steady Simple Extension for LDB2

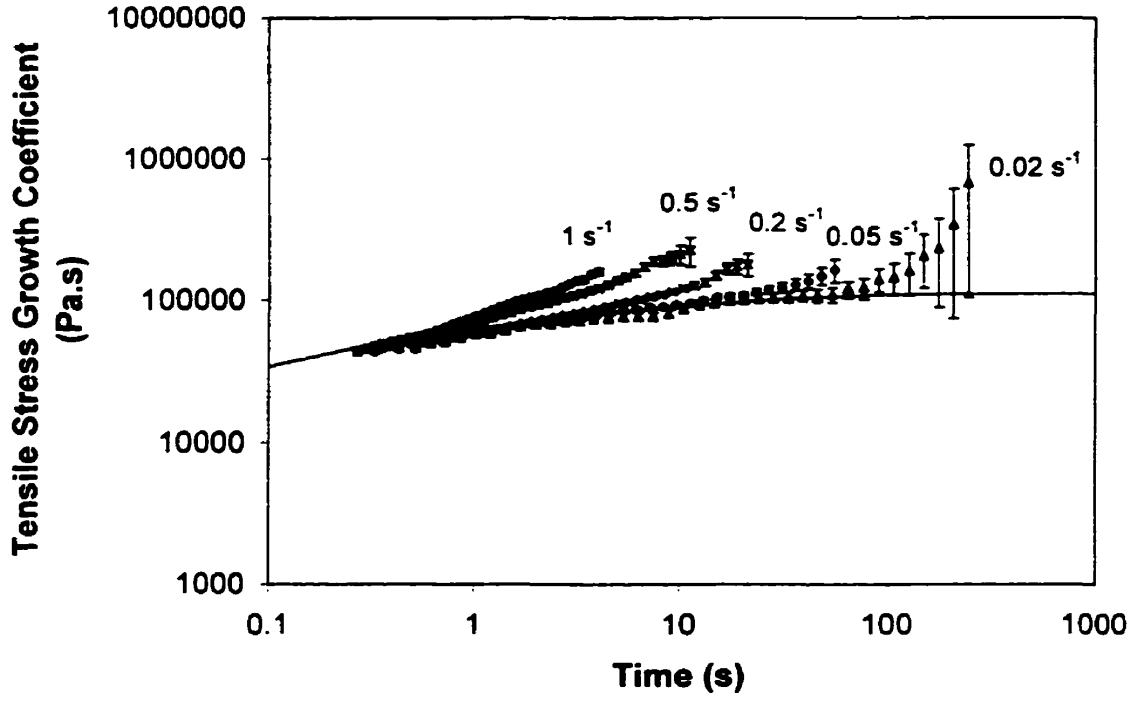

Figure 7.17 Start-up of Steady Simple Extension for LDB1

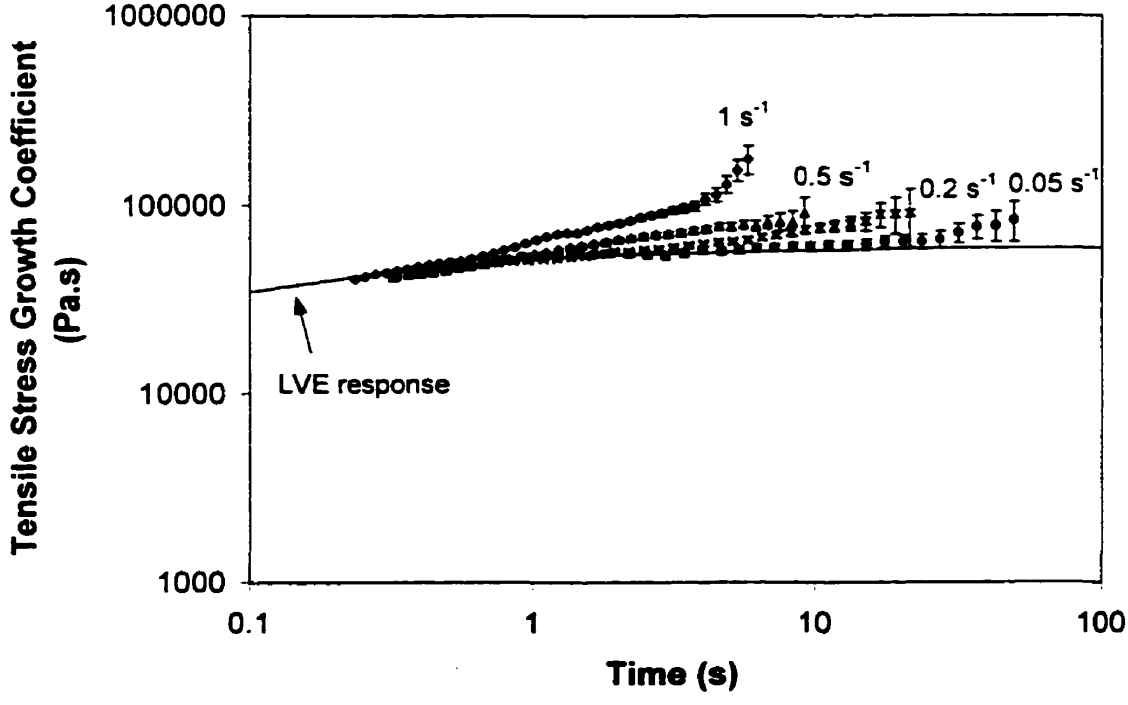

Figure 7.18 Start-up of Steady Simple Extension for LDL1

Table 7.2 Summary of Non-linear Behavior in Extensional Flow for Low Density mPEs at 130°C		
Resin	**DRI**	**$\dot{\varepsilon}$ at which strain hardening is first observed (s^{-1})**
LDL1	0	0.1*
LDB1	1.1	0.05
LDB2	3.9	0.02
LDB3	14	0.01

7.2.3 Effect of Long Chain Branching on Extensional Flow Behavior

The effect of LCB on extension flow behavior can be seen in Figures 7.19 and 7.20. In these figures the tensile stress growth coefficient is plotted for different resins at the same rate. The data for the high density mPEs are plotted in Figure 7.19. Since the tensile stress growth coefficient for HDL1 at 0.5 s^{-1} was indistinguishable from the LVE response, the LVE response of this material was plotted in Figure 7.19 to compare with the other high density mPEs. We see that an increased degree of LCB causes an increase in the tensile stress growth coefficient at a certain rate and time. Also, the behavior of HDL1 is significantly different from the behavior of the long chain branched materials. The data for the low density mPEs are plotted in Figure 7.20. An increased degree of LCB causes the same effect for these materials.

* Data for LDL1 are suspect due to the errors discussed in Section 7.1.3 and must be verified.

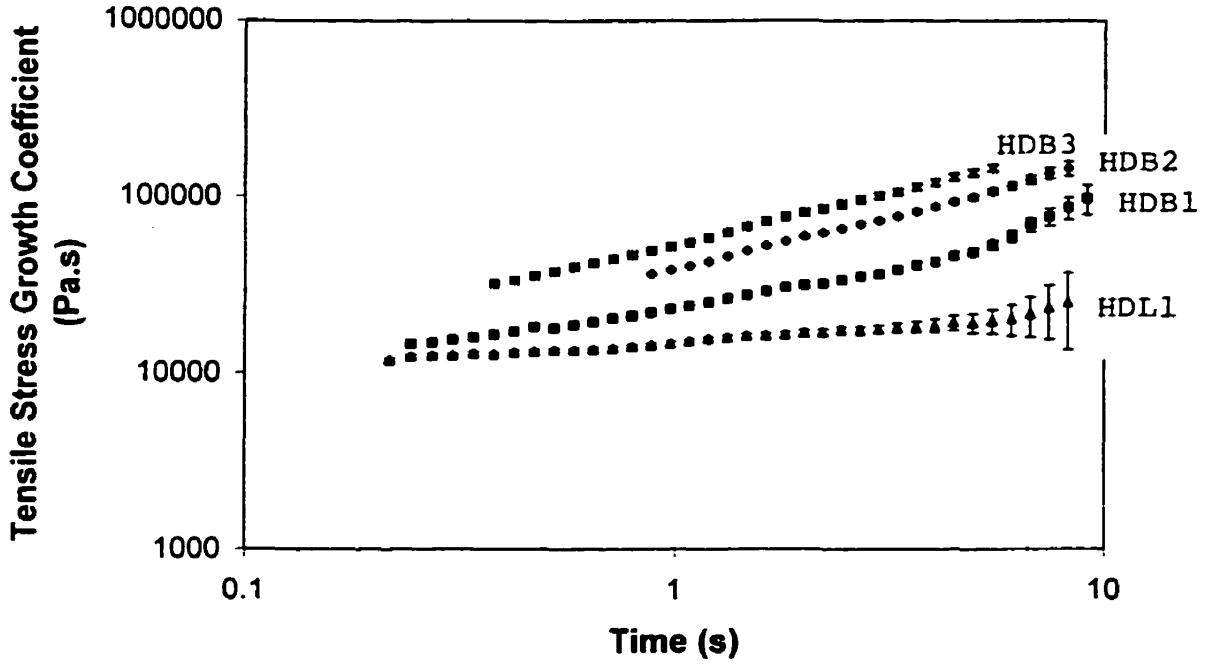

Figure 7.19 Effect of LCB on Extensional Flow Behavior at 0.5 s^{-1} for High Density mPEs

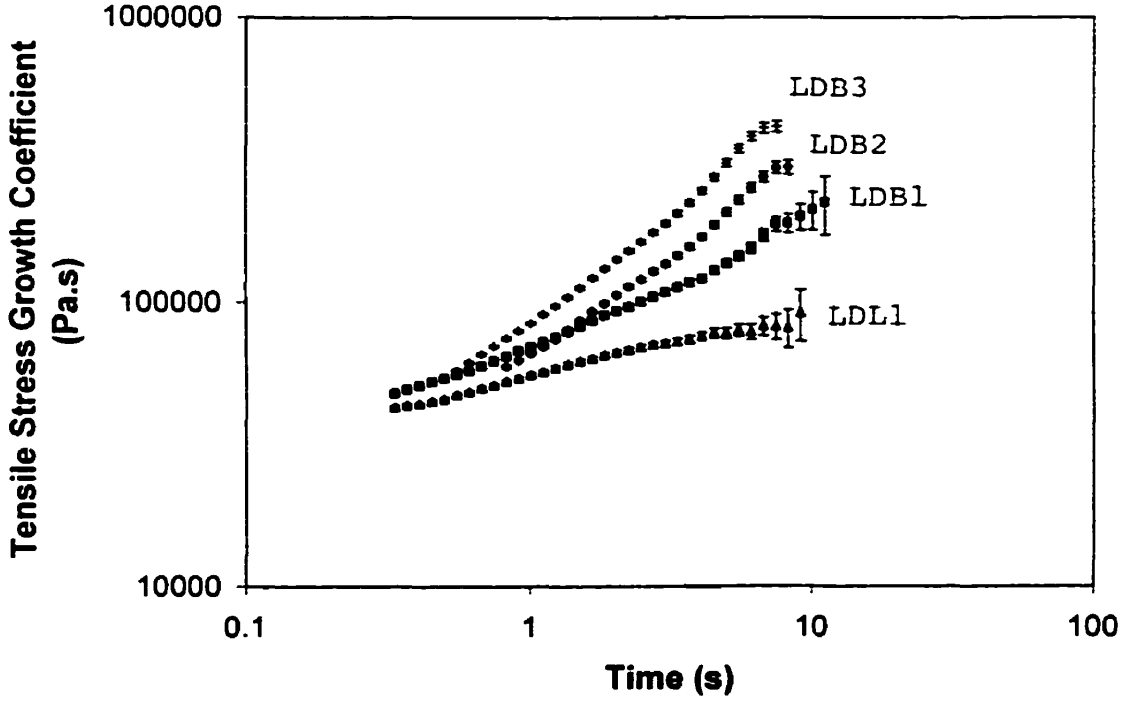

Figure 7.20 Effect of LCB on Extensional Flow Behavior at 0.5 s^{-1} for Low Density mPEs

7.2.4 Effect of Temperature on Extensional Flow Behavior

Extensional flow measurements were performed on LDB3 at both 130 (Figure 7.15) and 150°C (Figure 7.21). Data from three extension rates at each temperature are compared in Figure 7.22. As expected, an increase in temperature shifts the tensile stress growth coefficient curves down and to the right. These data were shifted using the temperature shift factors calculated from the LVE data (Section 5.2) and plotted in Figure 7.23. As, shown in this figure, the shifted rates for the 130°C data are equal to $a_T\dot{\gamma}_{130C}$. In this plot we see that the LVE temperature shift factors appear to shift the extension flow data correctly.

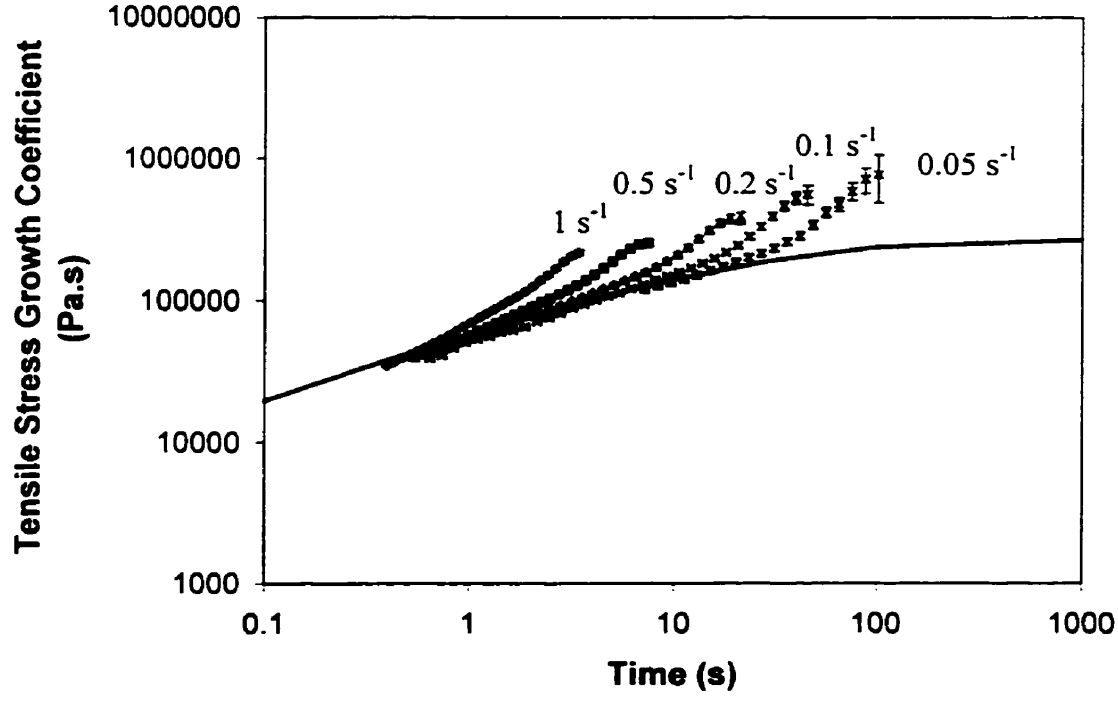

Figure 7.21 Start-up of Steady Simple Extension for LDB3 at 150°C

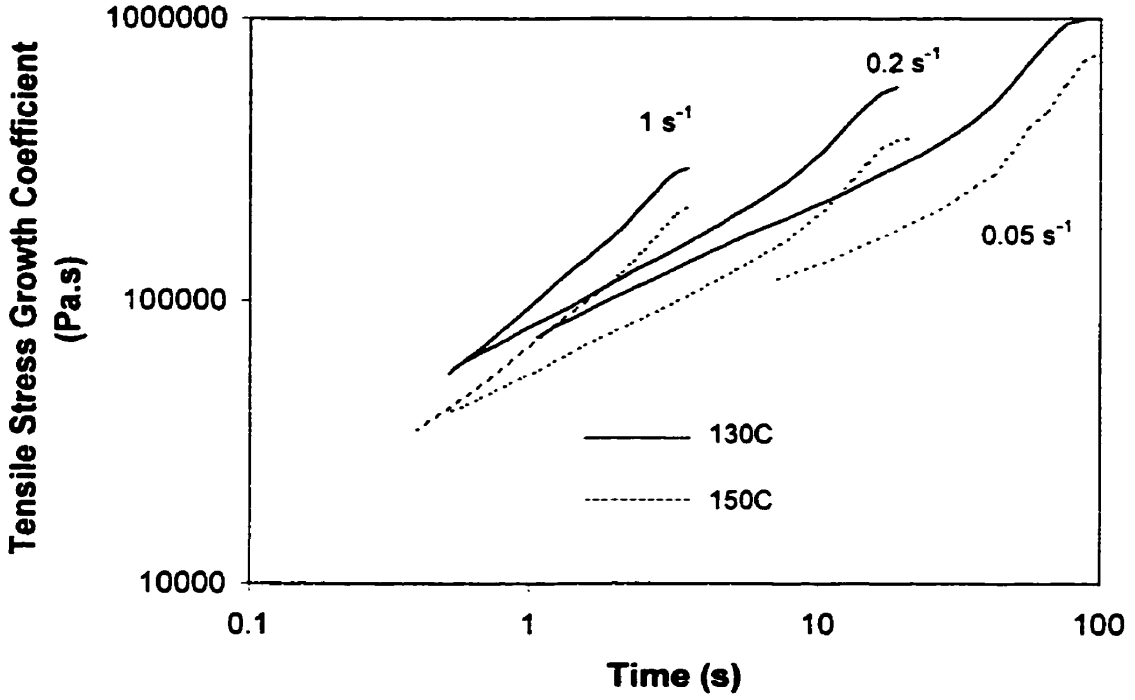

Figure 7.22 Effect of Temperature on Extensional Flow Behavior for LDB3

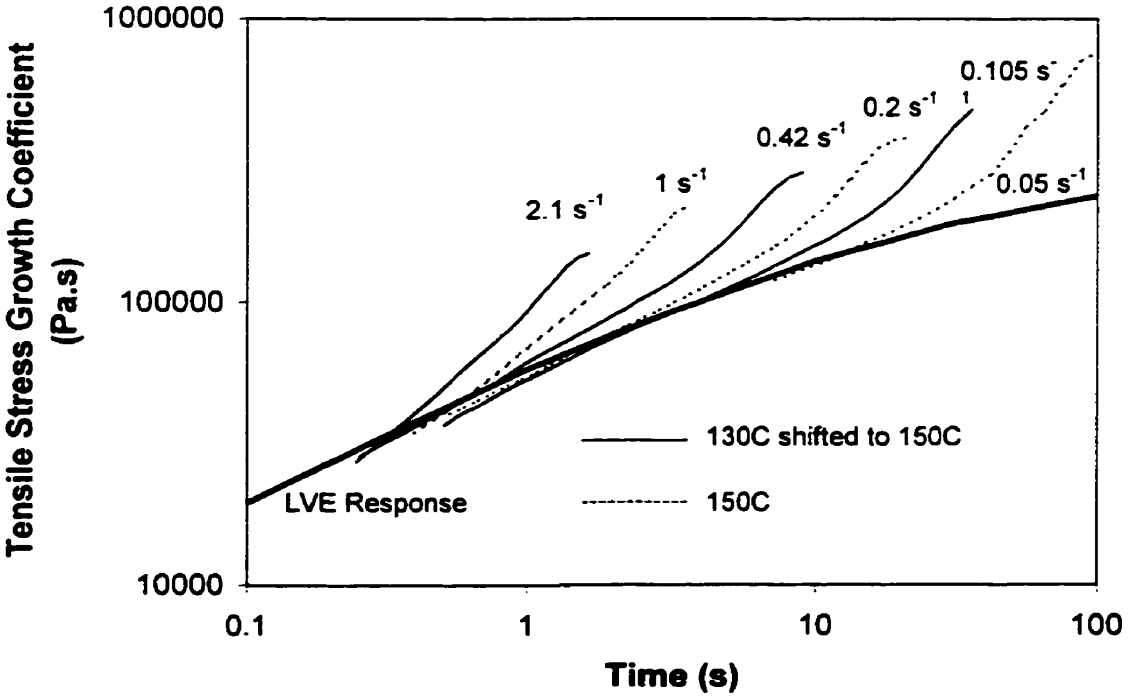

Figure 7.23 Time-Temperature Shifting of Tensile Stress Growth Coefficient Using Shift Factors from LVE Data
(LDB3, a_t=2.1, b_t=1.05)

List of References

[1] H. Münstedt, *J. Rheol.*, 23,4, 421-436 (1979)

[2] J. Meissner and J. Hostettler, *Rheol. Acta*, 33:1-21 (1994)

[3] J. Hepperle and T. Saito, unpublished work, Institute of Polymer Materials, University of Erlangen-Nuremberg, Erlangen, Germany (1998)

Chapter 8

Fit of the Wagner Constitutive Equation to Rheological Data

Under the conditions present in plastics forming processes, polymers exhibit nonlinear viscoelasticity. To simulate such a response one must use a constitutive equation such as the BKZ equation, which relates the stress to the strain history.

$$\tau_{ij}(t) = \int_{-\infty}^{t}\left[2\frac{\partial u}{\partial I_1}C_{ij}(t,t') - 2\frac{\partial u}{\partial I_2}B_{ij}(t,t')\right]dt' \qquad [8.1]$$

where: C is the Cauchy strain tensor and B is the Finger strain tensor

I_1 and I_2 are the first and second scalar invariants of the Finger tensor

u is a time-dependent elastic energy potential which is also dependent on I_1 and I_2

Wagner's simplification of the BKZ equation is a widely used constitutive equation (Equation 8.2)[1]. In Wagner's equation the memory function is described by the product of a time dependent memory function (Equation 8.3) and the damping function. A damping function that has been found to be useful is the one proposed by Papanastasiou and coworkers (Equation 8.4)[2]. In this equation, **a** and β are material dependent constants. For most flows, Wagner's equation must be solved numerically. In the present work, the numerical technique developed by Jeyaseelan and Dealy[3] was used for all simulations.

$$\tau_{ij}(t) = \int_{-\infty}^{t} m(t-t')h(I_1,I_2)B_{ij}(t,t')dt' \qquad [8.2]$$

$$m(t,t') = \sum \frac{G_i}{\lambda_i} \exp\left(-\left[\frac{t-t'}{\lambda_i}\right]\right) \qquad [8.3]$$

$$h(I_1, I_2) = \frac{1}{1 + a[\beta I_1 + (1-\beta) I_2 - 3]} \qquad [8.4]$$

8.1 Determining the Parameters in Wagner's Equation

In Wagner's equation there are two material functions; the memory function, m(t,t'), and the damping function. The memory function is based on a generalized Maxwell model as shown in Equation 8.3. The parameters, G_i, λ_i, are determined by fitting dynamic linear viscoselastic data. In the present work we used the IRIS software package to do this.

For shear flows, $I_1 = I_2$, and Equation 8.4 for the damping function simplifies to Equation 8.5. The most direct way to determine **a** in Equation 8.5 is by step strain experiments. In these experiments the non-linear relaxation modulus, $G(t,\gamma)$, is measured (described in Section 6.2). Using Equation 8.6, the value of the damping function can be determined at various strains. The value of **a** is then calculated by fitting these data to Equation 8.5.

$$h(I) = \frac{1}{1 + a(I-3)} \qquad [8.5]$$

$$G(t,\gamma) = G(t) \bullet h(\gamma) \qquad [8.6]$$

As described in Section 6.2, this was done for three of the high density mPEs (Table 8.1). The fit of Equation 8.5 to the experimental data is shown in Figure 8.1. The quality of the fit is best for HDB3 and worst for HDL1. Equation 8.5 is not able to describe the small strain behavior, of HDB1 and HDL1. For HDB1, the fit is better at higher strains.

Table 8.1 Values of "a" for Three mPEs		
Resin	$\frac{LCB}{10^4 C}$	a
HDL1	0	0.059
HDB1	0.12	0.096
HDB3	0.42	0.149

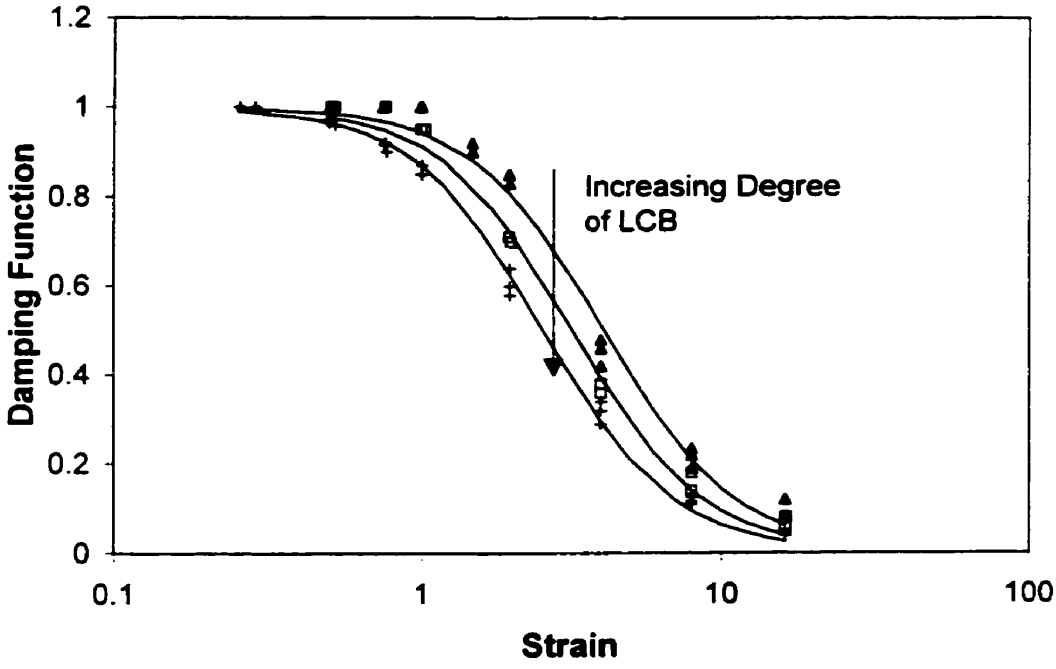

Figure 8.1 Damping Functions for HDL1, HDB1 and HDB3
Curves represent best fit to Equation 8.15

The value of β (Equation 8.4) must be determined from extensional flow data. An attempt was made to use stress growth data from the start-up uniaxial extension to estimate β, since these were the only extensional flow data available for these materials, but the data were not of sufficiently good quality (see Section 7.1.3 for a discussion about the errors in these data). Since we were only really interested in evaluating the Wagner model for shear flows in this work the lack of a value for β was not a concern.

8.2 Simulation Results for Steady Simple Shear

The Wagner model was used to generate viscosity curves, and theses are compared with experimental data in Figures 8.2 through 8.4. The agreement for the of the model predictions to the experimental data is fair with some deviations at high rates. Despite this, the relative behavior of these three materials is preserved in the model predictions. For example, in both experimental and predicted viscosity curves the amount of shear sensitivity is greater for HDB3 than for HDB2 and HDL1.

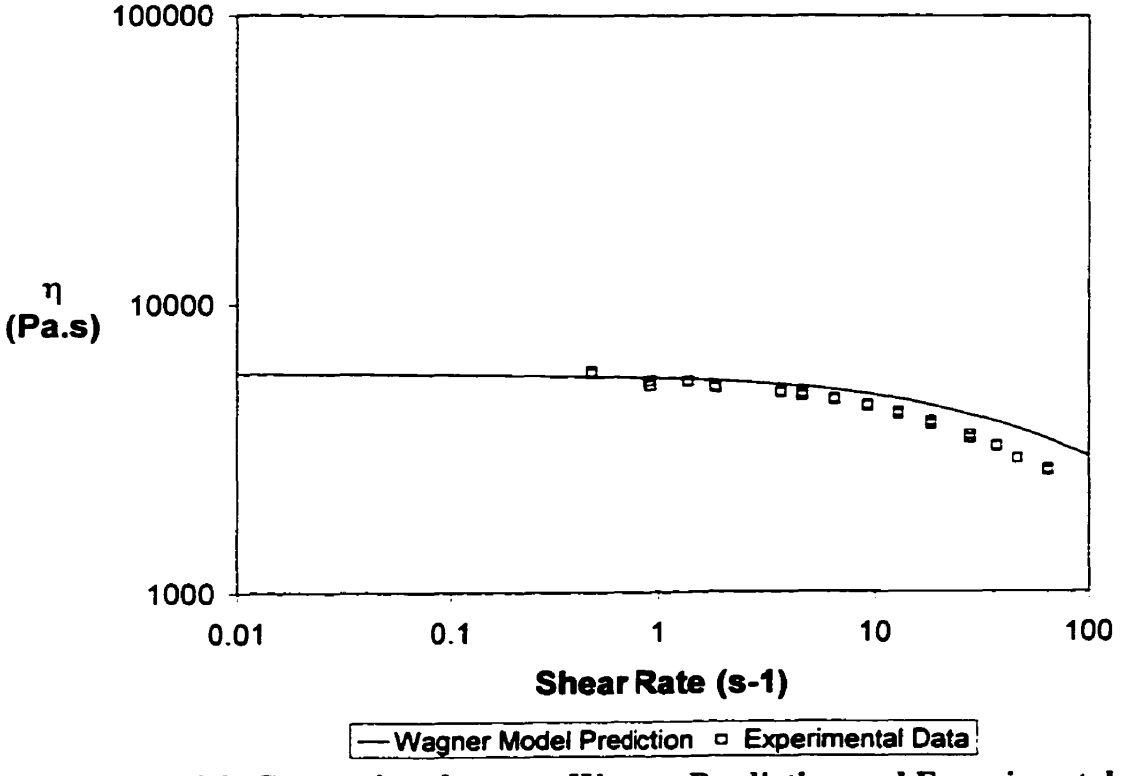

Figure 8.2 Comparison between Wagner Prediction and Experimental Measurements of the Viscosity Curve of HDL1

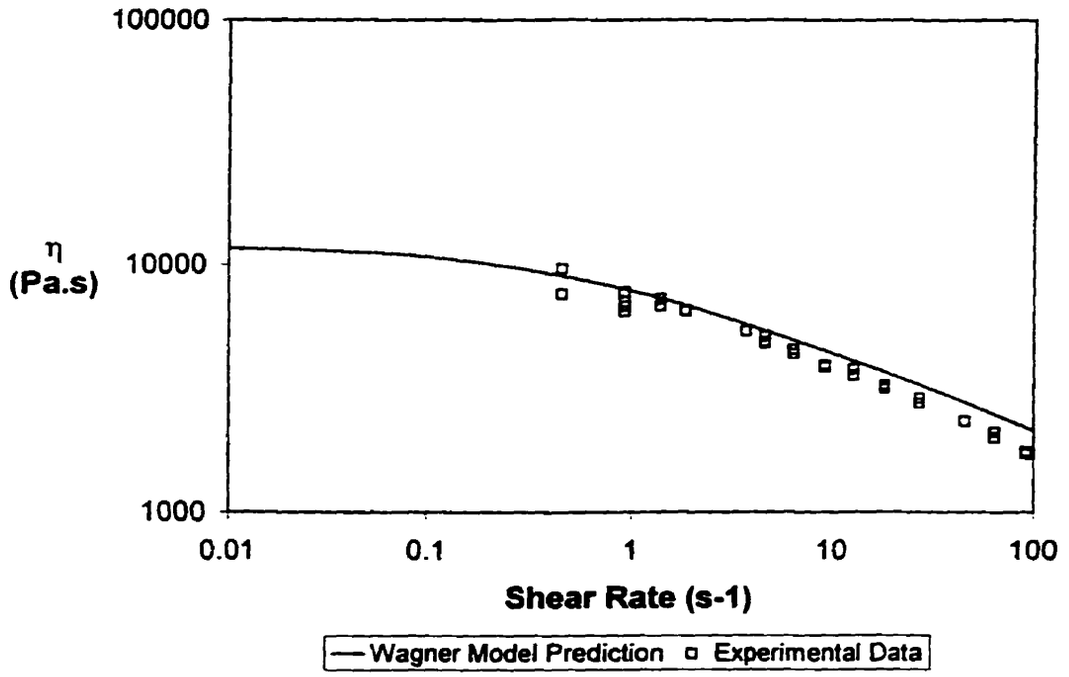

Figure 8.3 Comparison between Wagner Prediction and Experimental Measurements of the Viscosity Curve of HDB1

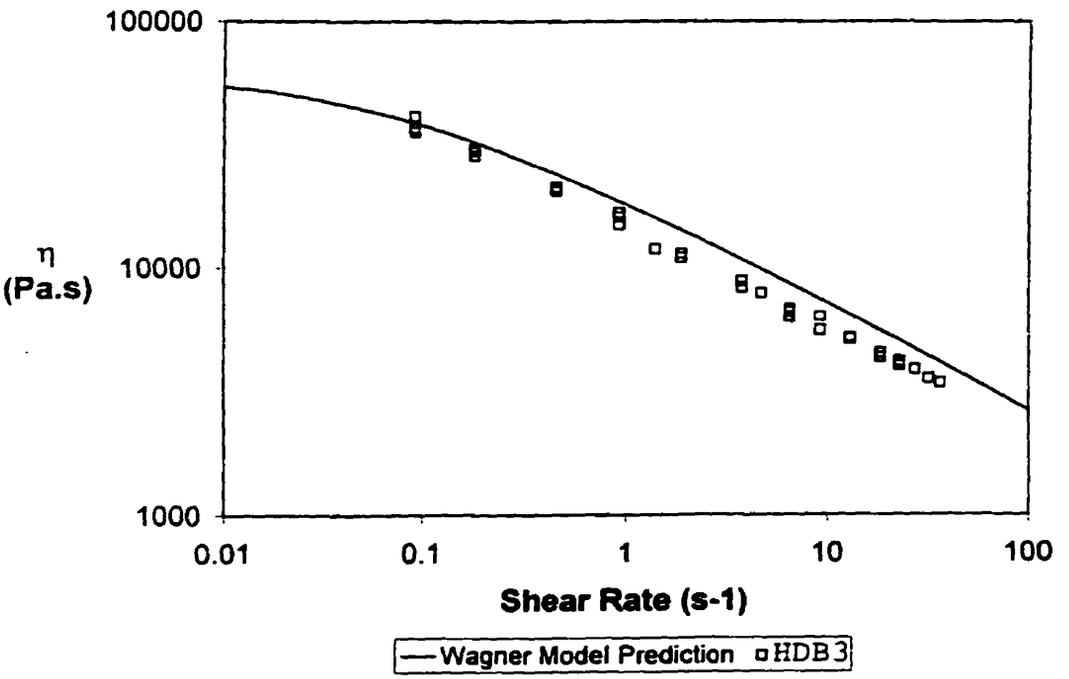

Figure 8.4 Comparison between Wagner Prediction and Experimental Measurements of the Viscosity Curve of HDB3

8.3 Simulation Results for Large Amplitude Oscillatory Shear

Large amplitude oscillatory shear, LAOS, was also simulated, and the predictions of the model were compared with experimental data (Figures 8.5 through 8.10). In general the simulation results agree very well with the experimental data for all three materials. The amplitude and phase angle of the first harmonic, σ_1 and δ_1, are in excellent agreement in all cases. The amplitude of the third harmonic, σ_3, is under-predicted by the Wagner model in all cases. The phase angle of the third harmonic is in excellent agreement for HDL1 and HDB3 and is slightly over predicted for HDB1.

Based on the results for steady simple shear and LAOS, and given the inherent difficulty in modeling non-linear viscoelastic behavior we conclude that the Wagner model predicts the behavior of the three mPEs in shear flows with reasonable accuracy.

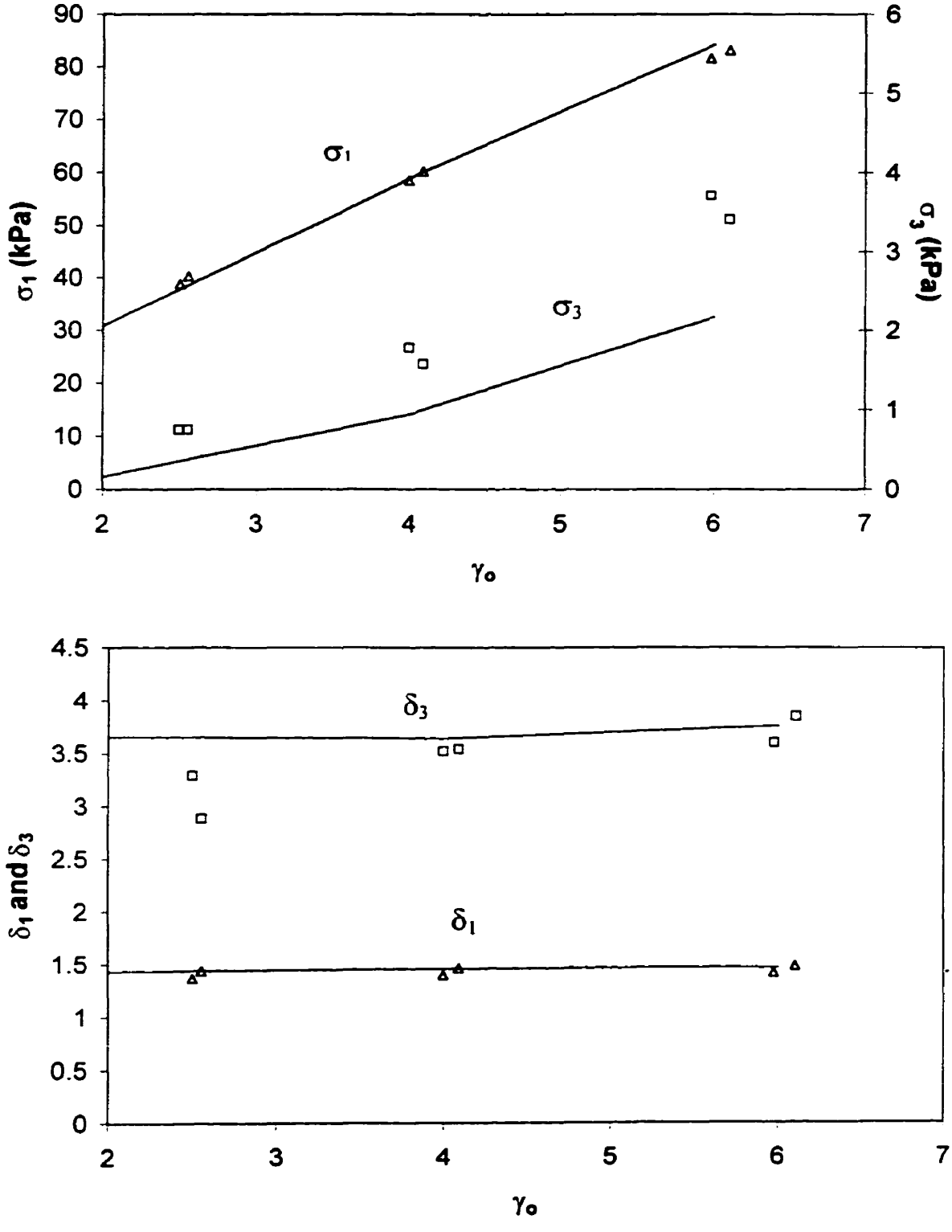

Figure 8.5 Comparison between Wagner Model Prediction and Experimental Data of LAOS Response for HDL1 at $\omega = \pi\ s^{-1}$
(Curves represent Wagner Model predictions and symbols represent experimental data)

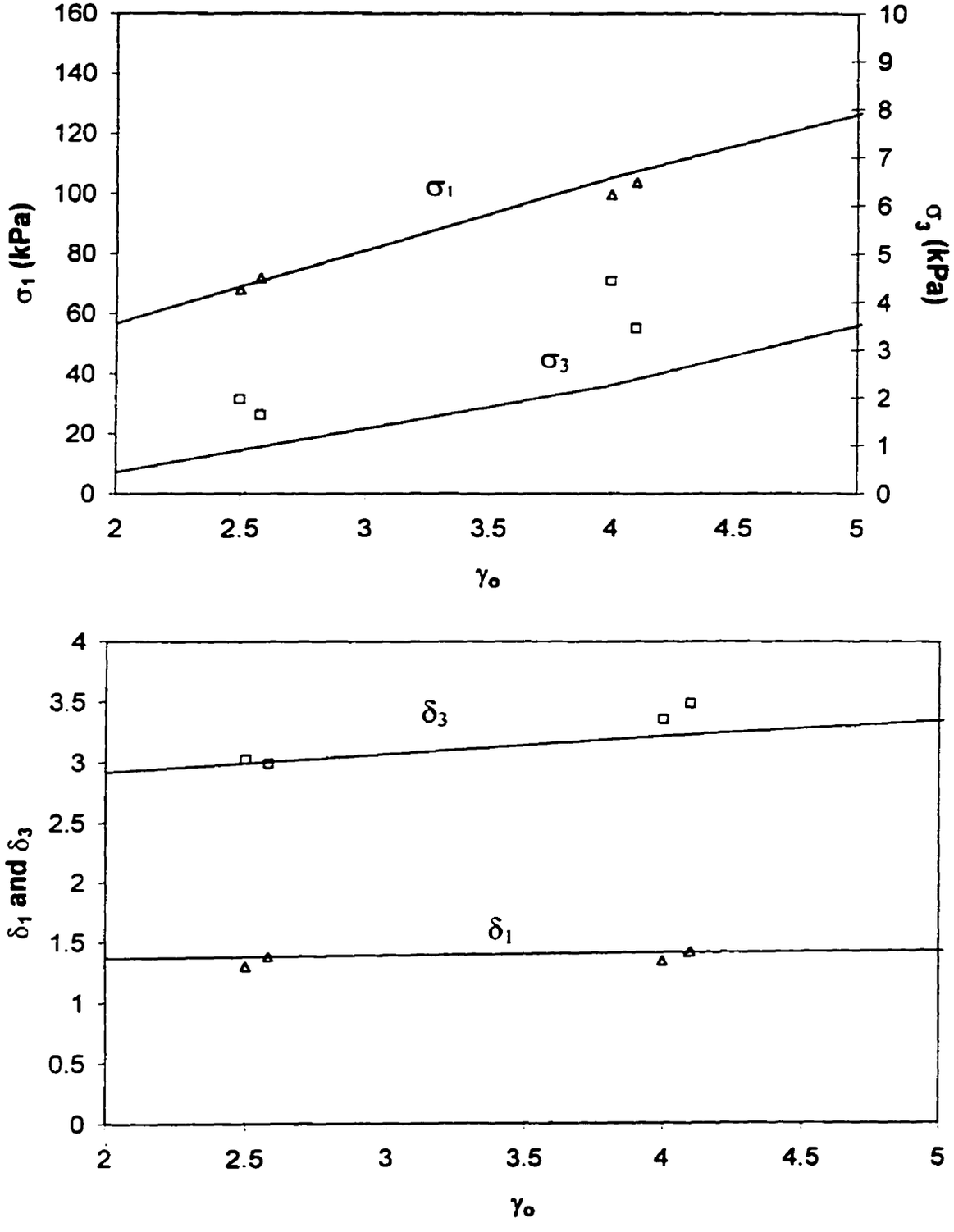

Figure 8.6 Comparison between Wagner Model Prediction and Experimental Data of LAOS Response for HDL1 at $\omega = 2\pi\ s^{-1}$
(Curves represent Wagner Model predictions and symbols represent experimental data)

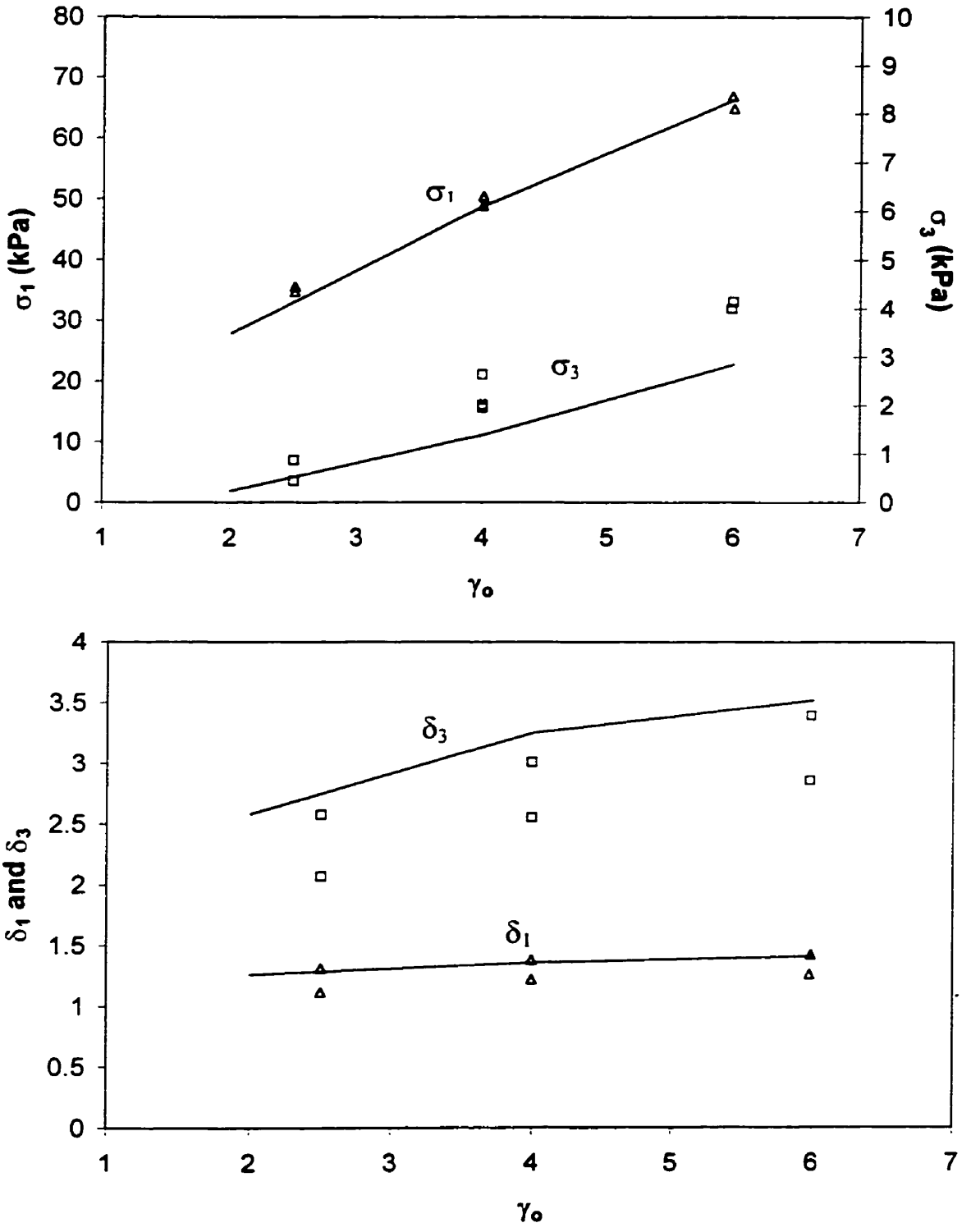

Figure 8.7 Comparison between Wagner Model Prediction and Experimental Data of LAOS Response for HDB1 at $\omega = \pi\ s^{-1}$
(Curves represent Wagner Model predictions and symbols represent experimental data)

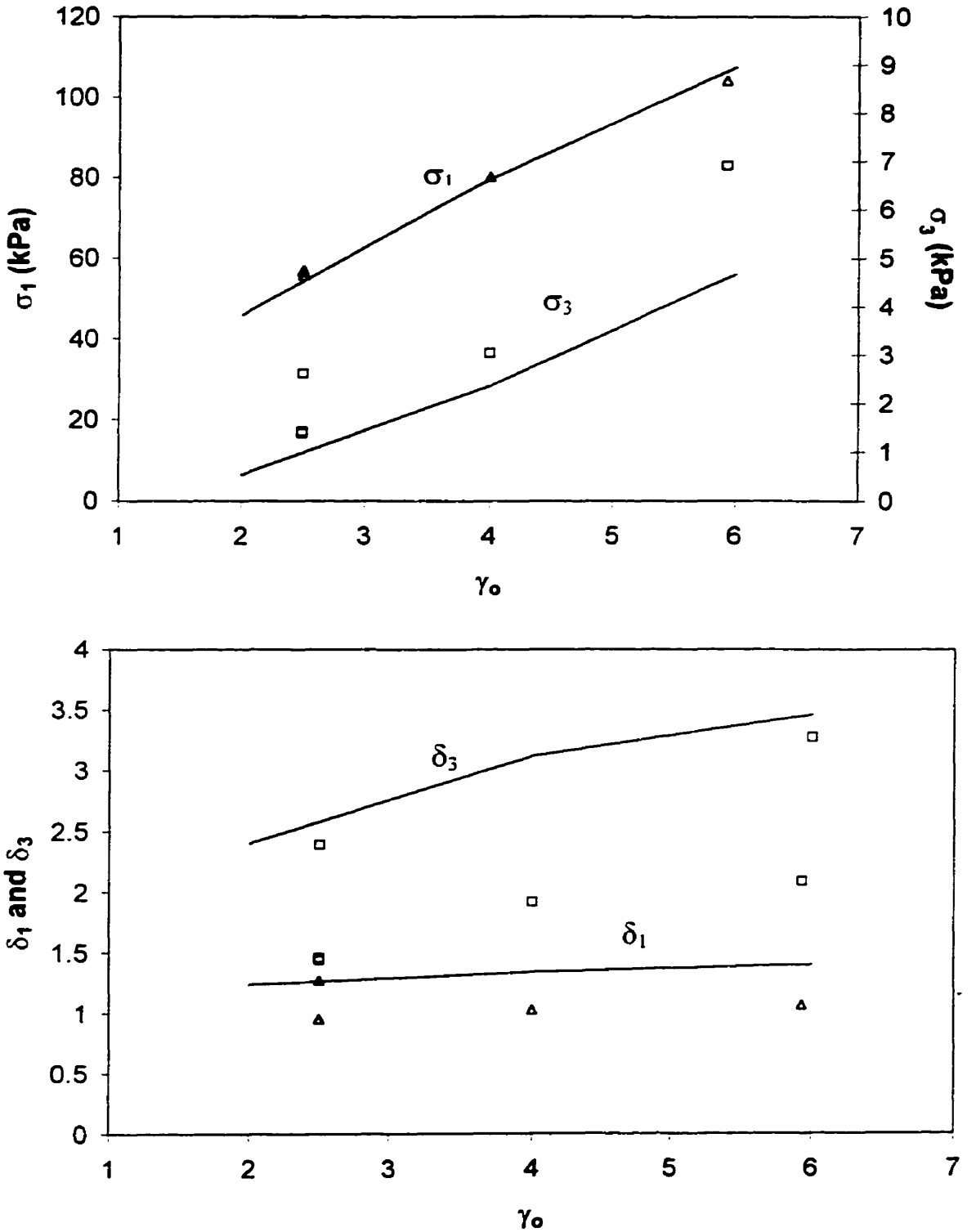

Figure 8.8 Comparison between Wagner Model Prediction and Experimental Data of LAOS Response for HDB1 at $\omega = 2\pi\ s^{-1}$
(Curves represent Wagner Model predictions and symbols represent experimental data)

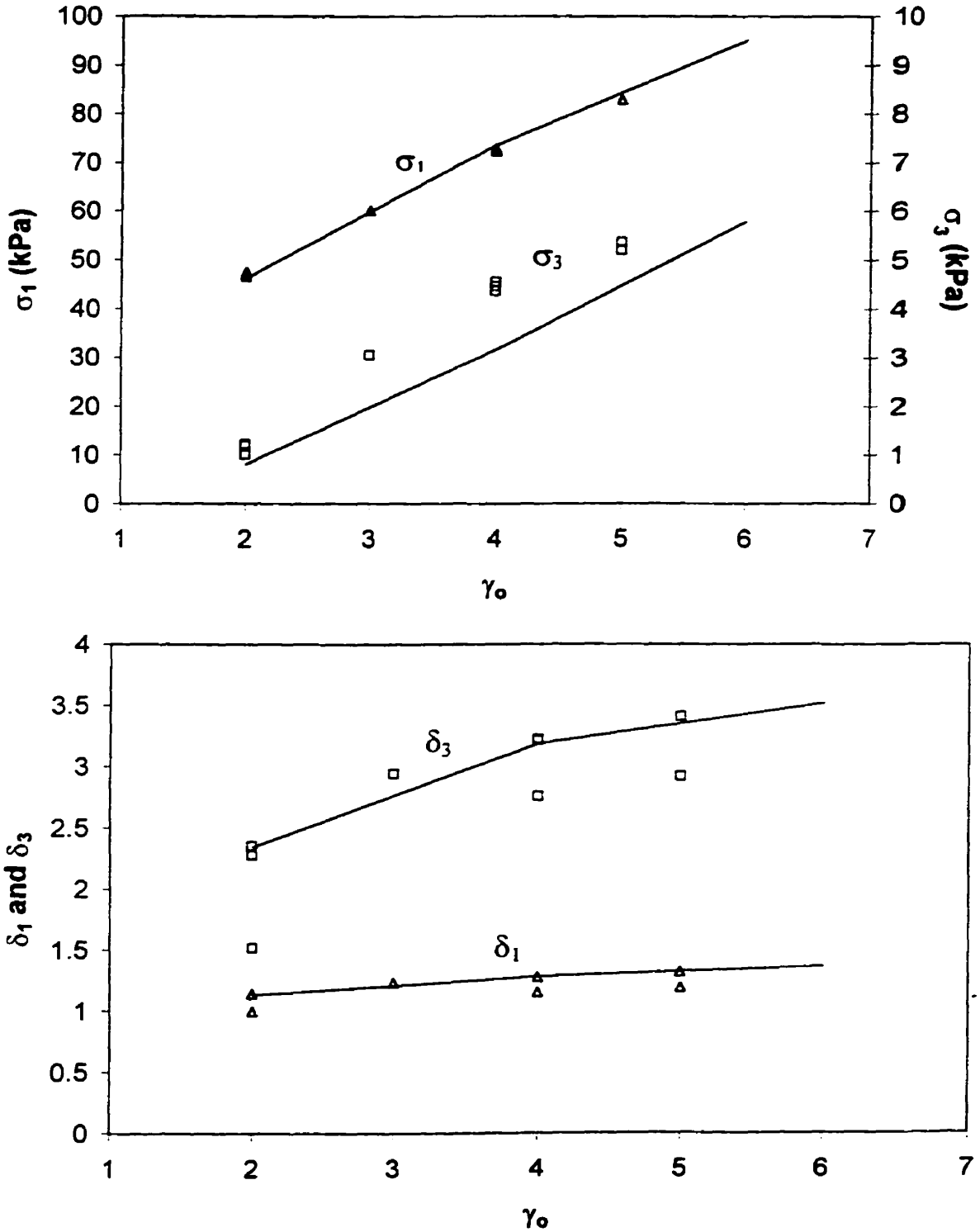

Figure 8.9 Comparison between Wagner Model Prediction and Experimental Data of LAOS Response for HDB3 at $\omega = \pi\ s^{-1}$
(Curves represent Wagner Model predictions and symbols represent experimental data)

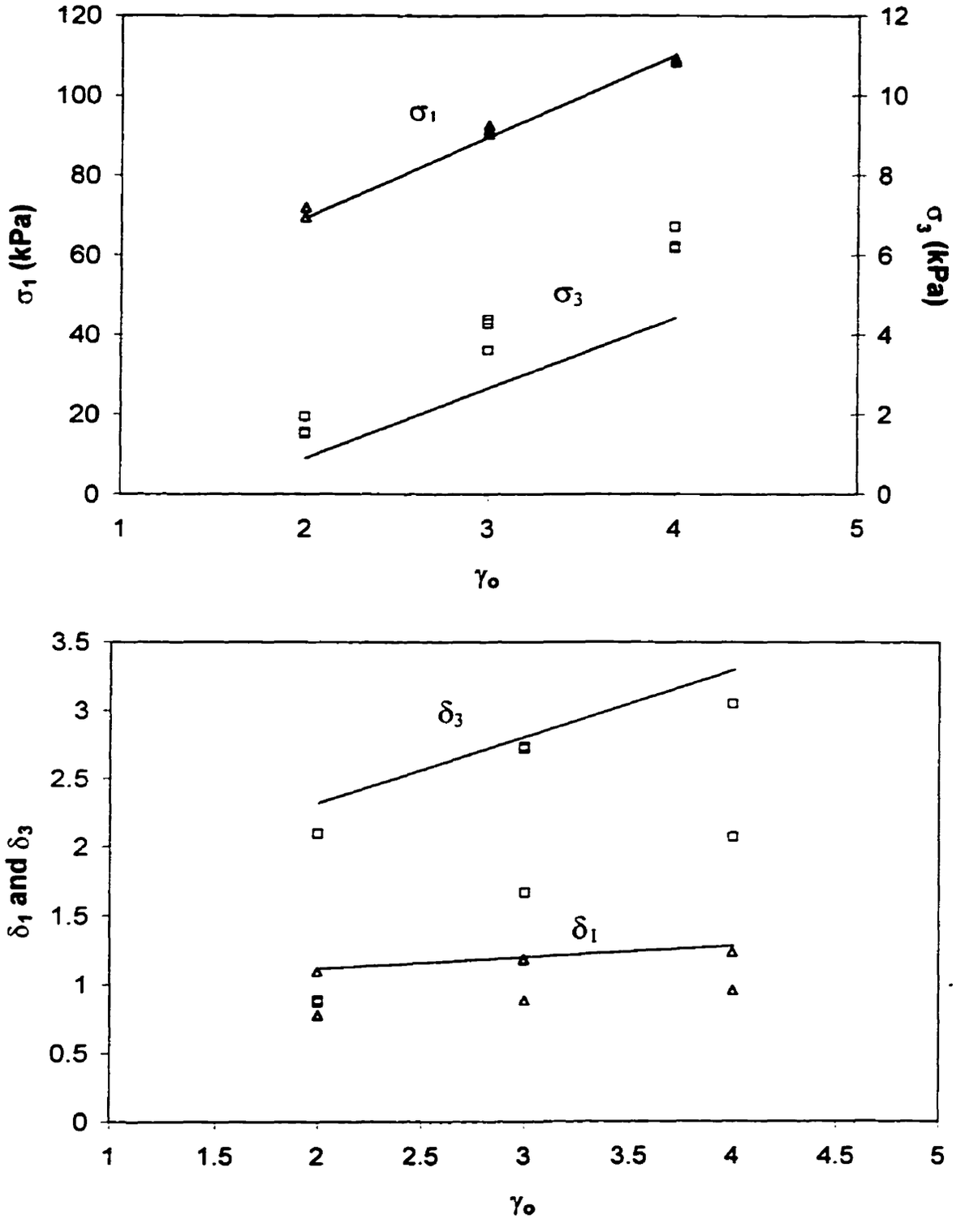

Figure 8.10 Comparison between Wagner Model Prediction and Experimental Data of LAOS Response for HDB3 at $\omega = 2\pi\ s^{-1}$
(Curves represent Wagner Model predictions and symbols represent experimental data)

List of References

[1] Wagner, M.H., *Rheol. Acta*, Vol. 15:136 (1976)

[2] Papanatasiou, A.C. *et al*, *J. Rheol.*, Vol. 27, 387-410 (1983)

[3] Jeyaseelan, R.S. and J.M. Dealy, unpublished work (1996)

Chapter 9.
Using Rheological Data to Provide Information about LCB

Since rheological behavior depends strongly on molecular structure in fairly predictable ways, rheologists have always been interested in solving the inverse problem: using rheological data to provide information about molecular structure. Although there has been some controversy about the feasibility of solving these ill-posed problems a number of researchers have had significant success, especially with the calculation of MWD for linear polymers. One of the techniques that has been demonstrated to be reliable for linear polyethylenes was developed by Shaw and Tuminello[1] and refined by various other researchers[2,3]. This technique is particularly useful, because it requires only LVE data, is simple to apply, and is robust.

A more complicated problem is to extract information about the molecular structure of long chain branched polymers from rheological data. De-coupling the effects of MWD and LCB on rheological phenomena is a key problem for researchers to solve, because changes in these two molecular characteristics can have some similar effects on rheological behavior. For example, broadening the MWD increases the longest relaxation time, as does an increase in LCB.

As was discussed in Chapter 2, it is sometimes difficult to quantify low levels of LCB using established analytical techniques. Therefore, there is a great deal of interest in evaluating alternative techniques for the quantification of LCB.

9.1 Criteria for a Technique to Infer the Level of LCB from Rheological Data

A useful rheological technique for inferring the level of LCB must meet three criteria:

1. It must distinguish between linear and branched mPEs.
2. It must distinguish between branched mPEs and traditional polyethylenes.
3. It must allow us to infer the level of LCB.

To meet the first criterion, a technique must involve a parameter that is independent of M_w but highly sensitive to LCB. Since mPEs typically have polydispersity indexes of 2, the shape of the MWD is not a complicating factor in meeting this criterion. However, traditional polyethylenes (LLDPE and HDPE) can have significantly broader MWDs. Therefore, to meet the second criterion the parameter must also be independent of MWD. Finally, to be useful to infer the level of LCB, the parameter must have a unique value for any given degree of LCB within a reasonable range.

The Dow Rheology Index[4] (DRI) meets the first criterion and also allows the ranking of resins in terms of level of LCB. This parameter is a measure of the extent to which the viscosity curve of branched mPEs deviates from that of linear mPEs. The DRI is based on a resin's shear thinning behavior and is related to the degree of long chain branching. It is defined in terms of the parameters arising from a nonlinear regression fit of the generalized Cross viscosity function (Equation 9.1) to experimental complex viscosity and/or viscosity data (assuming the Cox-Merz rule to be valid).

$$\eta(\dot{\gamma}) = \frac{\eta_o}{1 + (\tau_o \dot{\gamma})^n} \qquad [9.1]$$

It has been found that linear mPEs obey the following relation[4].

$$\eta_o = 3.65 \times 10^6(\tau_o)$$
where
η_o [=]poise
τ_o [=]seconds [9.2]

The DRI is a measure of the departure from this behavior and is defined as[4]:

$$DRI = \frac{3.65 \times 10^6(\tau_o / \eta_o) - 1}{10} \quad [9.3]$$

where the units are as in Equation 9.2. Linear mPEs always have a DRI value of zero, while an increasing DRI value corresponds to an increasing degree of LCB. However, the DRI parameter is designed only for materials with narrow MWDs ($M_w/M_n \approx 2$), and this technique, therefore, will not be useful for distinguishing between long chain branched mPEs and traditional polyethylenes. The DRI values for LDB1, LDB2 and LDB3 are 1.1, 3.9 and 14 respectively.

9.2 Using Extensional Flow Behavior to Obtain Information about LCB

Previous results for traditional branched polyethylenes (LDPE) have suggested that a material's behavior under extension is strongly affected by the presence of LCB. LDPEs, which have high degrees of branching with many branch lengths, exhibit strain hardening behavior in extensional flow. Strain hardening behavior is characterized by an increase in the tensile stress growth coefficient above the LVE response (equal to 3 times the shear stress growth coefficient). Strain hardening is observed at intermediate rates only, resulting in an extensional viscosity curve that increases to a maximum that is higher than three times the zero shear viscosity and then decreases. Generally, linear polymers do not exhibit strain hardening, and their extensional viscosity curves therefore

decrease monotonically with rate. This means that strain hardening is independent of MWD. One measure of degree of strain hardening is the ratio of the maximum extensional viscosity to 3 times the zero shear viscosity. Münstedt and Laun[5] demonstrated the dependence of strain hardening on LCB using three polyethylenes (Table 9.1).

Table 9.1 Dependence of Strain Hardening on LCB[5]

Sample	Mw	Mw/Mn	$\frac{\eta_{E(max)}}{3\eta_o}$	Density (g/cm^3)	LCB per 1000C
LDPE 6	467 000	25	7	0.918	30
LDPE 9	256 000	10	2.8	0.928	15
HDPE 3	152 000	14	1	0.960	0

Based upon accepted beliefs about the sensitivity of extensional flow behavior to LCB, the present study was initially aimed at using extensional flow data to quantify LCB in mPEs. However, as was shown in Chapter 7, the mPEs did not exhibit steady state behavior within the experimentally accessible portion of the tensile stress growth function, and it was therefore impossible to construct extensional viscosity curves for these materials. This meant that the ratio used by Münstedt and Laun to quantify strain hardening was not useful for mPEs.

To establish precisely the information contained in the tensile stress growth coefficient that is not provided by the LVE data, a reduced tensile stress growth function was defined as shown by Equation 9.4.

$$\eta^+_{ER}(t,\dot{\varepsilon}) = \frac{\eta^+_E(t,\dot{\varepsilon})}{3\eta^+_o(t)} \qquad [9.4]$$

In Equation 9.4, the linear shear stress growth coefficient was calculated using the discrete spectrum (Section 5.3). Figures 9.1 and 9.2 show the reduced tensile stress

growth functions for the high and low density mPEs at 0.5 s^{-1}. At a rate of 0.5 s^{-1}, the $\eta^+_{ER}(t)$ functions for the linear mPEs are different from those for the branched mPEs, but the $\eta^+_{ER}(t)$ functions for the branched materials are indistinguishable. Furthermore, at lower rates the $\eta^+_{ER}(t)$ functions for the linear materials were indistinguishable from those of the branched materials. This means that while the $\eta^+_{ER}(t)$ function at higher rates is affected by the presence of LCB, it is not highly dependent on degree of LCB (at these levels). Hingmann and Marczinke[6] did find a dependence of the $\eta^+_{ER}(t)$ function on degree of LCB for polypropylene for higher branching levels. However, the accessible extensional flow data for the materials in this study do not contain much more information about degree of LCB than is contained in the LVE data, and the data most likely to be useful for inferring the level of LCB are thus the LVE data.

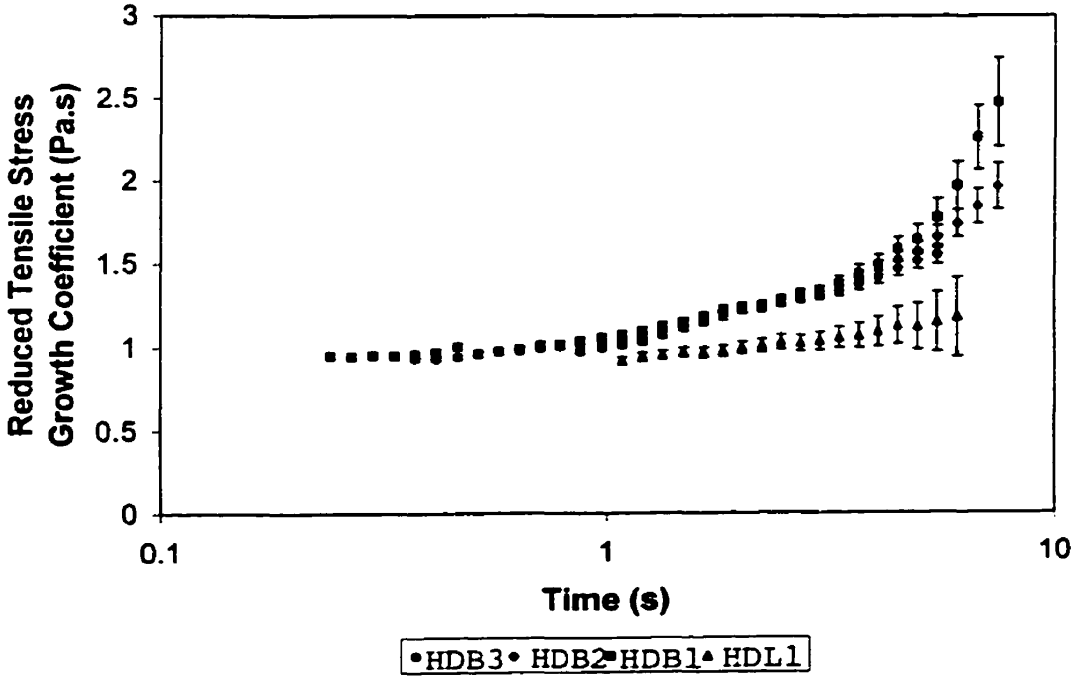

Figure 9.1 Effect of LCB on Reduced Tensile Stress Growth Coefficient for High Density mPEs at 0.5 s^{-1}

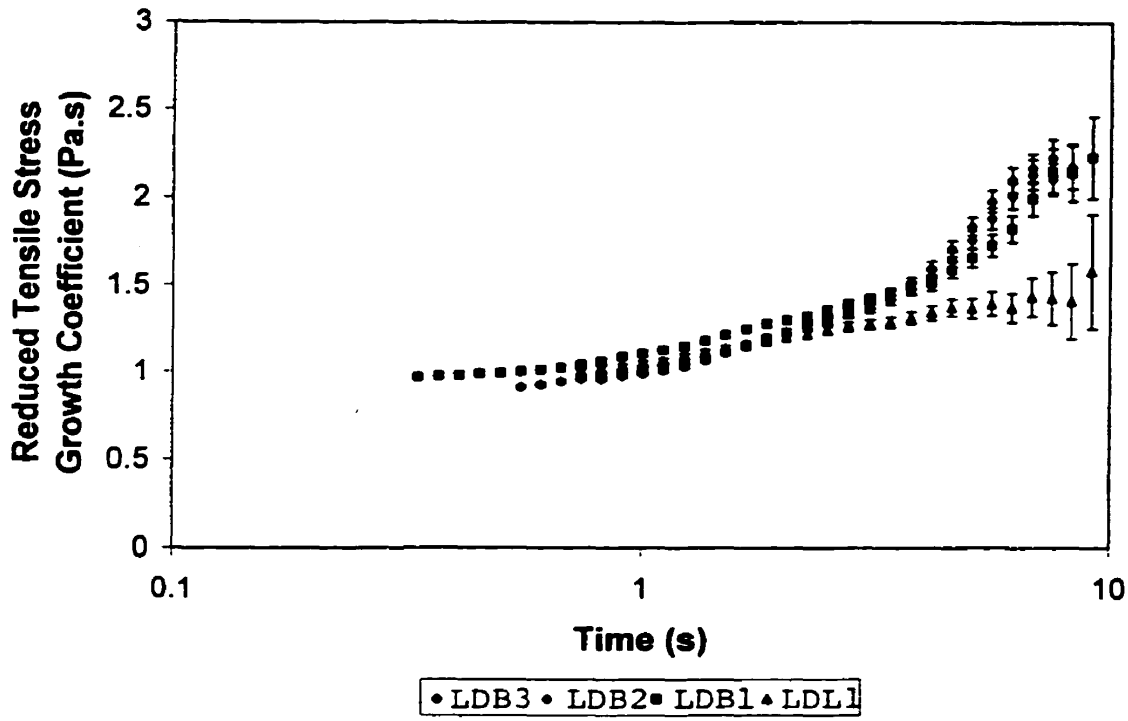

Figure 9.2 Effect of LCB on Reduced Tensile Stress Growth Coefficient Low Density mPEs at 0.5 s^{-1}

9.3 Separating the Effects of LCB and MWD on LVE Behavior

Separating the effects of LCB and MWD on rheological behavior is not a straightforward task. It is certainly not possible to determine the molecular structure of a polymer from rheological data alone without any prior knowledge about the molecular structure. If the material is known to be linear for example, then a reliable estimate of the MWD can be obtained using the LVE data. If a material is branched, however, the MWD predicted from LVE data using a technique such as that developed by Shaw and Tuminello will deviate from the true MWD. The degree of deviation in the predicted MWD is related to the degree of LCB. Therefore, comparing the gel permeation chromatography MWD with the MWD predicted from LVE data can provide information about the degree of LCB.

9.3.1 A Technique for Inferring MWD from Complex Viscosity Data for Linear Polyethylenes.

For the present study the correlation between MWD and complex viscosity is a modified version of the technique developed by Shaw and Tuminello[1]. The mixing rule given by Equation 9.5 is used along with the assumption that a polydisperse system can be modeled as a mixture of N monodisperse fractions each having a complex viscosity curve that consists of a Newtonian plateau followed immediately by a power law region.

$$\eta^{1/\alpha} = \sum_{i=1}^{N} w_i \eta_i^{1/\alpha} \qquad [9.5]$$

Equation 9.6 can then be derived (mathematical details are described by Malkin and Teishev[7]) to describe the dependence of the cumulative MWD on the complex viscosity curve.

$$W(m) = 1 + \frac{1}{\nu}\left(\frac{\eta^*}{\eta_o}\right)^{1/\alpha}\left(\frac{\omega}{\omega_c}\right)^{\nu/\alpha}\left.\frac{d\ln\eta^*}{d\ln\omega}\right|_{\omega=\omega_c m^{-\alpha/\nu}} \qquad [9.6]$$

In the above equation the critical frequency (ω_c) is the intersection of the low shear rate plateau and the power law portion of the log-log viscosity curve, and the reduced molecular weight is defined as follows.

$$m \equiv M/\overline{M}_w \qquad [9.7]$$

The slope in the power law region is equal to -ν. The logarithmic differential molecular weight distribution (Equation 9.8) is obtained by taking the derivative of Equation 9.6 with respect to log(m).

$$w(\log m) = \left[\frac{-\ln(10)}{mv^2}\right]\left[\frac{\eta^*}{\eta_o}\right]^{1/\alpha}\left[\alpha\frac{d^2\ln\eta^*}{d\ln\omega^2} + v\frac{d\ln\eta^*}{d\ln\omega} + \left(\frac{d\ln\eta^*}{d\ln\omega}\right)^2\right] \qquad [9.8]$$

The reduced molecular weight is related to the frequency as shown below.

$$\omega = \omega_c m^{-\alpha/v} \qquad [9.9]$$

The use of Equation 9.8 to calculate the MWD implies the availability of experimental complex viscosity data that include the Newtonian plateau and the power law region. For most polydisperse polymeric systems it is not possible to measure the complex viscosity over the entire range of interest. Therefore, the data are extrapolated at both ends using well-behaved viscosity models. The extrapolation at the low frequency end of the curve was accomplished using Equation 9.10 with the discrete linear relaxation spectrum.

$$\eta^*(\omega) = \sqrt{\left(\sum_{i=1}^{N}\frac{\omega G_i\lambda_i^2}{1+(\omega\lambda_i)^2}\right)^2 + \left(\sum_{i=1}^{N}\frac{G_i\lambda_i}{1+(\omega\lambda_i)^2}\right)^2} \qquad [9.10]$$

The Vinogradov fluidity model, Equation 9.11, was used to extrapolate at high rates. In this equation, the negative of the power law slope, v, is determined by fitting experimental data. It was found that for the mPEs included in this study the optimum value for v was always 1. This is not generally the case with traditional polyethylenes.

$$\frac{\eta_o}{\eta^*} = \sum_{i=1}^{N} A_i\omega^{iv/N} \qquad [9.11]$$

Once the complex viscosity curve has been extrapolated to a zero second derivative at both ends, the logarithmic differential MWD is calculated from the complex

viscosity data using Equations 9.8 and 9.9. This calculated MWD is referred to as the "viscosity MWD".

As described in Section 4.1.1, the true MWD can be measured using gel permeation chromatography (GPC). GPC data are often reported in terms of weight fractions (wt_i) corresponding to molecular weights (M_i). These data must be converted to the discrete logarithmic MWD function using Equations 9.12 through 9.14. The weight fraction data are first transformed into a discrete representation of the MWD function (Equation 9.12) and then normalized as shown in Equation 9.13.

$$f_i' = \frac{wt_i}{M_i} \qquad [9.12]$$

$$f_i = \frac{f_i'}{\sum f_i'(M_{i+1} - M_i)} \qquad [9.13]$$

Finally, the data are put into the form of the discrete logarithmic MWD function (Equation 9.14), which is of the same form as the viscosity MWD.

$$w_i(\log M_i) = f_i M_i \mathrm{Ln}(10) \qquad [9.14]$$

For linear polymers the viscosity MWD as determined above and the discrete logarithmic MWD function calculated from GPC data should be the same.

9.3.1.1 The Effect of Various Molecular Characteristics on the Accuracy of the Viscosity MWD for Linear Polyethylenes

The accuracy of the viscosity MWD is illustrated by the data for HDL1 in Figure 9.3. For this material we have excellent agreement between the viscosity MWD and the GPC MWD. To examine the effects of various molecular characteristics on the viscosity

MWD seven additional linear polyethylenes were chosen to permit the systematic variation of M_w, polydispersity index (PI) and comonomer content. The quality of the viscosity MWDs for these materials was then compared to that of HDL1. Two measures of the quality of the viscosity MWD were used: the peak ratio (Equation 9.15) and the breadth ratio (Equation 9.16).

$$\text{Peak Ratio} = \frac{\text{GPC MWD peak m}}{\text{viscosity MWD peak m}} \qquad [9.15]$$

$$\text{Breadth Ratio} = \frac{\text{GPC MWD breadth at w(log m)} = 0.5}{\text{viscosity MWD breadth at w(log m)} = 0.5} \qquad [9.16]$$

The characteristics of the materials included in this study are summarized in Table 9.2 and are described in detail in Tables 4.3 and 4.4 in Chapter 4. Unless indicated otherwise the LVE data that were used to calculate the viscosity MWDs presented in this chapter were measured at 150°C with a data point density of 7 points per decade of frequency.

Table 9.2 Linear Polymers Included in Viscosity MWD Evaluation

Resins	Molecular Characteristic of Interest
HDL2 and HDL3	Mw range of 41 900 to 122 200
LDL1, LDL2, LDL3	Butene content range of 11.4 to 21.2 wt.%
LLDPE1 and LLDPE2	Broad MWD octene copolymers

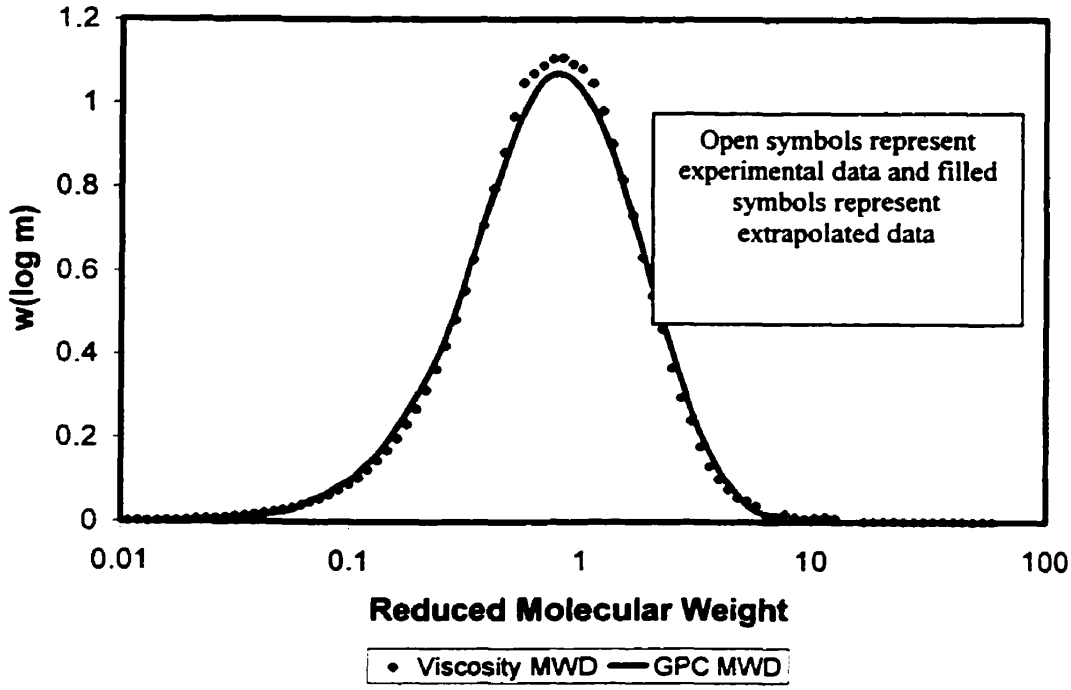

Figure 9.3 Comparison of Viscosity and GPC MWD for HDL1
(Butene copolymer (1.44 wt.%) with Mw= 100 900 and PI = 2.08)

The viscosity and GPC MWDs for HDL2 and HDL3 are compared in Figures 9.4 and 9.5, and the effect of M_W on the quality of the viscosity MWD is summarized in Table 9.3. Lowering M_W results in a movement of the experimental window towards the higher molecular weight end of the distribution (Figures 9.4 and 9.5). This movement of the experimental window reduces the amount of information that is available for the MWD prediction and results in a poorer prediction. The poorer quality of the prediction affects the breadth of the viscosity MWD but not the location of the peak (Table 9.3). The quality of the viscosity MWDs predicted for the two higher molecular weight materials is excellent.

Table 9.3 Effect of M_W on Viscosity MWD Quality

Resin	M_W	Peak Ratio	Breadth Ratio
HDL2	41 900	1.06	1.18
HDL1	100 900	0.96	1.04
HDL3	122 200	0.97	1.09

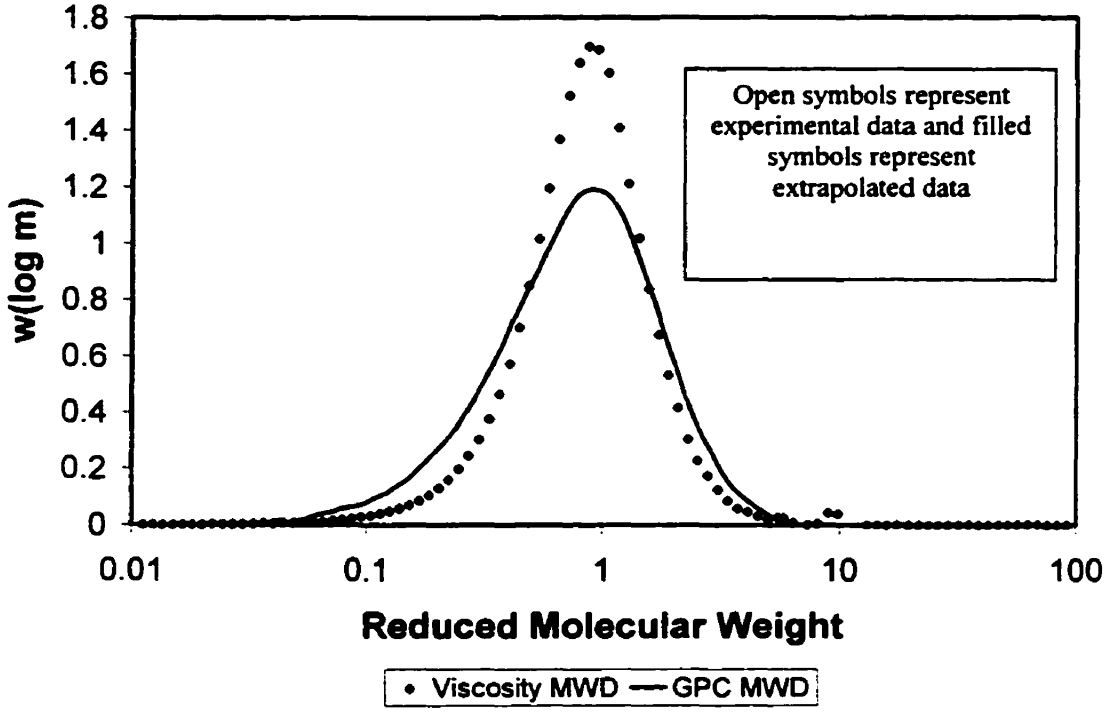

Figure 9.4 Comparison of Viscosity and GPC MWD for HDL2

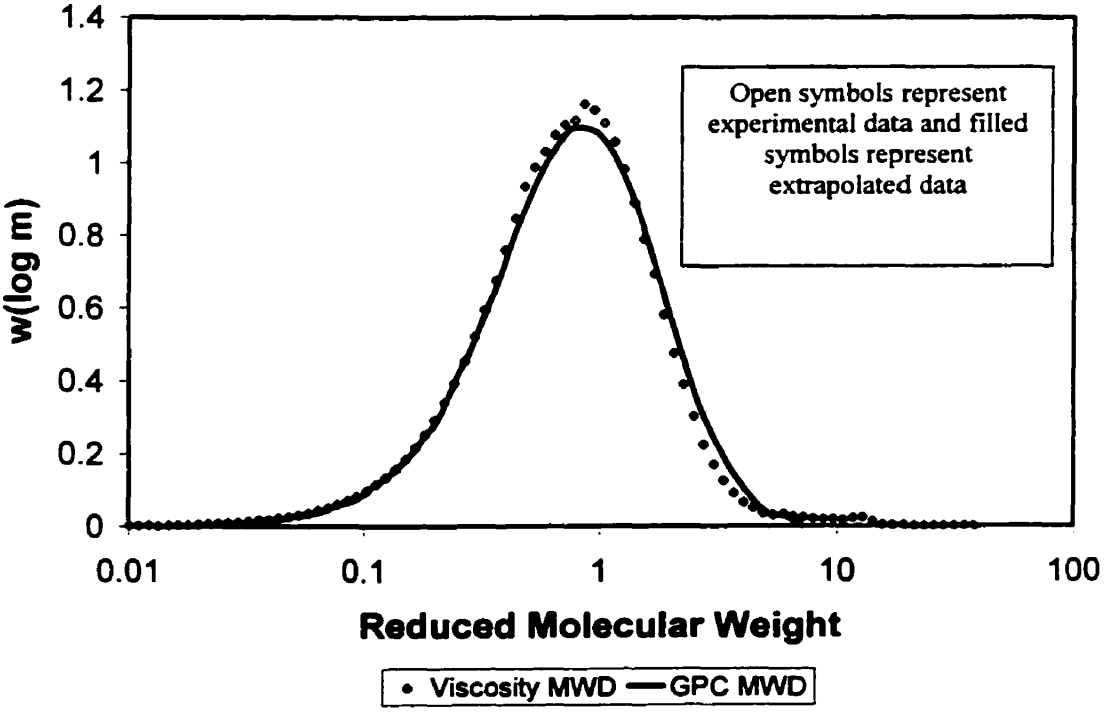

Figure 9.5 Comparison of Viscosity and GPC MWD for HDL3

The effect of short chain branching on the viscosity MWD was studied using LDL1, LDL2 and LDL3 (Figures 9.6 through 9.8). The results shown in the figures and summarized in Table 9.4 indicate that short chain branching resulting from co-polymerization with butene (up to 21.2 wt.% butene) has no effect on the viscosity MWD.

Table 9.4 Effect of Short Chain Branching on Viscosity MWD Quality

Resin	wt. % butene	Peak Ratio	Breadth Ratio
HDL1	1.44	0.96	1.04
LDL1	11.4	0.97	1.06
LDL2	14.83	0.92	1.04
LDL3	21.1	0.90	1.05

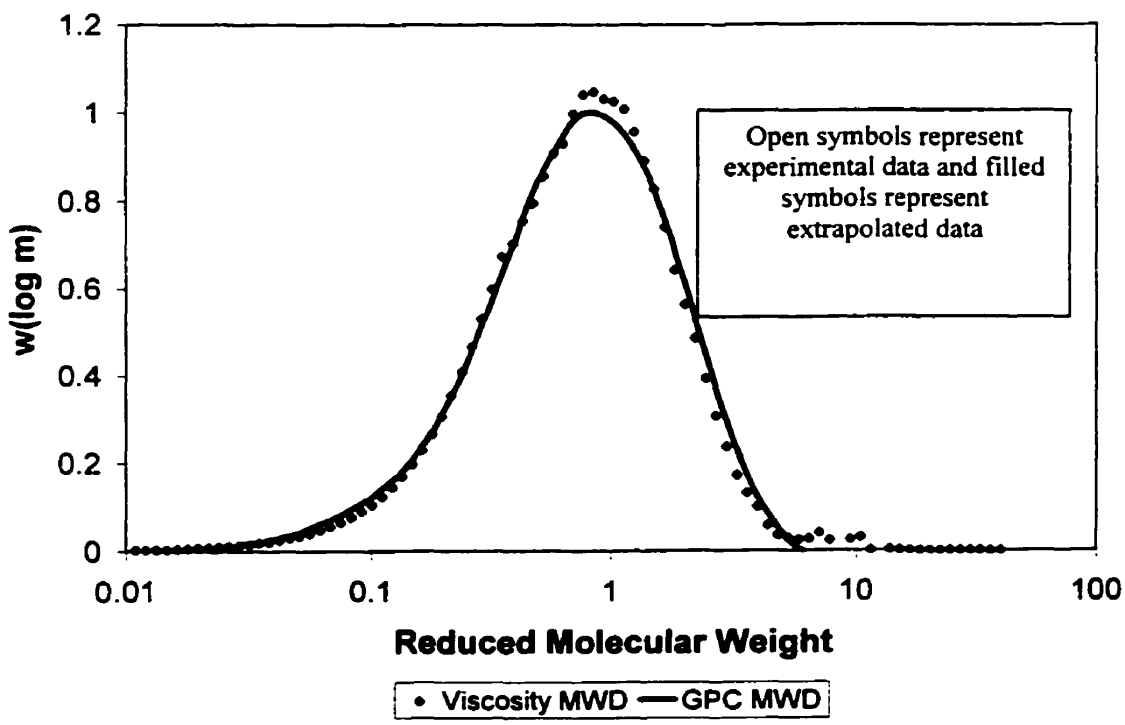

Figure 9.6 Comparison between Viscosity and GPC MWD for LDL1
(LVE Data Measured at 130°C)

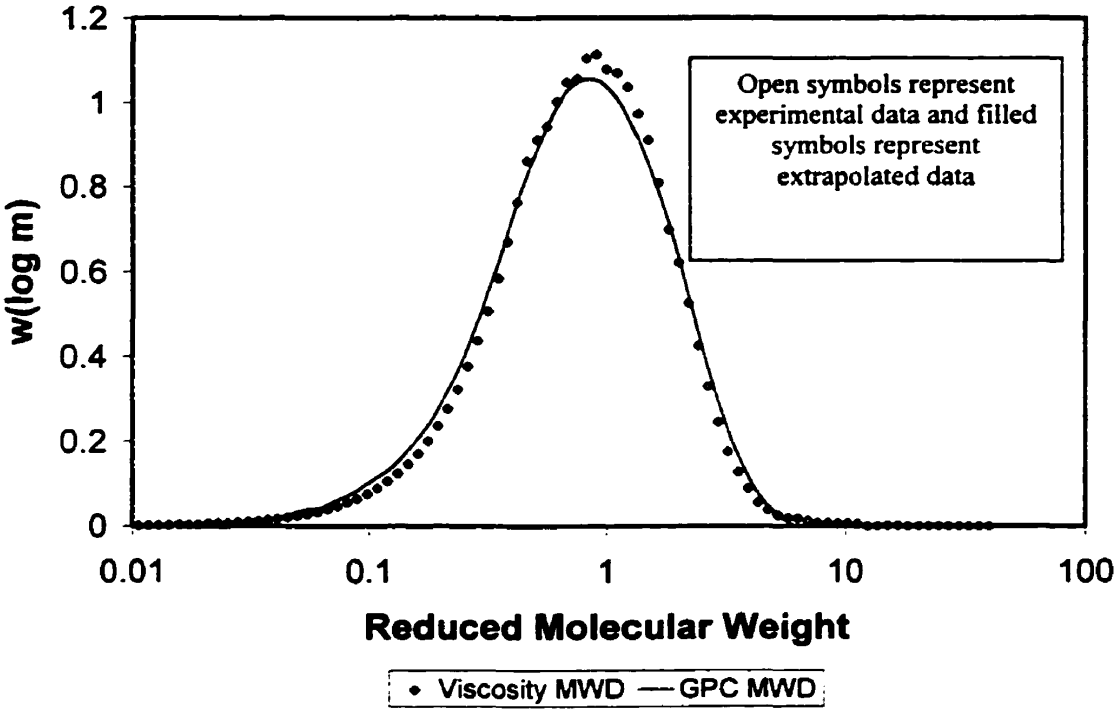

Figure 9.7 Comparison between Viscosity and GPC MWD for LDL2

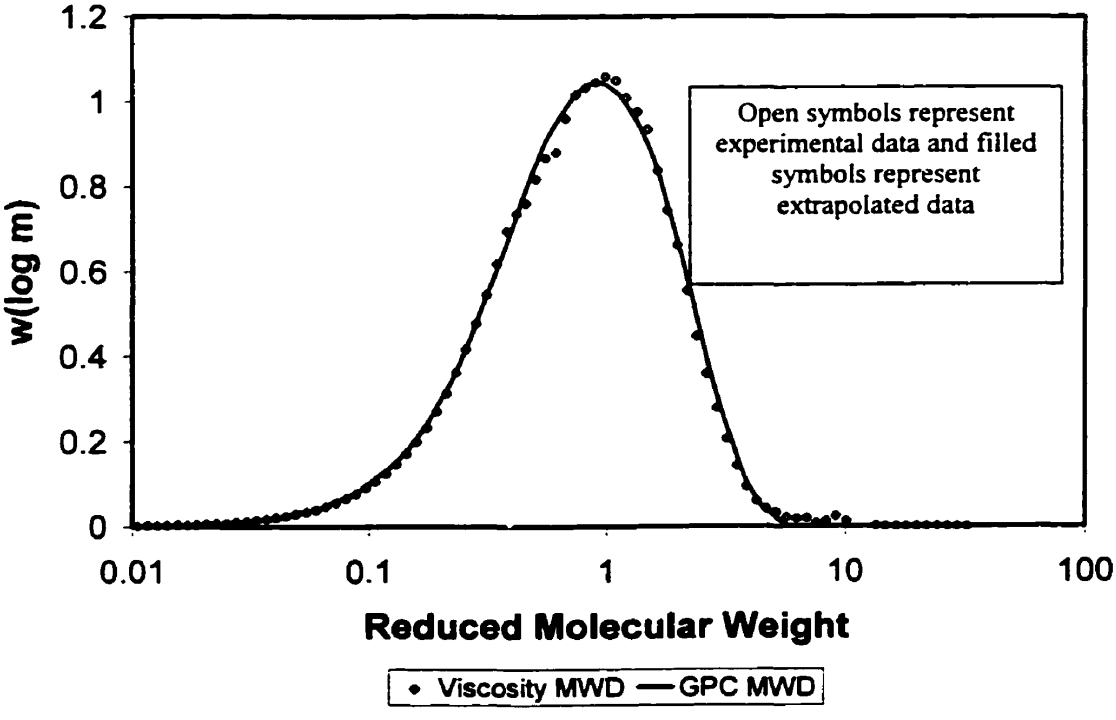

Figure 9.8 Comparison between Viscosity and GPC MWD for LDL3

The effect of polydispersity on the viscosity MWD was studied using LLDPE1 and LLDPE2 (Figures 9.9 and 9.10), the results are summarized in Table 9.5. While the viscosity MWDs of LLDPE1 and LLDPE2 are not in as good agreement with the GPC data as is the viscosity MWD for the narrower MWD HDL1, the agreement is still very good. Based on the data in Table 9.5 there is no correlation between polydispersity and the quality of the peak molecular weight prediction.

Table 9.5 Effect of Polydispersity on Viscosity MWD Quality

Resin	M_W	M_W/M_N	Peak Ratio	Breadth Ratio
HDL1	100 900	2.1	0.96	1.04
LLDPE2	145 500	3.5	1.11	.99
LLDPE1	158 000	4.54	1.07	.96

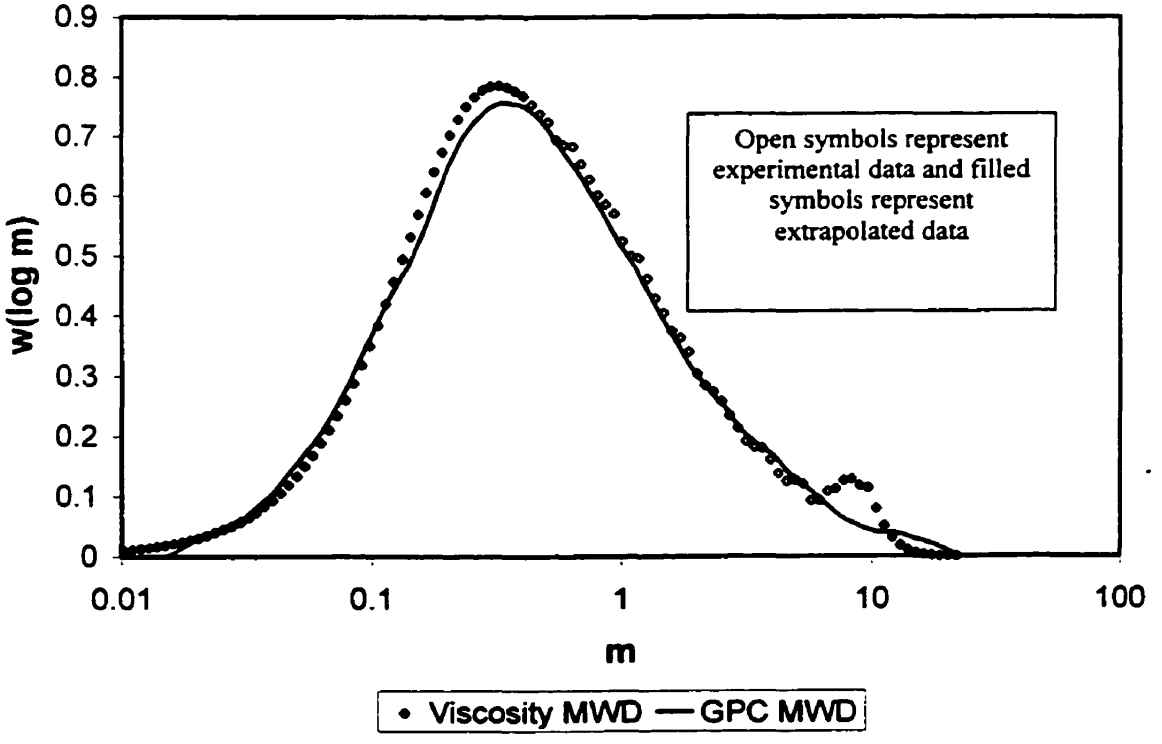

Figure 9.9 Comparison between Viscosity and GPC MWD for LLDPE1
(LVE Data measured at 150°C, 9 points/decade frequency)

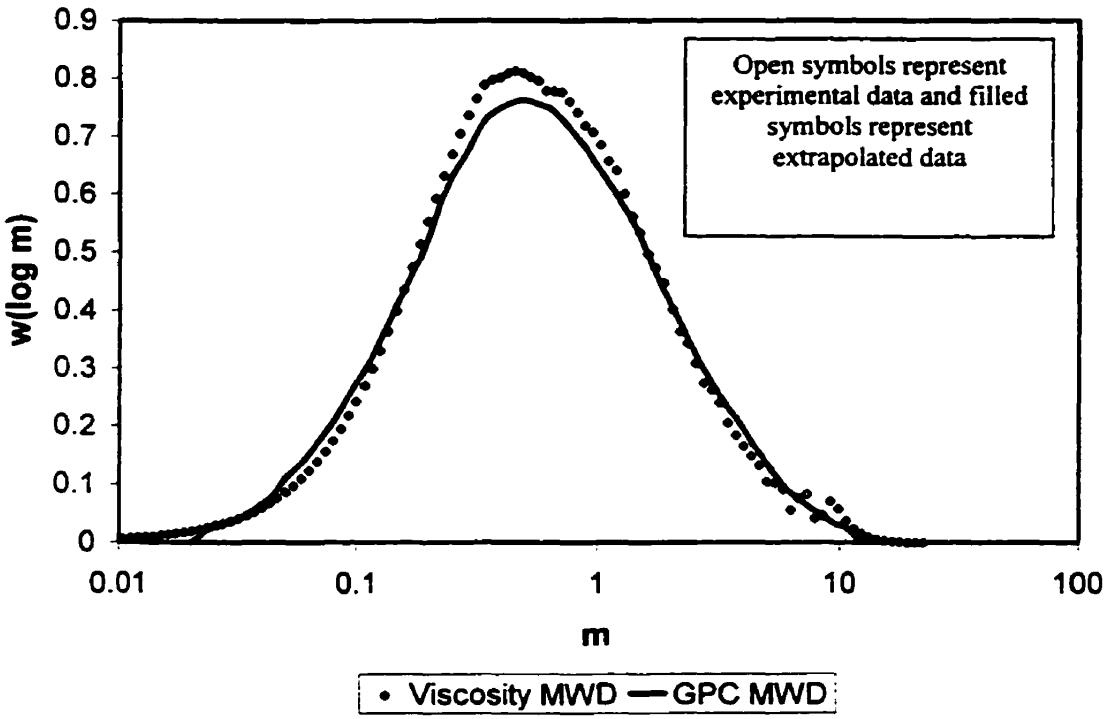

Figure 9.10 Comparison between Viscosity and GPC MWD for LLDPE2
(LVE Data measured at 150°C, 9 points/decade frequency)

9.3.1.2 The Effect of LVE Data Measurement Temperature on the Viscosity MWD

The effect of the measurement temperature on the quality of the viscosity MWD was evaluated using the low density mPE LDL1. LVE measurements were performed at 130, 150 and 170°C, and the viscosity MWD was calculated from the data at each temperature. In Figure 9.11, the viscosity MWDs calculated from LVE data measured at 130°C and 170°C are compared with the GPC MWD. The increase in measurement temperature moves the experimental window to higher molecular weights, which corresponds to lower frequencies. This results in a slightly poorer prediction of the details of the MWD, particularly in the region just before the peak. The results of this study are summarized in Table. 9.6. Increasing the temperature affects primarily the breadth of the viscosity MWD, although there is a small change in the peak location at 170°C. Overall, these data indicate that in the temperature range 130°C to 170°C there is little effect of

temperature on the viscosity MWD for LDL1. As is discussed in the next section, increasing the temperature and thereby moving the experimental window to higher molecular weights can reduce the quality of the viscosity MWD. Therefore, for the materials studied in this work, the lowest temperature at which the material is completely molten is the optimum testing temperature.

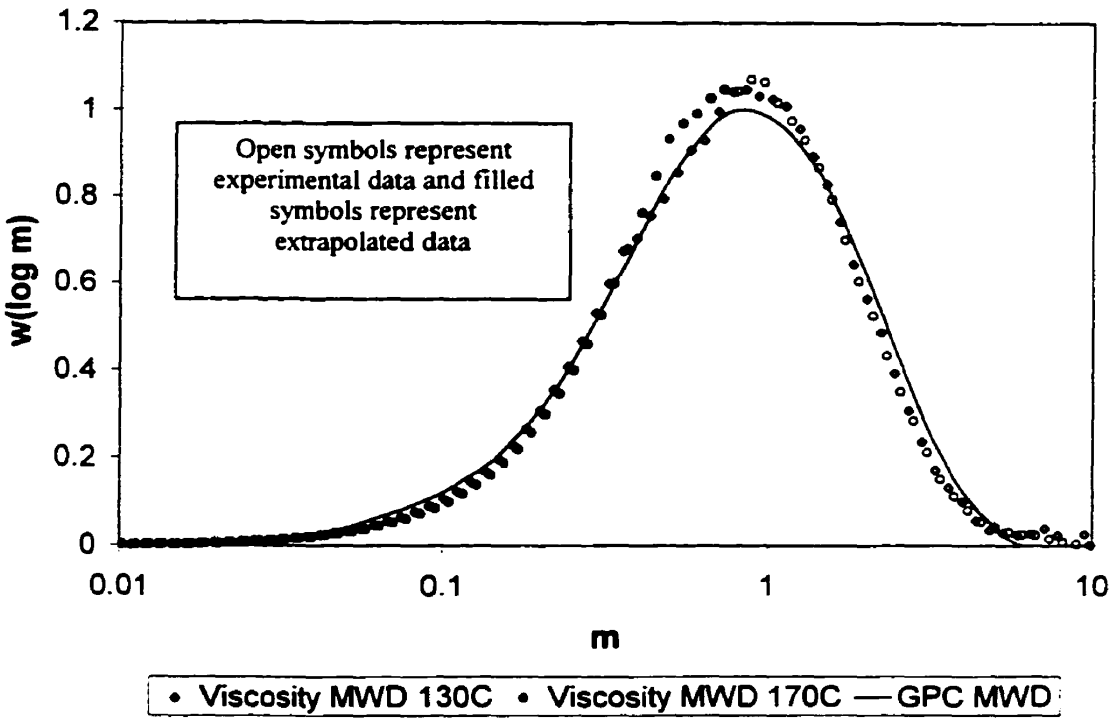

Figure 9.11 The Effect of LVE Measurement Temperature on the Viscosity MWD for LDL1

Table 9.6 Effect of LVE Data Measurement Temperature on Viscosity MWD Quality for LDL1

Measurement Temperature (°C)	Peak Ratio	Breadth Ratio
130	0.97	1.06
150	0.97	1.09
170	0.96	1.09

9.3.1.3 The Effect of LVE Data Density and Range on the Viscosity MWD

The effects of data range and density on the viscosity MWD have been previously investigated[2,3]. Increasing the range and the density of the LVE data results in a better MWD prediction. In terms of range, the ideal LVE data set would include the Newtonian plateau and the power law region. However, this is usually experimentally impossible, and as is shown in reference 2 the most important LVE information resides in the region around the minimum in the second derivative of the logarithmic complex viscosity curve $\left(\frac{d^2 \ln \eta^*}{d \ln \omega^2}\right)$. The likelihood of predicting an accurate MWD with a given set of LVE data can be evaluated by plotting the second derivative curve against the reduced frequency (ω/ω_c)as in Figure 9.12. In this figure we see that the experimental window for HDL1 at 150°C includes the minimum in the second derivative, which leads to the excellent quality of the viscosity MWD prediction for HDL1.

Any shift of the experimental window is likely to affect the quality of the viscosity MWD. An increase in measurement temperature, as shown in the previous section, will shift the experimental window to a lower reduced frequency. If the experimental window no longer covers the minimum in the second derivative, the quality of the MWD will be compromised. A decrease in molecular weight also shifts the experimental window to lower reduced frequencies. This was the cause of the poor quality of the viscosity MWD in the case of HDL2 that was presented in Section 9.3.1.1. HDL2 has a very low molecular weight, resulting in the experimental window shown in Figure 9.13, which does not include the minimum in the second derivative.

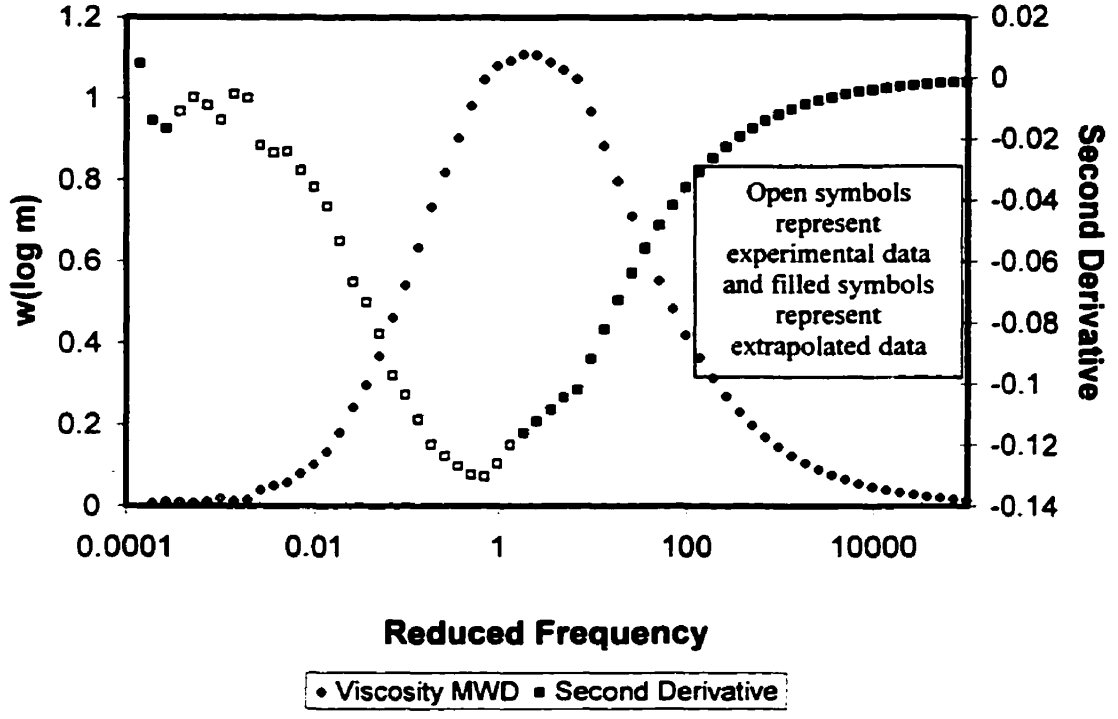

Figure 9.12 Second Derivative and Viscosity MWD Curves for HDL1

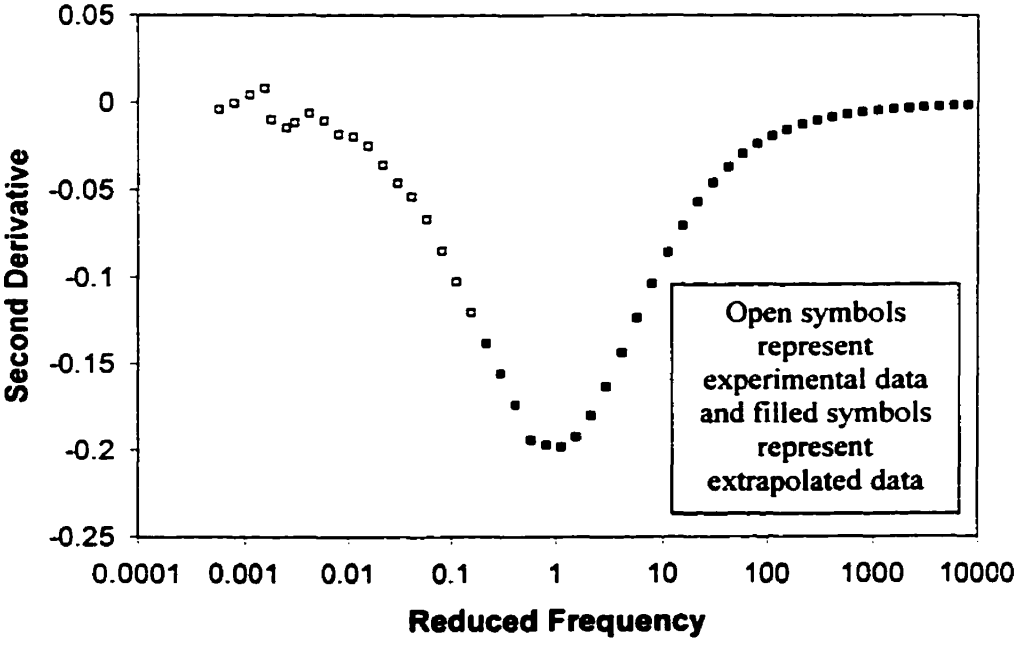

Figure 9.13 Second Derivative Curve for HDL2

A high frequency truncation study was performed using the data for HDL1 to determine the relationship between the breadth of the experimental window and the quality of the viscosity MWD. The data were truncated at the three frequencies shown in Figure 9.14, and the viscosity MWDs were recalculated from the truncated data (Figure 9.15). The results are summarized in Table 9.7. When the data were truncated at frequencies below 6.95 rad/s IRIS was not able to calculate the discrete spectrum. We assume that this was a result of insufficient information for the fitting procedure. In Table 9.7 we see that the quality of the viscosity MWD deteriorates as the experimental window is narrowed. The viscosity MWD becomes narrower, and the peak moves to higher molecular weights as more high frequency data are lost. The breadth of the viscosity MWD is the first characteristic that is affected by the truncation. The peak molecular weight is significantly affected only in truncation 3, shown in Table 9.7, and even in this extreme situation the error in the peak molecular weight is not large. We conclude from this study that data sets including information up to reduced frequencies lower than 0.13 can still predict the location of the peak molecular weight reliably. In the case of multiple peaks in the viscosity MWD, we can refer to the proximity of the experimental window to the second derivative minimum that corresponds to the MWD peak in question to evaluate the quality of the data. A measure of this proximity is the relative location, R, defined in Equation 9.17. According to the results of the truncation study, data sets with relative locations below 0.19 can still predict the location of the peak molecular weight.

$$R \equiv \frac{\text{maximum experimental } \omega}{\omega \text{ at second derivative minimum}} \qquad [9.17]$$

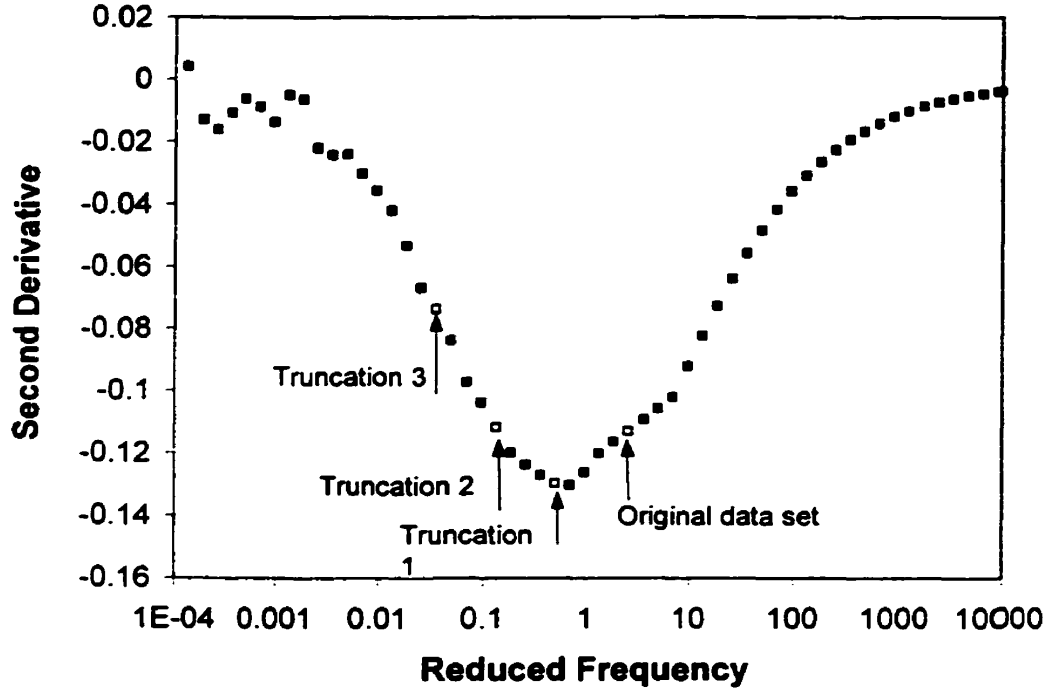

Figure 9.14 Truncation Limits for HDL1 Data

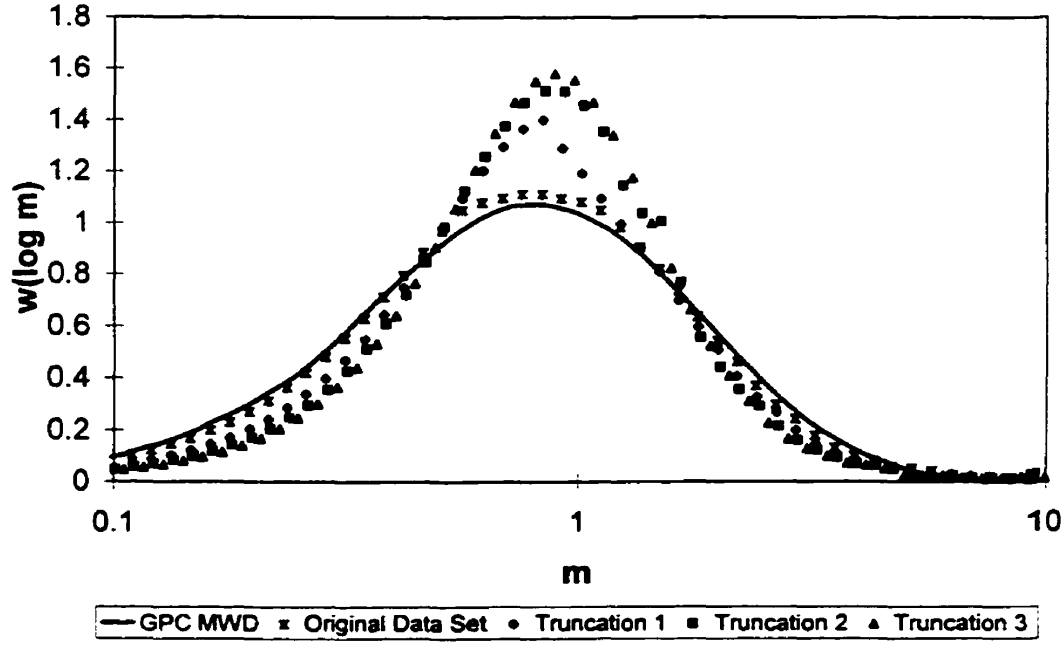

Figure 9.15 Effect of Data Truncation on Viscosity MWD (HDL1)

Table 9.7 Data Truncation Study – HDL1					
Data Set	**Experimental frequency range (rad/s)**	**Maximum ω/ω_c in Exptl Data**	**Relative Location of Exptl Window**	**Peak Ratio**	**Breadth Ratio**
Original	0.036 - 500	2.58	3.73	0.96	1.04
Truncation 1	0.036 - 96.54	0.50	0.72	0.96	1.12
Truncation 2	0.036 - 25.90	0.13	0.19	0.95	1.20
Truncation 3	0.036 - 6.95	0.04	0.05	0.90	1.17

Liu and coworkers[2] showed that the LVE data density governs the resolution of the viscosity MWD. If the data are too sparse, important details of the MWD will be lost, e.g., bimodality in the MWD. To resolve two characteristics of the MWD, one occurring at m_1 and the second occurring at m_2, the condition in Equation 9.18 must be met.

$$\rho_{Data} \geq \frac{6.5}{3.4\left|\mathrm{Log}(m_1) - \mathrm{Log}(m_2)\right|} \qquad [9.18]$$

where ρ_{Data} is points per decade of frequency

In the current work, the density of the LVE data was 7 points per decade of frequency except for the low density mPEs at 150°C and 170°C when the density was 5 points per decade and for LLDPE1 and LLDPE2 when the density was 9 points per decade. Using Equation 9.18, this technique indicates that for the 9, 7 and 5 points/decade data sets the viscosity MWD will resolve features that are 0.21, 0.27 and 0.38 decades of molecular weight apart respectively.

Based upon the accuracy of the peak molecular weight predictions presented earlier it appears that the viscosity MWD technique (applied in this work) actually has a better resolution for this feature of the MWD than was indicated by the above analysis. For all of the linear materials studied in this work, the errors in the peak molecular weight

predictions were less then 0.044 decades of molecular weight (data density of 7 points per decade of frequency). This corresponds to the relation given by Equation 9.19.

$$\text{Resolution in Peak m} = \frac{2}{3.4\rho_{Data}} \qquad [9.19]$$

Using Equation 9.19, we can estimate that the error in the peak molecular weight for the data sets that have densities of 5 and 9 points per decade would be at most 0.059 and 0.033 decades respectively (error is ½ of resolution). It is useful to note that an uncertainty in the viscosity MWD peak molecular weight of 0.044 decades corresponds to an uncertainty in the logarithm of the peak ratio of 0.044.

The results presented in Section 9.3.1 show that the technique used for the calculation of the viscosity MWD of linear polyethylenes is robust, particularly in terms of the peak molecular weight prediction. Based upon the truncation study using data for HDL1, we find that as long as sufficient data for the fitting of the viscosity models is available the peak molecular weight can be predicted with good accuracy. The LVE data density governs the resolution in the peak molecular weight. For 7 points per decade of frequency the resolution in the peak molecular weight is 0.084 decades of molecular weight. This correspond to an uncertainty in the peak molecular weight ratio of 11% (for a peak ratio of 1), which is larger than, and could therefore possibly explain, all of the errors due to differences in molecular structure, measurement temperature, and data truncation that were found in this work.

9.3.2 The Effect of LCB on Viscosity MWD

The viscosity MWD technique presented in Section 9.3.1 is valid only for linear materials. Since the complex viscosity curve is affected by MWD and long chain branching (LCB), a viscosity MWD calculated for a branched material does not represent the GPC MWD. For a branched material, the viscosity MWD can be interpreted as the

MWD of a linear polymer that would have the same complex viscosity curve as that of the branched material. The viscosity MWD was calculated for the branched materials, HDB1-4 and LDB1-3, and the results are compared to the GPC MWDs in Figures 9.16 through 9.22. We recall that HDB1-4 have increasing levels of LCB as do LDB1-3. The presence of LCB has several effects on the viscosity MWD. The viscosity MWD of a branched material in comparison to the GPC is broadened, the primary peak is shifted to a lower molecular weight, and a secondary peak is added at high molecular weights. As can be seen in Figures 9.16 through 9.22, the degree of distortion in the viscosity MWD as compared to the GPC MWD increases as the degree of LCB increases. It was found that the shifting of the peak was the best measure of the difference between the viscosity and the GPC MWD, and as shown in the next section, this shift can be correlated with the degree of LCB. The LVE data used to determine the viscosity MWDs presented in this section were measured at 150°C unless otherwise indicated.

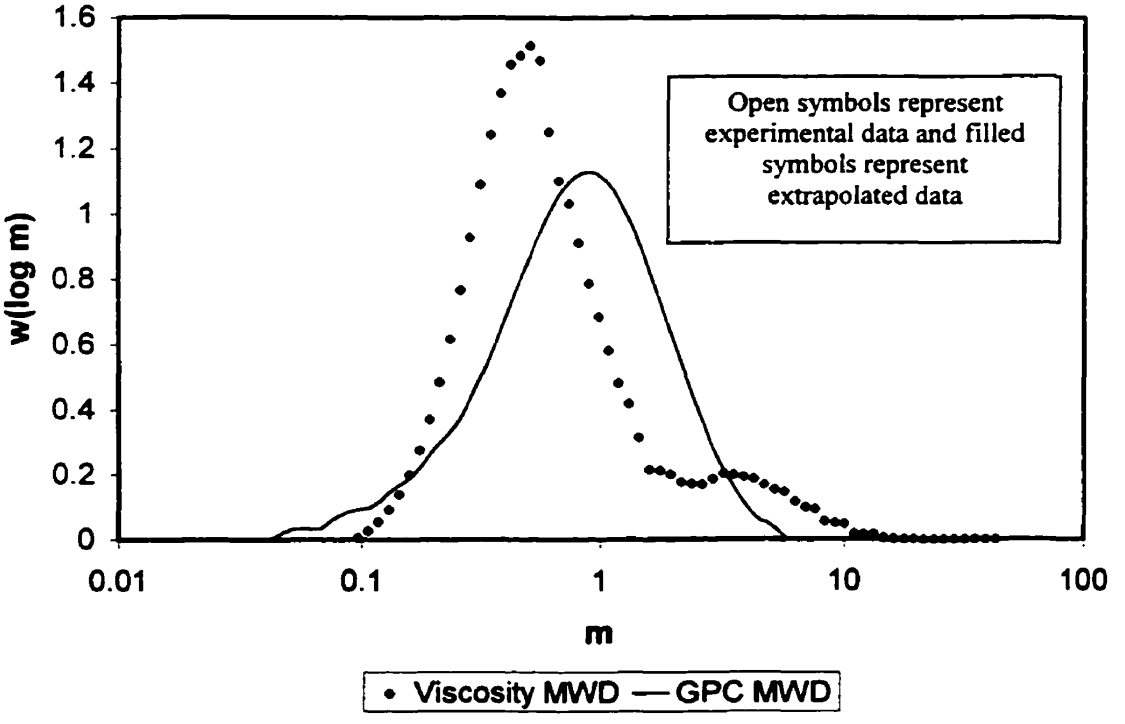

Figure 9.16 Comparison between Viscosity and GPC MWD for HDB1

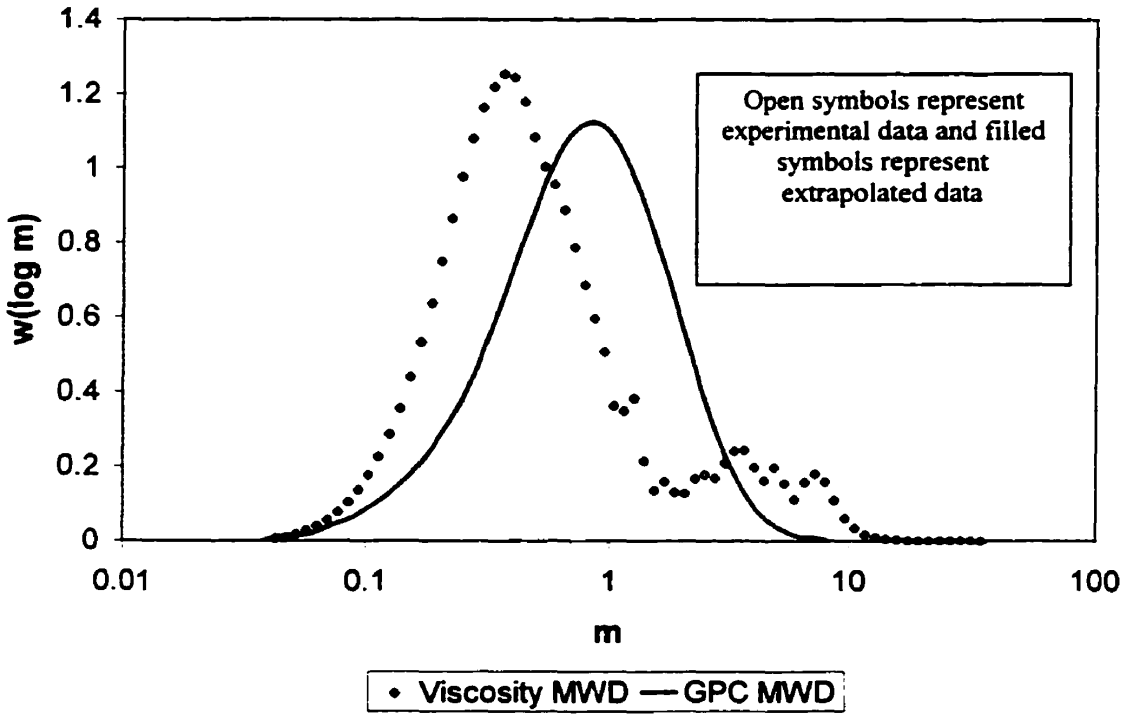

Figure 9.17 Comparison between Viscosity and GPC MWD for HDB2

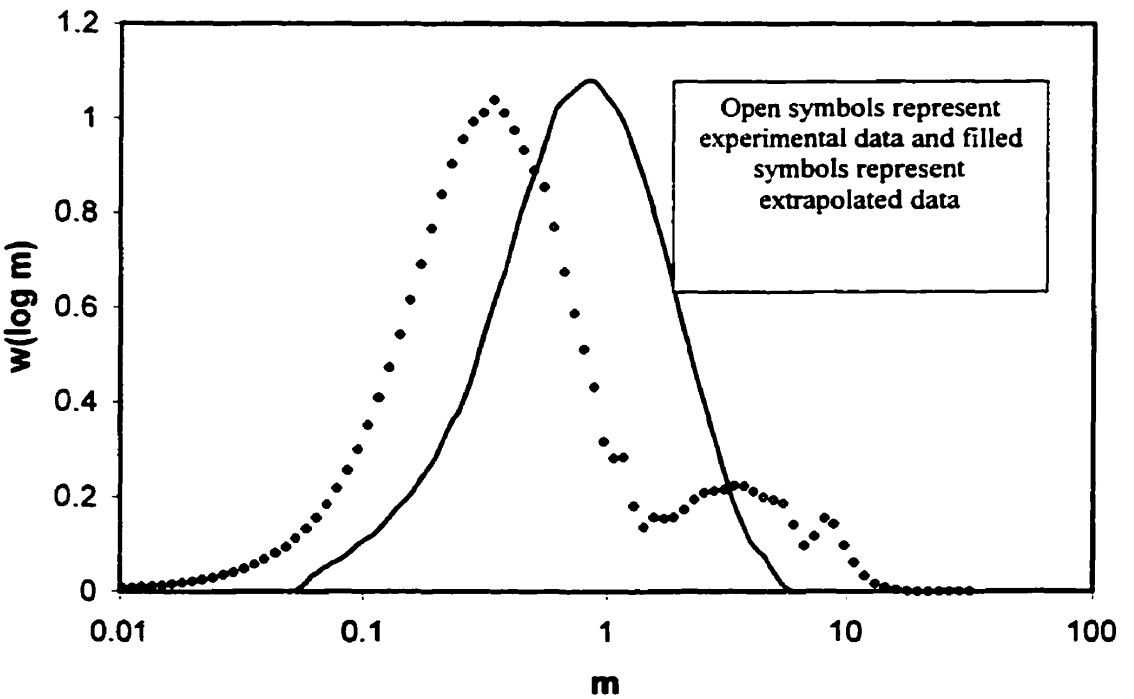

Figure 9.18 Comparison between Viscosity and GPC MWD for HDB3

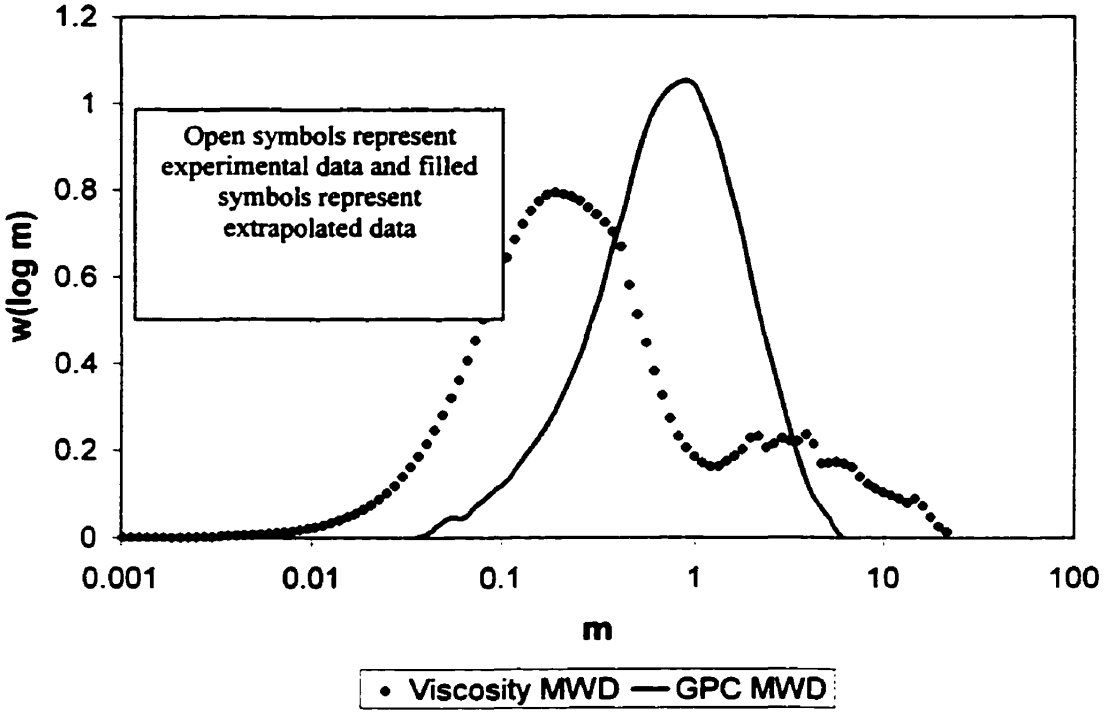

Figure 9.19 Comparison between Viscosity and GPC MWD for HDB4

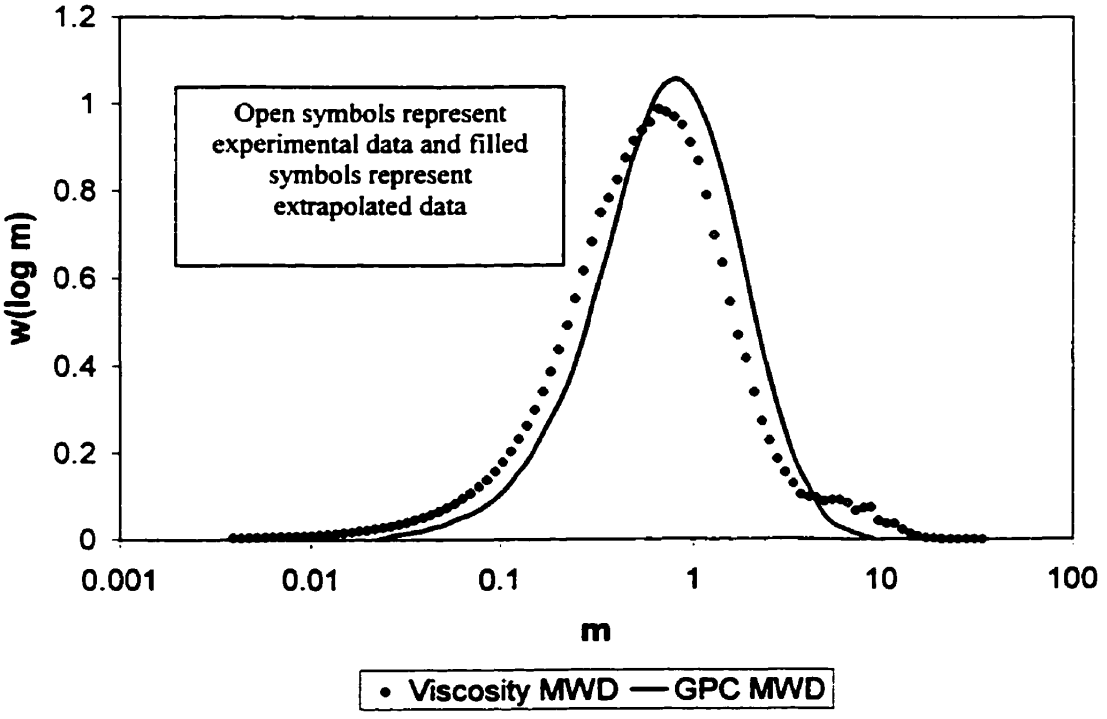

Figure 9.20 Comparison between Viscosity and GPC MWD for LDB1
(LVE Data Measured at 130°C)

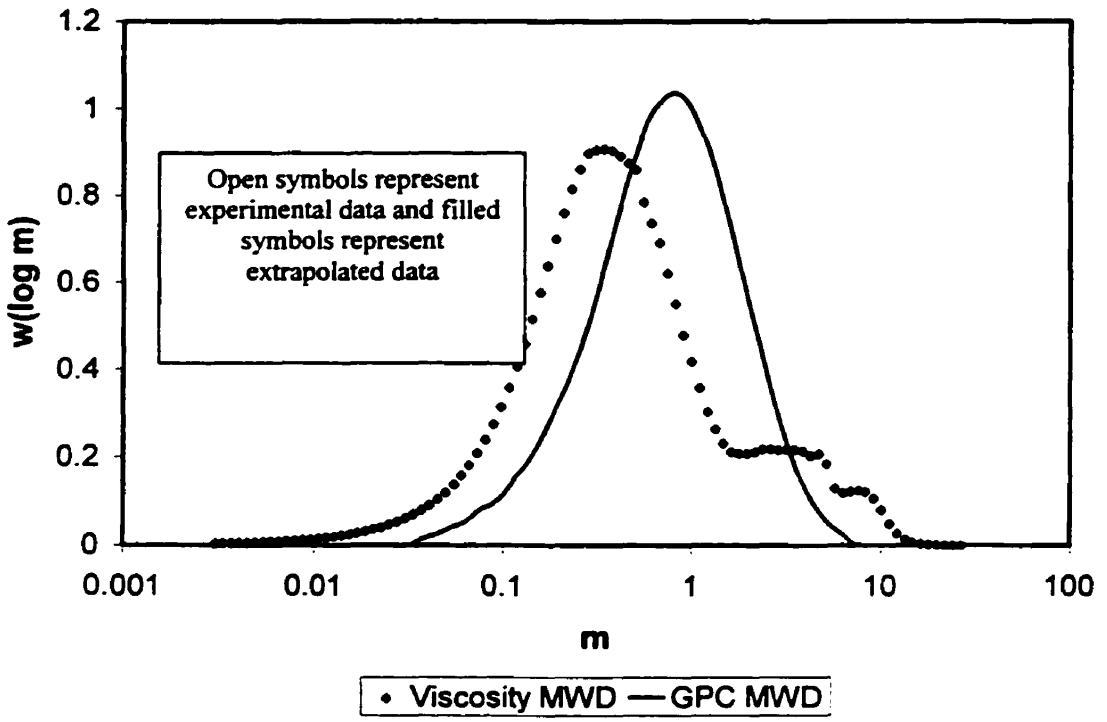

Figure 9.21 Comparison between Viscosity and GPC MWD for LDB2
(LVE Data Measured at 130°C)

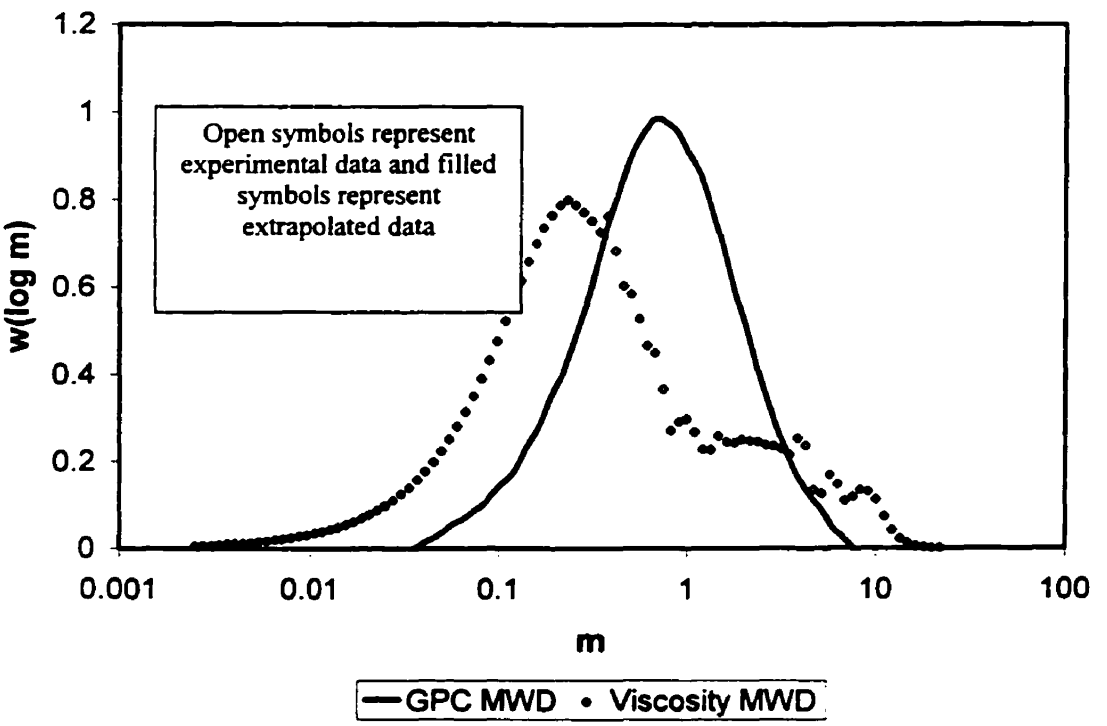

Figure 9.22 Comparison between Viscosity and GPC MWD for LDB3
(LVE Data Measured at 130°C)

Since the peak of the viscosity MWD is an important parameter, it is necessary to ensure that the predictions for this value are correct. For the branched materials, with the exception of LDB1, the experimental window does not cover the primary peak. However, as was demonstrated previously, the criterion for evaluating the quality of the prediction of the location of a peak MWD involves the location of the experimental window relative to the corresponding minimum in the second derivative curve. Figure 9.23 shows the second derivative of HDB3. By inspection, we see that the experimental window is close enough to the relevant minimum in the second derivative to give a good prediction of the location of the peak. A more objective measure is the relative location parameter, **R**, as defined by Equation 9.17. The **R** values corresponding to the primary peaks for all the branched materials are presented in Table 9.8. The lowest **R** value for the branched materials, 0.52, is significantly higher than the **R** value of 0.19 that was seen with the second truncation of the HDL1 (Section 9.1.3.1). Even with an **R** of 0.19 the peak molecular weight prediction was very good. Assuming that the **R** parameter is valid for the branched materials we can thus have confidence in the predicted locations of the primary peaks in the viscosity MWDs of the branched materials.

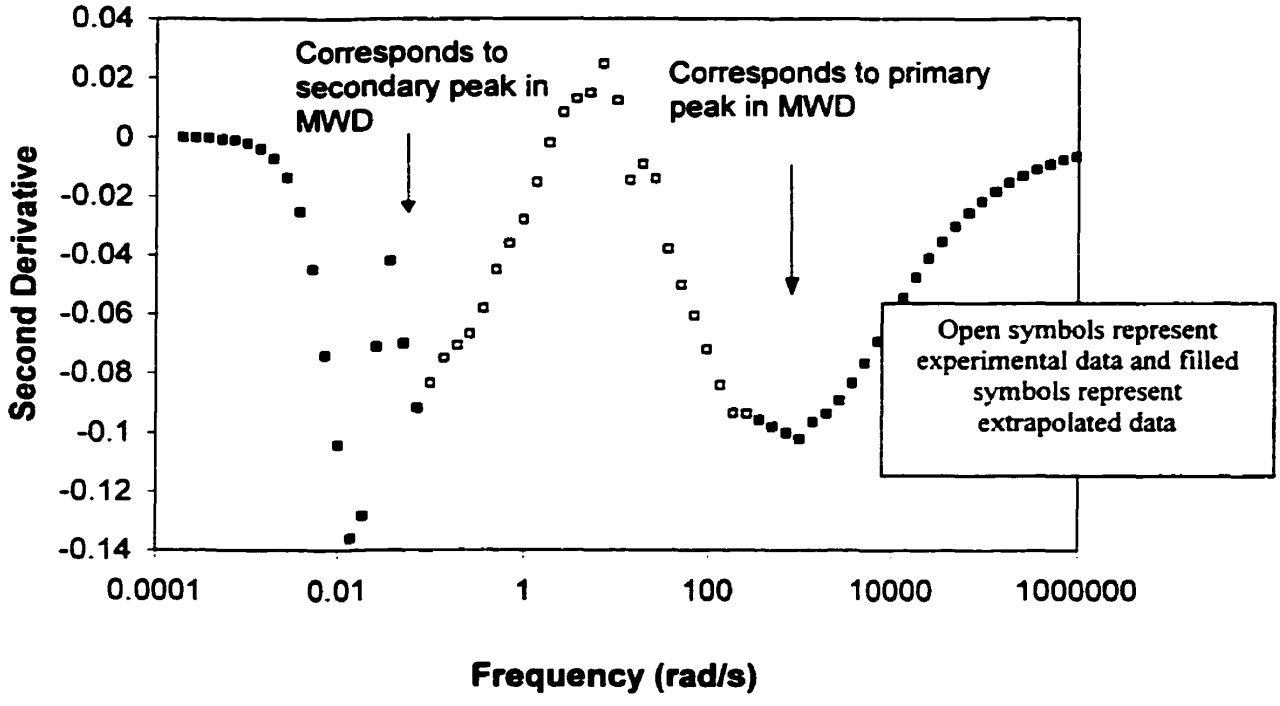

Figure 9.23 Second Derivative Curve for HDB3

Table 9.8 Relative Locations with respect to Primary Peaks in MWD for Branched mPEs					
High Density mPEs			Low Density mPEs		
Resin	LCB/ 10^4 C	R	Resin	DRI	R
HDB1	0.12	0.72	LDB1	1.1	19.3
HDB2	0.37	0.72	LDB2	3.9	3.73
HDB3	0.42	0.52	LDB3	14	0.52
HDB4	1.21	2.68			

A high frequency truncation study of the data for HDB3 was performed to evaluate the applicability of the **R** parameter to branched materials. As for HDL1, high frequency data were truncated, and the viscosity MWD was recalculated until the shortest data set that allowed for the same peak molecular weight was found. The results of this study are shown in Figure 9.24. The truncated data set included data up to a frequency of 258.28 rad/s and had an **R** of 0.19. This limiting value of **R** is in agreement with the

results for HDL1. From this we conclude that **R** is a valid criterion for evaluating the quality of the viscosity peak molecular weight for branched materials and that as long as **R** is ≥ 0.19 the peak molecular weight prediction is reliable.

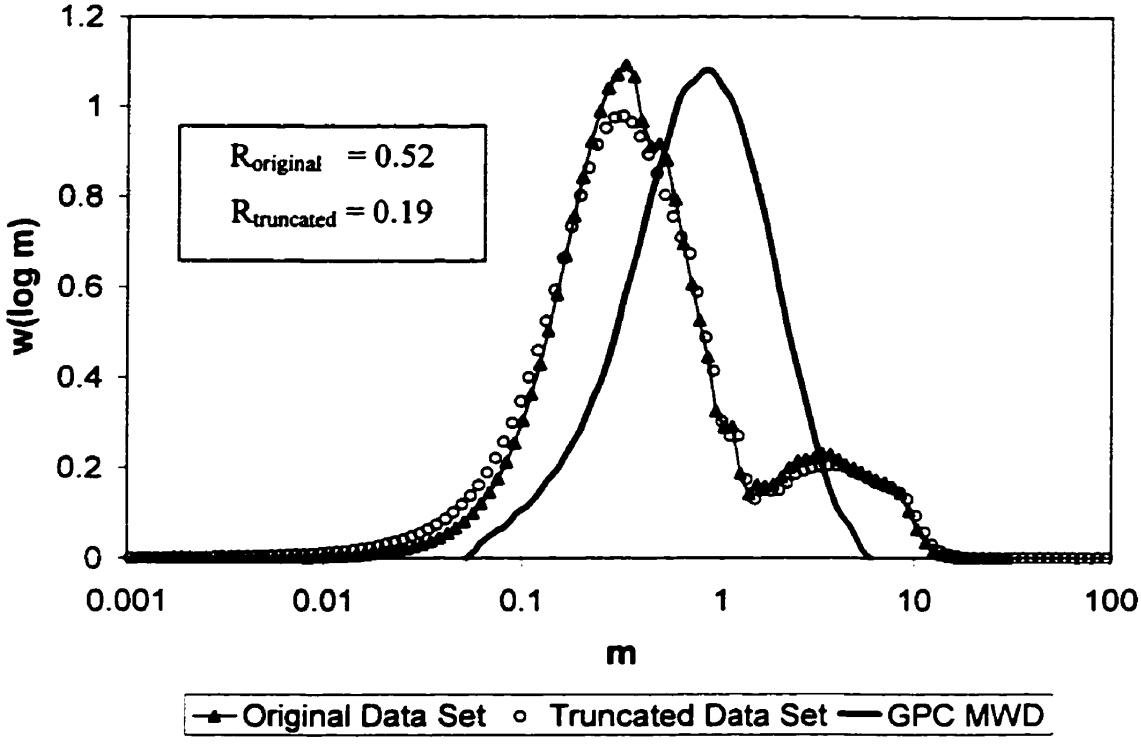

Figure 9.24 Results of HDB3 Truncation Study

9.4 Correlating the Distortion of the Viscosity MWD to Degree of LCB

It was found that the feature of the viscosity MWD that was most sensitive to the degree of LCB was the shift in the primary peak as compared to the GPC MWD. To quantify the shift of the primary peak we use the peak ratio, defined by Equation 9.15. The peak ratio values for the branched materials are given in Table 9.9. As noted earlier, the peak ratios for all of the linear materials are in the range 1.0±0.11, implying that there is a significant difference between the linear materials and the (long chain) branched mPEs.

Using the data for the high density mPEs, for which we had C^{13}-NMR measurements of degree of LCB, a correlation was developed between peak ratio and degree of LCB (Equation 9.20). With this correlation, peak ratios less than 1 automatically indicate a linear material. For peak ratios greater than or equal to 1 a parabolic function of the logarithm of the peak ratio was found to give the degree of LCB. This function has only one fitted parameter, and it was found that functions with more parameters did not improve the fit of the data. Equation 9.20 is compared to the experimental data for the high density mPEs in Figure 9.25.

$$\frac{LCB}{10^4\,C} = \begin{cases} \dfrac{\text{GPC Peak}}{\text{Viscosity Peak}} < 1, & 0 \\ \dfrac{\text{GPC Peak}}{\text{Viscosity Peak}} \geq 1, & 2.66\left[\text{Log}\left(\dfrac{\text{GPC Peak}}{\text{Viscosity Peak}}\right)\right]^2 \end{cases} \qquad [9.20]$$

$$r^2 = 0.998$$

Table 9.9 Peak Ratios (Equation 9.15) for Branched mPEs

High Density mPEs				Low Density mPEs			
Resin	**Actual LCB/ 10^4 C**	**Peak Ratio**	**Predicted LCB/10^4 C**	**Resin**	**DRI**	**Peak Ratio**	**Predicted LCB/10^4 C**
HDB1	0.12	1.73	0.15	LDB1	1.1	1.27	0.03
HDB2	0.37	2.31	0.35	LDB2	3.9	2.33	0.36
HDB3	0.42	2.51	0.45	LDB3	14	2.96	0.60
HDB4	1.21	4.69	1.20				

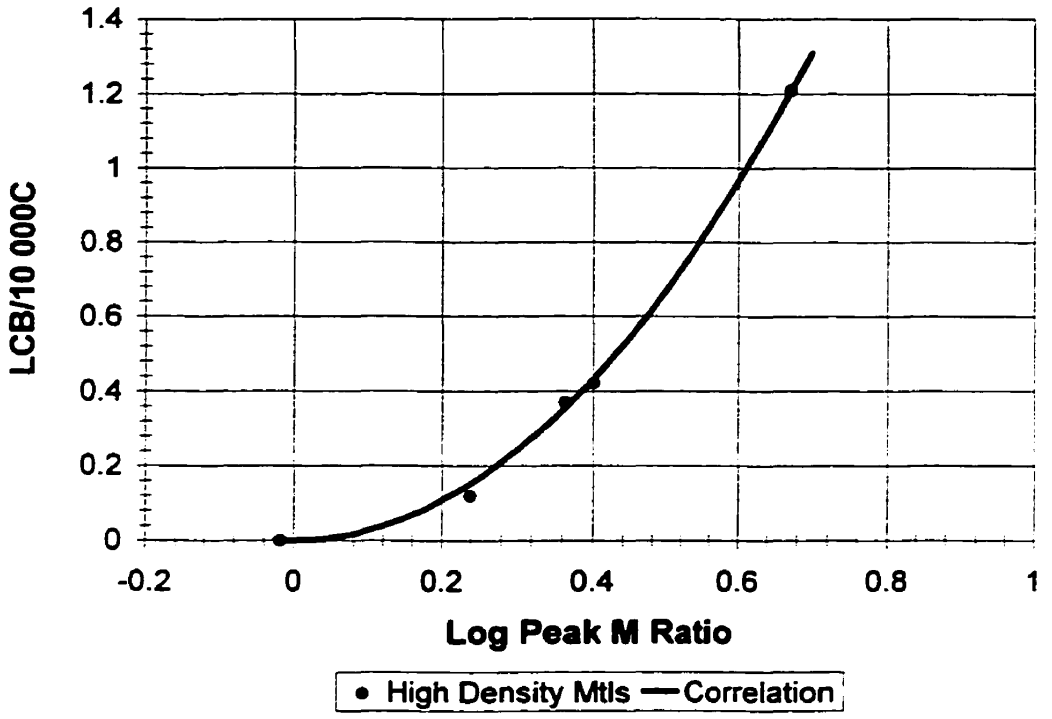

Figure 9.25 Relationship between Degree of LCB and Peak Molecular Weight Ratio

To test the possibility of falsely predicting LCB in a linear material, this correlation was used with all of the linear materials discussed in Section 9.3.1, and the highest degree of LCB that was predicted was 0.005 LCB/10^4C. The uncertainty in the viscosity peak molecular weight due to data density for LVE data with 7 points/decade is 0.044 decades. Therefore, the largest peak ratio that should be obtained for a linear material is 1.11, which corresponds to 0.005 LCB/10^4C. Therefore, only when the predicted level of LCB is greater than 0.005, can it possibly indicate the presence of LCB. For branched materials, assuming the same uncertainty in the peak molecular weight, the uncertainty in the predicted LCB can be calculated using Equation 9.21. In Equation 9.21, PR is the peak molecular weight ratio. It should be noted that the uncertainty in the predicted degree of LCB calculated using Equation 9.21 is only indicative of the uncertainty due to data density in the LVE data. Issues such as uncertainty in the correlation parameters due to limited data points have not been included in this analysis.

$$\Delta LCB = \frac{\partial LCB}{\partial \text{Log}(PR)} \bullet \Delta \text{Log}(PR) = 0.118[\text{Log}(PR)] \qquad [9.21]$$

The predicted degrees of LCB for LDB1-3 and the uncertainties in these predictions due to LVE data density are given in Table 9.10.

Table 9.10 Predicted Degree of LCB for Low Density Branched mPEs

Resin	LCB/10^4C	Uncertainty in LCB/10^4C
LDB1	0.03	0.01
LDB2	0.36	0.04
LDB3	0.60	0.06

It has been demonstrated that degree of LCB can be inferred using rheological data when combined with analytical molecular weight distribution data. The extensional flow data measured using the Rheomoetrics extensional rheometer (RME) are not useful for quantifying LCB or even ranking resins in terms of LCB. LVE data, on the other hand, appear to be sensitive to degree to LCB. The effects of MWD and LCB on the LVE behavior can be distinguished by comparing the viscosity MWD calculated using the complex viscosity curve with the GPC MWD. The difference between the viscosity and the GPC MWDs for branched materials is related to the degree of LCB. This relation is described by a simple correlation (Equation 9.20) that can be used to estimate the degree of LCB for a material that has unknown branching characteristics.

List of References

[1] Shaw, M.T. and W.H. Tuminello, *Polym. Eng. Sci.* 34, 159-165 (1994)

[2] Liu, Y., M.T. Shaw, and W.H. Tuminello, *Polym. Eng. Sci*, 38(1), 169-176 (1998)

[3] Wood-Adams, P.M. and J.M. Dealy, *J. Rheol.* 40(5), 761-778, (1996)

[4] Lai, S.Y. *et al*, ANTEC 40, 1814-1815 (1994)

[5] Münstedt, H. and H.M. Laun, *Rheol. Acta.*, vol. 20, 211, 1981

[6] Hingmann, R. and B.L. Marczinke, *J. Rheol.*, 38(3), 573-587 (1994)

[7] Malkin, A.Y. and A.E. Teishev, *Polym. Eng. Sci.* 31, 2449-2455 (1991)

Chapter 10.
Conclusions

1. The zero shear viscosity of linear mPEs depends exponentially on the weight average molecular weight with an exponent very close to that reported previously for other linear polyethylenes.

2. Comonomer content, based on butene comonomer, or degree of short chain branching has no effect on the linear viscoelastic behavior up to a butene content of 21.1 weight %.

3. Both the linear and nonlinear viscoelastic behavior of mPEs are affected by the presence of long chain branches, with the linear viscoelastic data being most sensitive to small differences in degree of long chain branching (LCB).

4. Increasing the degree of long chain branching of mPEs has an effect on the linear viscoelastic behavior that is similar to increasing the branch length of asymmetric star polymers. The zero shear viscosity is increased, and the relaxation spectrum is broadened with increased LCB. Also, long chain branched materials exhibit a plateau in their loss angle function that is not exhibited by linear materials.

5. mPEs follow most of the empirical relations developed by Cox, Merz and Gleissle to relate linear properties to viscometric functions.

6. Increasing the degree of LCB of mPEs results in more shear sensitivity.

7. Both linear and long chain branched mPEs exhibit separable stress relaxation behavior at large strains. Increasing the degree of LCB results in a damping function that is more sensitive to strain.

8. The Wagner model, with a memory function inferred from linear viscoelastic data and a damping function determined using step strain experiments, can adequately describe the behavior of mPEs in steady simple shear and large amplitude oscillatory shear.

9. Most of the effect of LCB on extensional flow behavior arises from the linear viscoelastic properties of a material, and transient extensional flow data are therefore not useful for inferring the level of LCB of mPEs.

10. Rheological data alone are not sufficient to infer level of LCB, and some knowledge of the molecular structure is necessary.

11. The viscosity MWD, calculated from the complex viscosity using a technique developed for linear polymers, can be used along with analytical molecular weight distribution data to infer the level of LCB using the technique developed in this work. The linear viscoelastic measurement conditions can be optimized to provide the best LCB prediction. Variations in molecular weight, polydispersity and degree of short chain branching within certain limits will not cause the false prediction of the presence of LCB in the case of a linear material.

Chapter 11.
Contributions to Knowledge

The effect of molecular structure on the rheology of polyethylene was studied in a systematic way. Because of the unique properties of the constrained geometry catalyst system we were able to study a precisely defined set of mPEs. The effect of molecular weight (MW), short chain branching (SCB), and long chain branching (LCB) on the rheological behavior of polyethylene were studied independently. A study such as this is unique for polyethylene. Most of the previous work in this area compared materials that were different in more than one molecular characteristic. In particular, studies of the effect of LCB on the rheological behavior of commercial polyethylenes were complicated by large variations in molecular weight distribution (MWD).

The zero shear viscosity was found to depend exponentially on the weight average molecular weight, confirming previously reported results. Degree of SCB, for butene copolymers, was shown to have no significant effect on the linear viscoelastic behavior up to a butene content of 21.1 weight %. The lack of effect of SCB on rheological behavior is often assumed, but this is the first time that is has been confirmed using materials with identical polydispersities. Low levels of LCB were found to affect both linear and non-linear viscoelastic behavior with the linear viscoelastic data being the most sensitive to degree of LCB. Zero shear viscosity and breadth of relaxation spectrum increased with degree of LCB. Additionally branched mPEs exhibited a plateau in their loss angle curve that is not present for linear polyethylenes. This plateau has been reported before for model star polymers but not for commercial branched materials. Temperature sensitivity increased with degree of LCB. In terms of linear viscoelastic behavior, branched mPEs behaved in a very similar fashion to star branched polymers in

that increasing the degree of long chain branching of mPEs has effects that were qualitatively similar to those of increasing the branch length in asymmetric star polymers.

Branched mPEs follow the empirical relations developed by Cox, Merz and Gleissle that relate linear properties to viscometric functions. This is not found with highly branched traditional low density polyethylene and is therefore a new finding.

The degree of LCB significantly affects the viscosity curves of mPEs. As mentioned previously, the zero shear viscosity is increased with degree of LCB. Also, the shear sensitivity of the material is increased resulting in a high rate viscosity that can be lower than that of a linear material of the same molecular weight.

Linear and branched mPEs exhibit separable stress relaxation behavior and that the sensitivity of the damping function to strain increases with degree of LCB. This has never been reported before for polyethylene.

This work showed that extensional flow data are not as sensitive to low levels of LCB as was previously thought from studies of highly branched LDPE. In particular, the effects of LCB on transient extensional flow behavior can be explained in terms of changes in the linear viscoelastic properties.

This work has shown that the effect of low levels of LCB on the rheological behavior is significantly different from the effect of high levels of LCB. An extrapolation of the rheological behavior of highly branched low density polyethylenes to the low levels of LCB present in mPEs is therefore not possible.

Transient extensional flow data are not suitable for inferring degree of LCB, and since other rheological properties are affected by both MWD and LCB some knowledge of the molecular structure is necessary to infer degree of LCB. The conclusion that

extensional flow data are not useful for inferring degree of LCB is not in accordance with the conventional view arising from studies of highly branched low density polyethylene.

A technique was developed for inferring low levels of LCB using complex viscosity data and analytical MWD information. In this technique, the viscosity MWD is calculated from the complex viscosity using a technique developed for linear polymers and compared to the actual MWD (as measured by gel permeation chromatography). The presence of LCB causes the viscosity MWD to be very different from the actual MWD; the primary peak in the distribution is shifted to a lower molecular weight and a false peak is added at high molecular weights. We have correlated the shift of the primary peak to the degree of LCB using a simple equation. This procedure is robust and variations in M_W, MWD and SCB are not likely to result in false predictions of LCB for linear materials. We have also presented a technique for evaluating the reliability of the predicted degree of LCB that involves only complex viscosity data.

Bibliography

Archer, A.R. and S.K. Varshey, work submitted for publication (1998)

Baumgaertel, M. and H.H. Winter, *Rheol. Acta*, 22, 425 (1983)

Bersted, B.H. *et al*, *J. Appl. Polym. Sci.*, Vol. 26, 1001 (1981)

Bersted, B.H., *J. Appl. Poly. Sci.*, Vol. 30, 3751-3765 (1985)

Bersted, B.H., *Encyclopedia of Fluid Mechanics*, Vol. 7, Chapter 22, Gulf Publishing Company (1988)

Carella, J.M. *et al*, *Macromoleculs*, Vol. 19, 659, (1986)

Carella, J.M., Macromolecules, 29, No. 25, 8280-8281 (1996)

Colvin, R., Modern Plastics, 62-67, May (1997)

Constantin, D., *Poly. Eng. Sci.*, 24, 268 (1984)

Cox, W.P. and E.H. Merz, *J. Polym. Sci.*, 28:619 (1958)

Dealy, John M. and Kurt F. Wissbrun, *Melt Rheology and its Role in Plastics Processing: Theory and Applications*, Van Nostrand Reinhold New York, 1990

Gell, C.B. *et al*, *J. Polym. Sci. B: Polym. Phys.*, 35, 1943-1954 (1997)

Giacomin A.J.and J.M. Dealy, in *Techniques in Rheological Measurement*, edited by A.A. Collyer, Chapman and Hall, London, 1993.

Gleissle, W. in *Rheology, Vol. 2*, edited by G. Astarita, G. Marrucci and L. Nicolais (Proc. 8th Intern. Congr. Rheol.) Plenum Press, New York, p. 457 (1980).

Graessley, W.W. *et al*, *Macromolecules*, 9, 127-141 (1976)

Graessley, W.W. and J. Roovers, *Macromolecules*, 12, 959 (1979)

Hepperle, J. and T. Saito, unpublished work, Institute of Polymer Materials, University of Erlangen-Nuremberg, Erlangen, Germany 1998

Jeyaseelan, R.S. and J.M. Dealy, unpublished work, 1996

Kim, Seungoh, unpublished work, McGill University (1998)

Kim, Y.S., et al, *J. Appl. Polym. Sci.*, 59, 125-137 (1996)

Koopmans, R.J. SPE ANTEC, 43 , 1006-1009, (1997)

Koran, F., *Anomalous Wall Slip Behavior of Low Density Polyethylenes*, Master's Thesis, Department of Chemical Engineering, McGill University, July 1994

Lai, S.Y. and G.W. Knight, SPE-ANTEC, 39, 1188-1192 (1993)

Lai, S.Y. *et al*, United States Patent, 5 272 236 (1993)

Lai, S.Y. *et al*, SPE-ANTEC, 40, 1814-1815 (1994)

Larson, R.G., *Rheol. Acta.*, 24:327 (1985)

Laun, H.M. and H. Münstedt, *Rheol. Acta*, 15, 517 (1976)

Laun, H.M. and H. Münstedt, *Rheol. Acta*, 17, 415 (1978)

Laun, H.M. and H. Schuch, *J. Rheol.*, 33(1), 119-175 (1989)

Laun, H.M., *Rheol. Acta*, 17, 1-15 (1978)

Laun, H.M., *J. Rheol.*, 30:459 (1986)

Liu, Y., M.T. Shaw, and W.H. Tuminello, *Polym. Eng. Sci*, 38(1), 169-176 (1998)

Macosko, C.W. and Kasehagen, work submitted to *J. Rheol.* for publication (1998)

Malkin, A.Y. and A.E. Teishev, *Polym. Eng. Sci.* 31, 2449-2455 (1991)

Meissner, J. and J. Hostettler, *Rheol. Acta*, 33:1-21 (1994)

Mirabella, F.M. and L. Wild, *American Chemical Society Advances in Chemistry Series 227*, 23-44 (1990)

Münstedt, H. and H.M. Laun, *Rheol. Acta*, 18, 492 (1979)

Münstedt, H. and H.M. Laun, *Rheol. Acta*, 20, 679 (1981)

Münstedt, H. and H.M. Laun, *Rheol. Acta.*, 20, 211 (1981)

Münstedt, H., *J. Rheol.*, 23:4, 421-436 (1979)

Osaki, K. *et al*, *Macromolecules*, 23:20, 4392 (1990)

Osaki, K, *Rheol. Acta.*, 32, 429-437 (1993)

Pang, S. and A. Rudin, *American Chemical Society Symposium Series 521*, 254-269 (1993)

Papanatasiou, A.C. *et al*, *J. Rheol.*, 27, 387-410 (1983)

Pederson, S. and A. Ram, *Polym. Eng. Sci.*, 18, 990 (1978)

Raju, V.R., *et al*, *J. Polym. Sci., Poly. Phys. Ed.*, 17, 1223 (1979)

Raju, V.R., *et al*, *J. Polym. Sci., Polym. Phys. Ed.*, 17, 1183-1195 (1979)

Raju, V.R., G.G. Smith, G. Marin, J.R. Knox, W.W. Graessley, *J. Polym. Sci.: Phys. Ed.*, 17, 1183-1195 (1979)

Ramanathan, R. et al, SPE ANTEC, 41, 1073-1077 (1995)

Randall, J.C., *American Chemical Society Symposium Series 142*, 93-118 (1980)

Rochefort, W.E., *et al*, *J. Polym. Sci: Polym. Phys. Ed.*, 17, 1197 (1979)

Rudin, A. *et al*, *J. Liquid Chrom.*, 7 (9), 1809-1821 (1984)

Schwank, Don, *Modern Plastics*, August (1993), p. 49-50

Shaw, M.T. and W.H. Tuminello, *Polym. Eng. Sci.* 34, 159-165 (1994)

Vega, J.F., et al, *Macromolecules*, 29:3, 960-965 (1996)

Vega, J.F., et al, *Macromolecules*, 31:11, 3639-3647 (1998)

Wagner, M.H., *Rheol. Acta*, 15:136 (1976)

Wasserman, S.H., SPE ANTEC, 43, 1129-1133 (1997)

Wissbrun, K.F., *J. Rheol.*, 30:1143 (1986)

Wood-Adams, P.M. and J.M. Dealy, *J. Rheol.* 40(5), 761-778, (1996)

Yoshikawa, K. *et al*, *Polymer Rheology and Processing*, Edited by A.A. Collyer and L.A. Utracki, Chapter 2, Elsevior Science Publishers Ltd. (1990)

Zapas, L.J., *J. Res. N. B. S,* 75a:33 (1971)

Appendix A.

Linear Viscoelastic Data

Table A.1 Dynamic Moduli Data for High Density mPEs at 150°C						
	HDL1		HDB1		HDB2	
ω rad/s	G' Pa	G" Pa	G' Pa	G" Pa	G' Pa	G" Pa
0.018638	--	--	13.03334	213.0084	76.57794	577.208
0.025898	--	--	23.57418	294.9436	136.1534	754.7262
0.036	2.381858	208.5366	38.89326	402.1786	236.1932	965.8944
0.05	4.359322	289.0956	64.7528	546.8924	343.7462	1286.622
0.069475	6.882828	401.026	107.8561	740.9424	531.5048	1673.746
0.096535	12.44524	554.6748	171.9522	991.5428	755.904	2146.928
0.134136	20.46138	767.8202	265.9622	1321.302	1047.842	2743.964
0.186382	34.67512	1061.23	408.6188	1743.774	1456.748	3422.71
0.25898	58.35384	1464.108	607.6494	2280.432	2017.236	4289.636
0.359848	96.97444	2017.638	882.9226	2960.196	2695.976	5310.034
0.5	170.5856	2783.748	1273.82	3811.318	3624.93	6508.376
0.694748	278.902	3821.83	1774.306	4874.298	4634.03	7978.586
0.965347	456.592	5238.576	2424.69	6205.046	5887.47	9754.598
1.34134	742.631	7154.926	3253.686	7860.926	7465.218	11919.44
1.8638	1205.12	9737.474	4303.164	9926.576	9348.868	14597.44
2.58972	1944.946	13184.96	5636.022	12506.06	11686.76	17848.34
3.59839	3111.09	17757.54	7317.762	15772.48	14553.46	21968.72
5	4927.406	23742.8	9440.6	19888.62	18090.14	27125.64
6.94751	7699.108	31440.48	12187.96	25055.36	22546.1	33517.36
9.65356	11845.42	41193.44	15743.14	31559.26	28151.96	41420.84
13.4136	17946.66	53364.62	20296.26	39600.52	34788.14	51958.6
18.6382	26574.8	68067.94	26548.52	49693.04	44346.24	62863.54
25.8975	38625.32	85576.72	34688.14	61933.76	55988.32	76789.12
35.9844	54862.06	105719.8	45359.38	76584.58	70686.72	93087.18
50	76227.32	128241.4	59371.72	93853.82	89294.32	111699.8
69.4746	103307.6	152663.6	77409.3	113661.8	112516.6	132340.8
96.5352	136849.8	178219.6	100386.9	135845.4	141066.2	154801.8
134.137	177005.8	203913.8	128970.4	160001.8	175434.4	178290
186.383	223578.6	228891.4	163754.2	185488.6	215972.6	202019.8
258.977	276050.8	252129.8	204765.4	211168	262362.6	225120.8
359.844	333376.2	273823.4	251808.4	236545.2	314560.6	247285.8
500	394078.6	293604.6	303864	261673.8	371237.8	267532

Table A.2 Dynamic Moduli Data for High Density mPEs at 150°C				
	HDB3		HDB4	
ω rad/s	G' Pa	G" Pa	G' Pa	G" Pa
0.005	--	--	211.8664	752.7026
0.006948	--	--	311.6256	990.4494
0.009654	--	--	456.834	1288.206
0.013414	--	--	654.5114	1644.062
0.018638	222.5204	902.6668	921.771	2072.44
0.025898	333.866	1186.226	1268.35	2582.546
0.036	499.216	1534.518	1712.364	3177.908
0.05	723.0098	1967.778	2310.008	3884.492
0.069475	1029.136	2492.696	3013.882	4697.832
0.096535	1428.306	3123.944	3880.956	5623.034
0.134136	1939.25	3876.946	4922.524	6680.164
0.186382	2594.86	4769.126	6169.3	7893.534
0.25898	3406.924	5822.408	7637.374	9275.954
0.359848	4404.38	7062.498	9352.354	10860.34
0.5	5637.884	8498.494	11464.7	12658.04
0.694748	7069.446	10240.13	13761.4	14809.64
0.965347	8798.274	12296.96	16433.22	17305.64
1.34134	10831.1	14768.36	19518.1	20241.44
1.8638	13240.1	17754.62	23087.26	23751.86
2.58972	16116.72	21382.28	27259.14	27921.66
3.59839	19555.5	25851.58	32160.2	32953.82
5	23710.14	31331.52	37969.36	38976.84
6.94751	28776.14	38050.96	44908.1	46175.4
9.65356	35051.72	46246.18	53264.92	54699.98
13.4136	43140.76	56347.14	63396.04	64706.56
18.6382	52748.4	68121.44	75732.68	76369.8
25.8975	65168.28	82195.82	90805.14	89722.74
35.9844	80763.84	98545.1	109163.6	104695.2
50	100207.9	117077.2	131471	121152.2
69.4746	124130	137659.6	158672.2	138314.2
96.5352	153308	159926	190963.8	155995.6
134.137	188143.4	183343.4	229415.2	172842.8
186.383	228968	207078.4	274237	187179
258.977	275329.8	230428	325303.2	197312.2
359.844	326393.4	253281.6	384446.8	200529
500	382688.8	274913.2	448927.6	193465.8

Table A.3 Dynamic Moduli Data for Low Density mPEs at 130°C								
	LDL1		LDB1		LDB2		LDB3	
ω rad/s	G' Pa	G" Pa	G' Pa	G" Pa	G' Pa	G" Pa	G' Pa	G" Pa
0.006948	--	--	--	--	--	--	299.219	954.5153
0.009654	--	--	--	--	--	--	429.9025	1223.28
0.013414	3.71314	266.3746	48.8757	474.6178	220.8	921.3308	603.3325	1562.84
0.018638	8.350374	370.657	78.6036	645.5482	329.8446	1201.288	836.2535	1969.348
0.025898	13.65832	511.4344	121.6356	869.907	482.9822	1554.002	1136.85	2462.165
0.036	23.36022	702.9088	185.524	1166.66	694.0426	1989.904	1534.528	3052.61
0.05	41.75928	973.4304	286.6032	1558.48	1009.806	2535.834	2091.858	3775.333
0.069475	66.60738	1339	416.4378	2069.674	1394.526	3192.1	2733.953	4612.385
0.096535	108.0436	1837.434	604.9374	2736.572	1899.116	3985.3	3539.93	5575.25
0.134136	168.2136	2518.358	856.2804	3604.402	2537.894	4936.266	4535.663	6711.428
0.186382	264.373	3447.92	1204.348	4739.444	3348.304	6067.93	5745.023	8022.178
0.25898	421.3752	4719.46	1673.822	6215.616	4349.582	7419.206	7193.573	9537.818
0.359848	668.9602	6445.458	2309.878	8134.002	5582.124	9030.266	8932.53	11288.48
0.5	1094.56	8794.68	3208.29	10638.1	7108.506	10949.42	11041.88	13299.75
0.694748	1749.778	11913.92	4417.786	13854.66	8907.376	13281.36	13420.35	15680.18
0.965347	2807.47	16067.72	6110.206	17983.98	11106.02	16073.72	16262.7	18428.65
1.34134	4473.442	21496.06	8455.49	23212.64	13753.86	19447.64	19608.18	21638.3
1.8638	7055.342	28495.8	11716.18	29786.94	16978.82	23531.14	23550.55	25412.6
2.58972	10972.82	37313.4	16229.24	37890.96	20928.22	28447.3	28116.7	29773.53
3.59839	16708.8	48225.44	22400.12	47806.9	25784.24	34400.48	33523.2	34907.38
5	24959.5	61251.7	30762.06	59439.66	31875.48	41459.38	40006.23	40904.4
6.94751	36253.32	76575.54	41828.42	73178.66	39347.72	49908.62	47649.88	47930.58
9.65356	51452.7	94024.02	56280.12	88813.26	48667.9	59771.34	56692.48	56158.28
13.4136	71327.2	113191	74843.1	106070.8	60261.58	71153.3	67401.93	65215.08
18.6382	96251.4	133512.8	97861.48	124545.8	74555.34	83921.2	80448.5	76187.05
25.8975	126906.6	154335.2	126064	143678.6	92184.44	98075.24	95777	88112.88
35.9844	163294.6	174662.2	159521.2	162441.2	113395.8	113215.8	113981.5	101224.3
50	205570.2	193420.8	198533.8	180134.8	139010.2	128908.6	135333	115430.
69.4746	253381.8	209628.6	242617.4	195550	169087.8	144386	160404.3	129834
96.5352	306310	221994.6	291852.4	207587.4	204128.6	158844.6	189047	144841.8
134.137	363773.6	229448.4	345393	215167.2	244413.2	171383.4	222335.3	159600.8
186.383	424842.4	230353.2	402755.2	216445	289524.6	180001.4	259148.5	173703
258.977	488971	223223.4	462895.8	210541.2	339329.4	183413.8	299568.8	186122.3
359.844	555279.4	206226.6	525487.6	194752.8	393908.4	179307.4	343791	195871
500	623393.8	176536	590082.8	167688.4	451920.6	164847.2	391061.3	203855.5

Table A.4 Arrhenius Activation Energies for Low Density mPEs (130 to 170°C)	
Resin	Ea/R (K)
LDL1	4070
LDB1	4704
LDB2	5259
LDB3	6414

Table A.5 Discrete Spectra for High Density mPEs (150°C)		
Resin	G_i (Pa)	λ_i (s)
HDL1	545 500	0.001723
	172 600	0.01299
(5 modes)	21 490	0.08644
	769.3	0.7991
	13.9	9.398
HDB1	1 174 000	0.0002296
	260 900	0.003296
(7 modes)	73 340	0.01769
	15 860	0.1103
	4 376	0.6895
	871.4	3.642
	63.34	20.59
HDB2	480 000	0.0009319
	198 800	0.004609
(7 modes)	81 940	0.01911
	25 750	0.09373
	9 271	0.5376
	3 341	3.008
	594.6	18.84
HDB3	581 000	0.000529
	219 000	0.002745
(8 modes)	130 200	0.009982
	48 760	0.04453
	18 070	0.2387
	7 775	1.375
	2 510	7.408
	456.1	40.8

Table A.5 Discrete Spectra for High Density mPEs (150°C) continued		
Resin	G_i (Pa)	λ_i (s)
HDB4	336 200	0.002479
	137 800	0.01128
(9 modes)	55 020	0.04889
	23 710	0.22
	11 990	0.9842
	6 289	4.069
	2 780	17.1
	796.9	75.21
	96.35	892.4

Table A.6 Discrete Spectra for High Density mPEs (150°C)		
Resin	G_i (Pa)	λ_i (s)
HDL2	128900	0.002157
(2 modes)	138.5	0.1619
HDL3	575100	0.005141
	144500	0.05001
(4 modes)	4391	0.728
	127	14.79
HDL4	439200	0.0155
	499100	0.09408
(6 modes)	321100	0.4639
	86510	2.104
	10610	11.24
	2380	101.3

Table A.7 Discrete Spectra for Low Density mPEs (150°C)		
Resin	G_i (Pa)	λ_i (s)
LDL2	427500	0.003811
	170400	0.02665
(5 modes)	18420	0.1774
	223.9	2.366
	2.398	30.54
LDL2	371400	0.004333
(5 modes)	231200	0.02747
	58340	0.1566
	2949	1.039
	65.29	11.8

Table A.8 Discrete Spectra for Linear Low Density Polyethylenes (150°C)		
Resin	G_i (Pa)	λ_i (s)
LLDPE1	255900	0.002613
	137000	0.01207
(7 modes)	69560	0.05563
	26390	0.2791
	7692	1.466
	1838	8.031
	402.2	51.64
LLDPE2	195400	0.002271
	174000	0.007332
(7 modes)	114900	0.03371
	44150	0.1752
	10610	0.9586
	1639	5.615
	175.9	37.19

Table A.9 Discrete Spectra for Low Density mPEs at 130°C		
Resin	G_i (Pa)	λ_i (s)
LDL1	468 100	0.005407
	180 900	0.05057
(4 modes)	13 520	0.4769
	172.4	10.01
LDB1	332 000	0.00366
	207 800	0.01722
(7 modes)	82 140	0.07675
	18 390	0.3675
	3 394	2.004
	730.3	10.58
	90.76	54.07
LDB2	290 100	0.002837
	145 500	0.01214
(8 modes)	63 010	0.04872
	23 810	0.2069
	9 796	0.895
	4 354	3.649
	1 536	15.36
	287.2	75.78

Table A.9 Discrete Spectra for Low Density mPEs at 130°C continued		
Resin	G_i (Pa)	λ_i (s)
LDB3	352 200	0.001097
	174 800	0.005931
(9 modes)	86 260	0.02642
	37 090	0.1221
	17 250	0.5644
	8 211	2.513
	3 437	10.89
	981.6	43.49
	317.7	178

Appendix B.

Experimental Conditions for Step Strain Experiments

Table B.1 Conditions for Step Strain Experiments

Resin	Strain (γ)	Strain Rate ($\dot{\gamma}$) (s^{-1})	Δt (s)
HDL1	0.5	55.3	0.038
	0.75	55.3	0.043
	1	64.5	0.045
	1.5	55.3	0.056
	2	64.5	0.06
	4	64.5	0.09
	8	64.5	0.15
	16	64.5	0.27
HDB1	0.5	73.7	0.036
	0.75	73.7	0.039
	1	73.7	0.043
	2	73.7	0.056
	4	73.7	0.08
	8	73.7/92.2	0.14/0.11
	16	92.2	0.20
HDB3	0.25	18.433	0.043
	0.5	18.433	0.056
	0.75	18.433	0.07
	1	18.433	0.08
	2	23.04	0.11
	4	23.04	0.20
	8	23.04	0.37
	16	23.04	0.71

Appendix C

Nonlinear Shear Flow Data

Table C1. Viscosity Measured Using the Sliding Plate Rheometer (150°C)						
$\dot{\gamma}$	η (Pa.s) **HDL1**	η (Pa.s) **HDB1**	η (Pa.s) **HDB2**	η (Pa.s) **HDB3**	η (Pa.s) **HDB4**	η (Pa.s) **LDB3**
0.009217	--	--	--	--	--	81646.25
0.018433	--	--	--	--	--	72875.83
0.02765	--	--	--	--	--	61845
0.046083	--	--	--	--	100165.7	53165
0.064516	--	--	--	--	--	51821.67
0.092166	--	--	--	38079.71	75585.46	46655
0.184332	--	--	22119.57	29637.68	56228.99	--
0.276498	--	--	--	--	--	29994.22
0.460829	5835.141	8644.252	16442.52	21041.21	35842.47	25209.98
0.645161	--	--	--	--	--	21785.25
0.921659	5347.072	7111.352	13083.88	15972.52	23691.85	18412.45
1.382488	5416.064	7040.521	11408.59	11888.57	18277.42	--
1.843318	5176.343	6530.114	9742.268	11144.87	16363.91	13303.46
2.764977	--	--	--	--	--	10600.45
3.686636	4972.878	--	7856.433	8463.068	11701.14	--
4.608	4871.962	4971.065	7668.186	7875.434	--	--
6.451613	4701.643	4473.807	6300.372	6543.191	9318.51	--
9.21659	4464.034	3900.401	5441.575	4907.297	7720.65	--
12.903	4190.111	3690.615	--	--	--	--
18.43318	3860.468	3212.174	5005.813	4458.851	5788.385	--
23.04147	3438.517	--	4246.008	4108.184	5241.306	--
27.64977	3221.261	2818.626	3829.295	--	4828.557	--
46.083	2905.966	2341.102	3107.654	--	--	--
64.516	2654.535	2051.042	--	--	--	--
92.166	--	1736.107	--	--	--	--

Table C2. Viscosity and First Normal Stress Difference Measured with RMS800 (Cone and Plate) at 150°C						
	HDL1		HDB1		HDB2	
$\dot{\gamma}$	η (Pa.s)	N_1 (Pa)	η (Pa.s)	N_1 (Pa)	η (Pa.s)	N_1 (Pa)
0.01	6359	--	--	--	35911	68.55666
0.03	--	--	13426	--	--	--
0.06	6205	33.97316	12656	178.3667	27987	719.8032
0.1	--	--	11739	338.2175	25091	--
0.3	6102	259.0908	10287	1470.388	18450	3686.647
0.6	6017	618.7907	8406	2592.1	13739	5647.882
1	5714	1123.856	7513	4590.909	11938	8318.716
3	5453	4051.275	--	--	--	--
6	4993	8927.096	--	--	--	--

Table C3. Viscosity and First Normal Stress Difference Measured with RMS800 (Cone and Plate) at 150°C				
	HDB3		LDB3	
$\dot{\gamma}$	η (Pa.s)	N_1 (Pa)	η (Pa.s)	N_1 (Pa)
0.01	65906	181.4882	79325	182.1736
0.06	--	--	53205	2268.428
0.1	38037	2676.989	47544	3969.054
0.3	24571	5268.475	29323	8164.946
0.6	18281	8293.909	21799	12554.37
1	14192	10431.18	15956	13370.38

Table C4. Damping Function determined from Step Strain (150°C)			
γ	h(γ)		
	HDL1	HDB1	HDB3
0.25	--	--	1
0.5	1	1	0.965
0.75	1	1	0.91
1	1	0.95	0.86
1.5	0.91	0.82	0.7
2	0.84	0.705	0.59
4	0.453	0.37	0.315
8	0.215	0.16	0.117
16	0.107	0.07	0.045

Table C5. Large Amplitude Oscillatory Shear Results for HDL1 (150°C)					
γ_o	F (Hz)	σ_1 (kPa)	δ_1	σ_3 (kPa)	δ_3
2.498	0.5	38.81	1.3728	0.75	3.2942
2.551	0.5	40.27	1.4389	0.75	2.8836
3.996	0.5	58.53	1.401	1.78	3.5234
4.088	0.5	60.18	1.4643	1.57	3.5423
5.974	0.5	81.6	1.4215	3.71	3.6039
6.101	0.5	83.1	1.483	3.41	3.853
2.498	1	67.96	1.2984	1.97	3.0253
2.578	1	71.83	1.38	1.64	2.994
3.998	1	99.58	1.3425	4.43	3.3563
4.1	1	103.63	1.4157	3.45	3.4898

Table C6. Large Amplitude Oscillatory Shear Results for HDB1 (150°C)					
γ_o	F (Hz)	σ_1 (kPa)	δ_1	σ_3 (kPa)	δ_3
2.501	0.5	34.68	1.3123	0.44	2.5733
2.499	0.5	35.55	1.11503	0.87	2.0669
3.994	0.5	48.9	1.3814	2.64	3.0102
3.996	0.5	50.43	1.2216	2.01	2.5514
3.996	0.5	50.33	1.2195	1.96	2.5499
5.991	0.5	64.84	1.4241	4.14	3.3946
5.98	0.5	66.91	1.2636	3.99	2.8578
2.497	1	56.76	0.9502	1.39	1.4598
2.501	1	55.78	1.2744	2.61	2.3936
2.499	1	57.05	0.9512	1.42	1.4412
3.997	1	80.1	1.0229	3.04	1.9177
5.929	1	104.13	1.0665	6.91	2.0938
5.929	1	104.16	1.0664	6.91	2.09

Table C7. Large Amplitude Oscillatory Shear Results for HDB2 (150°C)					
γ_o	F (Hz)	σ_1 (kPa)	δ_1	σ_3 (kPa)	δ_3
2.498	0.5	50.8	1.0732	1.29	1.8507
2.499	0.5	50.98	1.09	1.32	1.889
3.996	0.5	69.8	1.1769	3.52	2.596
3.997	0.5	69.2	1.1616	3.48	2.6056
5.978	0.5	88.8	1.2164	5.95	2.9124
5.979	0.5	88.83	1.2366	6.22	2.9171
2.499	1	78.66	0.8881	2.02	1.2745
2.499	1	77.78	0.8686	2	1.2649
3.997	1	105.22	0.9637	4.8	1.9207
3.998	1	106.79	0.9767	4.69	1.9067
5.927	1	133.85	1.0333	10.3	2.1462

Table C8. Large Amplitude Oscillatory Shear Results for HDB3 (150°C)					
γ_o	F (Hz)	σ_1 (kPa)	δ_1	σ_3 (kPa)	δ_3
1.996	0.5	46.56	1.1409	1.23	2.3519
1.996	0.5	47.05	1.1433	1.21	2.2781
1.999	0.5	47.56	0.9983	1.01	1.5211
2.996	0.5	60.12	1.2318	3.05	2.9403
3.995	0.5	72.39	1.2737	4.36	3.2246
3.995	0.5	72.75	1.2728	4.46	3.2179
3.996	0.5	72.29	1.1484	4.54	2.7551
4.993	0.5	82.83	1.3142	5.2	3.4079
4.995	0.5	82.96	1.1866	5.36	2.922
1.997	1	69.51	1.0983	1.95	2.0982
1.999	1	72.05	0.7778	1.55	0.874
1.999	1	71.85	0.783	1.52	0.8889
2.996	1	91.41	1.1788	4.29	2.7238
2.996	1	90.45	1.1871	4.38	2.7352
2.999	1	92.54	0.8861	3.61	1.6654
3.995	1	109.37	1.2347	6.72	3.0501
3.997	1	108.49	0.9549	6.18	2.0704
3.997	1	108.6	0.9571	6.22	2.069

Appendix D.

Numerical Technique for Solving the Wagner Equation

Solving a separable BKZ model in simple extension or shear flow

Ranjit S. Jeyaseelan
Chemical Eng., McGill University
Montreal, Canada H3A 2A7

ABSTRACT

We propose a more efficient method for solving separable BKZ models. than numerical integration. This is illustrated in both simple extension and shear flows. This method is also particulary well suited for simulating the flow of fluids with multiple relaxation times.

A SEPARABLE BKZ MODEL

The Wagner equation is a versatile, separable BKZ model, wherein the extra stress tensor $\underset{\approx}{\sigma}$ is given by the following hereditary integral [1] :

$$\underset{\approx}{\sigma}(t) = \int_{-\infty}^{t} m(t-t')\, h[I]\, \underset{\approx}{B}(t,t')\, dt' \qquad (1)$$

where $\underset{\approx}{B}$ is the Finger tensor, m is the memory function :

$$m(t-t') = \sum_i \frac{G_i}{\lambda_i} e^{-(t-t')/\lambda_i} \qquad (2)$$

and h is the damping function. In the examples presented here, the following form is used :

$$h(I) = \frac{1}{1+a(I-3)} \qquad (3)$$

and I is a general invariant of $\underset{\approx}{B}$, defined in terms of the first and second invariants. I_1 and I_2 [2] :

$$I \equiv \beta I_1 + (1-\beta) I_2 \tag{4}$$

In simple shear, since I_1 and I_2 are equal, nonlinear behavior is governed by only one parameter, a. The parameter β can be fitted to nonlinear behavior in extensional flow.

The Wagner equation with the damping function given by (3) cannot be solved analytically, except during the time interval $-\infty < t' < 0$ in the integral (1). Therefore, we have to perform numerical integration to obtain the solution for the stress in the time interval $0 < t' < t_n$, where t_n is the discretized present time.

A limiting factor in numerically solving (1-4) is that since the memory function in (2) changes exponentially with time, small time steps ($\Delta t \leq .005 s$) in the integration scheme are frequently necessary to obtain accurate solutions. Therefore, if the overall time for which we want the solution is large (say $1000 s$), the CPU time required is enormous.

To circumvent this problem, we extend an idea used by Wagner and Laun [3] and propose the following scheme to solve (1-4) : We make the approximation that during a small interval of time Δt (which is the step size in the integration scheme) the damping function has a constant value equal to the average of its values at the end-points of the interval. This approximation allows us to take the damping function out of the integral during each time step, and the rest of the integral can then be integrated analytically. With this approximation, instead of replacing the integral by an integration rule, we replace it with a series of integrals, each of which can be solved analytically :

$$\int_0^{t_n} m(t_n - t')\, h[I(t_n,t')]\, \underset{\approx}{B}(t_n,t')\, dt' \;\cong\; \sum_{i=1}^{n} h[I(t_n,t_{i-1})] \int_{t_{i-1}}^{t_i} m(t_n - t')\, \underset{\approx}{B}(t_n,t')\, dt' \tag{5}$$

where $h[I(t_n,t')]$ is the value of the damping function corresponding to the strain $\epsilon(t_n,t')$, and $h[I(t_n,t_{i-1})]$ is the value of the damping function corresponding to the strain $\epsilon(t_n,t_{i-1})$.

SIMPLE EXTENSION

In the start-up of simple extensional flow, equations (1-4) reduce to the following equation for the tensile stress growth coefficient as a function of the extension rate $\dot{\epsilon}$, and present time (t_n) :

$$\eta_E^+[\dot{\epsilon},t_n] \equiv \frac{\sigma_{11}-\sigma_{22}}{\dot{\epsilon}} = \frac{G(t_n)\,h[I(t_n,0)]\left\{e^{2\dot{\epsilon}t_n}-e^{-\dot{\epsilon}t_n}\right\}}{\dot{\epsilon}} + \frac{1}{\dot{\epsilon}}\int_0^{t_n} m(t_n-t')\,h[I(t_n,t')]\left[e^{2\dot{\epsilon}(t_n-t')}-e^{-\dot{\epsilon}(t_n-t')}\right]dt' \tag{6}$$

where G is the relaxation modulus and $h[I(t_n,0)]$ is the value of the damping function corresponding to the strain $\epsilon(t_n,0)$. For this case, the proposed scheme gives :

$$\begin{aligned}\eta_E^+[\dot{\epsilon},t_n] &= \frac{G(t_n)\,h[I(t_n,0)]\left\{e^{2\dot{\epsilon}t_n}-e^{-\dot{\epsilon}t_n}\right\}}{\dot{\epsilon}} \\ &+ \frac{1}{\dot{\epsilon}}\sum_{k=1}^{n}\bar{h}[I(t_n,t_{k-1})]\left\{G(t_n-t_k)\left[e^{2\dot{\epsilon}(t_n-t_k)}-e^{-\dot{\epsilon}(t_n-t_k)}\right]\right. \\ &\quad \left. - G(t_n-t_{k-1})\left[e^{2\dot{\epsilon}(t_n-t_{k-1})}-e^{-\dot{\epsilon}(t_n-t_{k-1})}\right]\right. \\ &+ 2\dot{\epsilon}e^{2\dot{\epsilon}t_n}\sum_i \frac{G_i\lambda_i e^{-t_n/\lambda_i}\left[e^{(1/\lambda_i-2\dot{\epsilon})t_k}-e^{(1/\lambda_i-2\dot{\epsilon})t_{k-1}}\right]}{1-2\dot{\epsilon}\lambda_i} \\ &+ \left.\dot{\epsilon}e^{-\dot{\epsilon}t_n}\sum_i \frac{G_i\lambda_i e^{-t_n/\lambda_i}\left[e^{(1/\lambda_i+\dot{\epsilon})t_k}-e^{(1/\lambda_i+\dot{\epsilon})t_{k-1}}\right]}{1+\dot{\epsilon}\lambda_i}\right\}\end{aligned} \tag{7}$$

where the average value of the damping function during each interval is :

$$\bar{h}[I(t_n,t_{k-1})] = \frac{h[I(t_n,t_k)]+h[I(t_n,t_{k-1})]}{2} \tag{8}$$

and $h[I(t_n,t_k)]$ is the value of the damping function corresponding to the strain $\epsilon(t_n,t_k)$.

SIMPLE SHEAR

Here we consider an additional approximation that the strain *during* each time step increases linearly with time. Such an approximation is necessary if we desire to impose a controlled stress

history, and solve (1-4) for the strain response.As an example we solve (1-4) for large amplitude oscillatory shear (LAOS). The proposed scheme gives the following equation for the shear stress :

$$\sigma_{12}(t_n) = G(t_n)h[I(t_n,0)]\gamma(n) + \sum_{k=1}^{n} \hat{h}[I(t_n,t_{k-1})] * \left\{[\gamma(n)-\gamma(k)]G(t_n-t_k) - [\gamma(n)-\gamma(k-1)]G(t_n-t_{k-1}) + \frac{\gamma(n)-\gamma(k-1)}{\Delta t}\sum G_j\lambda_j\left[e^{-(t_n-t_k)/\lambda_j} - e^{-(t_n-t_{k-1})/\lambda_j}\right]\right\} \quad (9)$$

where $\gamma(n) = \gamma_o \sin(\omega t_n)$, $\gamma(n,k) = \gamma_o \sin(\omega t_n) - \gamma_o \sin(\omega t_k)$ and the average value of the damping function during each time step differs only slightly from (8) :

$$\hat{h}[I(t_n,t_{k-1})] = h[I(t_n,\frac{t_k+t_{k-1}}{2})] \quad (10)$$

COMPARISON OF NUMERICAL INTEGRATION WITH PROPOSED SCHEME :

The discrete relaxation spectrum in Table 1 is for a typical molten polymer (LDPE, 130 ± 1 C). Figure 1 is a plot of the shear stress predicted by the Wagner model for this material in LAOS for 5 cycles at a strain amplitude of 5 and a frequency of 0.1 Hz. It is clear that the proposed method (solid cuve) for solving (1-4) is as accurate as that obtained by numerical integration (symbols). Numerical integration was performed using the trapezoidal rule, to obtain the solution at 100 points, and the step sizes (Δt) are indicated in Table 2. The solution using the proposed scheme was obtained for the same total flow duration as in numerical integration, with $n = 200$ in equation (9).

For the case of simple extension, Figure 2 shows that for 4 extension rates, solving (1-4) using the proposed scheme (curves) predicts the tensile stress growth coefficient as accurately as trapezoidal integration. The step sizes in numerical integration are shown in Table 3, and the solution was obtained at 100 points. The solution using the proposed scheme was obtained for the same total flow duration as in numerical integration, with $n = 100$ in equation (7).

The primary importance of the new scheme is the drastic reduction in computation time. Tables 2 and 3 compare the CPU time taken for both schemes. In some cases, the advantage of the new

scheme is over a thousand-fold. The value of Δt used in the trapezoidal scheme was chosen so as to give results nearly independent of step size.

While it is certainly possible to improve the efficiency of numerical integration by using more sophisticated rules such as Simpsons' or Gaussian quadrature, a thousand-fold improvement is unlikely without the use of an analytical approximation over some time period. Furthermore, numerical integration of the Wagner model in some cases such as simple shear flow with dynamic wall slip, may impose restrictions that do not permit the use of more sophisticated integration rules.

For multiple relaxation time fluids there is an important advantage in simulating polymer processing behavior using integral constitutive equations such as the Wagner model, instead of differential constitutive equations. With differential constitutive equations, the number of equations to be solved for the stress scales with the number of elements in the discrete relaxation spectrum. This is not so for the Wagner model, since the memory function can be evaluated separately as a function of time, and read as a single variable during the iteration for the stress. This remarkable property is not always realized; the asterisk in Table 3 indicates a case where declaring the memory function as an array was not possible because the size of the array was too large for the memory of the computer. While we may be able to increase this limit somewhat, it is certain that there will be other cases where the size would be too large to handle, especially if the fluid has a small relaxation time. This limitation does not exist for the proposed scheme of solving the integral constitutive equations since the array size for the memory function is much smaller (due to the much larger time steps). Therefore with the proposed scheme we will probably always be able to cut the CPU time down to that of a single relaxation time fluid.

REFERENCES

[1] Wagner, M.H., "Analysis of Time-Dependent Non-Linear Stress-Growth Data for Shear and Elongational Flow of a Low-Density Branched Polyethylene Melt," Rheol. Acta **15**, 136-142 (1976).

[2] Wagner, M.H., "Zur Netzwerktheorie von Polymer-Schmelzen," Rheol. Acta **18**, 33-50 (1979).

[3] Wagner, M.H. and Laun H.M., "Nonlinear Shear Creep and Constrained Elastic Recovery of a LDPE Melt," Rheol. Acta **17**, 138-148 (1978).

Table 1. Discrete relaxation spectrum for a typical molten polymer (LDPE, 130 ± 1 C)

λ_i (s)	G_i (Pa)
.0008227	341300
.005596	146300
.02887	69100
.1645	27910
.9798	11910
5.565	4580
29.88	1382
192.7	275.4

Table 2. CPU time taken on a Pentium 166 Mhz computer, for obtaining the shear stress predicted by the Wagner model for 5 cycles of LAOS, at a strain amplitude of 5.

Frequency (Hz)	CPU Time (Trapezoidal Integration) s	CPU Time (Proposed Scheme) s
1.0	3.29 [$\Delta t = .0005 s$]	0.11
0.1	16.53 [$\Delta t = .001 s$]	0.11
0.05	151.6 [$\Delta t = .001 s$]	0.11

Table 3. CPU time taken on a Pentium 166 Mhz computer, for obtaining the tensile stress growth coefficient predicted by the Wagner model in simple extension. The reason for the asterisk is explained in the text.

$\dot{\epsilon}$ (1/s)	CPU Time (Trapezoidal Integration) s	CPU Time (Proposed Scheme) s
1.0	0.44 [$\Delta t = .02 s$]	0.16
0.1	1.7 [$\Delta t = .05 s$]	0.11
0.01	16.81 [$\Delta t = .05 s$]	0.17
0.001	402.9 * [$\Delta t = .05 s$]	0.17

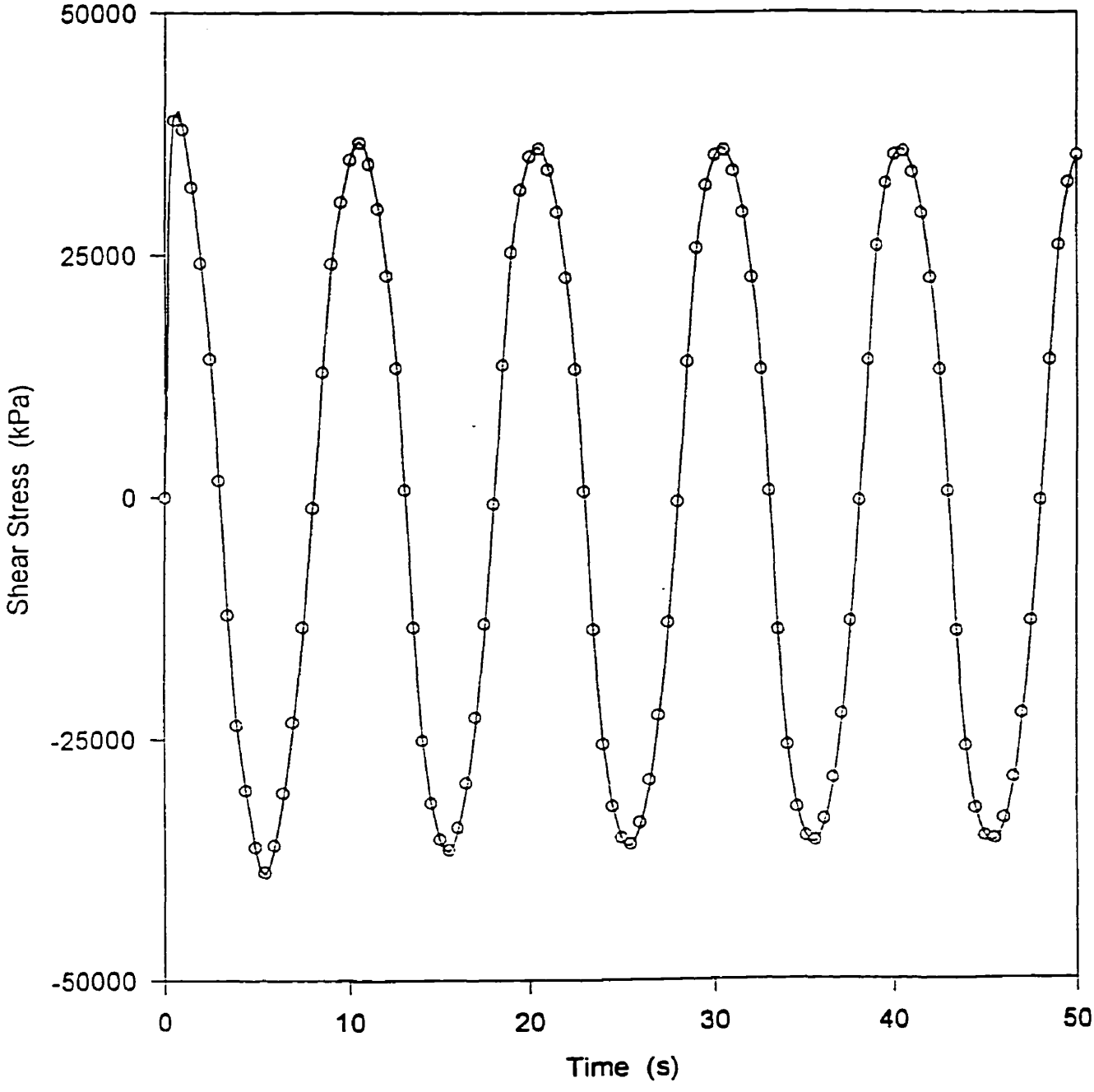

Fig. 1. Shear stress predicted by the Wagner model in LAOS for 5 cycles at a strain amplitude of 5 and a frequency of 0.1 Hz. Proposed method (solid cuve) for solving (1-4) is at least as accurate as that obtained by numerical integration (symbols).

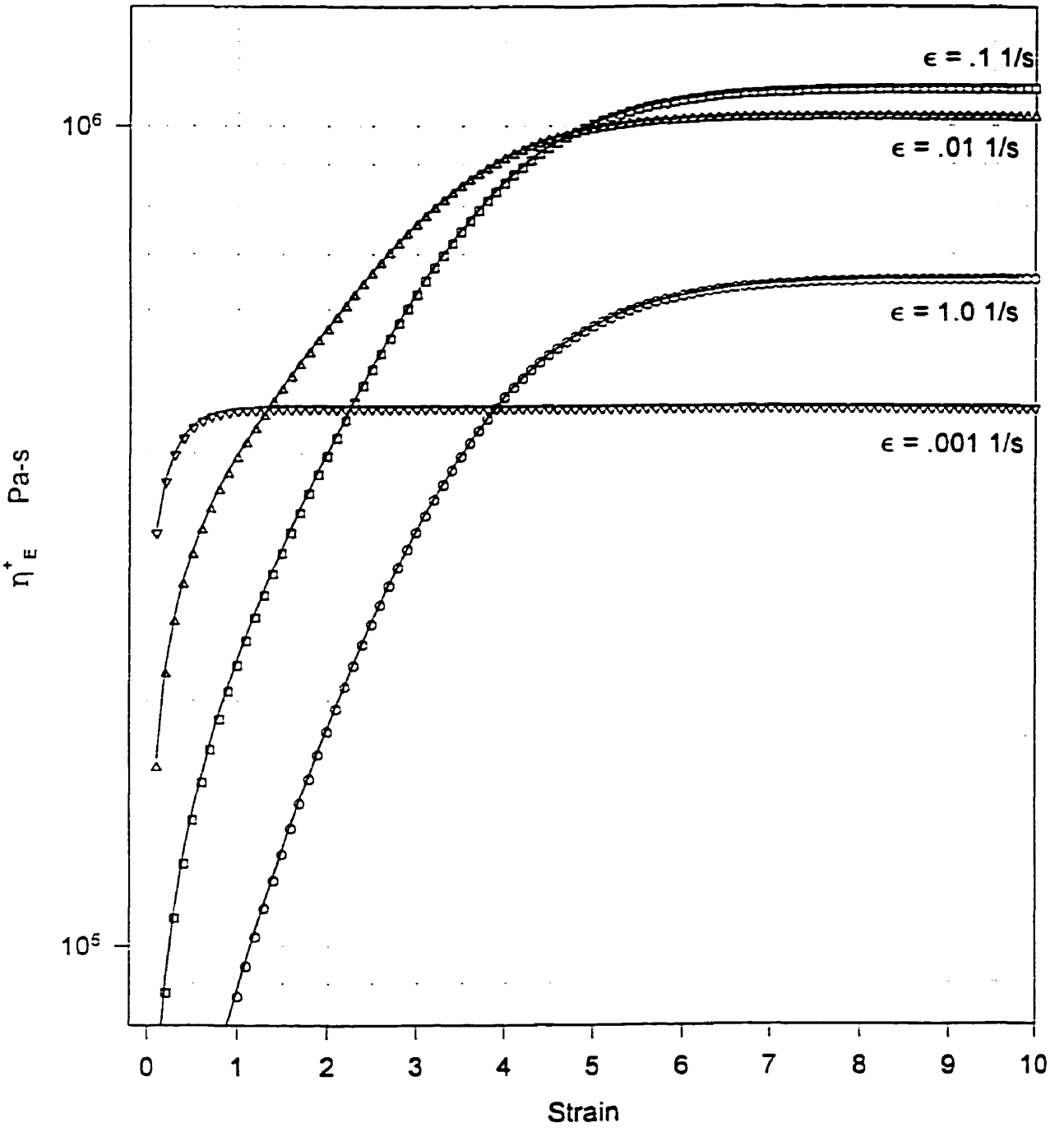

Fig. 2. Tensile stress growth coefficient predicted by solving (1–4) using the proposed scheme (curves), and by trapezoidal integration (symbols).

Curve 1: DSC
File info: n6257 Mon Jul 29 09:34:17 1996
Sample Weight: 4.411 mg
LDL1

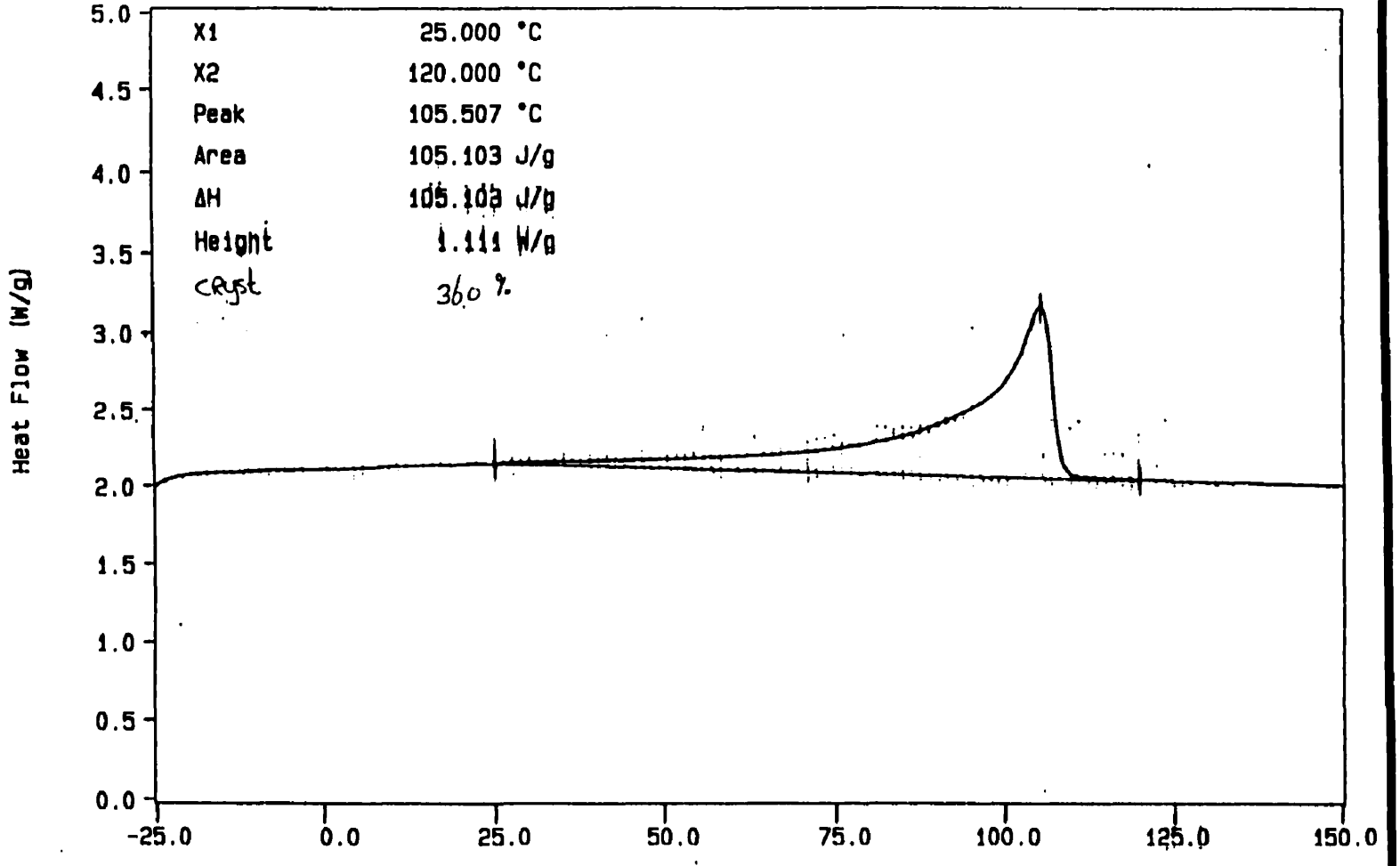

CCA-7 : 60 ml N2/min 2 channels
TEMP1: -30.0 C TIME1: 0.0 min RATE1: 10.0 C/min
TEMP2: 150.0 C

Marian
PERKIN-ELMER
7 Series Thermal Analysis System
Tue Jul 30 01:03:24 1996

Appendix E.

Differential Scanning Calorimetry Results

Curve 1: DSC
File info: n6257 Mon Jul 29 09:34:17 1996
Sample Weight: 4.411 mg
LDL1

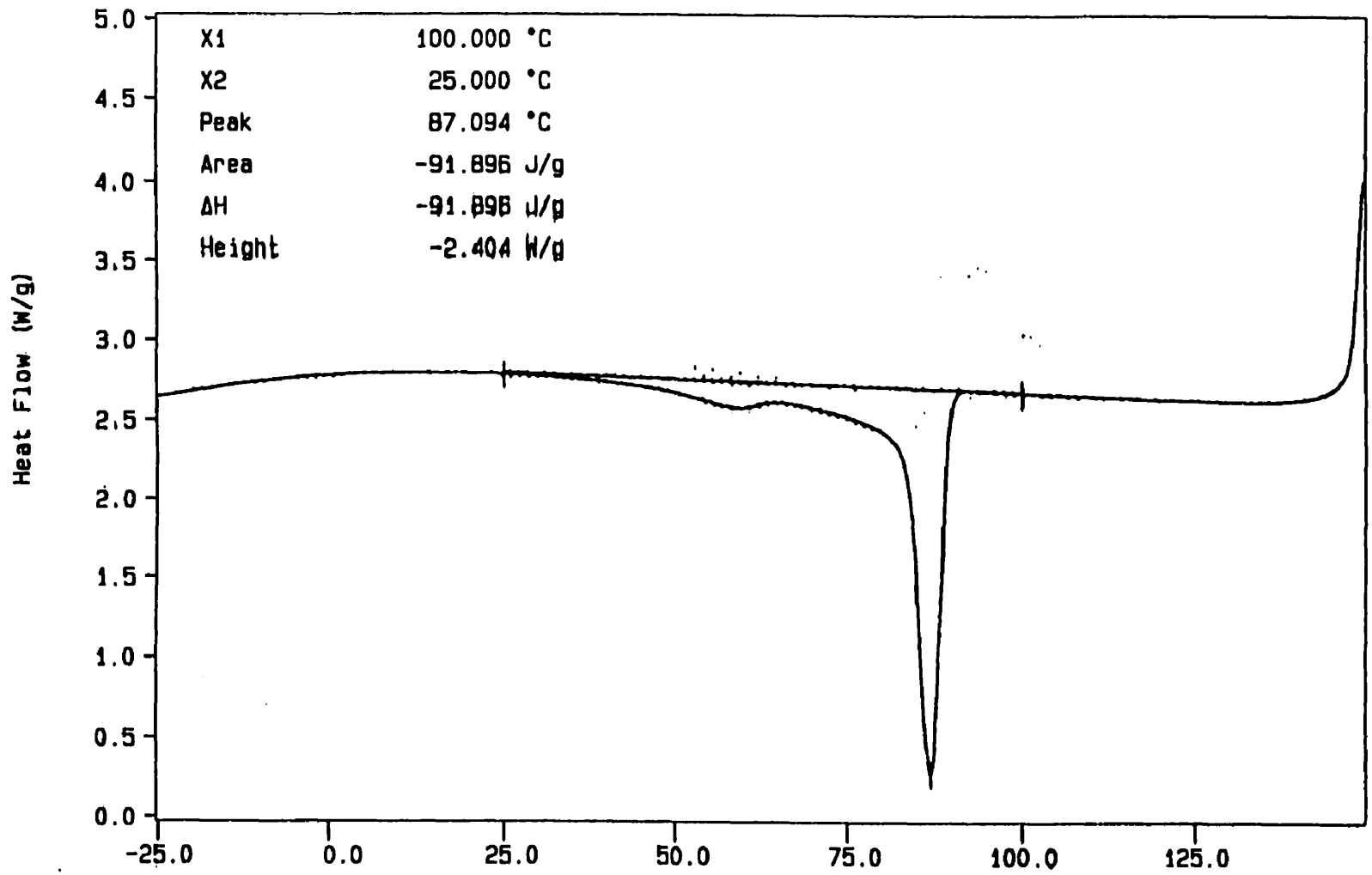

CCA-7 : 60 ml N2/min.2 channels
TEMP1: 150.0 C TIME1: 5.0 min RATE1: 10.0 C/min
TEMP2: -30.0 C

Marian
PERKIN-ELMER
7 Series Thermal Analysis System
Tue Jul 30 01:01:51 1996

Curve 1: DSC
File info: n6248 Tue Jul 23 09:54:39 1996
Sample Weight: 6.469 mg
LDB1

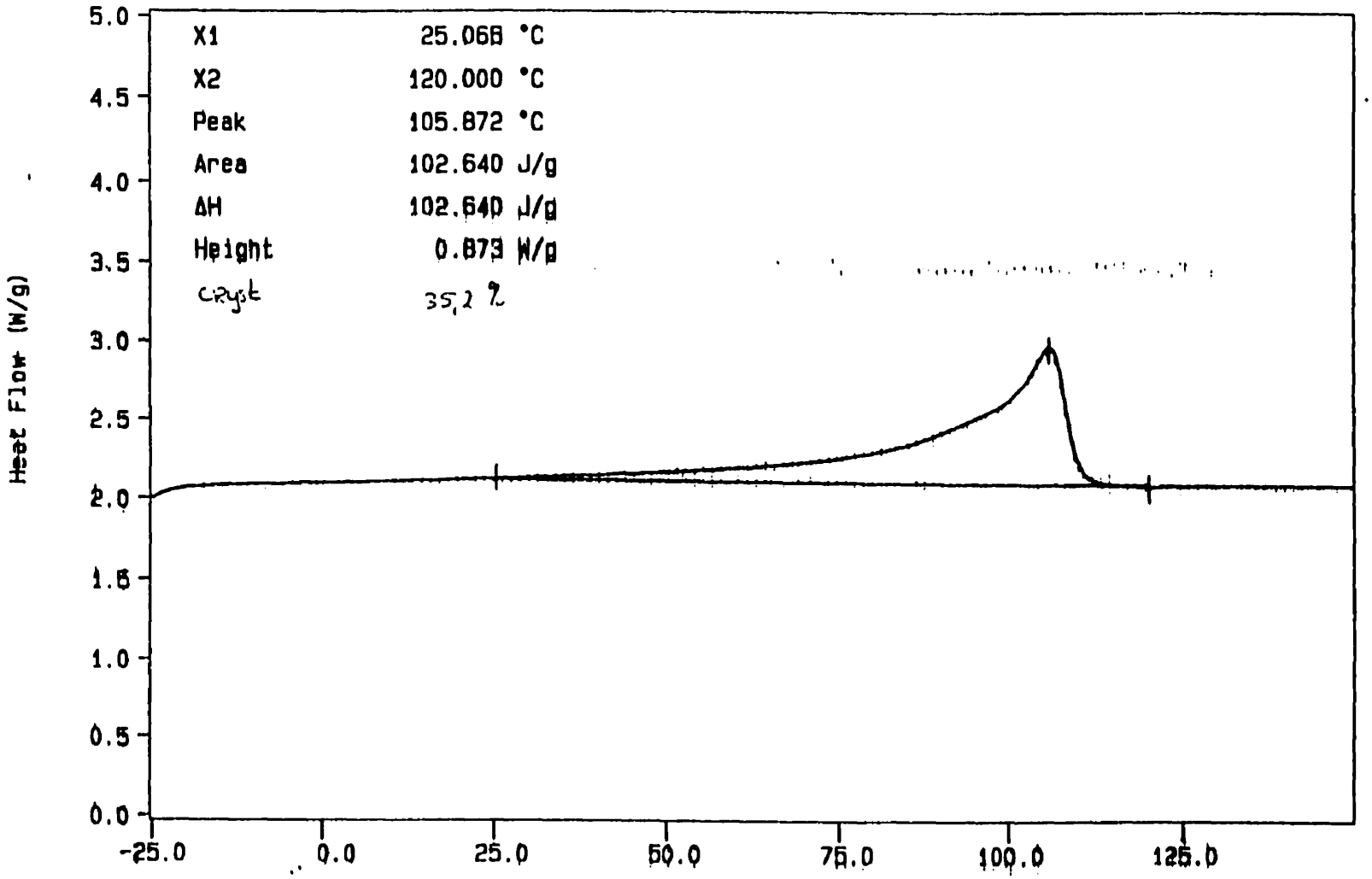

CCA-7 : 60 ml N2/min 2 channels
TEMP1: -80.0 C TIME1: 5.0 min RATE1: 10.0 C/min
TEMP2: 150.0 C

Marian
PERKIN-ELMER
7 Series Thermal Analysis System
Thu Jul 25 08:51:08 1996

Curve 1: DSC
File info: n6248 Tue Jul 23 09:54:39 1996
Sample Weight: 6.469 mg
LDR1

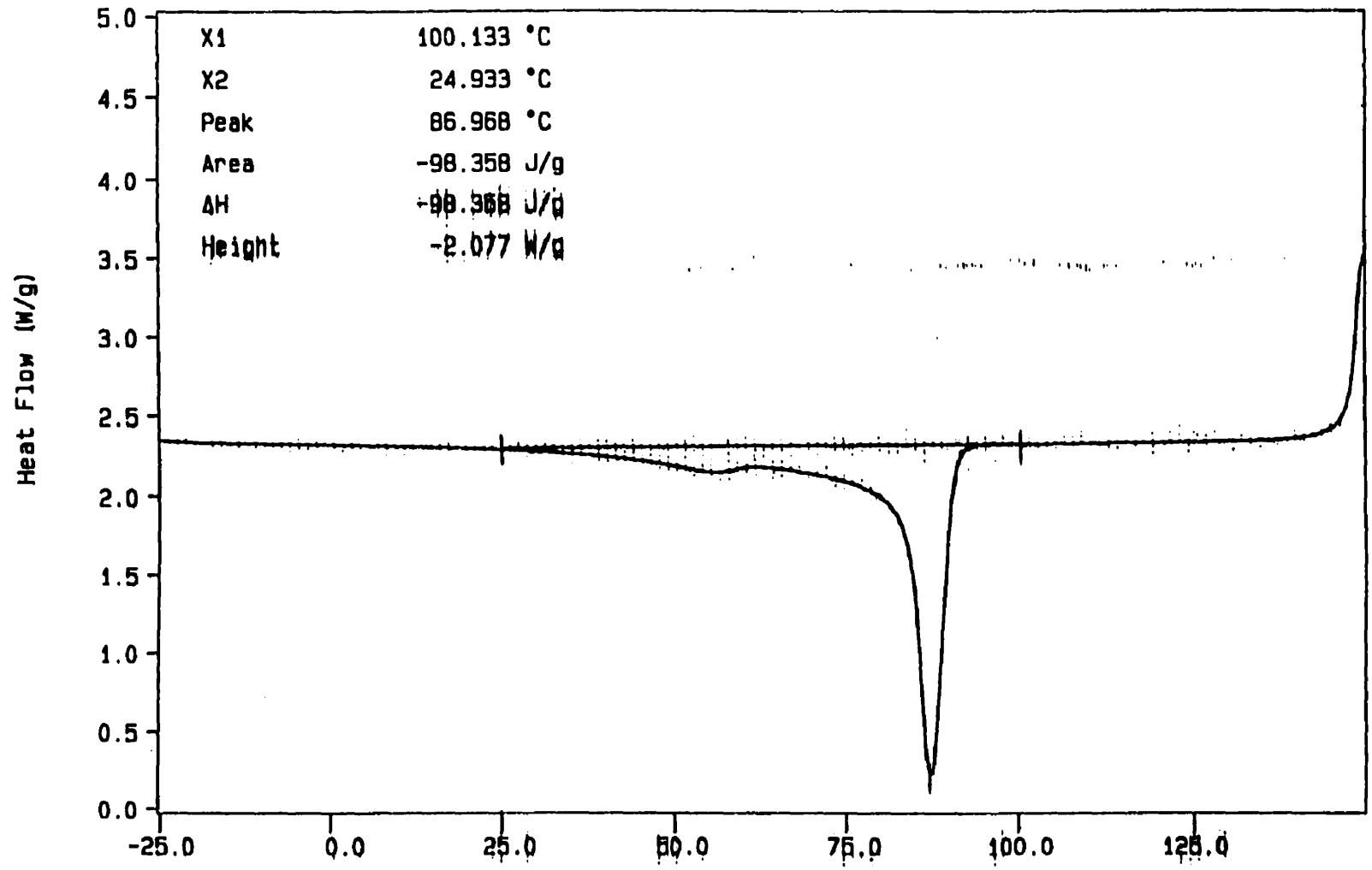

CCA-7 : 60 ml N2/min 2 channels
TEMP1: 150.0 C TIME1: 5.0 min RATE1: 10.0 C/min
TEMP2: -30.0 C

Marian
PERKIN-ELMER
7 Series Thermal Analysis System
Fri Jul 26 01:25:39 1996

Curve 1: DSC
File info: n6254 Thu Jul 25 02:56:15 1996
Sample Weight: 4.776 mg
LDB2

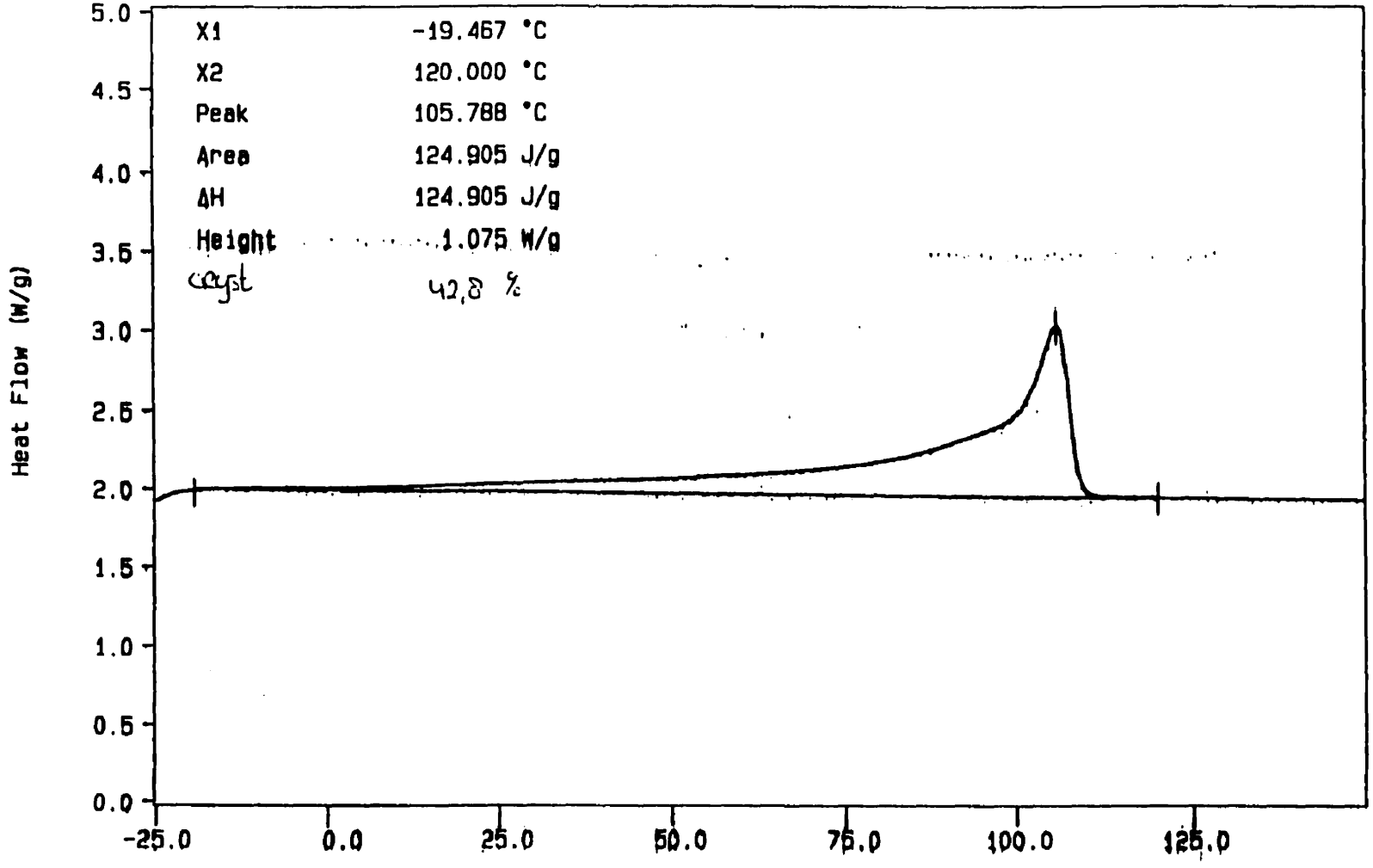

CCA-7 : 60 ml N2/min 2 channels
TEMP1: -30.0 C TIME: 0.0 min RATE: 10.0 C/min
TEMP2: 150.0 C

Marian
PERKIN-ELMER
7 Series Thermal Analysis System
Thu Jul 25 08:48:10 1996

Curve 1: DSC
File info: n6254 Thu Jul 25 02:56:15 1996
Sample Weight: 4.776 mg
LDB2

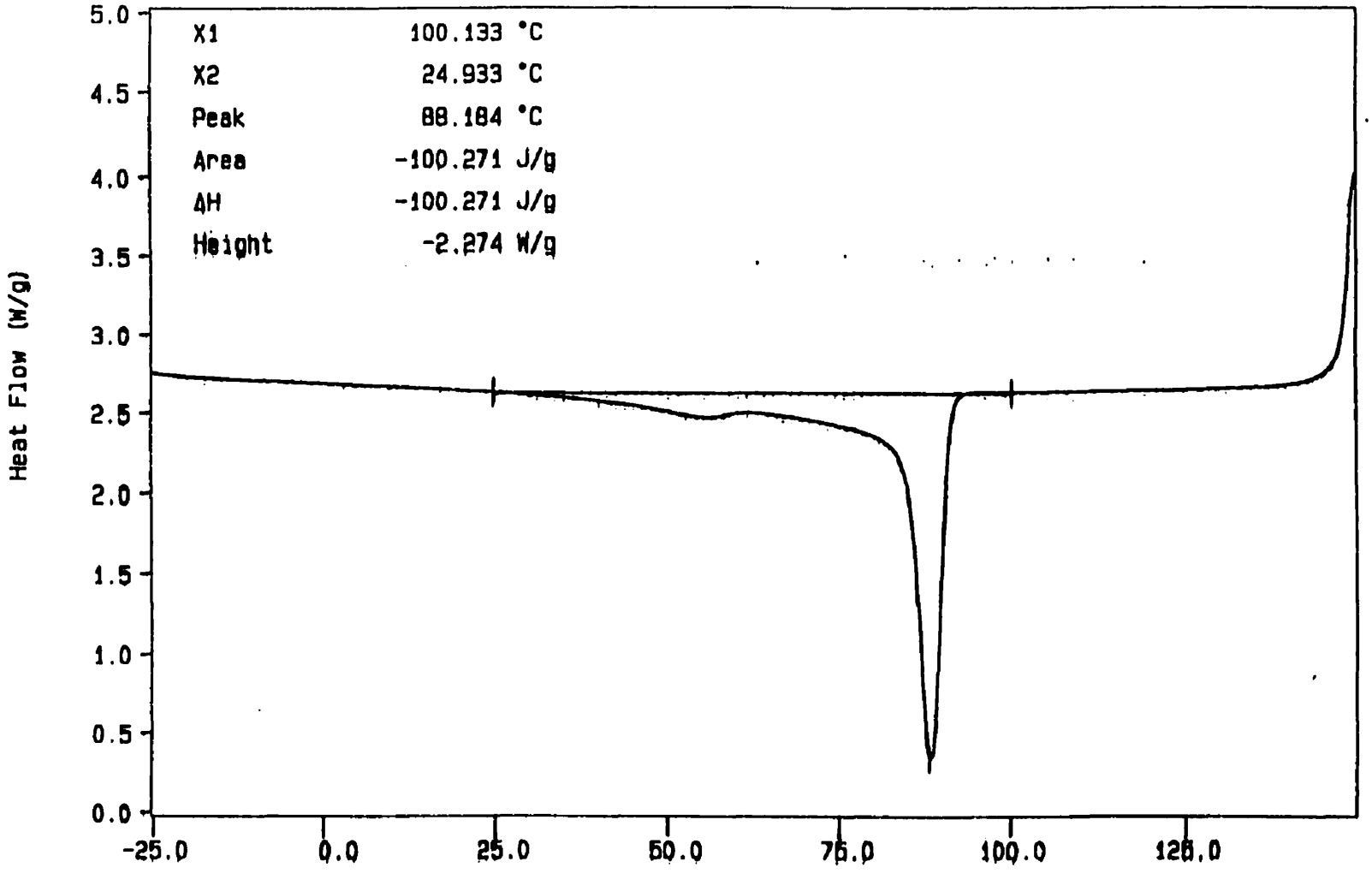

CCA-7 : 60 ml N2/min 2 channels
TEMP1: 150.0 g TIME1: 5.0 min RATE1: 10.0 C/min
TEMP2: -30.0 d

Marian
PERKIN-ELMER
7 Series Thermal Analysis System
Thu Jul 25 08:46:03 1996

Curve 1: DSC
File info: n6256 Mon Jul 29 08:18:40 1996
Sample Weight: 6.242 mg
LDB3

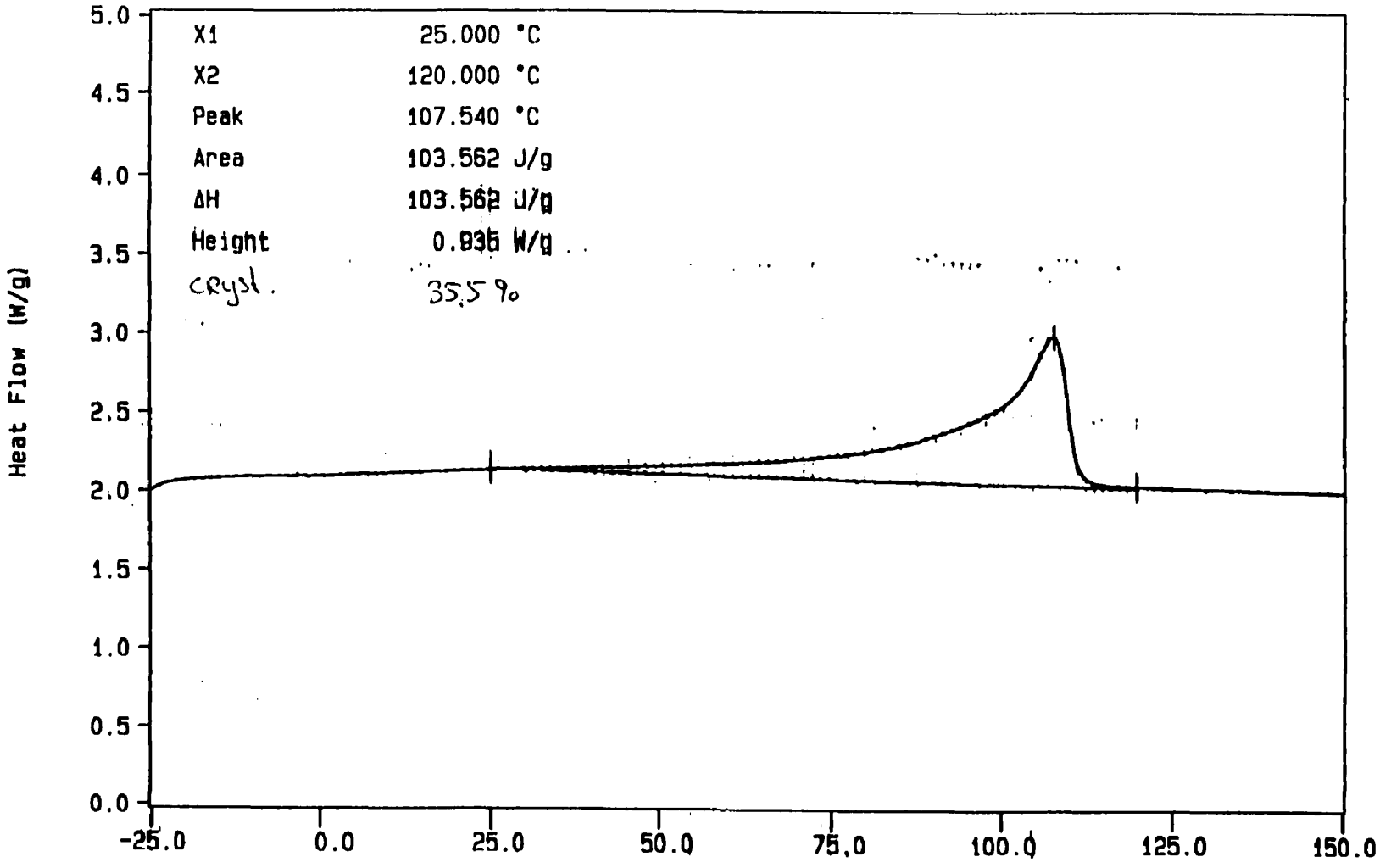

CCA-7 : 60 ml N2/min 2 channels
TEMP1: -30.0 C TIME1: 0.0 min RATE1: 10.0 C/min
TEMP2: 150.0 C

Marian
PERKIN-ELMER
7 Series Thermal Analysis System
Mon Jul 29 08:28:12 1996

Curve 1: DSC
File info: n6256 Mon Jul 29 08:18:40 1996
Sample Weight: 6.242 mg
LDB3

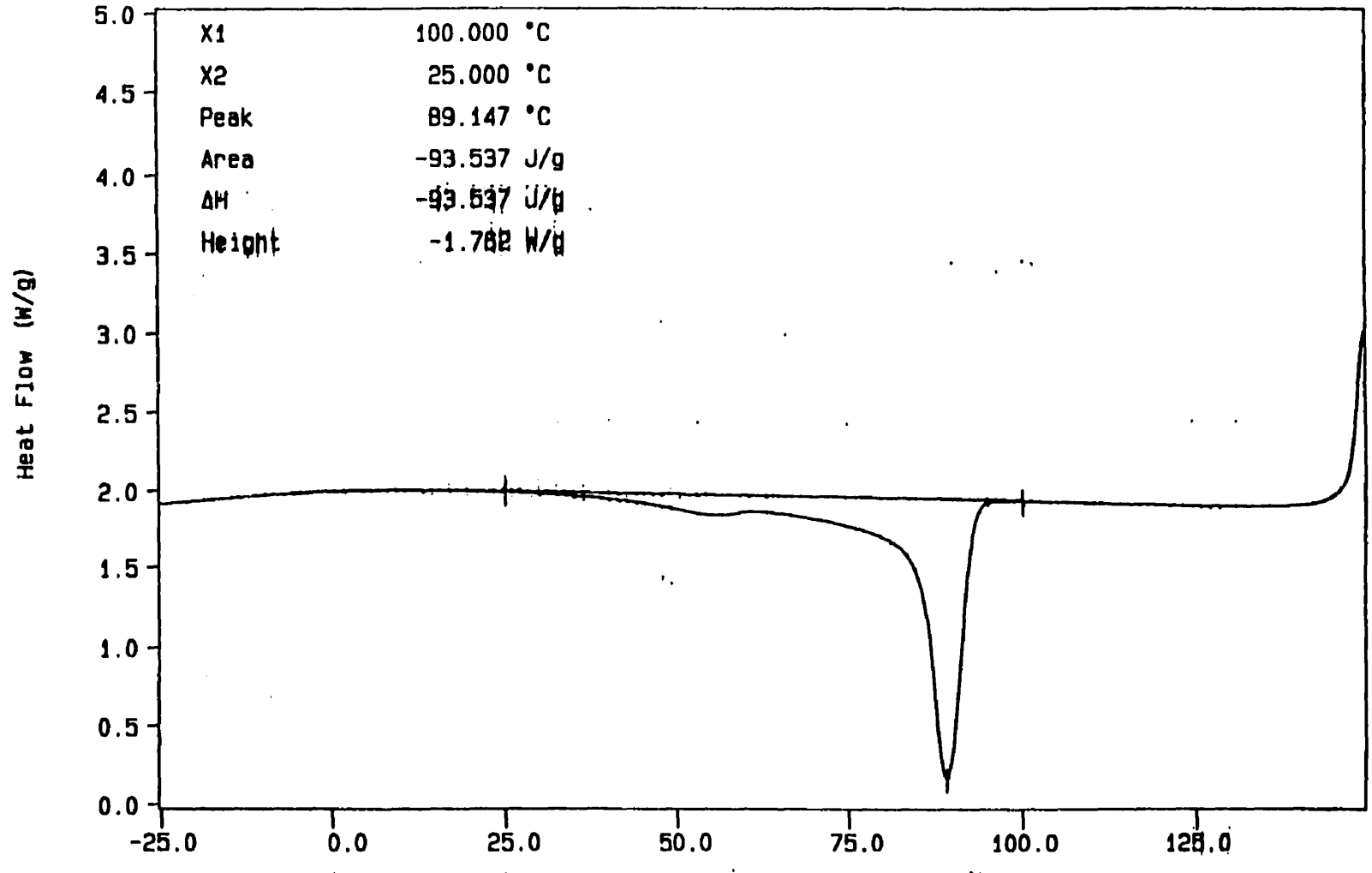

CCA-7 : 60 ml N2/min 2 channels
TEMP1: 150.0 C TIME1: 0.5 min RATE1: 10.0 C/min
TEMP2: -30.0 C

Marian
PERKIN-ELMER
7 Series Thermal Analysis System
Mon Jul 29 08:27:07 1996

Appendix F.

Table of Nomenclature

Greek Letters			
α	exponent for M_w dependence of η_o	η^+_{ER}	reduced tensile stress growth coefficient
β	material dependent parameter in damping function	η_o	zero shear viscosity
δ	loss angle	λ	relaxation time
Δx	plate displacement	ρ	density
ε	Hencky strain	σ	stress
$\dot{\varepsilon}$	Hencky strain rate	σ_E	extensional stress
γ	strain	σ_o	stress amplitude
γ_o	strain amplitude in oscillatory shear and strain in step strain	τ_{ij}	Component 'ij' of the extra-stress tensor
$\dot{\gamma}$	strain rate	τ_o	parameter in Cross viscosity model
η	viscosity	υ	negative of the power law slope of viscosity curve
$\eta^*(\omega)$	complex viscosity	ω	frequency
$\eta'(\omega)$	real component of complex viscosity	ω_c	critical frequency
$\eta''(\omega)$	imaginary component of complex viscosity	ψ^+_I	first normal stress growth coefficient
η^+_E	tensile stress growth coefficient	ψ_I	first normal stress coefficient
η_E	extensional viscosity	Γ	viscosity enhancement factor
η^+	stress growth coefficient	Γ_{asym}	viscosity enhancement factor for assymetric stars (defined in Equation 2.7)

Roman Letters			
J_s^o	recoverable compliance	m	reduced molecular weight in Chap. 9 and Cross model power-law index parameter in Eqn. 1.1
A	area	M	molecular weight
a	material dependent parameter in damping function	m(t-t')	memory function
A_o	initial area	M_{arm}	molecular weight of a branch or arm
a_T	shift factor for time-temperature superposition	M_e	critical molecular weight for entanglement
B_{ij}	component 'ij' of the Finger tensor	M_W	weight average molecular weight
b_T	modulus shift factor for time-temperature superposition	M_Z	Z average molecular weight
C_{ij}	component 'ij' of the Cauchy strain tensor	M_{Z+1}	Z+1 average molecular weight
E_a	Arrhenius activation energy	PR	peak molecular weight ratio
F	force	R	relative location (Eqn 9.17)
f	number of arms (star polymers)	R	ideal gas constant
g	ratio of mean squared radii of gyration	T	temperature
G(t)	linear shear stress relaxation modulus	t	time

Roman Letters			
$G'(\omega)$	storage modulus	T_o	reference temperature
$G''(\omega)$	loss modulus	t_o	time passed since beginning of experiment in step strain test
$G^*(\omega)$	complex modulus	v	velocity
G_d	amplitude ratio in oscillatory shear	W	width
H	height	w	weight fraction
$h(I_1,I_2)$	damping function	w(log m)	differential molecular weight distribution function
H_o	initial height	w_B	weight fraction branched molecules
I_1,I_2	first and second invariant of the Finger strain tensor	w_L	weight fraction linear molecules
L	length	W_o	initial width